Photoexcitation of Aldehyde Derivatives to Access Chiral Added Value Products

PhD Candidate: Antonio Di Sabato

Supervisor: Prof. Patrizia Gentili

PhD in Chemical Science
XXXV Cycle

Department of Chemistry

Faculty of Mathematical, Physical and Natural Sciences

La Sapienza University of Rome

Table of Contents

1. Introduction

1.1 Organic Photochemistry

The field of organic photochemistry is usually considered born in 1912 with Giacomo Ciamician's pioneering lecture at the 8th International Congress of Applied Chemistry[1], entitled "The Photochemistry of the Future"[2]. Ciamician and his contemporaries generally adopted for their experiments the cheapest and most widely available light source: sunlight. Yet, the power of our star is inherently difficult to harness, given its daily, seasonal and geographical high variability, combined with an emission spectrum that covers the visible range and extends far into the infrared region, while higher energy UV photons, more suitable to induce vibronic transitions, are efficiently shielded by the ozone layer. Throughout the XX century, mercury vapours lamps and incandescent bulbs have been the only alternatives powerful enough to be used in chemical reactions; both of them exhibit a broad and uneven profile of emission, thus limiting their use to very specific case studies.
Starting from the early 2000 though, the availability of cheap CFL (*Compact fluorescent lamp*) and LED (*light emitting diode*) sources helped shedding a new light on photochemistry.
The photochemistry of carbonyl compounds has been investigated since the initial studies in this field. As it is well known, the carbonyl compounds has two nonbonding lone pairs on the oxygen atom; interesting one-electron properties of these compounds, such as ionization potentials or n,π^* transitions, show that the two lone pairs are not equivalents, but they occupy the nondegenerate n_p and n_{sp} orbitals. In particular, the first ionization potential of simple ketones indicates the involvement of the n_p electron,

showing that n_p orbital is at higher energy than the π bonding and n_{sp} orbitals (Scheme **1.1**)[3].

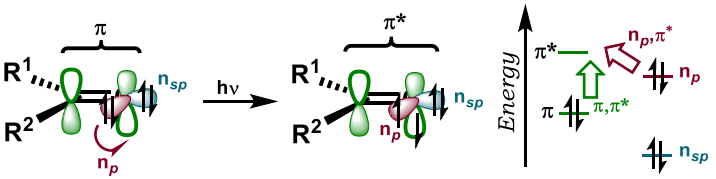

Scheme 1.1 Molecular orbitals involved in the carbonyl group transitions

These observations point out that, albeit two transitions are possible, π→π* and n→π*, for simple ketones and aldehydes the lowest excited state is n_p,π*; however, the transition n→π* is forbidden for symmetry reasons, so that ketones and aldehydes have a very weak n→π* absorption (ε = 20 - 50 $M^{-1}cm^{-1}$) and generally it is hidden from the stronger π→π* transition. By intersystem crossing (ISC), the ^{1}(n,π*) singlet state decays rapidly to ^{3}(n,π*) triplet one, being these two excited states very close in energy. In the case of aryl ketones, it is also possible to have an ISC from S_1(n,π*) to T_1(π,π*), being the energy of the last one very similar to that of T_1(n,π*); which of the excited levels lies at lower energy depends on the solvent and on the nature of substituents on the benzene ring. Generally, the ISC for aromatic and aryl alkyl ketones is more efficient (few picoseconds) and quantum yields are close to unit ($\Phi_{ISC} \approx 1$); ISC rates of alkyl ketones, instead, are below 10^8 s and singlet reactions can occur[4].
The knowledge of the nature of the lowest excited state is very important to understand the photophysical properties and photochemical reactivity of carbonyl compounds.

1.2 The Norrish Reactions

A Norrish reaction is a photochemical reaction occurring on substrates possessing an aldehyde or ketone moiety. After

irradiation at the appropriate wavelength (typically around 300-400 nm, depending on the nature of the substrate), it is possible to elicit the n→π* transition of the carbonyl group, bringing the substrate to the excited singlet state ($^*S_1$). This excited intermediate can undergo bond homolisys at the α position with respect to the carbonyl, forming two free radical fragments. Depending on the exact chemical structure and on the relative bond dissociation energies, these free radicals may evolve towards different products: a simple recombination reforms the starting material, accompanied, when possible, by racemisation at the α-carbon; alternatively, the acyl radical can lose a molecule of carbon monoxide, forming a new carbon radical fragment that, after recombination, produces an alkane. The final effect of this transformation is the decarbonylation of the reagent. The abstraction of an α-hydrogen from the carbonyl fragment leads to a ketene and an alkane, while the abstraction of a β-proton from the alkyl fragment generates an aldehyde and an alkene. These possible reaction pathways are known as **Norrish Type I reactions** (Scheme **1.2**)[5]. Nonetheless, it is important to stress that, once the molecule lies in the $^*S_1$ state, it may simply return to the ground state by radiative or radiationless channels.

There is a good correlation between the rates of α-cleavage with the C-CO bond dissociation energies; for example, the excitation energy to S_1 for alkyl ketones (E_{S1} (acetone) = 373 kJ/mol) and acetophenone (Es_1 = 330 kJ/mol) are high enough to allow the C-CO bond cleavage and to release the *tert*-butyl and benzyl radicals. In other words, the quantum yields (Φ_I range 0.2 - 0.4) and the α-cleavage rates constants are related to the radical stability. Usually these rate constant from singlet n,π* excited states are in the range 10^8 - 10^9 s^{-1} and are comparable to those of intersystem crossing.

When the lifetime of the $^*S_1$ excited state is long enough, the system can evolve to the triplet state ($^*T_1$) through an $^*S_1 \rightarrow {}^*T_1$ *Inter-System Crossing* (ISC). In the presence of a γ-hydrogen in the substrate, the oxygen atom may perform an intramolecular H-atom abstraction to form a 1,4-biradical. Once formed, this species

may follow another type of fragmentation, the so-called **Norrish Type II Reaction**, by cleavage of the C_α-C_β bond, forming an alkene and an enol which rapidly tautomerizes to its corresponding carbonyl form (Scheme **1.2**). Alternatively, the 1,4-biradical may couple in an intramolecular fashion to give, as a product, a cyclobutanol, in a process commonly referred to as **Norrish-Yang Cyclization** (N-Y, Scheme **1.2**).

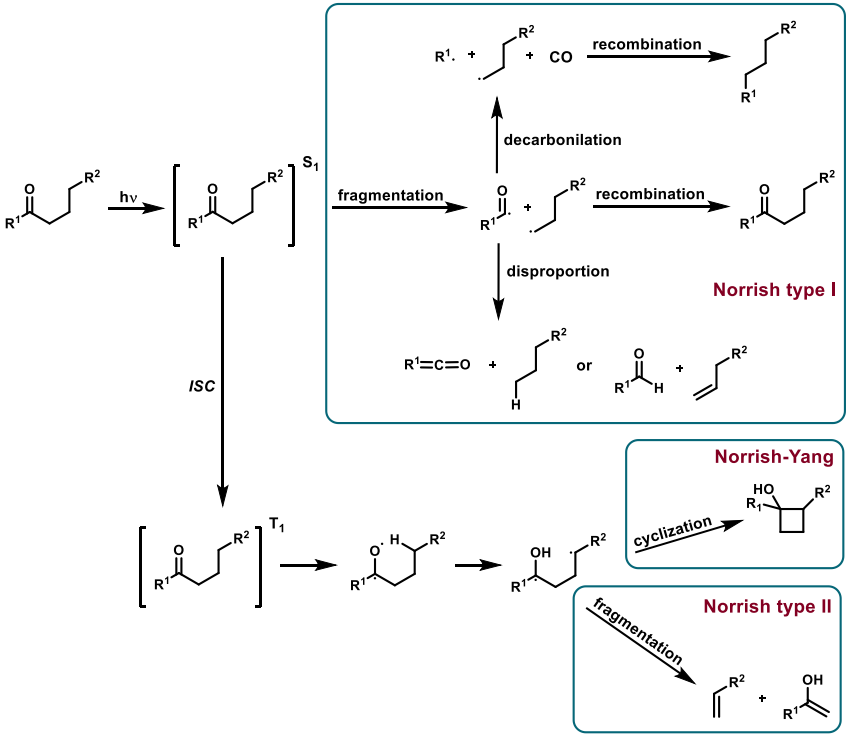

Scheme 1.2 Overview of the Norrish reactions.

Partition of 1,4-biradical among elimination, cyclization and reversion reactions is affected by several factor. 1,4-biradicals obtained from alkyl aryl ketones, for example, have lifetimes

ranging from about 20 ns, as in cyclohexane and benzene, to approximately 120 ns in DMSO and methanol. The solvent H-bond ability increases the lifetime of 1,4-biradical, probably inhibiting the re-H-abstraction, which leads to parent ketone, and modifying conformations and interactions between the radical sites[6].

The 1,4-biradical intermediate can exist in two different conformations (Scheme **1.3**): *gauche* (*cisoid*) and *anti* (*transoid*), the former generating the N-Y cyclization product, the latter giving rise to Norrish Type II fragments. Ring closure can occur only in the *cisoid* conformation, where the *p*-orbitals on the C_1 and C_4 are arranged frontally, allowing their overlap to form the new σ bond. Conversely, in the *transoid* conformation, the orbitals orientation is parallel with respect to the $\sigma_{C2\text{-}C3}$ bond, facilitating bond cleavage and favouring new π bonds formation. In both cases, before evolving to the products, to ensure spin conservation, the system shall return to the singlet state through an *ISC*, since triplet-excited products formation is energetically unlikely[7].

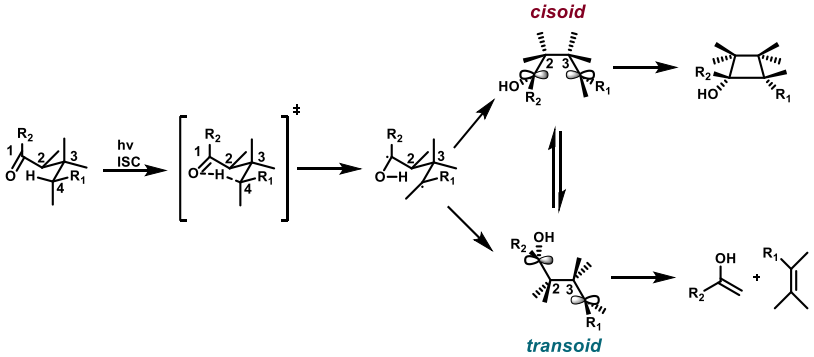

Scheme 1.3 *Cisoid* and *transoid* conformations of the 1,4-biradical.

Two main aspects are especially relevant for the applicability of the N-Y reaction in organic synthesis, i.e., the chemoselectivity of cyclization vs. Norrish I and II fragmentation reactions and the stereoselectivity of the ring closure. The latter generates at least two stereogenic centres from an achiral precursor. Both the

incidence of the Norrish II fragmentation and the stereoselectivity of cyclization are related to conformational changes in the triplet state. To ensure *p*-orbitals overlap and construction of the cyclobutanol scaffold, the 1,4-biradical may rotate the C_1-C_2 and C_3-C_4 bonds, bringing the -OH group and substituent R_2 on opposite sides (*trans* ring closure) or on the same side (*cis* ring closure) of the ring plane. Contrarily, rotation around the C_2-C_3 bond leads to the appropriate conformation for the bond to break through a Norrish II mechanism (Scheme **1.3**).

1.2.1 Chemoselectivity and Stereoselectivity in the Norrish-Yang reaction

As shown in the work by Griesbeck's and Moorty's groups[7–11], competing reaction pathways may arise during the photolysis of alkanophenones derivatives: when the substituents are in *syn* configuration, the cyclobutanol is the prevalent species observed, while the *anti* diastereoisomer produces almost exclusively fragmentation products (Scheme **1.4**).
This phenomenon occurs because the 1,4-biradical tends to always adopt the most stable conformation, where the substituents are further apart. This arrangement happens to be *transoid* for the *anti* diastereoisomer, and so leading to fragmentation products, while for the *syn* isomer the most stable conformation is the *cisoid* one, allowing for the formation of the 4-membered cycle.

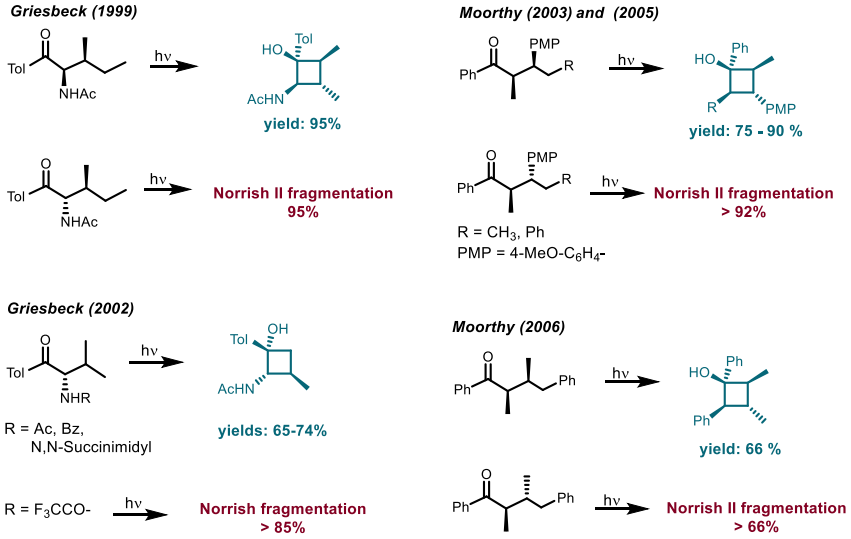

Scheme 1.4 Norrish-Yang cyclization *vs.* Norrish II fragmentation.

Has been observed how bulkier substituents tend to arrange themselves in a *trans* configuration; anyway, solvent polarity may influence the diastereoselectivity in the ring closure. The bulkiness of the -OH group, in fact, also depends on its solvation, as polar or H-bonding solvents may increase the steric hindrance of the hydroxyl moiety by enlarging its coordination sphere, leading to a bias towards the *trans* ring closure. As an example, the photocyclization of β-anisylbutyrrophenones yields preferentially the *cis* diastereoisomer when performed in apolar solvents, such as benzene or cyclohexane, while the *cis:trans* ratio is about 1:1 when the reaction is conducted in polar solvents, like DMSO or MeOH (scheme **1.5**)[12]. It should be noted anyway that in both cases large portions of the converted starting material underwent Norrish II fragmentation instead of cyclization.

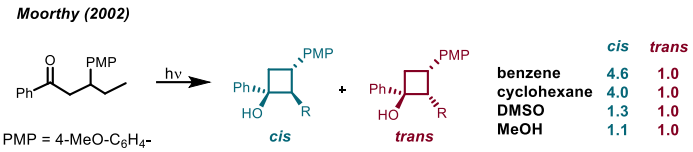

Scheme 1.5 Solvent-dependant diastereoselectivity in Norrish-Yang cyclization

Another case where the change in reaction conditions completely reverses the stereoselectivity of the N-Y cyclization is the photoexcitation of 2-benzyloxyacetophenone to give substituted dihydrobenzofuranols. The simple reaction of the substrate in solution affords exclusively the *cis* isomer, while the addition of 5 equivalents of tetrabutylammonium fluoride in the reaction mixture results in a 93:7 prevalence of the *trans* isomer (Scheme **1.6**)[13]. This is due to a cation-π interaction between the tetraalkylammonium ion and the benzylic ring, together with hydrogen bond of the fluoride to the hydroxyl group of the biradical intermediate.

Diastereoselectivity can also be imparted by structural biases in the reagent, such as the presence of cyclohexyl[14] or decalin ring systems [15] or atropoisomeric motifs[16].

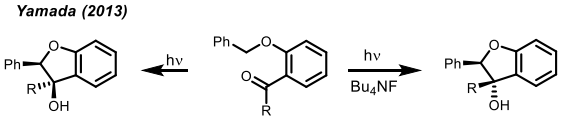

Scheme 1.6 Tetrabutylammonium-assisted Norris-Yang cyclization.

Notably, all the examples shown so far involve the photocyclization of aryl ketones to afford 1-arylcyclobutan-1-ols. Over the years though, the scope of the Norrish-Yang reaction has also been expanded to 1,2-diketones[14,17] and α-keto-oximes[18,19], to provide 2-hydroxycyclobutanones derivatives, as well as to α-[20,21] and β-ketoamides[22,23] to yield β-lactams.

It should be highlighted that, although the photochemistry of aldehydes was extensively studied, these compounds form exclusively fragmentation products by means of Norrish I or II reaction mechanism and generally fail to afford any cyclization product[24–26].

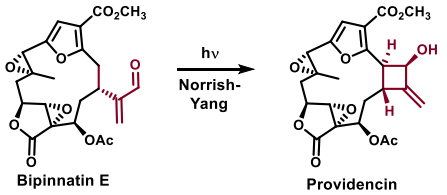

Scheme 1.7 Biosynthesis of providencin.

A remarkable exception is that of bipinnatin E and providencin, two furanocembranoids with mild anticarcinogenic activity, isolated from Caribbean gorgonian corals. The structural difference between these molecules is the presence of an *exo*-methylene substituted cyclobutanol ring fused on C_1 and C_2 in providencin, while bipinnatin E has an acyclic α-β unsaturated aldehyde on the C_2 position. Bipinnatin E could be easily transformed into providencin by means of the Norrish-Yang cyclization, and this is the most likely mechanism for the biosynthesis of this compound (Scheme **1.7**)[27,28]. The presence of the highly strained 14-membered ring and the defined stereochemistry on the six stereogenic centres drive the reactivity towards the product with the correct configuration on the newly formed chiral centres[28].

1.3 2-(hydroxyimino)aldehydes

2-(hydroxyimino)aldehydes (HIAs), of generic structure RC(=NOH)CHO, are a class of organic compounds sporadically investigated in the scientific literature, despite their high

technological and application potential. Their most straightforward synthesis employs the corresponding aliphatic aldehyde and sodium nitrite as nitrosating agent, in the presence of $FeCl_3$, through an enamine organo-SOMO catalytic process (Scheme **1.8**)[29]. An alternative methodology involves the use of either $AlCl_3$ and *n*-Bu_4NNO_2 or (*i*-Pr)$_3$SiCl and $AgNO_2$ on silyl enol ethers obtained from the parent aldehyde[30].

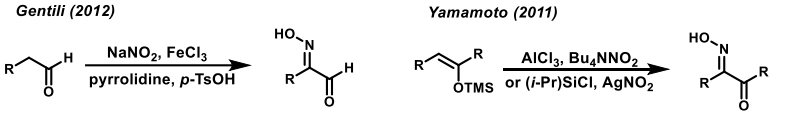

Scheme 1.8 Synthesis of 2-(hydroxyimino)aldehydes.

The proprieties of HIAs are shaped by the presence of the adjacent carbonyl and oxime functionalities, which impart a peculiar reactivity to these compounds. For example, the presence of the aldehyde in conjugated position with respect to the C=NOH double bond renders the oxime much easier to deprotonate. In fact, the pK_a of HIA is typically around 8-9, making them more similar in acidity to hydroxamic acids (pK_a = 7.7-9.9) then to simple oximes (pK_a in the 10-12 range)[31].

Another interesting propriety of HIAs, noticed in my group just before the start of my PhD, is the possibility for them to form metal complexes. In particular, trying to perform an azide-alkyne Huisgen cycloaddition of an HIA-containing molecule with Cu^{2+} catalysis, the formation of a green precipitate was observed, accompanied by a detrimental effect on the reaction yield. This phenomenon was ascribable to the formation of a copper-HIA complex, which was thus removed from the reaction environment, shutting down the desired reactivity. As will be thoroughly described in Chapter **3** of this work, further studies followed to explore the capability of several HIAs to complex Cu^{2+} or other metal ions. As a matter of fact, simple oximes have been extensively used to complex different metals[32], along with oxime

derivatives, such as α-oxo-oximes[33], α-cyano-oximes[34], 2-pyridylcarbaldehyde oximes[35,36], among the others.

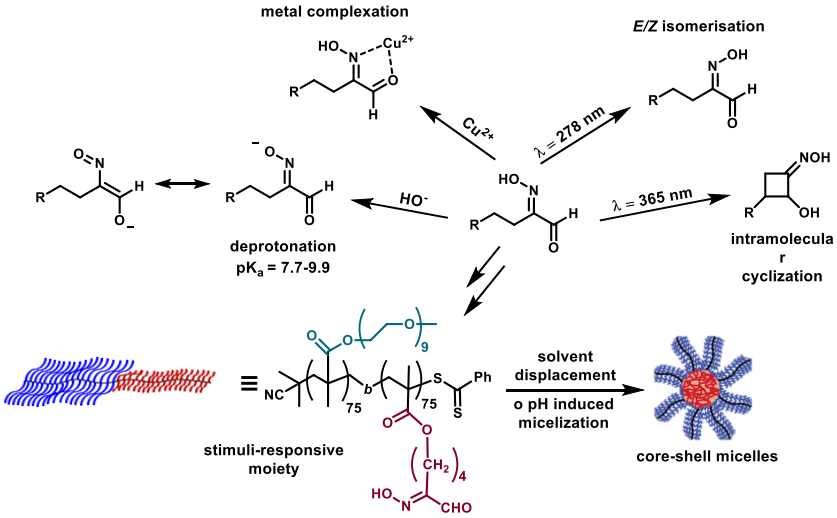

Scheme 1.9 Proprieties of 2-(hydroxyimino)aldehydes.

HIAs also exhibit a rich photochemistry, being possible to trigger independently the allowed π→π* transition of the oxime and the much weaker prohibited n→π* transition of the carbonyl group, which occur at λ ≅ 250 nm and λ ≅ 330 nm, respectively. The excitation of the π→π* transition of the oxime leads to the weakening of the C=N bond, enabling the system to undergo *E*/*Z* isomerisation. In this way the HIAs, which initially show almost every time an exclusively *E* configuration, reach a photostationary equilibrium with a well-defined substrate-dependant *E*/*Z* ratio. This transformation is reversible by keeping the sample, for times ranging from days to weeks, at 40 °C in the dark, after which the HIAs return to their initial *E*/*Z* ratio[31].

The initial studies on the photoexcitation of HIAs were conducted using high pressure mercury lamps with peak intensity at wavelengths around 350 nm and large bandwidths of around 100

nm. Such a light source is capable of exciting both the oxime and the carbonyl transitions. In fact, it was observed that along with the relatively fast (~2 h) substituent dependant *E*/*Z* isomerism, Norrish-Yang photoisomerization (described in Section **1.2**) to 2-hydroxycyclobutanone oximes (CBOs) occurred over longer irradiation times (>20 h). The discovery of such reactivity led to the development of a research project exploring the synthetic utility and chemical behaviour of the CBO products, the scope of the N-Y photocyclization, and its stereochemical outcome. This project absorbed a consistent fraction of my PhD and will be described in detail in Chapter **2**.

The HIA functionality has been also installed on a methacrylate scaffold that was used as monomer in the construction of random and block copolymers, together with oligo(ethylene glycol) methyl ether methacrylates (OEGMA) monomers (Scheme **1.9**)[37]. *Poly*-OEGMAs are known to self-assemble when a critical aggregation temperature is reached; thus, when these two monomers are combined, *multi-stimuli responsive* polymers are obtained, which can spontaneously aggregate or disassemble in response to chemical and physical variations, namely changes in temperature and pH, light, the presence of metal ions or combinations of two or more of these stimuli[38].

2. Norrish-Yang Reaction of HIAs[39]

In the synthetic aspect of the present chapter, the HIAs scope in the Norrish-Yang reaction was explored while also addressing the criticalities of scaling-up and isolation of stereoisomers. From a more mechanistic point of view, the stereoselectivity of the ring closure was determined experimentally by detailed NMR analysis, and DFT calculations were performed to help elucidate the energetic factors involved. Molecular dynamics is used to explore CBO-solvent interactions and their role in post-cyclization oxime *E*/*Z* isomerism.[40] NMR-based absolute configuration assignment is also explored.

2.1 Discovery and Early Experiments

Our initial studies on different aliphatic HIAs were carried out by irradiation with high-pressure mercury lamps (λ = 365 nm with a large bandwidth of about 100 nm) that cover the forbidden n-π* carbonyl transition, and, to some extent, allowed the oxime π-π* transition. Thus, both Norrish-type reactions and *E*/*Z*-oxime configurational isomerization were potentially triggered. In fact, we observed that along with the relatively fast (2 h) substituent dependant *E*/*Z* isomerism, N-Y photoisomerization to cyclobutanol oximes (CBOs) occurred over longer irradiation times (> 20 h) leaving, however, large and variable fractions of unreacted HIA. We found no evidence of concurring Norrish I and II fragmentations. In subsequent studies, we began using LED sources (λ = 365 ± 10 nm) to stimulate the aldehyde group selectively on HIAs linked to polymethacrylates and to 1,2,3-triazoles. The overall outcome was the same in all cases, i.e., HIA conversion was quantitative within 3-4 h and the only detected photoproducts were CBOs. Only in those cases in which a different substituent, such as a remote

salicylaldehyde ring, competes for the same wavelength does the HIA fail to yield the corresponding CBO.[41,42] This proves that HIAs and LED sources are a promising combination in terms of excellent conversions, convenient reaction time, and the absence of undesired products, for the synthesis of secondary cyclobutanols from aldehydes. It is worth noting that, in general, the clean N-Y reaction is not easily obtained, and, more specifically, to our knowledge the synthetically relevant N-Y reaction of aldehydes, which afford four-membered rings bearing the secondary alcohol, has previously only been reported by my group.[37,40] In fact, the photochemistry of aldehydes generally results in fragmentation reactions that are of importance in atmospheric chemistry,[24,25] for light-induced fragrance release,[43] and for photocleavable polymeric materials[44]. In the case of HIAs, instead, it was observed that the exclusive N-Y reaction occurs in solution without the need for conformationally demanding substituents or templates. However more work needed to be done to elucidate the stereochemistry of products and to impart any synthetic value to the N-Y cyclization of HIAs.

2.2 Photoinduced Norrish–Yang Cyclization of 2-(Hydroxyimino)aldehydes

First, variously substituted 2-(hydroxyimino)aldehydes **1a-j** were efficiently synthesized, starting from the corresponding aldehydes via α-oximation reaction (see Chapter **5**).[29] The presence of either a secondary or tertiary C_3 position (R^2 = H and R^2 ≠ H, respectively) was envisioned since the latter case would lead to the generation of a third stereogenic centre during the photoisomerization (**2g-j**).
Mass spectrometry analyses of HIA **1a** and CBO **2a**, carried out in negative ion mode, showed different fragmentation patterns. While **1a** displayed only a peak corresponding to the $[M\text{-}H]^-$ ion, **2a** also exhibits the peaks corresponding to the loss of H_2O, HCN, and CO molecules (see Chapter **5**). Both *E*/*Z*-oxime configurations are

observed in **2a** (*E*/*Z* = 15:1 in DMSO-d_6), even though the HIA precursor **1a** is only present as an *E*-oxime isomer. Oxime isomerization during and after the photoreaction will be discussed in section **2.6** of this chapter. Whereas in Moorthy's work, the competition between Norrish II and Norrish-Yang reactions is independent of the polarity of the solvent,[45–49] in the case of HIAs, fragmentation and cyclization occur alternatively. In fact, when apolar solvents were employed, such as DCM or benzene, decomposition of the starting material was observed, yielding a complex mixture of products (Table **2.1**, entries **5**-**6**). Conversely, by carrying out the reaction in polar solvents like MeOH-d_4 and MeCN-d_3, the corresponding CBO **2a** was isolated as a single product with complete conversion and improved diastereoselectivity of 2.5:1 in favour of the *trans* isomer (Table **2.1**, entries **3**-**4**). While the diastereomeric ratio (*dr*) values were comparable, the reaction carried out in MeOH-d_4 was faster, with complete conversion in 1.5 h compared to the 5 h in MeCN-d_3. Moreover, the use of a more powerful LED source improved reaction time without affecting the *dr* or leading to undesired products (Table **2.1**, entries **1**-**2**).

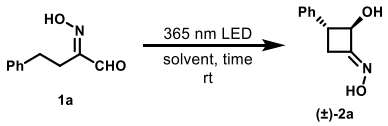

1a (±)-2a

Entry[a]	Solvent	Time (h)	*dr*[b]
1[c]	DMSO-d_6	4.0	1.4:1
2	DMSO-d_6	3.0	1.4:1
3	MeOH-d_4	1.5	2.5:1
4	MeCN-d_3	5.0	2.5:1
5	DCM-d_2	3.0	decomposition[d]
6	Benzene-d_6	4.5	decomposition[d]

Table 2.1 [a] The substrate (0.060-0.075 mmol) was dissolved in the appropriate deuterated solvent (600-750 µL, C = 0.1 M) in an NMR quartz tube. The sample was placed in a photoreactor using 1450 mW LED radiant flux. [b] *dr* values corresponding to the *trans*:*cis* diastereomers determined via ^{1}H-NMR. [c] Same reaction conditions, except for 1030 mW LED radiant flux. [d] decomposition yielded a complex mixture of products.

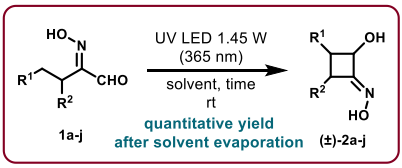

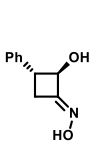

(±)-**2a**

DMSO-d_6, 3 h, dr = 1.4:1[b)]
MeOH-d_4, 1.5 h, dr = 2.5:1[b)]

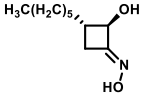

(±)-**2b**

DMSO-d_6, 5 h[c)], dr = 1.3:1[b]
MeOH-d_4, 4 h, dr = 1.7:1[b)]

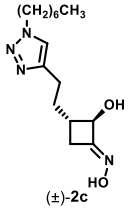

(±)-**2c**

DMSO-d_6, 4.5 h[c)], dr = 1.3:1[b)]
MeOH-d_4, 4 h, dr = 1.3:1[b)]

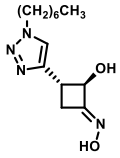

(±)-**2d**

DMSO-d_6, 4.5 h[c)], dr = 1.3:1[b)]
MeOH-d_4, 2 h, dr = 1.7:1[b)]

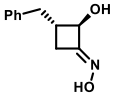

(±)-**2e**

DMSO-d_6, 6.5 h, dr = 1:1.1
MeOH-d_4, 5 h, dr = 1:1.1

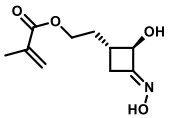

(±)-**2f**

DMSO-d_6, 5 h, dr = 1:1
MeOH-d_4, 3.5 h, dr = 1.1:1

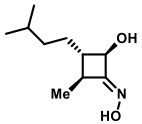

(±)-**2g**

DMSO-d_6, 1.5 h, dr = 5:1
MeOH-d_4, 1 h, dr = 2.5:1

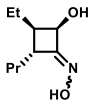

(±)-**2h**

DMSO-d_6, 1.5 h, dr = 10:1[b,e)]
MeOH-d_4, 0.5 h, dr >99:1[b)]

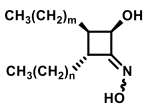

(±)-**2i'** m=8, n=7[d)]
(±)-**2i''** m=9, n=6[d)]

DMSO-d_6, 3 h[c)], dr >99:1[b)]
MeOH-d_4, 0.8 h, dr >99:1[b)]

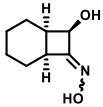

(±)-**2j**

DMSO-d_6, 2.5 h, dr >99:1[b)]
MeOH-d_4, 4.5 h[c)], dr >99:1[b)]

Scheme 2.1 Scope of HIAs in the N-Y cyclization. [a] The substrate (0.060-0.075 mmol) was dissolved in the appropriate deuterated solvent (600 – 750 µL, C = 0.1 M) in an NMR quartz tube. The sample was placed in the photoreactor using 1450 mW LED radiant flux; [b] *dr* values corresponding to the *trans*:*cis* ring-closure products determined via ^{1}H NMR; [c] Same reaction conditions, except 1030 mW LED radiant flux; [d] since the H-abstraction could occur on the two different alkyl chains of substrate **1i**, the exact structure of the product could not be determined; [e] a second diastereoisomer was observed (ca.10%), ascribable to the relative *cis* configuration of Et and Pr substituents.

Consequently, we selected DMSO-d_6 and MeOH-d_4 as the best solvents to proceed toward the evaluation of the general applicability of the reaction on variously substituted HIAs **1a-g** (Scheme **2.1**). On the one hand, monitoring the course of the reaction is easier in DMSO, owing to better resolution of diastereoisomeric peaks and to the presence of reliable -OH signals. On the other hand, the use of MeOH could lead to higher diastereoselectivity and allows easier isolation of the synthesized CBOs by simple solvent evaporation. Indeed, the products were fully characterized to confirm an excellent degree of purity without any further purification.

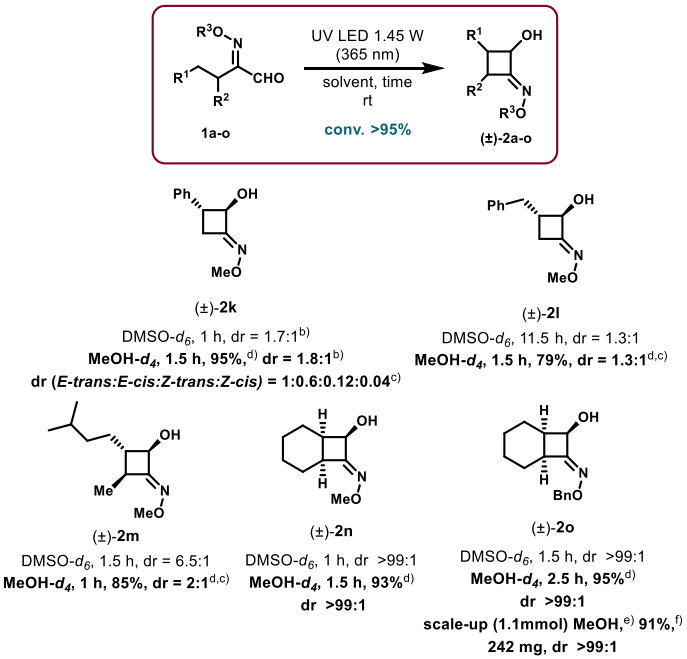

Scheme 2.2 Scope of HIAs with alkylated oxime group in the N-Y. [a] The substrate (0.060-0.075 mmol) was dissolved in the appropriate deuterated solvent (600-750 µL, C = 0.1 M) in an NMR quartz tube. The sample was placed in the photoreactor using 1450 mW LED radiant flux; [b] *dr* values corresponding to the *trans*:*cis* ring-closure products determined via ^{1}H NMR; [c] all diastereoisomers were isolated via flash column

chromatography and characterized; [d] isolated yield after flash column chromatography; [e] scale-up experiment starting from 1.1 mmol of **1j** dissolved in 4.3 ml MeOH (C = 0.25 M). Reaction completion achieved in 13h.

A further synthetic advantage is provided by functionalization of the oxime -OH group (**1k**-**o**), which resulted in stability of the obtained CBOs on silica, thus enabling also the isolation of all diastereoisomers via flash column chromatography, achieving good to excellent product recovery (up to 95% yield).
It is worth noting that in MeOH-d_4, variable amounts of the hemiacetal form of **1k**-**o** were observed, thanks to the distinct position of the >C=NOCH_3 and >C=NOCH_2Ph signals (3.8 and 5.05 ppm, respectively). However, the carbonyl/hemiacetal equilibrium did not affect either the product yield or reaction times. In all of the tested cases, excellent conversion was observed in the formation of the desired CBOs (Scheme **2.2**).
Both aliphatic and aromatic R_1 substituents were well tolerated in terms of conversion to CBO. Most importantly, the functionalization of the oxime moiety allowed product purification via column chromatography with good to excellent yields and, in the case of products **2k**, **2l**, and **2m**, all of the generated diastereoisomers were successfully isolated and characterized separately (see Chapter **5**). Moreover, the presence of different functional groups such as esters and double bonds was well tolerated in the radical cyclization. In fact, compound **2f** was isolated with complete conversion and no detectable side products. Finally, to demonstrate the applicability of the procedure, a scale-up experiment (1.1 mmol) was carried out with substrate **1o**, isolating the corresponding CBO **2o** with comparable yield (91%) and the same excellent diastereoselectivity (>99:1 *dr*), further validating the synthetic value of this methodology.

2.3 Spectroscopic and Stereochemical Analyses of Cyclobutanol Oximes

As shown in Scheme **2.2** and **2.3**, all C_3-substituted HIAs gave the corresponding cyclobutanol oximes with excellent stereocontrol and, being the CBO moiety a confined small ring with many functional groups in the proximal vicinity, the spectroscopic determination of the relative configuration of the obtained compounds was a key challenge.

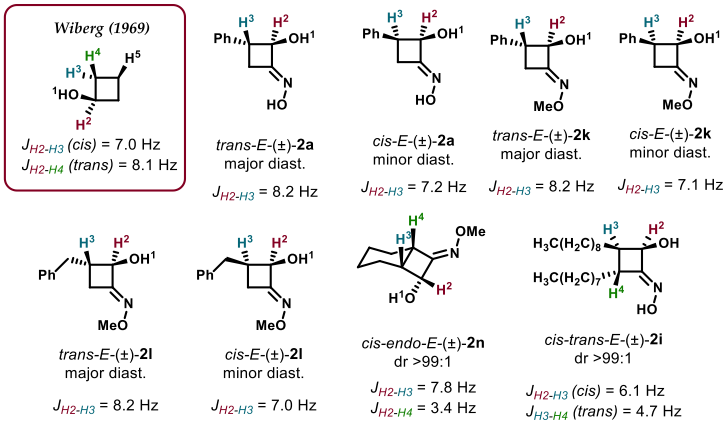

Figure 2.1 *J*-coupling constants of the synthesised CBOs.

In fact, in the case of products **2a-f** and **2k-l** the possible diastereomers are derived only from a *cis* or *trans* ring closure (between OH and R^1), while the introduction of an additional substituent in compounds **2g-j** and **2m-o** implicates the generation of a third stereocentre during the photoisomerization so that up to eight stereoisomers can be formed. Several factors (solvent polarity, hydrogen bond, stereoelectronic requirements, substituent steric hindrance) can potentially play a role in determining the *cis* or *trans* ring closure and, consequentially, the

stereoselectivity of the reaction. The assignment of *cis*/*trans* ring signals was determined by a combination of spin-decoupled ^{1}H, ^{13}C, HSQC, and NOESY NMR spectroscopy (see Chapter **5**).
In the case of products **2a-j** and **2k-l**, the values of the *J*-couplings between protons H^2 and H^3 in both major and minor diastereoisomers were in good agreement with literature data on substituted cyclobutanols,[50] hence identifying the major diastereoisomer as the *trans*-CBO (Figure **2.1**). Similarly, the relative configuration of products **2j** and **2n-o** was assigned mainly on the basis of *J* coupling values, confirming the formation of the *endo* product for the CBOs **2e,i,j**. Furthermore, the NOESY NMR (see Chapter **5**) showed a weak contact between the alcoholic H^1 and the alkylic H^5, which is also compatible with the most probable distances in the endo structure (see Chapter **5**).

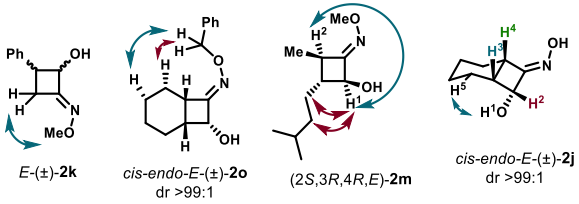

Figure 2.2 NOESY contacts relevant to CBOs structure elucidation.

Additionally, NOESY NMR on the methylated CBO **2k** exhibited a clear correlation between the methyl group and CH_2, allowing us to assign the configuration of the oxime double bond as *E* in both isomers. In compound **2o**, the benzylic CH_2 group showed NOE contact with two cyclohexane protons, confirming the *E* configuration of the oxime double bond (Figure **2.2**). Finally, all analysed CBOs gave the same CID fragmentation pattern as that of **2a**, both in negative and positive ion modes.
Once the NMR diagnostic signals were assigned, we were able to evaluate the diastereoselectivity of the ring closure as a function of substitution and solvent. We first focused our attention on substrates with R_2 = H, which would afford the corresponding

CBOs bearing only two stereogenic centres (Scheme **2.1**, **2a-f**). The diastereoselectivity was limited in these cases, with *dr* in the 1.1:1-1.7:1 *trans:cis* range, both in DMSO and MeOH. Subsequently, HIAs having $R^2 \neq H$ were tested, to evaluate the influence of the introduction of a third incipient chiral centre on the reaction outcome (Scheme **2.1**, **2g-j**). Interestingly, the reactions carried out in DMSO-d_6 showed better diastereoselectivity in favour of a *cis* closure of the cyclobutane ring.[49] Indeed, in DMSO, we observed the formation of a single diastereoisomer of CBOs **2h**, **2i**, and **2j** (Scheme **2.1**). It should be noted that, in the case of HIA **1i**, H-abstraction can occur at two equivalent Cγ positions, R^1 and R^2 being just slightly different in length (product **2i** in Scheme **2.1**). However, the two resulting regioisomers are not distinguishable by either NMR or MS analysis. It appears that the presence of an additional substituent ($R^2 \neq H$) causes the inversion of the ring closure stereoselectivity from *trans* to *cis* (products **2h-j**). Interestingly, in the case of product **2g** (R^2 = Me), the ring closure still favours the *trans* diastereoisomer. Presumably, the smaller steric hindrance of the methyl group (**2g**) compared to propyl (**2h**), is not sufficient to invert the diastereoselection. O-functionalized HIAs showed a similar behaviour; in the case of methylated compounds **1k**-**l** (R^2 = H), the diastereoselectivity (*dr* up to 1.8:1) decreased in comparison with the corresponding non-methylated compound **1a** (*dr* = 2.5:1), whereas excellent stereoselectivity was observed for both methylated **1n** ($R^2 \neq H$) and benzylated **1o** ($R^2 \neq H$), affording the same level of diastereocontrol in the *cis* ring closure (>99:1 *dr*) (Scheme **2.2**). Considering that HIA **1g** was prepared starting from (±)-citronellol, we envisioned that the preparation of both optically pure HIAs derived by (*R*)- or (*S*)-citronellol, both commercially available, could give us crucial information on the stereochemical features of the process. Indeed, we prepared HIAs (*S*)-**1g** and (*R*)-**1g** and the corresponding methylated one (*R*)-**1m**. The obtained substrates were probed under photoirradiation conditions, and the results were analysed by both NMR and HPLC on a chiral stationary phase, in

comparison with the corresponding racemic analogues. The product (4*S*)-**2g** was obtained with excellent conversion and a diastereomeric ratio of 5:1 (Scheme **2.3**).

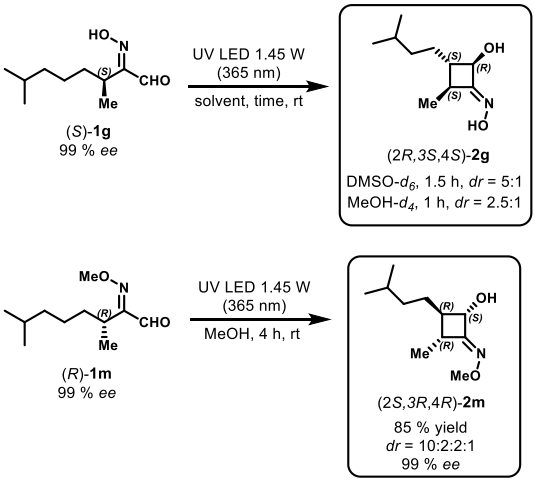

Scheme 2.3 Photoinduced Norrish-Yang cyclization of optically pure HIAs, (*S*)-**1g**, and the corresponding methylated one (*R*)-**1m.**

The same level of diastereocontrol was observed on the racemic product (±)-**2g** (Scheme **2.3**), and similar results were observed with the methylated product (4*R*)-**2m**. Additionally, for this compound, all the diastereoisomers were purified by column chromatography and characterized separately. The purification was performed as well on the racemic product (±)-**2m** and the major diastereoisomers were analysed by HPLC on a chiral stationary phase, showing complete retention of the optical purity with 99% *ee* values. These outcomes showed that no racemization process occurs during the photochemical isomerization reaction, which generates the two new stereocentres in a complete enantioselective process. Moreover, it allowed us to unambiguously assign the absolute configuration of the major diastereoisomer of the obtained optically pure CBOs as (2*S*,3*R*,4*R*,*E*)-**2m**, on the basis of the known configuration of C_4

combined with the relative configuration determined via NMR analyses.

2.4 IR Multiple Photodissociation Spectroscopy

The stereochemical assignments were further validated by relying on IR multiple photon dissociation (IRMPD) spectroscopy. Using this technique, it is possible to obtain the IR spectra of ions, which are mass-selected and trapped in the cell of a mass spectrometer, by plotting the abundancies of the fragments that are produced by the interaction of the ions with resonant photons as a function of the photon energy.[51,52] IRMPD spectroscopy has proven to be a valuable tool for the characterization of reaction intermediates,[53–56] and it has also shown potential for the discrimination of stereoisomers.[53,57–59] It is thus a promising approach for the unambiguous identification of the herein-presented compounds.
Compounds **2o**, *cis*-**2m**, and *trans*-**2m** were characterized as bare protonated species. Photofragmentation mass spectra are reported in Figures **5.15-17** in chapter **5**. Main fragmentation channels are also described and agree with the structural features of the ions. Interestingly, [*cis*-**2m**+H]$^+$ and [*trans*-**2m**+H]$^+$ show some differences in the fragmentation channels, in particular, the loss of a water molecule is only present in the dissociation pathway of [*cis*-**2m**+H]$^+$.
Figure **2.3** reports the IRMPD spectrum of [**2o**+H]$^+$ together with the calculated IR spectrum of the optimized structure designed to have the hypothesized stereoisomerism, *cis-endo-E*-**2o**. For comparison purposes, the geometries of the *exo* stereoisomer, *cis-exo-E*-**2o**, and the *Z* isomer *cis-exo-Z*-**2o** were also optimized and the corresponding spectra are reported. Protonation of the alcohol group for *cis-endo-E*-**2o** was also tested, but the optimization process led to the N-protonated form. The experimental spectrum shows the best agreement with the calculated one of *cis-endo-E*-**2o**, confirming the assigned stereoselectivity of the synthetic

procedure. It has to be noted that the calculated isomers are not interconvertible, thus relative energies cannot be used to predict the actual isomer population.

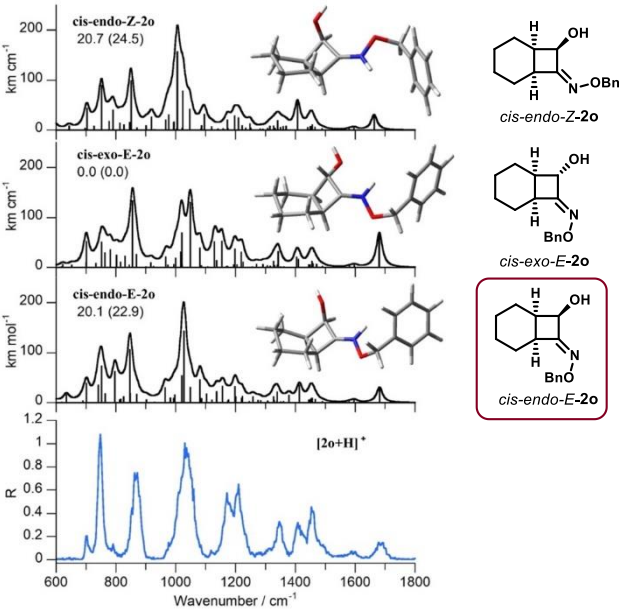

Figure 2.3 From bottom to top: recorded IRMPD spectrum of [**2o**+H]$^+$, simulated IRMPD spectra of *cis-endo-E*-**2o**, *cis-exo-E*-**2o**, and *cis-endo-Z*-**2o**, respectively.

Vibrational modes assignment is reported in table **5.1** in chapter **5**. Indeed, the calculated vibrations of the stereoisomers *cis-exo-E*-**2o** and *cis-endo-Z*-**2o** do not significantly differ from the ones of *cis-endo-E*-**2o**. However, it is possible to highlight a few characteristic features. Regarding *cis-exo-E*-**2o**, the most evident difference is the presence of a partially split band comprising at 1049 cm^{-1} the NO stretching coupled with the OH bending and at 1021 cm^{-1} the NO bend and CC stretch. This is in contrast with the single broad IRMPD band at 1033 cm^{-1} that is better interpreted by the same couple of vibrational modes calculated for *cis-endo-E*-**2o** at 1029 and 1022 cm^{-1}, respectively. Also, the two

experimental bands at 1213 and 1173 cm^{-1} are better reproduced by the cluster of calculated vibrational modes of *cis-endo-E*-**2o** in that spectral range. The spectrum of the protonated *Z* isomer of compound **2o**, *cis-endo-Z*-**2o**, albeit showing a somehow good agreement with the experiment, presents a slight shift in the frequency of the CN stretching mode with respect to the corresponding IRMPD band: values are 1664 and 1683 cm^{-1}, respectively. Indeed, the experimental frequency is better reproduced by *cis-endo-E*-**2o** with its calculated value of 1682 cm^{-1}. The pronounced signal at 1033 cm^{-1} is also not well simulated by the NO stretching calculated for *cis-endo-Z*-**2o** at 1006 cm^{-1}, while the cluster of vibrational modes around 1200 cm^{-1} again does not accurately reproduce the experiment. In summary, the comparison allows the assessment of *cis-endo-E*-**2o** as the sampled isomeric form of [**2o**+H]$^+$.

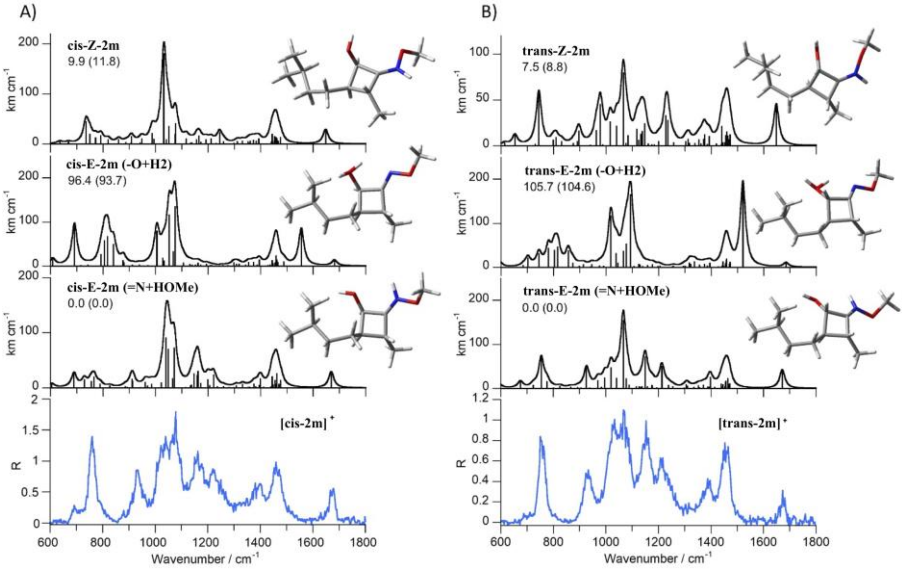

Figure 2.4 Recorded and calculated spectra of the two major diastereoisomers of CBO **2m**.

To confirm the opposite stereoselectivity of the *trans* ring closure in the presence of the methyl group as R_2 in product **2m** (*vide*

supra), the isolated pure diastereoisomers *cis*-**2m** and *trans*-**2m** were also characterized using IRMPD spectroscopy, and the experiments interpreted by DFT calculations. The results are reported in Figure **2.4**.

Both IRMPD spectra of [*cis*-**2m**+H]$^+$ and [*trans*-**2m**+H]$^+$ are in good agreement with the calculated spectra of the corresponding *E* isomers protonated on the nitrogen atom: *cis*-*E*-**2m** and *trans*-*E*-**2m**, respectively (Figure **2.4a** and **2.4b**, respectively). The vibrational mode assignment for both species is reported in Tables **5.2** and **5.3**. Compounds *cis*-**2m** and *trans*-**2m** differ in the configuration of one of their stereocentres, in particular the C_2 atom. Indeed, both their IRMPD spectra present comparable vibrational features as highlighted in Tables **5.2** and **5.3**; however, the spectral range below 800 cm^{-1} shows some differences which can be correlated to the different stereochemistry of compounds *cis*-**2m** and *trans*-**2m**.

Calculated vibrations of *cis*-*E*-**2m** in that range show the presence of several modes of similar intensity related to the NH bend coupled with other vibrational modes, which is in agreement with the broadening of the lower portion of the IRMPD signal at 757 cm^{-1} and the emerging of a smaller feature at 690 cm^{-1}. On the contrary, the IRMPD spectrum of [*trans*-**2m**+H]$^+$ presents a single signal at 750 cm^{-1} consistent with the presence in the calculated *trans*-*E*-**2m** spectrum of a dominant signal at 755 cm^{-1}, i.e., the out-of-plane NH bending. Protonation on the alcoholic functionality was also taken into account for both [*cis*-**2m**+H]$^+$ and [*trans*-**2m**+H]$^+$ leading to the structures *cis*-*E*-**2m**(-O$^+$H$_2$) and *trans*-*E*-**2m**(-O$^+$H$_2$), respectively. Their presence in the sampled population can indeed be discarded on the basis of the evident disagreement of computed spectra with experimental ones. Finally, the calculated spectra of the *Z* isomers of *cis*-**2m** and *trans*-**2m**, *cis*-*Z*-**2m** and *trans*-*Z*-**2m**, respectively, are reported and compared to the IRMPD spectra to assess their absence in the sampled gas-phase population and confirm the samples to be single diastereoisomers. Though simulating most of the vibrational

bands, the calculated spectra of *cis-Z*-**2m** and *trans-Z*-**2m** show poor agreement with the experiment. It should be noted that the theoretical CN stretching modes (1648 cm^{-1} for both *cis-Z*-**2m** and *trans-Z*-**2m**) are blue-shifted with respect to the corresponding IRMPD bands at 1673 cm^{-1} in a similar fashion as already observed for [**2o**+H]$^+$. These results confirm the spectroscopic assignment of the relative configuration of the major diastereoisomer as *trans*-**2g/m**, opposite to products **2hj**.

2.5 Mechanistic Insight through DFT Calculations

Once having unambiguously assigned the relative configuration of the final products and having studied the dependence of the reaction outcomes on the HIA structure, we focused on the postulation of a reaction mechanism on the basis of DFT calculations, which could also rationalize the diastereoselectivity observed. The proposed reaction mechanism follows the one presented by Tang and Paton[28] and is illustrated qualitatively in Figure **2.5**. The blue line corresponds to the T_1 triplet potential energy surface (PES). The red ones are for singlet states.

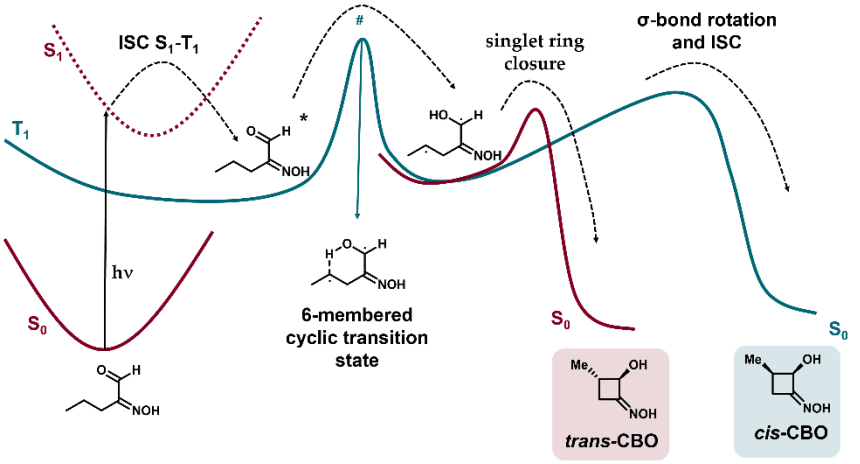

Figure 2.5 Simplified scheme illustrating the proposed reaction mechanism for the HIA model compound **1p**. The potential energy curves in blue and red are a representation of the reaction pathway for the triplet and singlet states, respectively.

Model compound **1p** was chosen as representative for HIAs with R^2 = H to simplify DFT calculations. The initial photoexcitation brings the molecule to the S_1 state.[60] This state in compounds like **1p** and **1j** absorbs at 310 nm (~ 4 eV above S_0) and is dominated by a $^1(n, \pi^*)$ excitation. The second excited state S_2, dominated by a $^1(\pi, \pi^*)$ excitation, is located at 5.4−5.5 eV above S_0 (~230 nm). Hence, the only state that can be pumped by the LED irradiation is S_1. While we cannot completely exclude that the $^1(\pi, \pi^*)$ state could play a role, we verified that, at least in the very first stage of the mechanism, its energy remains around 2 eV above that of S_1, therefore, in the following, we assume that it does not partake in the reaction. An ISC to the T_1 triplet state $^3(n, \pi^*)$ follows. We note that this nonradiative S_1 ⇝ T_1 transition is a nonefficient process activated by vibronic couplings.[61] The triplet PES has a first minimum where the molecule is in the carbonylic form. The latter undergoes unimolecular H-abstraction to form a 1,4-diradical hydroxyl. This step is hindered by an activation barrier of around 20 kcal/mol and the transition state is characterized by a cyclic

six-membered ring. As also noted in Paton's and Tang's work, in the diradical hydroxyl intermediate, the distance between the two unpaired electron sites is large enough for the two spin arrangements, triplet (↑↑) and singlet (↑↓) to have essentially the same energy. The final step in the reaction path consists of a ring closure in the singlet state due to the pairing of the two radical sites. The ring closure brings the two radical sites into the final cyclic products. The ring closure does not seem to be characterized by a downhill energetic path toward the final products. We have found that this step is hindered by a barrier. The different stereochemistry is essentially due to the relative position of the OH group before closure.

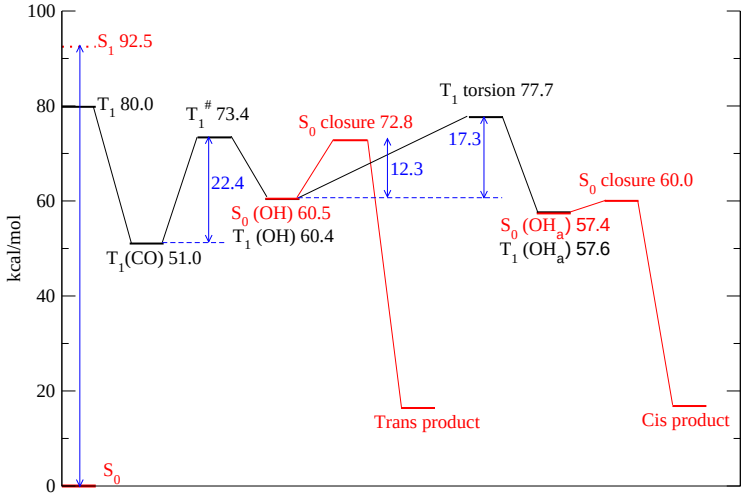

Figure 2.6 Energetic profile of the reaction of HIA model compound **1p**. The triplet stationary points are drawn in black and the singlet ones in red. The numbers represent the energy differences with the ground state S_0 in its minimum geometry and are expressed in kcal/mol.

The quantitative version of the above scheme for the model compound HIA **1p** is shown in Figure **2.6**. The reactive process starts on the left where the photoabsorption brings the reactant to

the S_1 state (located approximately 90 kcal/mol above the ground state). The vertical energy of the corresponding triplet is 80 kcal/mol. These numbers are compatible with those previously reported. The minimal structure of the triplet state in its carbonylic form, T_1(CO), is located 51.0 kcal/mol above S_0 and is reported in Figure **2.7a**.

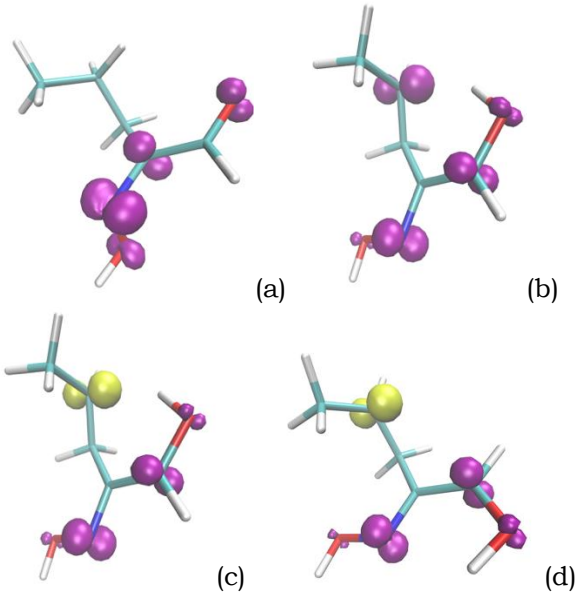

Figure 2.7 Relevant minimum energy structures along the reaction of compound HIA **1p**. The purple/yellow iso-surface represents the spin density. (a) Carbonylic triplet **T_1(CO)**; (b) hydroxyl diradical triplet **T_1(OH)**; (c) hydroxyl diradical singlet **S_0(OH)**; (d) hydroxyl radical singlet **$S_0(OH_\alpha)$.**

Its structure is characterized by a noncoplanar geometry of the oxime group with respect to the carbonyl with the unpaired spins residing mainly on the C=N bond and only slightly on the two oxygen atoms (purple isosurface in Figure **2.7**). The triplet can undergo unimolecular H-abstraction to form the hydroxyl structure. The barrier ($T_1^{\#}$) to the reactive process is 22.4 kcal/mol and leads to the hydroxyl diradical intermediate T_1(OH). The latter

structure is shown in Figure **2.7b**. The oxime group, in this structure, is coplanar with the hydroxyl and the unpaired spins are mainly delocalized over the carbon and nitrogen. This minimum is less stable than T_1(CO) by about 9 kcal/mol. In the diradical, owing to the localization and the distance of the unpaired spin, the energy of the triplet state is almost degenerate with the singlet (ΔE = 0.01 kcal/mol). The local minimum geometry of the singlet S_0(OH) is also very similar to that of T_1(OH) and is reported in Figure **2.7c**. At this point, the S_0(OH) molecule can undergo a ring closure and transform into the final product CBO **2p** with a *trans* ring closure. By tracing a minimum energy path of the closure, we estimated a barrier of around 12-13 kcal/mol. Some of the sampled geometries along the path are shown in Figure **2.8a**.

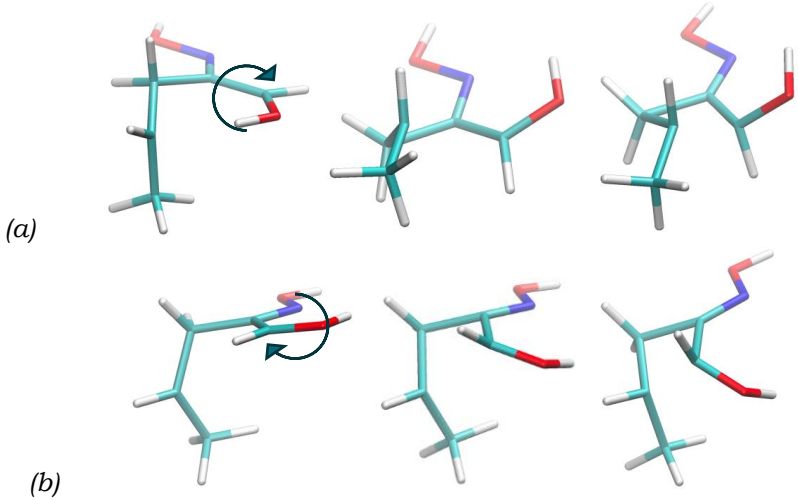

Figure 2.8 (a) Snapshots of the closing path for compound HIA **1p**. from **S_0(OH)** to the trans product. (b) Same for the path from **$S_0(OH_\alpha)$** to the cis product.

If the conversion from the triplet T_1(OH) to the singlet S_0(OH) is not fast, the former can undergo a rotation around the C-CHOH bond

to produce the conformer $T_1(OH\alpha)$ and its corresponding singlet state $S_0(OH\alpha)$ whose structure is reported in Figure **2.8b**. The transformation of $T_1(OH)$ into $T_1(OH\alpha)$ is hindered by a considerable rotational barrier of 17.3 kcal/mol. The ring closure from $S_0(OH\alpha)$ requires only 2-3 kcal/mol and leads to the *cis* product through the path illustrated in Figure **2.8b**.

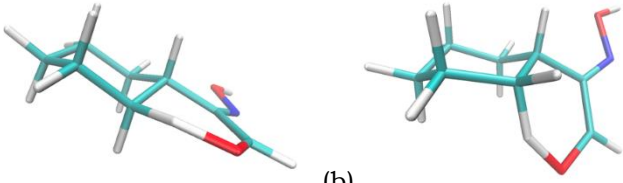

(a) (b)

Figure 2.9 Transition state structures for **1j** illustrating the two ways in which the H-abstraction can take place: (a) equatorial; (b) axial.

The data pertaining to compound HIA **1j** are presented in an analogous fashion in Figure **2.10**, where we see that the general reactive scheme closely follows the one illustrated for HIA **1p**. The H-abstraction in $T_1(CO)$ can take place either toward the equatorial or axial position of the target CH_2 and we have localized either transition states.

The equatorial abstraction (Figure **2.9a**) produces a conformation that invariably leads to a *trans* ring closure. The axial abstraction (Figure **2.9b**) leads to the observed *cis* final product. The barrier of axial H-abstraction is 23 kcal/mol, similar to the one found for HIA **1j**, while that of the equatorial is higher (28.3 kcal/mol). Thus, in Figure **2.10**, for clarity, we have reported only the lowest energy transition state that is also the one that leads to the observed final products. Once $T_1(OH)$ is formed, the molecules can undergo the same processes we have illustrated for HIA **1p**.

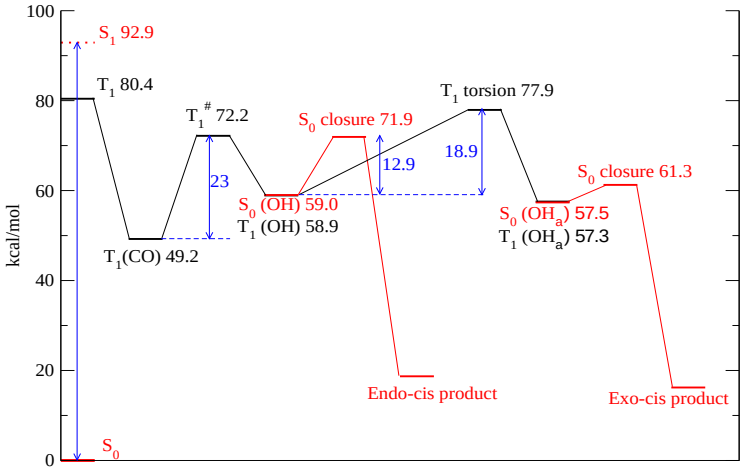

Figure 2.10 Energetic profile of the reaction of compound **1j**. The triplet stationary points are drawn in black and the singlet ones in red. The numbers represent the energy differences with the ground state S_0 in its minimum geometry and are expressed in kcal/mol.

The ring closure either produces the *endo-cis* or *exo-cis* stereochemistry depending on the position of the OH group in the initial singlet state before the formation of the C-C bond. The closure initiated in the S_0(OH) geometry leads to the observed *endo-cis* product, while a closure initiated in the S_0(OHα) leads to the *exo-cis* product (see Figure **2.11**).

The S_0(OH) and S_0(OHα) interconvert through a torsion around the C-CHOH bond that is hindered by an energetic barrier of almost 19 kcal/mol. It is evident from the data presented in Figures **2.6** and **2.10** that the possibility for the T_1 state to evolve towards particular stereochemistry is due to the competition between the rotational barrier and the closure one. If the rotational barrier is much lower than the latter, the reaction will not be fully stereoselective and both closure processes are possible. The outcome, in this case, is more likely to be determined by the

relative height of the two barriers along the closure barriers in the diradical singlet states S_0(OH) and S_0(OHα).

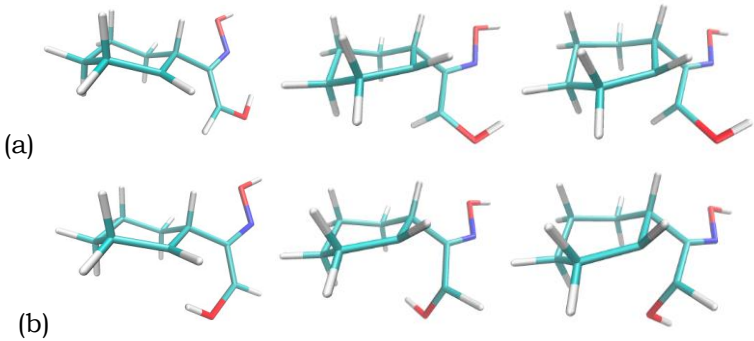

Figure 2.11 Closure paths for **1j**: (a) from **S_0(OH)** leading to the endo-cis product; (b) from **S_0(OHα)** leading to the *exo-cis* product.

Otherwise, if the rotational barrier is higher than that of the closure ones, the final product can only be the one arising from the T_1(OH) geometry because the two conformers T_1(OH) and T_1(OHα) cannot interconvert rapidly enough. In both molecules analysed here, the energy barrier to the torsional motion in T_1(OH) turns out to be higher than the one for the singlet ring closure, thereby preventing the T_1 state to access the T_1(OHα) conformer. In both **1j** and **1p**, we should therefore expect an almost complete stereoselectivity.[28] This is consistent with our experimental results for compound **1j**, which forms exclusively the *endo-cis* product. In contrast, when testing HIAs with R^2 = H, to which **1p** is the model compound, no ring closure stereoselectivity is observed. This effect may be ascribed to differences in the solvent coordination of **1j** and **1p** biradicals, which are not taken into account by the *in vacuo* calculations and are impossible to include even with continuum (implicit) solvent models. Coordination of the less sterically demanding **1p** biradical may lower its torsional barrier, resulting in decreased stereoselectivity. As mentioned in the introduction, in addition to the diastereoselectivity of the

Norrish-Yang ring closure, it is important to consider the possibility for the hydroxyl diradical (OH) to undergo Norrish II fragmentation. In a Norrish-type II reaction pattern, not only must the two radical carbon centres be in a *transoid* conformation,[47,49] but also the C_2-C_3 σ bond must be parallel to the *p* radical orbitals, to ensure both bond cleavage and the formation of the double bond in the resulting fragments. In our system, stereoelectronic and steric features, due to the presence of the oxime group, might prevent the correct parallel alignment in the *transoid* conformation. In fact, in the DFT calculations the energies of the singlet states of the hydroxyl diradical (OH) have been computed and the optimal geometries at the nearest local minima were determined, which turn out to be in a *cisoid* conformation (Figure **2.7c**), thus favouring the Norrish-Yang cyclization pathway over fragmentation.

2.6 Solvent-Dependent *E*/*Z* Isomerization of the Oxime Double Bond

Finally, our attention was drawn to the *E*/*Z* isomerism of the oxime group. All substrates exhibit > 95% *E* configuration prior to photoisomerization, regardless of the solvent, whereas different *E*/*Z* ratios (ranging from 99:1 to 1.4:1) in the CBO products are initially obtained in a solvent dependent manner. This matter is thereby described specifically with substrate **1j**. The corresponding CBO **2j** is initially obtained in DMSO-d_6 as a single diastereomer.
However, to our surprise, a second set of **2j** CBO signals appeared over time upon standing in DMSO-d_6 and in the dark at the expense of those of the original diastereomer, reaching a final ratio of 5:1 within 72 h after irradiation (see chapter **5** for the final ^{1}H-NMR spectrum).
For clarity, Figure **2.12** shows the evolution over time of the cyclobutane H_2 signal. It should be noted that both isomers exhibit the *cis* ring closure. In MeOH-d_4, instead, the same two sets of

signals appear already during the photoreaction in a 2.5:1 ratio. This ratio remained unchanged for several days upon storage in MeOH-d_4. The outcome in MeCN-d_3 and acetone-d_6 was the same as in methanol, i.e., the initial isomer ratio did not change over time. However, when MeOH-d_4 was removed and the samples were redissolved in DMSO-d_6, the NMR signals changed over time to finally reach the same 5:1 ratio as in the sample obtained directly in DMSO-d_6.

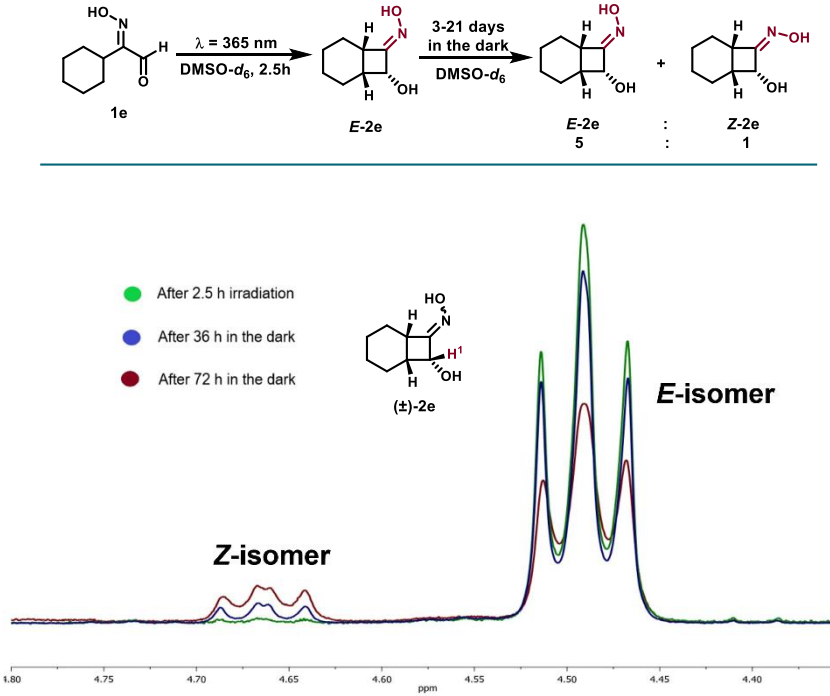

Figure 2.12 Expansion of ^{1}H-NMR spectra of **2j** (see Chapter **5**) at different times of storing in the dark at room temperature after the photoisomerization depicting diagnostic peaks of H^2 as example.

We ascribe the new set of CBO signals to DMSO-assisted *E*/*Z* isomerization of the oxime C=N bond. In fact, DMSO-assisted

double bond configurational isomerizations have been reported for α-oxo-oximes,[62] hydrazones,[63] and azolylmethylidene 2-indanone derivatives.[64] In all cases, the isomerizations were ascribed to the H-bonding between DMSO and the C=N−OH of the isomerizing double bond, with no need for photoactivation or acid catalysis. Specifically, noncatalyzed oxime isomerization can occur by rotation of the substituents around the C=N bond through a polar transition state, sensitive to solvent polarity.[65] Strong H-bonding between the labile oxime O-H hydroxyl group and DMSO, combined with the bulk of the two alkyl substituents on the already tense four-membered ring structure in products **2j**, could affect the C=N character, thus assisting the *E*/*Z* isomerization (Scheme **2.4**).

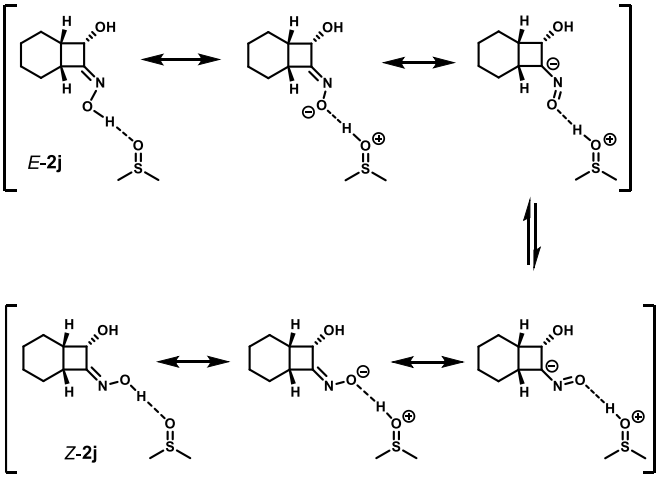

Scheme 2.4 Suggested mechanism of E/Z isomerization of CBO **2e**.

The same solvent-promoted *E*/*Z* CBO isomerization is observed in **2g-i** (Scheme **2.1**), whereas O-functionalized HIAs do not exhibit this behaviour, thus proving the crucial role of the oxime-OH group in this isomerization. Hence, to explore the role of the interaction between the oxime OH and DMSO or methanol, we

relied on molecular dynamics calculations. Molecular dynamics simulations were performed via the GROMACS (v. 2021.2) software package[66] on the major diastereomer (*cis-endo*) of free oxime **2j** and **2n**, the corresponding oxime methyl ether. Details about simulations can be found in Chapter **5**. In Figure **2.13**, radial distribution functions (RDFs) of DMSO and MeOH oxygen with respect to the oxime oxygen are shown to highlight the solvent-oxime interaction. An analogous curve is reported for reference in Figure **5.10** for **2j** and DCM, representative of a nonhydrogen bonding solvent. Interestingly, the curves of weakly interacting systems (*i.e.*, **2n**-DMSO and **2j**-DCM) exhibit similar features. On the other hand, the **2j**-DMSO and **2j**-MeOH (Figure **2.13a** and **2.13b**, respectively) curves exhibit a peak at r = 0.34 nm, which is absent in Figure **5.10**, thus pointing at a strong oxime-solvent interaction in both configurational isomers of **2j**. However, the peak of (*E*)-**2j**-DMSO is higher than that of (*Z*)-**2j**-DMSO, whereas no such difference is present with MeOH. Furthermore, the interactions of the CBO alcoholic oxygen with DMSO of both isomers are very similar to that of the oxime OH in (*Z*)-**2j** (Figure **5.11**). In other words, whereas the *Z*-oxime interacts similarly with both solvents, DMSO forms a stronger hydrogen bonding with the (*E*)-**2j** oxime, thus weakening the CNO-H bond and promoting *E*/*Z* C=NOH isomerization.

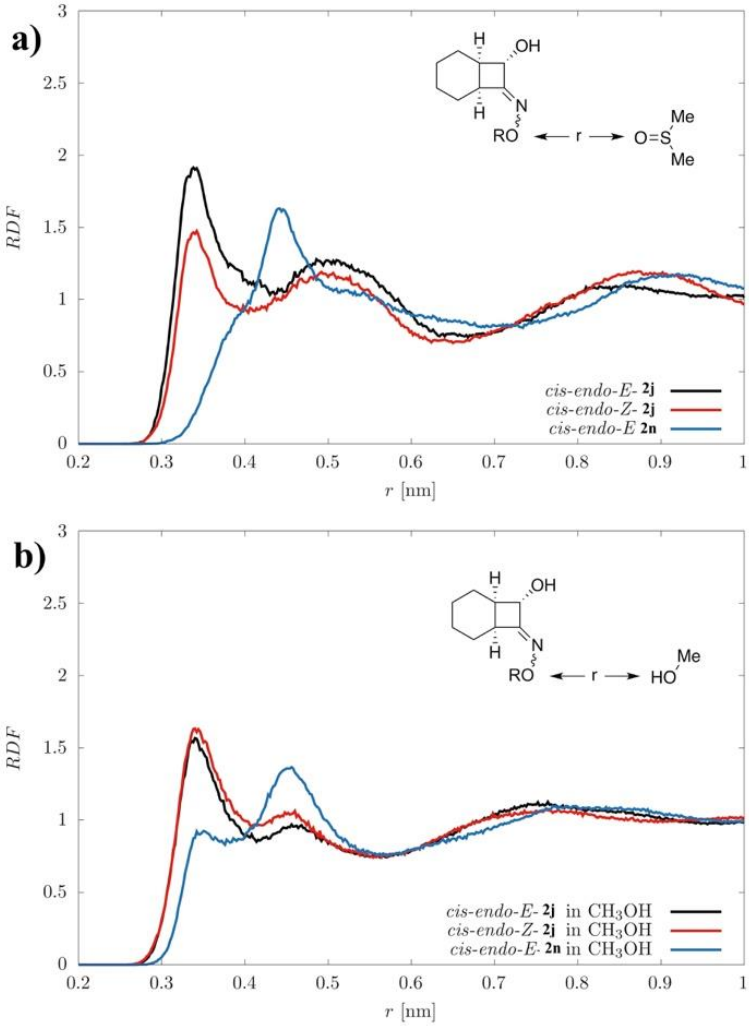

Figure 2.13 Radial distribution functions related to the interaction between CBO oxime oxygen and DMSO (a) and oxygen and MeOH (b), R = H (**2j**) e R = CH_3 (**2n**).

3. HIAs complexes with metal ions[40]

3.1 Complexes of Electron-Poor Oximes

Oximes and their derivatives have been extensively used as ligands for a variety of transition metal ions.[32–36] In recent years, studies focused especially on oximes having electron withdrawing groups (EWGs) in the α position, mainly α-cyanoximes. The presence of the -CN group makes these molecules more acidic than simple oximes, lowering their pK_a up to 7 orders of magnitude.
For protonated oximes the typical coordination site is the nitrogen (=*N*OH), while the conjugated anion, in the cases when it is stable, can form mixed oxime/oximate complexes. The metal N-coordination, indeed, can increase the acidity of =NOH group, such as in the case of 2-pyridineoximes (pK_a decreases from 10-11 to 3-5) and aldoxime (pK_a decreases from 12 to 10). X-ray crystallography of a variety of complexes formed by different α-cyanoximes with several metal ions shows multiple possible coordination geometries (Figure **3.1**).

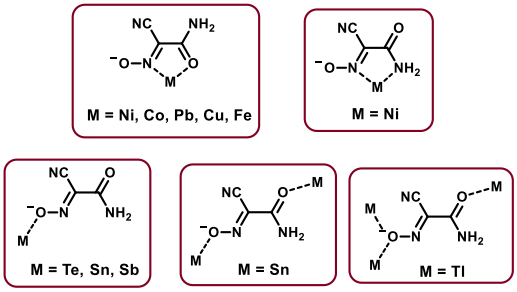

Figure 3.1 Geometries of α-cyanoximes complexes with different metals characterised by X-ray chrystallography.

Given the versatility of α-cyanoximes to complex a number of metal ions with different coordinations, they can be potentially employed in inorganic chemistry for the quantitative determination of metals in solution (for example Co(II) and Fe(II)), or in medicine, bound to Pt(II) or Pd(II), as alternatives to cisplatin, a very effective anticancer drug, but with many side effects.[67–69]
The presence of the electron withdrawing CHO group endows some similarity to α-cyanoximes. HIAs are, indeed, more acidic than the respective unsubstituted oximes (pK_a 7.7-9.9) thanks to the delocalization of the negative charge in the conjugate base; HIAs have two electrophilic (CHO and C=NOH) and two nucleophilic sites (nitrogen and oxygen atoms) analogously to α-cyanoximes (electrophilic sites: CN and C=NOH; nucleophilic sites: O and N). Based on these resemblances, similar behaviour to complex metal ions can be imagined also for HIAs.

3.2 Discovery of Cu(II)-HIA complexes and early experiments

Studies for the design of stimuli responsive functional molecules containing the HIA group, i.e. structures designed to serve specific tasks, were ongoing in my group in view of exploring their potential as UV-responsive moieties in lipophilic or water-soluble molecules, liposomes and macrocycles. The idea was to synthesis composite compounds containing the 2-(hydroxyimino)aldehyde functionality, resorting to the simple copper-catalysed azide-alkyne 1,4-Huisgen cycloaddition (CuAAC). To attain the goal, we carried out CuAAC reaction between two HIA-functionalized terminal alkynes and several azides having alkyl, oligo(ethylene glycol), benzyl and PEGylated phospholipid residues (Scheme **3.1**).

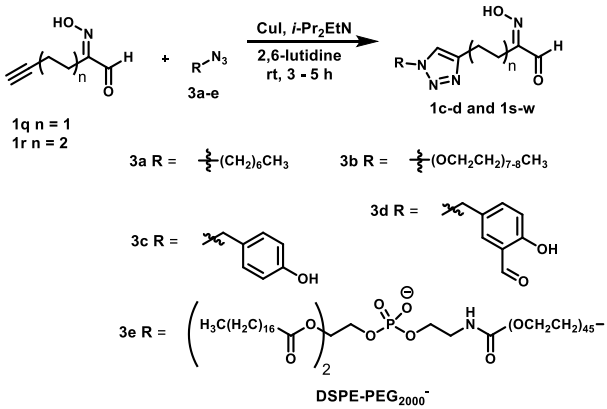

Scheme 3.1 Synthesis of 1,2,3-triazole-containing HIAs

The two HIA-alkynes **1q** and **1r** only differ by the length of the carbon chain separating the two functional groups. To link **1r** and **1q** to molecules of different nature we, then, utilized CuAAC with Cu(I) and no reductant in a degassed environment. The click reaction worked smoothly in 3–5 h on all azides **3a-e** and no significant differences are observed between alkyne **1q** and **1r** (Scheme **3.1**).

We thereby conclude that even though the neighbouring HIA may potentially interact with cuprous ions, it does not interfere with the CuAAC reaction in the above conditions. We also tested the popular Cu(II)/ reductant catalysed CuAAC on azide **3a** and 5-hexyn-1-ol and we compared its outcome in the presence of a stoichiometric amount of 2-(hydroxyimino)-3-octyltridecanal **1f**, a simple model HIA with no other substituents.[31] This way, we were able to check if the HIA group inhibits the Cu(II)/reductant catalytic system. The reaction was carried out in DMSO to ensure full solubility of **1f**. The reaction was slower compared to the click reactions in Scheme **3.1** even in the absence of **1f**. After 48 h, 70% yield of the triazole product was obtained, whereas the yield dropped to 15% when Cu(II) was added to the **1f**-containing mixture (Scheme **3.2**). A somewhat better outcome (30% yield)

resulted from adding pre-mixed copper-ascorbic acid to the reaction mixture, thus reducing Cu(II) prior to coming into contact with the HIA.

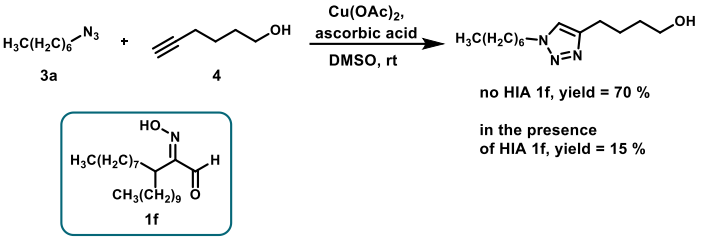

Scheme 3.2 CuAAC reaction in the presence and absence of **1f** in the reaction mixture.

To gain some insight into the interaction between HIA and copper ions, we looked into the effect of Cu(I) and Cu(II) addition to the UV-Vis spectrum of **1f** (Figure **3.2a** and **3.2b**). We do not observe any effect of **1f** on the UV-Vis spectrum up to 1:3 CuI/**1f** in acetonitrile (Figure **3.2a**).

In contrast, upon addition of $Cu(OAc)_2$ to **1f** (Figure **3.2b**), the appearance of a new band at λ = 432 nm and a broad absorption around 620 nm were observed, along with the suppression of the typical Cu(II) band at λ = 670 nm. The absorbance at 432 nm increased with the amounts of cupric ions added to solution (Figure **3.2b**, inset), thus suggesting the formation of Cu^{2+}-HIA complex. Moreover, chromatographically purified HIA **1t** were of a glow green colour and its absorption UV-vis spectrum showed an unexpected broad band extending just over 400 nm and no free Cu(II) band (λ = 600-700 nm).

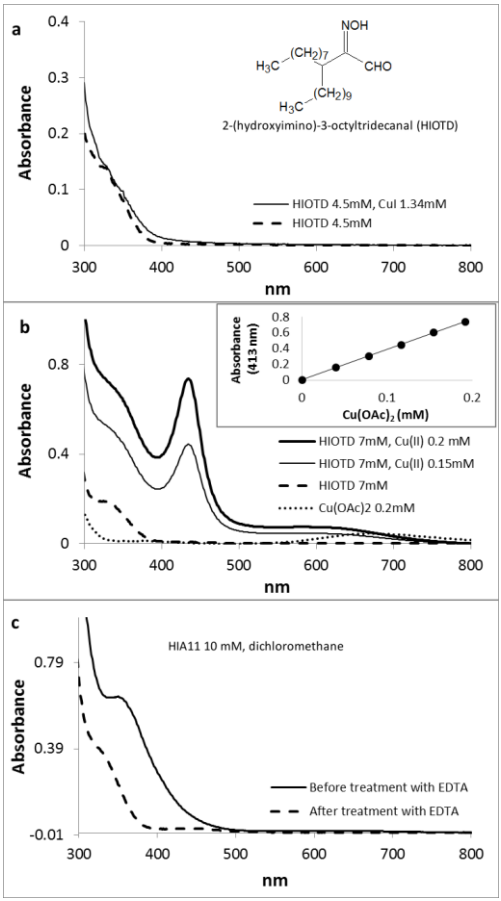

Figure 3.2 . UV-Vis spectra of (a) the model HIA **1f** in acetonitrile before and after addition of CuI; (b) **1f** in acetonitrile with increasing concentrations of $Cu(OAc)_2$; (c) **1t** in dichloromethane before and after treatment with EDTA for Cu^{2+} removal. Inset in (b) shows a linear increase of absorbance at λ = 432 nm as $[Cu^{2+}]$ is increased (ε = 3807 $M^{-1}cm^{-1}$).

As a working hypothesis based on the **1f**-Cu(II) spectra in Figure **3.2b**, we surmised that this absorption results from HIA **1t**-Cu(II) interaction and we attempted copper removal through treatment with an EDTA solution at pH 7.6-7.7. We avoided higher pH to limit deprotonation of the HIA moiety (pK_a of HIAs range 7.8-9),

which may lead to HIA decomposition.[31] The aqueous EDTA extracts exhibited a pale blue colour confirming extraction of Cu(II) (Chapter **5**), while the HIA **1t** spectrum shows the characteristic wavelength of the HIA n-π* transition, around 320 nm (Figure **3.2c**).[31] These results suggest HIA ligation of Cu(II) and the observed inhibition of the Cu(II)/ascorbic acid CuAAC by **1f** can, therefore, be rationalized in terms of selective ligation of Cu(II) by the HIA group.
This serendipitous discovery hinted to the possibility to develop a new family of HIA-containing ligands specific to the Cu^{II} ion, with possible application in ion recognition and selective ligation in solution.

3.3 Cu(II) complexation by HIAs

In order to confirm the formation of the HIA-Cu(II) complex and to determine its stoichiometry, UV-vis spectroscopy studies were performed on different HIAs in the presence of copper ions.
Initially, aliquots of a 4.6 mM solution of $Cu(OAc)_2$ were added to a 7.0 mM solution of HIA **1f** in acetonitrile and an absorption spectrum was recorded after each addition (Figure **3.3**). After the introduction of the copper salt, it was observed a new absorption band centred at λ = 432 nm, absent in the spectra of both **1f** and copper acetate, while the broad band at 670 nm, characteristic of the cupric ion, was not present in the spectrum. The absence of this absorption, combined with the increase in intensity of the one at 432 nm for progressive additions of $Cu(OAc)_2$ is a further indication of complex formation between the HIA and Cu(II).

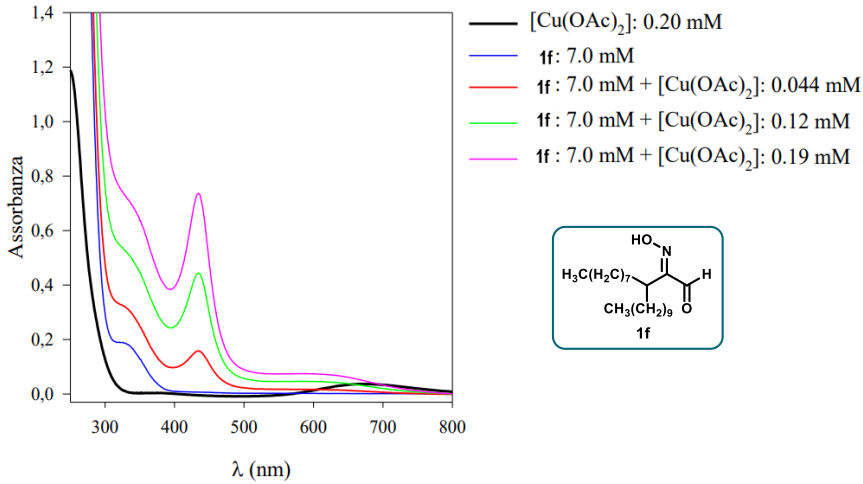

Figure 3.3 Absorption spectra of **1f** in the presence of increasing concentrations of $Cu(OAc)_2$.

3.3.1 Job's plot

Job's method[70–72], also known as continuous variations method, is a technique that allows to determine the stoichiometry of a coordination complex in solution by measuring the absorbance of the complex characteristic peak, while changing the ligand to metal ratio. This is achieved with the portionwise addition of a solution of the metal to an equimolar solution of the ligand, so that the total molarity of the solution stays constant even when the metal/ligand ratio varies. An UV-vis spectrum is recorded after every addition, and the absorbance of the complex is plotted against the ligand molar fraction (x_L). The maximum of the curve thus obtained (the Job's Plot) corresponds to the ratio of ligand to metal in the complex.

For the Job's method to be valid, three criteria have to be met: the complex must respect the Lambert-Beer law, the system total concentration has to remain constant and ionic strength in the solution must be buffered.

The validity of the Lambert-Beer law ($A = \varepsilon \ell c$) for the complex was verified by progressively adding $Cu(OAc)_2$ to a solution of HIA **1f** and by then measuring the absorbance at 432 nm. As shown in Figure **3.4**, the absorbance of the Cu^{2+}-HIA complex grows linearly, thus confirming the validity of the Lambert-Beer law and allowing to calculate the molar absorption coefficient, ε = 3807 $M^{-1}cm^{-1}$.

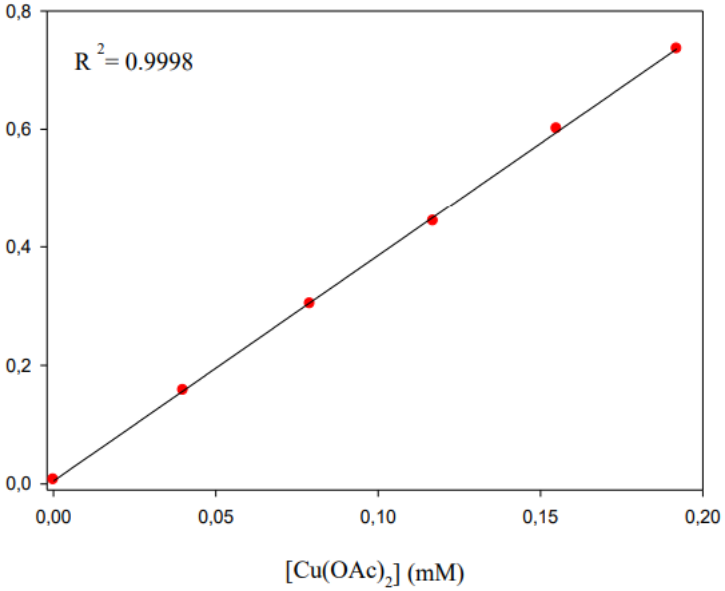

Figure 3.4 Lambert-Beer law validity for the **1f**-$Cu(OAc)_2$ complex.

Solutions with a concentration of 0.2 mM of $Cu(OAc)_2$ and HIA **1f** were prepared and portions of the copper solution were successively added to the solution of the HIA, while recording an UV-vis spectrum after every addition. It should be noted that, in order to keep the ionic strength constant, both the solutions of copper salt and HIA also contained a 15 mM concentration of Bu_4NBF_4. The absorbance at 432 nm was then plotted against the molar fraction of HIA **1f** and the stoichiometry of the complex was

obtained from the intersection of linear regression lines (Figure **3.5**).

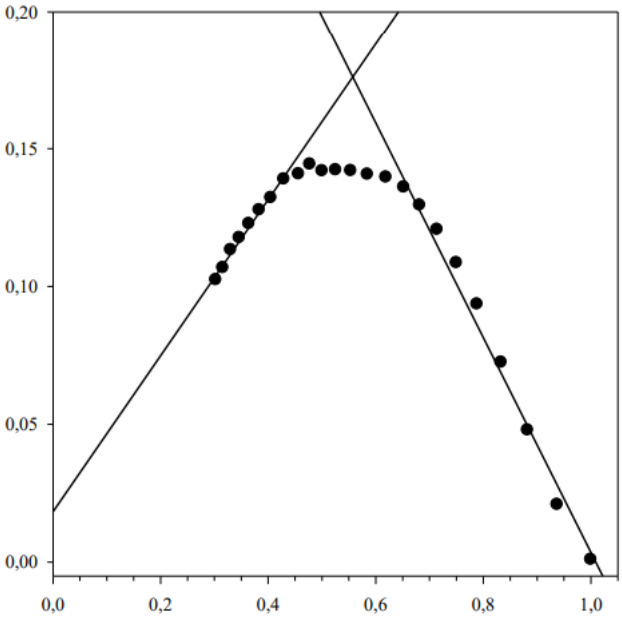

Figure 3.5 Job's plot for the complex **1f**-$Cu(OAc)_2$. On the x axis: molar fraction of **1f**. On the y axis: absorbance at 432 nm.

As it can be seen, the maximum of the curve is a plateau centred at x(**1f**) = 0.55, indicating that the complex has a Cu^{2+}/HIA ratio of circa 1:1, but also that either the formation of the complex is not particularly strong or that the 1:1 complex is the predominant species, along with other geometries/stoichiometries.
The same experiment, repeated with a higher total concentration, could have furnished a sharper maximum of the curve but precipitation of a green solid was observed. This is likely due to the presence of the long alkyl chains on the ligand that limit its solubility, and consequently the complex solubility, in a relatively polar solvent such as acetonitrile.

In order to avoid as much as possible solubility issues, while still having a ligand with no coordinating groups other than HIA, the following experiments were performed on compound **1h**. The characteristic absorption band of the complex formed by this HIA and Cu(II) is centred at λ = 422 nm and its intensity varies linearly with the concentration, thus obeying the Lambert-Beer law with a calculated ε = 914 $M^{-1}cm^{-1}$. It was then possible to follow the intensity of this peak and applying the continuous variations method (*vide supra*), this time with a total concentration in cuvette of 1.4 mM. The Job's plot of this complex (Figure **3.6**) shows a sharp maximum at *x*(**1h**) = 0.53, further confirming the 1:1 composition of the Cu(II)-HIA complex.

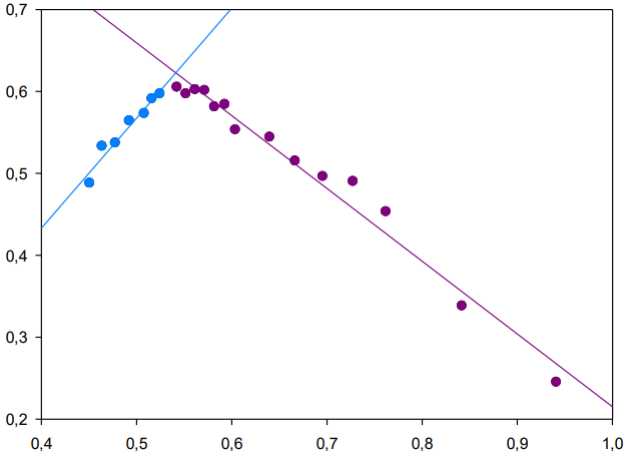

Figure 3.6 Job's plot for the complex **1h**-$Cu(OAc)_2$. On the x axis: molar fraction of **1h**. On the y axis: absorbance at 422 nm.

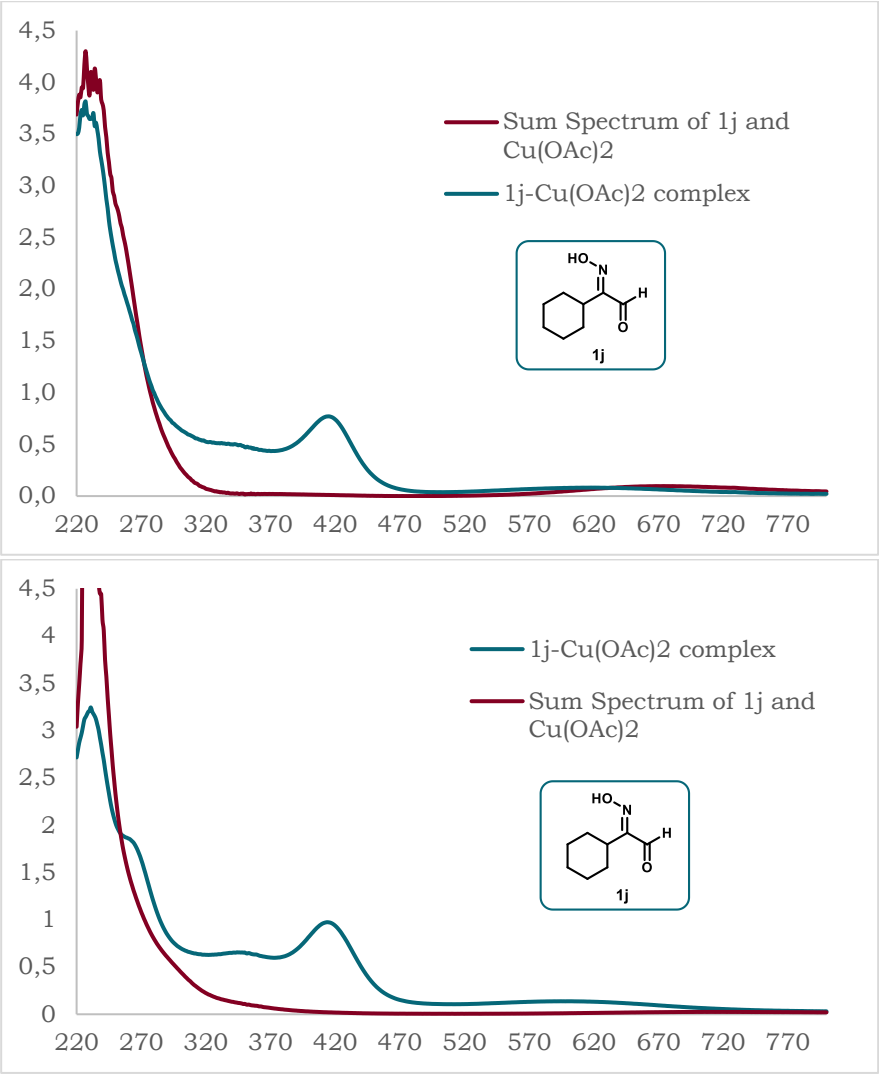

Figure 3.7 Spectra of **1j** and $Cu(OAc)_2$ before and after mixing. Top: spectra in MeCN; bottom: spectra in MeOH.

Similar results were obtained by using **1j** as ligand, both in MeCN and in MeOH, and the formation of a complex was observed by

recording the spectrum of two equimolar solutions of $Cu(OAc)_2$ and **1j** in the two separate compartments of a cuvette with a central septum. In this way it is possible to record the *sum spectrum* before mixing the solutions and to then observe any difference in the spectrum of the mixed species. In case no interaction occurs, the spectra before and after mixing will be identical, otherwise different absorptions will be present. It is worth noting that the absolute value of the absorbance will remain the same because at the beginning the solutions have a given concentration, but occupy just half the volume of the cuvette, therefore the effective optical path length the beam travels in each solution is half of the total optical path length. Upon mixing, the two species will have a total concentration that is half of the original one, but the effective optical path length will be doubled, thus maintaining the same total absorbance.

Similarly to the other HIAs tested, the UV-Vis spectrum of a 1:1 mixture of **1j** and $Cu(OAc)_2$ showed the appearance of the characteristic peak of the complex, this time centred at λ = 414 nm (Figure **3.7**).

In order to observe the influence of the oxime acidic proton on the complexation behaviour of HIAs, we resorted to compound **1n**, which is methylated on the oxygen atom and was already employed as a substrate in the Norrish-Yang cyclization (see Chapter **2**). In this case, the spectra recorded before and after mixing the solutions of **1n** and $Cu(OAc)_2$ are completely superimposable (see Chapter **5** for the full spectra), highlighting the complete lack of interaction between these two species. This result demonstrates that the presence of the free oxime group is necessary to ensure complex formation. Being Cu(II) a Lewis acid, it may contribute to lower the pK_a of the oxime and allow deprotonation even by the acetate anion. Another possible explanation is the formation of a mixed oxime/oximate complex with copper ions acting as bridging units. Further studies are still ongoing to better understand the geometry of the complex and the precise role of the oxime group.

3.4 Cu(II)-HIA Complex in the Norrish-Yang Reaction

In order to explore the feasibility of the Norrish-Yang reaction in the presence of metals, the complex formed by HIA **1h** and $Cu(OAc)_2$ was submitted to the photoexcitation conditions (see Chapter **2**).

This approach was faced with some criticalities: at concentrations above 1-2 mM the complex already tends to precipitate from the MeCN solution, compared with the concentration used for the photocyclization reaction, which is usually two orders of magnitude higher, around 0.1-0.2 M; at the concentrations used to study the complex, the NMR peaks of the HIA and CBO already barely emerge from the background noise, and, being Cu(II) a paramagnetic ion, contributes to further enlarge the peaks, rendering impossible to follow the reaction through NMR spectroscopy. Consequentially, UV-vis spectroscopy was chosen to monitor the progress of the reaction.

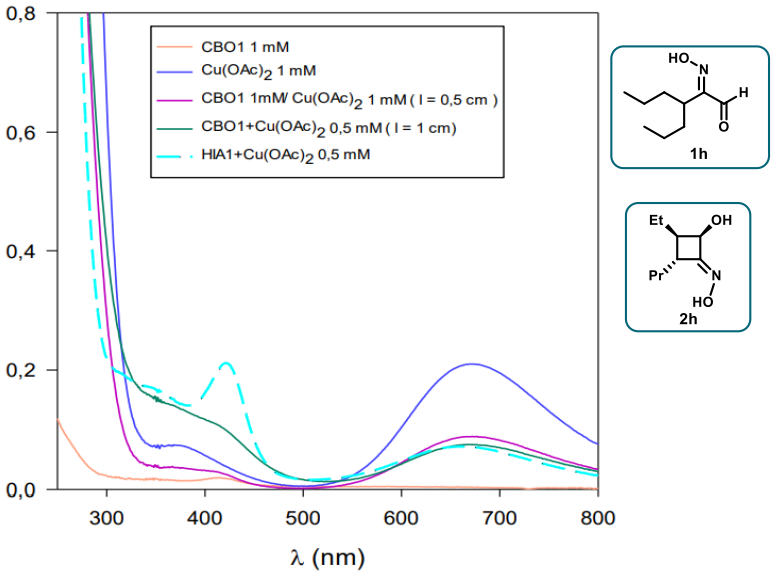

Figure 3.8 Comparison of the spectra of: CBO **2h** (orange); $Cu(OAc)_2$ (blue); sum spectrum of **2h** and $Cu(OAc)_2$ (purple); **2h**-$Cu(OAc)_2$ (green); **1h**-$Cu(OAc)_2$ complex (teal dashed).

Initially, CBO **2h** was synthesised in MeOH-d_4 with the methodology described in Chapter **2**. In this way it was possible to record the UV-vis spectrum of **2h** in the presence and absence of $Cu(OAc)_2$ using MeCN as a solvent. Even though for **2h** the formation of the complex with copper is not as evident as for HIAs, there are still notable differences between the sum spectrum and the spectrum after mixing, especially the appearance of a shoulder peak at around 415 nm (Figure **3.8**).

Once assessed the interaction between **2h** and $Cu(OAc)_2$, it was possible to verify the influence of Cu(II) on the outcome of the Norrish-Yang reaction. A 0.5 mM solution of $Cu(OAc)_2$-**1h** complex was thus prepared in MeCN in a quartz cuvette, photoexcitated at λ = 365 nm, and UV-vis spectra were recorded at regular intervals, until the spectrum assumes a profile analogous to the $Cu(OAc)_2$-**2h**.

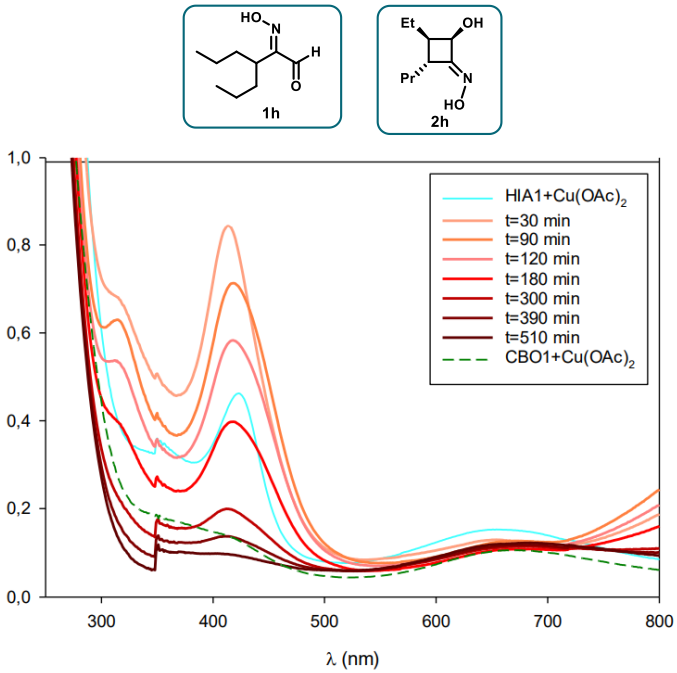

Figure 3.9 Spectra recorded during the photoexcitation of the **1h**-$Cu(OAc)_2$ complex (brown, orange and red lines). For comparison the spectra of **1h**-$Cu(OAc)_2$ (teal) and that of **2h**-$Cu(OAc)_2$ (green dashed) are also shown.

In Figure **3.9** are reported the spectrum of the initial solution of the $Cu(OAc)_2$-**1h** complex, the spectra recorded during the photostimulation at 365 nm, and the one of the $Cu(OAc)_2$-**2h** solution used as a comparison. During the first two hours of reaction, it is possible to observe a hyperchromic effect together with an ipsochromic shift, bringing the maximum of the curve at λ = 413 nm, and the appearance of a new peak at 315 nm. As the reaction progresses, the absorbance at 422 nm and 315 nm progressively diminish in intensity and the spectrum profile gets more and more similar to that of $Cu(OAc)_2$-**2h** mixture. This trend would suggest the formation of CBO **2h**, albeit much slower (8.5 h *vs* 0.5 h) than the photocyclization of **1h** by itself. Anyway, other

studies are necessary to understand the photochemical behaviour observed during the photostimolation at 365 nm. Further research is ongoing to accomplish a scale-up Norrish-Yang of several HIAs in the presence of cupric ions to isolate and characterize all products. It is also envisaged to investigate the possibility to perform the photocyclization with visible light, that is at the wavelength of the HIA-Cu^{2+} complex absorption band.

4. Enantioselective γ-perfluoroalkylation of Enals

4.1 Electron Donor-Acceptors (EDA) complexes

In 2013, during the development of new organo-photoredox methodologies, Melchiorre and co-workers noticed that, upon mixing catalytic amount of enamine and benzyl bromide, both colourless reagents, the resulting solution appeared yellow. This observation, supported by extensive spectroscopic analysis, was attributed to the formation of an Electron Donor-Acceptor (EDA) complex between the enamine and the benzylic bromide.[73,74]

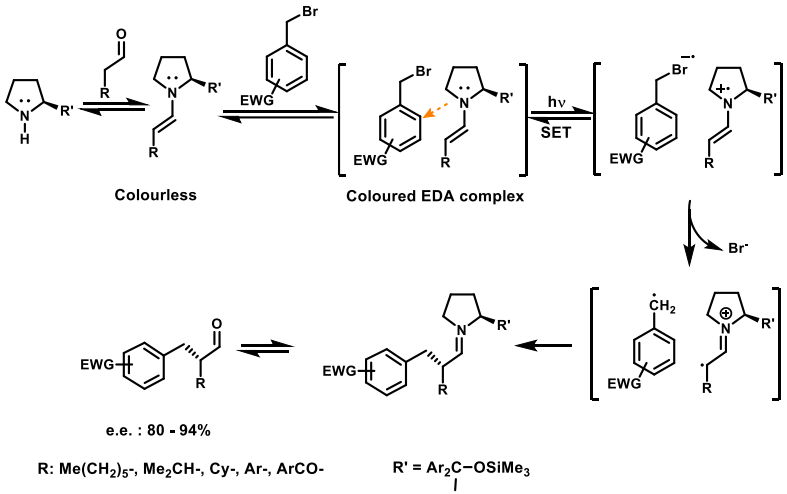

Scheme 4.1 Enantioselective organocatalytic alkylation of aldehydes *via* photoexcitation of EDA complex.

The formation of this complex is indicated by the appearance of a large absorption band in the visible range, indicating a charge transfer between the two species. It is therefore possible to selectively excite the EDA complex using visible light (λ = 460 nm) to trigger a Single Electron Transfer (SET) event between the two components of the EDA complex, with formation of a radical ions couple and the subsequent in-cage radical combination (Scheme **4.1**). Thus, the organocatalytic intermediate is involved in radical generation but also acts as a "radical trap" towards the electrophilic radical. This photo-organocatalytic dichotomy offered a powerful approach to develop stereocontrolled radical-based methodologies without any external photocatalyst.

4.2 Synthesis and Relevance of Fluorine-Containing Molecules

The established benefit of fluorine-containing fragments in medicinal chemistry relies on their ability to alter the physicochemical and pharmacokinetic properties of organic compounds.[75–78] In addition, it is acknowledged that increasing C(sp^3) incorporation and the presence of stereogenic centres positively correlate with the clinical success of small molecule therapeutics.[79,80] These aspects explain the importance of developing novel methods for the stereoselective incorporation of trifluoromethyl (CF_3) and perfluoroalkyl (R_F) units within organic molecules. However, only a few strategies are available for the catalytic installation of perfluoroalkyl-containing stereogenic centres.[81–86] For example, the combination of enamine organocatalysis and photoredox catalysis served to develop the enantioselective α-perfluoroalkylation of aldehydes (Scheme **4.2a**).[87] In a different photochemical approach, the asymmetric α-perfluoroalkylation of β-ketoesters was reported under phase transfer catalysis (PTC, Scheme **4.2b**).[88]

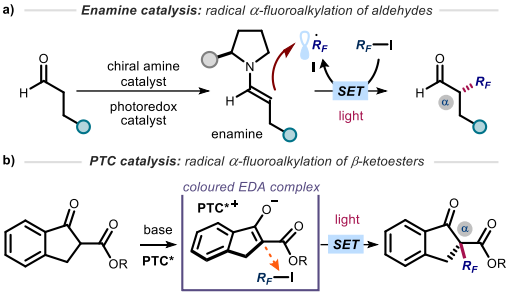

Scheme 4.2 Organocatalytic photochemical strategies for the stereoselective radical α-perfluoroalkylation of (**a**) aldehydes and (**b**) β-ketoesters. PTC: phase transfer catalyst; EDA: electron donor-acceptor; R_F: perfluoroalkyl chain.

Both protocols used visible light to generate perfluoroalkyl radicals (R_F·, **I**) via single electron transfer (SET), which were then intercepted stereoselectively. The photochemical radical generation was mastered either by an external photocatalyst (Scheme **4.2a**) or by excitation of a ground-state electron donor-acceptor (EDA) complex[73] between perfluoroalkyl iodides and a chiral enolate (Scheme **4.2b**). These methods led to the formation of C(sp^3)-CF_3 and C(sp^3)-R_F stereocentres at the α position of carbonyl compounds. In contrast, strategies that account for the stereoselective installation of perfluoroalkyl units at distal positions of the substrates *are not available*. The goal of this work is to close this gap in synthetic methodology by discovering a photochemical method for the asymmetric introduction of CF_3 and R_F groups at the remote γ position of α-branched enals **1** (Scheme **4.3**).

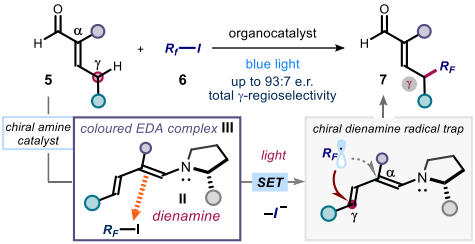

Scheme 4.3 Design plan for the stereocontrolled radical perfluoroalkylation of enals at the γ-carbon via excitation of an EDA complex **III** between a catalytic dienamine **II** and perfluoroalkyl iodides.

4.3 Enantioselective γ-Perfluoroalkylation of Enals

Our plan for the remote perfluoroalkylation relied on the reactivity of chiral dienamines **II**, generated upon activation of α-branched enals **5** with a chiral amine catalyst (Scheme **4.3**). Intermediates **II** are characterized by vinylogous nucleophilicity,[89–92] and have been used for the site-selective functionalization of enals **5** at their remote γ-carbon via traditional two-electron ionic pathways.[93–96] Recently, we demonstrated that the dienamine activation platform could be translated successfully also to radical chemistry.[97,98] The use of an external catalyst secured formation of electrophilic radicals, which were then stereoselectively intercepted by the chiral dienamine at remote position.[98] In the context of C(sp^3)-R_F bond formation, we surmised that the electron-rich nature of **II** could be leveraged to form photoactive EDA complexes upon aggregation with perfluoroalkyl iodides.[88] Visible light excitation of the EDA complex **III** would then drive the formation of perfluoroalkyl radical (R_F·, **I**), thus circumventing the need of an exogenous photocatalyst. Regio- and stereoselective trap would then offer a catalytic strategy for the remote γ-perfluoroalkylation of α-branched enals **5**.

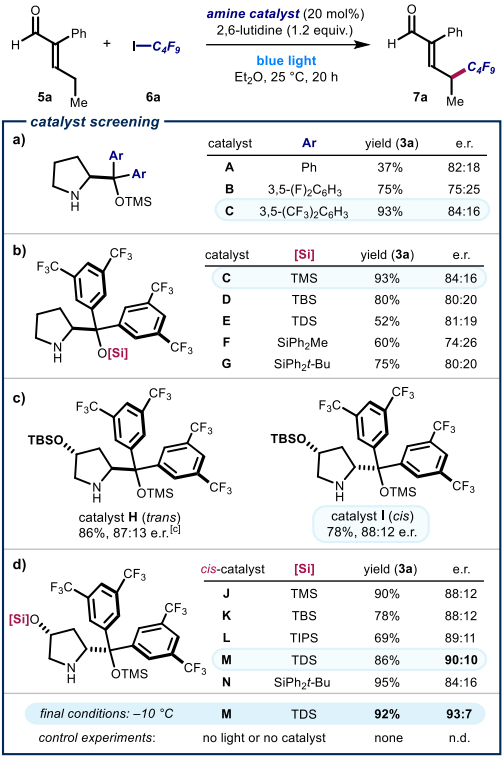

Scheme 4.4 Catalyst optimization. Reactions performed for 20 h in 0.3 mL of Et_2O using 0.2 mmol of **5a**, 0.6 mmol of **6a**, and 0.04 mmol of catalyst (20 mol%) under irradiation by a single high-power LED (λ_{max} = 460 nm, irradiance = 100 mW/cm²). Yield of **7a** determined by ^1H NMR analysis of the crude mixture using trimethyl orthoformate as the internal standard. Enantiomeric ratio (*e.r.*) of **7a** measured by chiral UPC² analysis after derivatization to the corresponding 2,4-dinitrophenyl hydrazone. Note that catalysts **A**–**H** gave product **7a** with an (*R*) absolute configuration; the figure shows the (*S*) major enantiomer of **7a** afforded by catalysts **I**-**M**. TMS: trimethylsilyl; TBS: *tert*-butyldimethylsilyl; TIPS: triisopropylsilyl; TDS: thexyldimethylsilyl.

The feasibility of our plan was evaluated by reacting 2-phenyl-2-pentenal **5a** with nonafluoroiodobutane **6a** in Et_2O using the commercially available TMS-protected diphenyl prolinol catalyst **A** (20 mol%, TMS: trimethylsilyl) and 2,6-lutidine as the additive

(Scheme **4.4a**). We noticed that the reaction mixture turned immediately yellow right after addition of all the reaction components, which individually were colourless (see below for further details). Irradiation by a blue light LED afforded the desired product (*R*)-**7a** with complete γ-regioselectivity and good enantiomeric ratio, albeit in low yield (37% yield, 82:18 *e.r.*). Other solvents, including THF and dichloromethane, were suitable, but diethyl ether proved optimal (Table **4.1**).

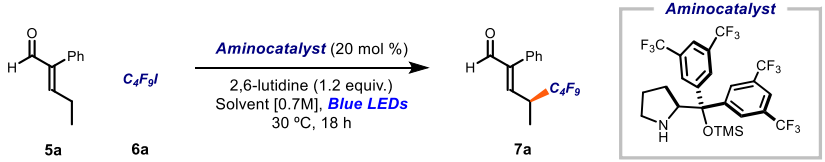

entry	solvent	yield **3a** (%)[a]	*e.r.* **3a** [b]
1	THF	63	83:17
2	Et_2O	96	83:17
3	Toluene	77	84:16
4	DCM	60	83:17
5	DMF	0	/
6[c]	Et_2O	95	83:17
7[d]	Et_2O	0	/
8[e]	Et_2O	0	/

Table 4.1 [a] Reaction performed on a 0.2 mmol scale using 3 equiv. of **5a**. Yield of **7a** determined by ^{1}H-NMR analysis of the crude mixture using trimethyl orthoformate as internal standard. [b] Enantiomeric ratio of **7a** determined by derivatization to the corresponding 2,4-dinitrophenyl hydrazine prior to injection in UPC^2. [c] Reaction time 2.5 hours. [d] Reaction conducted in the absence of aminocatalyst. [e] Reaction conducted in the absence of light.

To improve the stereoselectivity of the remote perfluoroalkylation, we modified the catalyst structure. Introduction of fluorinated aryl motifs (3,5-difluorophenyl and 3,5-bis(trifluoromethyl) substituents) in catalysts **B** and **C** improved the yield significantly, but the enantioselectivity remained unsatisfactory. Structural

variation of the best-performing catalyst **C** focused on the effect of different silyl ether substituents (catalysts **C**–**G**). These studies, detailed in Scheme **4.4b**, revealed that the smallest TMS group in catalyst **C** outperformed larger silyl ethers in terms of yield and enantioselectivity (93%, 84:16 *e.r.*). We next investigated the effect of a second stereogenic element on the catalyst's pyrrolidine core by synthesizing variants derived from 4-hydroxyproline (Scheme **4.4c**).[99,100] The *tert*-butyldimethylsilyl (TBS)- protected catalyst **H**, derived from *trans*-4-hydroxyproline, offered an increased stereocontrol (87:13 *e.r.*). The diastereomeric catalyst **I**, bearing the two pyrrolidine ring substituents in a *cis* relationship,[101,102] led to a slightly increased stereocontrol (the opposite enantiomer of the product (*S*)-**7a** was formed in 88:12 *e.r.*). This result suggested us to further optimize the structure of catalysts derived from *cis*-4-hydroxyproline (Scheme **4.4d**). Assessment of different silyl ether protecting groups at the 4-hydroxy moiety identified the bulky thexyldimethylsilyl (TDS)-protected catalyst **M** as the best-performing, since product **7a** was obtained in 90:10 *e.r.* Lowering the reaction temperature to –10 °C afforded **7a** in 93:7 *e.r.* and an excellent yield. Control experiments established that both the amine catalyst and light were essential for reactivity.

To evaluate the generality of the method, we applied the optimized conditions and the *cis*-catalyst **M** to react enal **5a** with iodides of different perfluoroalkyl lengths (Scheme **4.5a**). Pleasingly, products **7a**–**g** were obtained in good to high yields and enantiomeric ratios. Only reaction at the remote position occurred, exclusively leading to γ-functionalized products.

Crystals of compound **7g** were suitable for X-ray crystallographic analysis, which allowed the (*S*) configuration of the newly formed stereocentre to be assigned unambiguously. Ethyl difluoroiodoacetate could be used as the radical precursor, enabling the synthesis of α-difluoro ester **7h** in good yield and enantioselectivity. A sensitive sulfonyl fluoride was tolerated well, affording the heteroatom-dense product **7i**.

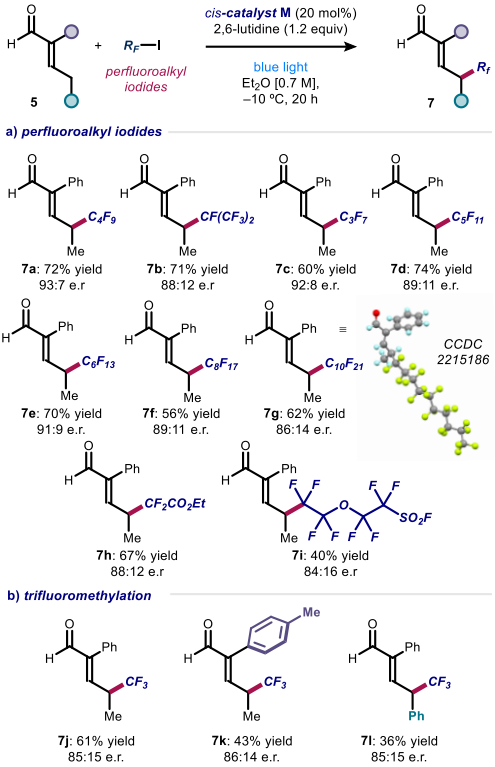

Scheme 4.5 Substrate scope for the asymmetric introduction of perfluoroalkyl and trifluoromethyl fragments at the remote γ position of α-branched enals. Reactions performed using **5** (0.2 mmol), enals **6** (0.6 mmol), 2,6-lutidine (0.24 mmol) in 0.3 mL of Et_2O under illumination by a single high-power LED (λ_{max} = 460 nm, irradiance = 100 mW/cm^2). Yields of the isolated products **7** and enantiomeric ratios are reported below each entry. Enantiomeric ratios measured by UPC^2 analysis on chiral stationary phase after derivatization of **7** to the corresponding 2,4-dinitrophenyl hydrazine derivatives.

Importantly, the asymmetric formation of a C(sp^3)-CF_3 stereogenic centre at the remote position of different enals was accomplished using CF_3I (products **7j–l,** Scheme **4.5b**). Other radical precursors, including perfluoroalkyl bromides and simple alkyl iodides, were

unsuccessful, highlighting the need of both a weak carbon-iodine bond and adjacent fluorine atoms (Figure **4.1**).

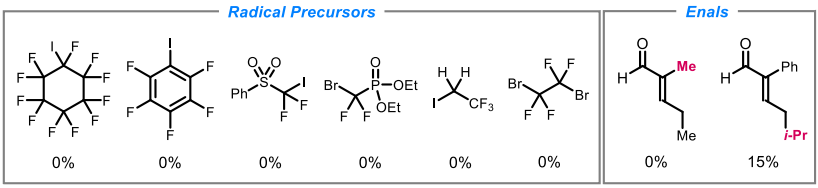

Figure 4.1 Survey of substrates which failed to give the product using enal **5** (3 equiv.), radical precursor **6** (0.2 mmol, 1 equiv.), catalyst **E** (20 mol%), 2,6-lutidine (1-2 equiv.) in Et_2O (0.7 M) at –10 °C for 20 h under blue light irradiation.

Next, a range of substituted and functionalized enals **1** were tested (Scheme **4.6**). Extended alkyl chain products were obtained in good yield and enantioselectivity (**7m**-**n**), with terminal halide (adduct **7o**), ester (**7p**), benzyl (**7q**) and phenyl (**7r**) groups were well tolerated. Various substituents on the α-phenyl group of enals were accepted, with products bearing alkyl (**7s-t**), 4-halogen (**7u-v**), and 4-methoxy (**7w**) groups all synthesized with consistently good results. With α-unsubstituted enals, achieving stereocontrol proved difficult, and the corresponding products **7x–z** were formed essentially in racemic form but with complete remote regioselectivity. A selective γ-perfluoroalkylation took place also with an enal derived from the naturally occurring diterpene *phytol* (product **7z**), achieving complete regioselectivity towards the more substituted methylene γ-position.

We then performed investigations to glean insight on the reaction mechanism (Figure **4.2**). UV-vis spectroscopic analysis confirmed that the individual components of the process were colourless, including the dienamine intermediate generated *in situ* from enal **5a** and the amine catalyst (green line in Figure **4.2a**). Right upon mixing perfluoroalkyl iodide **6a**, aminocatalyst, and enal **5a**, a new absorption band was observed in the visible region, which was

further corroborated by the appearance of a distinct yellow colour of the reaction mixture.

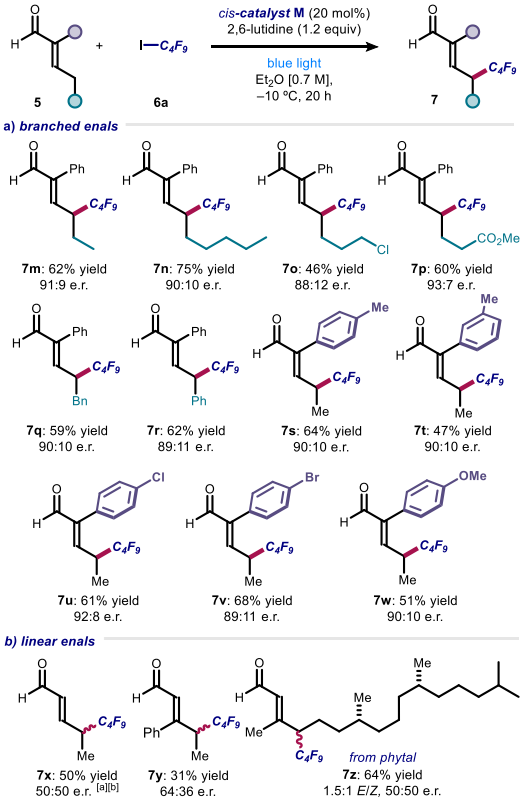

Scheme 4.6 Different enals that can participate in the light-driven remote perfluoroalkylation. Reactions performed using **6** (0.2 mmol), enals **5** (0.6 mmol), 2,6-lutidine (0.24 mmol) in 0.3 mL of Et_2O under illumination by a single high-power LED (λ_{max} = 460 nm, irradiance = 100 mW/cm^2). Yields refer to the isolated products **7**. Enantiomeric ratios measured by UPC^2 analysis on chiral stationary phase after derivatization of **7** to the corresponding 2,4-dinitrophenyl hydrazine derivatives. [a] Carried out at room temperature. [b] Isolated as the corresponding 2,4-dinitrophenyl hydrazone.

These observations are consonant with the formation of a visible-light absorbing EDA complex between the dienamine and R_F-I.

Mechanistically, we propose that light irradiation of the EDA complex **III** triggers an intracomplex SET, leading to the formation of perfluoroalkyl radical **I** after mesolysis of the C-I bond (Figure **4.2b**).

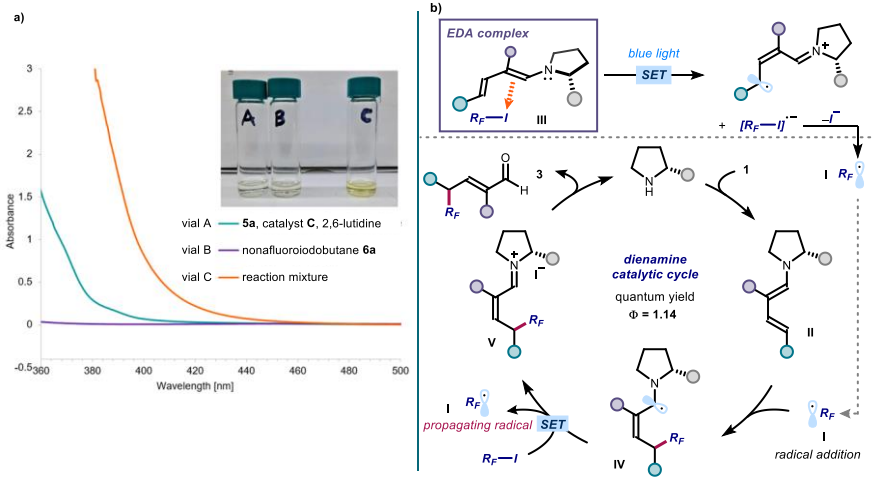

Figure 4.2 Mechanistic studies. (a) UV-vis measurements acquired on a Shimadzu UV-2401PC spectrophotometer with a quartz cuvette with path length of 1 cm. All samples in Et_2O. Vial A (green line): [catalyst **C**] = 0.6 M, [**5a**] = 0.6 M and [2,6-lutidine] = 0.6 M; Vial B (purple line): [**6a**] = 0.6 M; Vial C: [catalyst **C**] = 0.6 M, [**5a**] = 0.6 M, [**6a**] = 0.6 M and [2,6-lutidine] = 0.6 M. While the individual reaction components are all colourless, the vial C mixture containing all reaction components displays a yellow colour and an absorption band from approximately 450 nm. (b) Proposed radical propagation mechanism triggered by the excitation of the dienamine-based EDA complex **III**, which serves as the initiation event.

The electrophilic R_F· **I** is then intercepted by the chiral dienamine **II**, in a regio- and stereoselective fashion. The resulting α-amino radical **IV** would then either deliver an electron to **6** via SET,[103] or abstract an iodine atom from **6** via ATRA (atom-transfer radical addition),[104,105] to regenerate the perfluoroalkyl radical **I** thus propagating the radical chain. Hydrolysis of the iminium ion intermediate **V** releases product **7** and regenerates the

organocatalyst. We measured an overall quantum yield for the reaction between enal **5a** and nonafluoroiodobutane **6a** of Φ = 1.14, which is congruent with a radical chain process being operational[106,107]. It is important to notice that the *s-cis* dienamine conformation, depicted in Figure **4.2b**, would lead to the product (*S*) configuration on the stereogenic centre (as confirmed by X-ray crystallography), even though previous literature reports, studying similar dienamine intermediates, observed that the most stable conformation is the *s-trans*[94,108]. The outcome of the reaction could be explained by the Curtin-Hammett principle, whereas the minor *s-cis* conformer **II** is the actual reactive species for kinetic reasons, thus explaining the observed stereochemistry of the product.

In summary, we have developed the first enantioselective methodology that accounts for the remote installation of perfluoroalkyl-containing stereogenic centres. The chemistry exploits the ability of chiral catalytic dienamines to form photoactive electron donor-acceptor (EDA) complexes with perfluoroalkyl iodides, which under blue irradiation generate radicals through an SET mechanism. Key to achieving high levels of enantiocontrol and complete site selectivity for the more distal γ position of enals was the use of a sterically encumbered *cis*-4-hydroxyprolinol-derived catalyst.

5. Experimental Section

5.1 Materials and Methods

All analytical and technical grade solvents were used as received. All commercially available reagents were used as received. Column chromatography was carried out using *Merck* silica gel (230-400 mesh, 40-63 μm particle size, 60 Å pore size) or on activated neutral alumina (Brockmann I, 40-160 μm particle size, 58 Å pore size). Thin layer chromatography (TLC) was performed using glass plates precoated with a 0.25 mm thickness of silica gel and fluorescent indicator and visualized with UV light (254 nm), $KMnO_4$ solution or 2,4-Dinitrophenylhydrazine solution. ^{1}H-NMR and ^{13}C-NMR spectra were recorded in DMSO-*d*$_6$ (vials, *VWR*), $CDCl_3$ (bottle, *Aldrich*) or CD_3OD (vials, *Eurisotop*) on a *Bruker* Avance300 spectrometer (300 MHz). Chemical shifts are reported in ppm relative to the resonance of DMSO-*d*$_6$ (δ = 2.50), $CDCl_3$ (δ = 7.26) or CD_3OD (δ = 3.31) for ^{1}H-NMR and to the central peak of DMSO-*d*$_6$ (δ = 39.5), $CDCl_3$ (δ = 77.1) or CD_3OD (δ = 49.0) for ^{13}C-NMR. The multiplicity is abbreviated as follows: s (singlet), d (doublet), t (triplet), q (quartet), p (quintet), m (multiplet), bs (broad singlet). The coupling constant *J* is given in Hz (Hertz). Photostimulations were performed in 5 mm diameter clear fused quartz *Wilmad* Precision NMR sample tube. GC–MS analyses have been run on a HP 5892 series II GC, equipped with a 5% phenyl silicone 30m × 0.25mm × 25μm capillary column and coupled to a HP 5972 MSD instrument operating at 70 eV. High-resolution mass spectra (HRMS) were obtained with Bruker BioApex Fourier transform ion cyclotron resonance (FT-ICR) mass spectrometer. Collision induced dissociation (CID) were carried out by using ESI LTQ-XL (Thermo Scientific) at different collision energies. UPC^2 analysis on chiral stationary phase was performed on a Waters ACQUITY® instrument using IA-3, ID-3, IE-3, IG-3 and OJ-3 chiral

columns. The exact conditions for the analyses are specified in the experimental section of the individual compounds. UPC^2 traces were compared to racemic samples prepared using the optimised conditions with a 1:1 mixture of *R*- and *S*- catalyst **A** or a 1:1 mixture of (2*R*,5*R*)- and (2*S*,5*S*)-catalyst **C**, the latter being commercially available from Sigma Aldrich.

5.2 Photochemical setup

5.2.1 Photochemical Setup for the cyclization of 2-(hydroxyimino)aldehydes

The photoreactor for NMR-scale experiments consists of a lab-made LED chip assembly equipped with a sample holder. (Figure S1). The LED assembly is obtained by gluing a single LED chip (Nichia NVSU233A-D1 UV SMD-LED with PCB (10x10mm), λ = 365nm, 1030mW radiant flux or Nichia NVSU233B SMD-LED UV with PCB (10x10mm), λ = 365nm, 1450mW radiant flux, 3.75 V forward voltage from LUMITRONIX® LED-Technik GmbH) on an aluminum heat sink, using Fischer Elektronik heat-conducting adhesive WLK DK 4. The LED is powered with a constant current power supply (Meanwell LCM-40 Series, LUMITRONIX® LED-Technik GmbH). The sample holder consists of an aluminum block with a 7 mm housing to accommodate a 5mm NMR tube. The sample holder is screwed on top of the LED holder for easy replacement of the LED chip. The NMR tubing is placed in direct contact with the silicon lens that covers the light source and ensures a 60° viewing angle. Care should be taken not to damage the silicon lens. The system is kept at room temperature with the aid of a cooling fan.

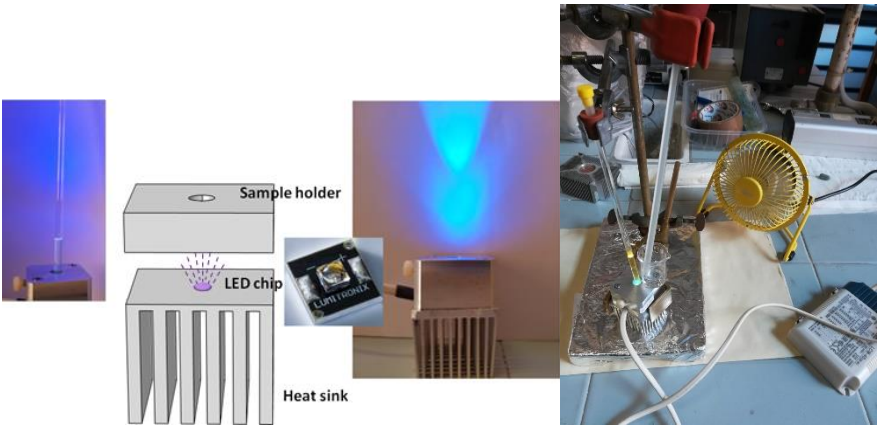

Figure 5.1 LED assembly for the photostimulation of HIAs to CBOs for NMR studies. Schematic is not drawn to scale.

5.2.1 Photochemical Setup for the γ-perfluoroalkylation of enals

The reaction setup consists of an aluminium supported single-LED connected to a power supply to modulate the light intensity. The single LED is provided of a plastic 3D-printed support above which is placed an aluminium fitter for the reaction vials. The latter is provided with inlet and outlet holes through which the refrigerating liquid flows. The setup is connected by rubber tubes to a Huber minichiller set to -12 °C which cools the aluminium plate and the reaction (the temperature of the reaction mixture was measured to be -10 °C). The setup is finally inserted in a homemade plastic cover to provide a closed space in which an Argon/Nitrogen atmosphere is created to prevent any water condensation during the reaction. The irradiance of the single LED is measured before every reaction trough the aid of a photodiode and is generally stable on 100 mW/cm^2.

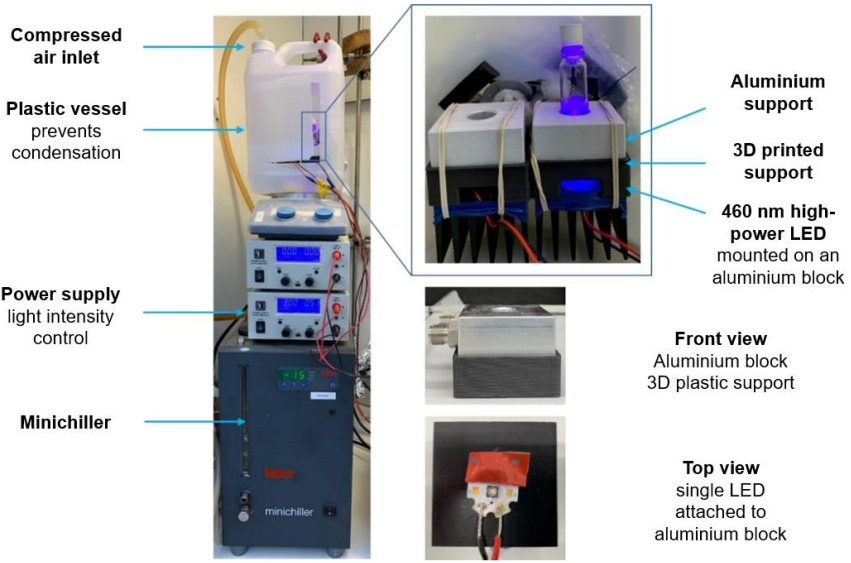

Figure 5.2 Photoreactor used for the enantioselective perfluoroalkylation of enals reaction.

5.3 Synthetic procedures

5.3.1 General procedure for aldehydes synthesis via Albright-Onodera oxidation[109]

To a solution of the alcohol (4.0 mmol, 1.0 equiv) in CH_2Cl_2 (10 mL) and DMSO (8.0 mmol, 2 equiv), P_2O_5 (7.2 mmol, 1.8 equiv) is added slowly to avoid overheating. The resulting slurry is stirred at room temperature for 1 h then cooled to 0 °C with an ice bath, then Et_3N (14.0 mmol, 3.5 equiv) is added dropwise. The resulting clear solution is stirred at room temperature for about 30 min (reaction completion is monitored via GC-MS analysis), then quenched with cold (4 °C) 1 M HCl (15 mL). The organic layer is separated, then washed with H_2O (1 x 15 mL) and brine (3 x 15

mL) and dried over Na_2SO_4. The solvent is removed by evaporation at reduced pressure and the residue is purified through column chromatography to afford the aldehydes as colourless liquids.

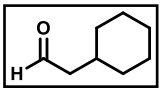

2-cyclohexylethanal. Reaction performed on 500 mg (3.91 mmol) of 2-cyclohexylethan-1-ol. Flash chromatography was performed with a mixture of CH_2Cl_2/Et_2O as eluant in ratio 50:1. Colourless liquid, 380 mg (3.02 mmol), 77 % yield.
^{1}H-NMR (300 MHz, $CDCl_3$) δ 9.75 (t, *J* = 2.4 Hz, 1H), 2.29 (dd, *J* = 6.8, 2.4 Hz, 2H), 1.98 – 1.80 (m, 1H), 1.76 – 1.62 (m, 5H), 1.37 – 0.91 (m, 5H). Data are in agreement to those reported in the literature.[109]

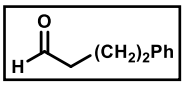

4-phenylbutanal. Reaction performed on 500 mg (3.33 mmol) of 4-phenylbutan-1-ol. Flash chromatography was performed with a mixture of petroleum ether/Et_2O in gradient from 10:1 to 8:1. Colourless liquid, 383 mg (2.59 mmol), 78 % yield.
^{1}H-NMR (300 MHz, $CDCl_3$) δ 9.76 (t, *J* = 1.6 Hz, 1H), 7.39 – 7.10 (m, 5H), 2.67 (t, *J* = 7.5 Hz, 2H), 2.46 (td, *J* = 7.3, 1.6 Hz, 2H), 2.02 – 1.92 (m, 2H). Data are in agreement to those reported in the literature[110].

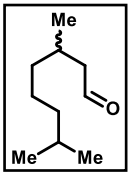

3,7-dimethyloctanal. Reaction performed on 500 mg (3.16 mmol) of 3,7-dimethyloctan-1-ol. The aqueous phase was extracted with 20 mL of Et_2O given the low solubility of the product in CH_2Cl_2. Flash chromatography was performed with a mixture of petroleum ether/Et_2O as eluant in ratio 20:1. Light yellow oil, 460 mg (2.94 mmol), 93 % yield.
^{1}H NMR (300 MHz, $CDCl_3$) δ 9.76 (t, *J* = 2.4 Hz, 1H), 2.40 (ddd, *J* = 16.0, 5.8, 2.1 Hz, 1H), 2.22 (ddd, *J* = 15.9, 7.8, 2.6 Hz, 1H), 2.12 – 1.98 (m, 1H), 1.56 – 1.48 (m, 1H), 1.34 – 1.11 (m, 6H), 0.96 (d, *J* =

6.7 Hz, 3H), 0.86 (d, J = 6.7, 1.5 Hz, 6H). Data are in agreement to those reported in the literature[111].

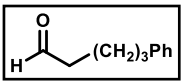

5-phenylpentanal. Reaction performed on 1000 mg (6.10 mmol) of 5-phenylpentan-1-ol. Flash chromatography was performed with a mixture of pentane/Et_2O in gradient from 30:1 to 15:1. Colourless oil, 834 mg (5.15 mmol), 83 % yield

^{1}H NMR (300 MHz, $CDCl_3$) δ 9.76 (t, J = 1.7 Hz, 1H), 7.38 – 7.10 (m, 5H), 2.66-2.64 (m, 2H), 2.54 – 2.40 (m, 2H), 1.68 (m, 4H). Data are in agreement to those reported in the literature[111].

5.3.2 General procedure for aldehydes synthesis via Parikh-Doering oxidation[111]

1.0 mmol of alcohol (1.0 equiv), 7 mL CH_2Cl_2 and 0.54 mL (4.0 mmol, 4.0 equiv) Et_3N are introduced in a flame-dried two-necked round bottomed flask equipped with a nitrogen inlet and magnetic stirring. The flask is chilled in an ice bath, then a solution of 0.48 g (3.0 mmol, 3.0 equiv) SO_3·Pyridine complex in 3 mL DMSO is added. Stirring is continued at 0°C for 1 h, then for 3 h at room temperature. The following workup procedure is aimed at minimizing product loss and maximizing removal of DMSO from the reaction crude. The reaction mixture is diluted with CH_2Cl_2 or Et_2O and washed with a 1:1 (v/v) mixture of NH_4Cl (sat) and brine. Most of the CH_2Cl_2 (if used) is removed by rotary evaporation and the residue is taken up with Et_2O. The aqueous phase is extracted with fresh Et_2O to minimize product loss. The combined organic phases are washed again with the NH_4Cl/ NaCl (sat), then with brine alone to remove as much DMSO as possible. After drying over anhydrous Na_2SO_4, the solvent is removed, and the residue is purified by silica gel chromatography.

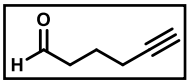

5-hexynal. Reaction performed on 1.80 g (18.4 mmol) of 5-hexyn-1-ol. Flash chromatography was performed with a mixture of petroleum ether/Et_2O in gradient from 20:1 to 8:1. Whereas Et_2O was removed by distillation, the product could not be isolated from solvent hydrocarbons. After a first distillation through a Vigreux column, we held on to the product-rich residue and we submitted the richest distilled fraction to a second distillation in an attempt to further concentrate the product. We thus obtained two product-rich lightly yellow oily residues and the yield of 5-hexynal was estimated by ^{1}H-NMR analysis. The residual solvent was assumed to be equivalent to hexane (C_6H_{14}), so that the integral of all signals below 1.8 ppm are worth 14H. Based on the amounts of the two fractions, we estimate 940 mg (9.79 mmol; 54% yield) as 73% (w/w) in hexanes.

^{1}H-NMR (300 MHz, $CDCl_3$) δ 9.77 (t, *J* = 1.3 Hz, 1H); 2.58 (td, *J* = 7.2, 1.3 Hz, 2H); 2.24 (td, *J* = 6.8, 2.5 Hz, 2H); 1.96 (t, *J* = 2.5 Hz, 1H); 1.82 (m, 2H). Data are in agreement to those reported in the literature[112].

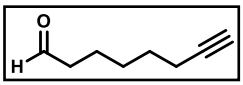

7-octynal. Reaction performed on 430 mg (3.41 mmol) of 7-octyn-1-ol. Flash chromatography was performed with a mixture of hexane/EtOAc in gradient from 15:1 to 12:1. Light yellow oil, 354 mg (2.85 mmol), 84 % yield.

^{1}H-NMR (300 MHz, $CDCl_3$) δ 9.77 (t, *J* = 7.3 Hz, 1H); 2.45 (td, *J* = 7.3, 1.7 Hz, 2H); 2.21 (td, *J* = 7.0, 2.7 Hz, 2H); 1.94 (t, *J* = 2.7 Hz, 1H); 1.66-1.48 (m, 6H). Data are in agreement to those reported in the literature[112].

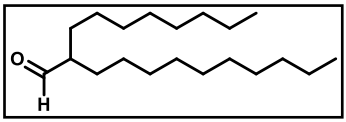

2-octyldodecanal. Reaction performed on 925 mg (3.10 mmol) of 2-octyldodecan-1-ol. Colourless liquid, 830 mg (2.80 mmol), 90 % yield.

^{1}H-NMR (300 MHz, $CDCl_3$) δ 9.54 (d, *J* = 3.18 Hz, 1H); 2.18-2.24 (m, 1H); 1.67 -1.57 (m, 2H), 1.25-1.45 (m, 30H); 0.87 (t, *J* = 6.42 Hz, 6H). Data are in agreement to those reported in the literature[113].

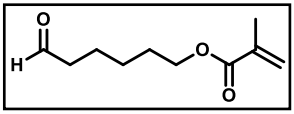

6-oxohexyl 2-methylprop-2-enoate. Under N_2 atmosphere, to an ice-cold solution of 1,6- hexanediol (2.00 g, 16.9 mmol) in anhydrous THF (20 mL) were added successively Et_3N (1.17 mL, 8.46 mmol), DMAP (0.206 mg, 1.69 mmol), and methacrylic anhydride (1.26 mL, 8.46 mmol). The mixture was stirred at 0° C for 1 h. MeOH (2.7 mL) was added and stirring was maintained for 10 minutes. After solvents evaporation under reduced pressure, the crude mixture was diluted with ethyl acetate (25 mL) and washed with HCl 1M, saturated $NaHCO_3$ and brine. The organic phase was dried over Na_2SO_4, filtered, and the solvents evaporated under reduced pressure. 1.052 g of a mixture of 6-hydroxyhexyl 2-methylprop-2-enoate and the dimethacrylate by-product was obtained and used in the next step without further purification. Under N_2 atmosphere, to the crude mixture obtained in dichloromethane (32 mL), was added Et_3N (2.7 mL, 19.6 mmol), followed, after cooling in an ice bath, by a solution of SO_3-Pyr complex (2.110 g, 13.7 mmol) in DMSO (13.3 mL). The mixture was stirred at room temperature for 24 h. The crude mixture was washed with NH_4Cl (sat), $NaHCO_3$ (sat) and H_2O. The solvent was removed by rotary evaporation, and the mixture was re-dissolved with Et_2O (30 mL), then washed with brine and H_2O. The organic phase was dried over Na_2SO_4, filtered, and the solvents evaporated. The residue was purified by silica gel chromatography with a hexane/ethyl acetate gradient to afford 835 mg of 6-oxohexyl 2-methylprop-2-enoate as a colourless liquid (4.54 mmol), 54 % overall yield.

^{1}H-NMR (300 MHz, $CDCl_3$) δ 9.7 (t, *J* = 1.6 Hz, 1H); 6.07 (m, 1H); 5.5 (m, 1H); 4.1 (t, *J* = 6.5 Hz, 2H); 2.4 (m, 2H); 1.9 (t, *J* = 1.2 Hz,

3H); 1.6 - 1.73 (m, 4H); 1.35 - 1.46 (m, 2H). Data are in agreement to those reported in the literature[114].

5.3.3 Synthesis of 3-propylhexanal

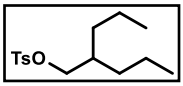

2-propylpentyl 4-methylbenzenesulfonate. 130 mg (1.0 mmol, 1.0 equiv) of 2-propyl-1-pentanol and 286 mg (1.5 mmol, 1.5 equiv) of *p*-toluensulfonyl chloride are dissolved in 2 mL of CH_2Cl_2. The resulting solution is cooled to 0 °C, then Et_3N (417 µL, 303 mg, 3.0 mmol, 3 equiv) is added dropwise and the reaction mixture is allowed to react at 25 °C. After 20 h the reaction is diluted with 13 mL of CH_2Cl_2 then the organic layer is washed with HCl 1 M (1 x 15 mL), water (1 x 10 mL), saturated aqueous $NaHCO_3$ (1 x 15 mL) and brine (1 x 15 mL), dried over Na_2SO_4 and the solvent removed by evaporation at reduced pressure. The title compound is obtained as a colourless oil (278 mg, 0.98 mmol, 98 % yield) and used without further purification.
^{1}H-NMR (300 MHz, $CDCl_3$) δ 7.78 (d, *J* = 8.3 Hz, 2H), 7.34 (d, *J* = 8.0 Hz, 2H), 3.90 (d, *J* = 5.4 Hz, 2H), 2.45 (s, 3H), 1.76 – 1.50 (m, 1H), 1.23 – 1.18 (m, 8H), 0.92 – 0.69 (m, 6H). Data are in agreement to those reported in the literature[115].

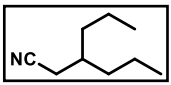

3-propylhexanenitrile. 2-propylpentyl 4-methylbenzenesulfonate (222 mg, 0.78 mmol, 1.0 equiv) is dissolved in 3 mL DMSO, then KCN (76 mg, 1.17 mmol, 1.5 equiv) is added and the reaction is warmed to 90 °C. After 3 h the reaction is cooled down to room temperature, diluted with 15 mL of saturated Na_2CO_3 and extracted 4 times with Et_2O. The combined organic layers are washed with brine, dried over Na_2SO_4 and evaporated at reduced pressure to afford 92 mg (0.66 mmol, 85 % yield) of 3-propylhexanenitrile as a colourless oil.

^{1}H NMR ($CDCl_3$, 300 MHz) δ 2.32 (d, *J* = 5.9 Hz, 2H), 1.74–1.68 (m,1H), 1.44–1.23 (m, 8H), 0.94–0.87 (m, 6H). Data are in agreement to those reported in the literature[116].

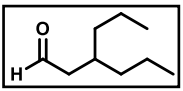

3-propylhexanal. In a flame-dried two-necked round bottom flask 92 mg (0.66 mmol, 1.0 equiv) of 3-propylhexanenitrile are dissolved in 11 mL of anhydrous hexane then a 1 M solution of diisobutylaluminum hydride in heptane (DIBAL-H, 1.66 mL, 2.5 equiv) is added under an Ar atmosphere. After 3 h, 9 mL of 96 % EtOH and 5.5 mL of H_2O are added dropwise to hydrolyze the excess of DIBAL-H and stirred for 1 h. The reaction mixture is then extracted with Et_2O (3 x 10 mL), the organic layers washed with 3 M HCl (1 x 20 mL), H_2O (1 x 20 mL), saturated $NaHCO_3$ (1 x 20 mL), brine (1 x 20 mL) and dried over Na_2SO_4. The product is purified via flash chromatography using as eluant a mixture of pentane/Et_2O in ratio 30:1. The product-containing fractions were distilled through a Vigreux column at ambient pressure to remove the solvents present, since evaporation with Rotavapor led to complete product loss. Although it was possible to remove all the Et_2O this way, still accompanied with partial evaporation of the product, hydrocarbons were still present in the distillation residue. Given the ^{1}H-NMR ratio of the multiplets at δ = 1.32 – 1.20 (comprising both 3-propylhexanal and hydrocarbon methylene hydrogens) and at δ = 0.92 – 0.86 (representative of the terminal methyl protons), the solvent still present in the sample was assumed to be heptane. Therefore the clear colourless liquid obtained is estimated to be a 37 % (w/w) solution of 3-propylhexanal in heptane (118 mg of solution, estimated 44 mg of 3-propylhexanal, 0.31 mmol, 47 % yield).

^{1}H NMR ($CDCl_3$, 300 MHz) δ 9.76 (t, *J* = 2.4 Hz, 1H), 2.33 (dd, *J* = 6.6, 2.4 Hz, 2H), 2.08 – 1.85 (m, 1H), 1.38 – 1.15 (m, 8H + 24H from heptane), 0.94 – 0.80 (m, 6H + 14H from heptane). Data are in agreement to those reported in the literature[117].

5.3.4 Synthesis of 3-octyltridecanal

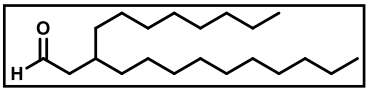

3-octyltridecanal. Under Ar atmosphere and at 0 °C, *t*-BuOK (0.94 g, 8.4 mmol) was added to a solution of $CH_3OCH_2PPh_3Cl$ (2.9 g, 8.3 mmol) in anhydrous THF (30 mL). The mixture was kept under magnetic stirring at room temperature for 4 h. 2-octyldodecanal (0.83 g, 2.8 mmol) dissolved in anhydrous THF (5 mL) was added at 0 °C and the mixture was kept under magnetic stirring at room temperature for 17 h. The mixture was filtered and the solvent evaporated under reduced pressure. The crude was dissolved in Et_2O (20 mL), washed with saturated NH_4Cl solution, dried over Na_2SO_4 and the solvent evaporated at reduced pressure. The residue was dissolved in THF (9 mL), then an aqueous HCl solution (1 M, 2.1 mL) was added and the mixture was stirred for 2 h at 75 °C. Et_2O (10 mL) was added and the mixture was washed with H_2O (5 mL). The aqueous phase was extracted with Et_2O (15 mL); the organic phases was washed successively with saturated $NaHCO_3$ and brine and dried over anhydrous Na_2SO_4. White solid, 0.35 g (1.1 mmol), 40 % yield.
^{1}H NMR ($CDCl_3$, 300 MHz) δ 9.76 (t, J = 2.4 Hz, 1H); 2.32 (dd, J = 6.6, 2.5 Hz, 2H); 1.94 (m, 1H); 1.37 (m, 32H); 0.88 (t, J = 6.5 Hz, 6H). Data are in agreement to those reported in the literature[114].

5.3.5 General procedure for α-oximation of aldehydes[29]

In a two-necked round bottom flask equipped with magnetic stirring are introduced in this order, under a N_2 atmosphere, 10 mL DMF, pyrrolidine (0.6 mmol, 0.2 equiv), *p*-toluenesulfonic acid (0.6 mmol, 0.2 equiv) and the aldehyde (3.0 mmol, 1.0 equiv). Then $NaNO_2$ (3.0 mmol, 1.0 equiv) is added, followed by $FeCl_3 \cdot 6H_2O$ (3.0 mmol, 1.0 equiv) in small portions to avoid excessive heating. The reaction is stirred for 4-6 h at room temperature (completion is monitored by TLC using hexane/ethyl acetate 5:1 as eluant). The

mixture is diluted with 30 mL EtOAc and 20 mL of a 1:1 (v/v) mixture of NH_4Cl (sat) and brine and stirred for 20 minutes at room temperature. The organic layer is set aside and the aqueous phase is extracted with 20 mL fresh EtOAc to minimize product loss. The pooled organic solutions are washed once more with 20 mL of NH_4Cl (sat)/brine mixture, then three times with brine. After drying over anhydrous Na_2SO_4, EtOAc is removed by rotary evaporation. The product is purified by silica gel chromatography.

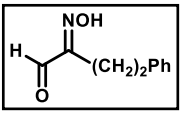

2-(hydroxyimino)-4-phenylbutanal (1a). Reaction performed on 350 mg (2.36 mmol) of 4-phenylbutanal. Flash chromatography was performed with a mixture of petroleum ether/Et_2O in gradient from 5:1 to 4:1. White to light yellow solid, 290 mg (1.64 mmol), 69 % yield, m.p. = 61-63 °C.

^{1}H-NMR (300 MHz, DMSO-*d*$_6$) δ 12.97 (s, 1H), 9.36 (s, 1H), 7.31 – 7.21 (m, 2H), 7.18 – 7.14 (m, 3H), 2.75 – 2.54 (m, 4H).

^{13}C$\{^1H\}$**-NMR** (75 MHz, DMSO-*d*$_6$) δ 191.6, 158.9, 140.8, 128.3, 128.1, 126.1, 30.6, 23.3.

ESI-HRMS (negative): calculated for $C_{10}H_{10}NO_2$ $[M-H]^-$, 176.07170; found 176.07201 ± 4.0 x10^{-4} u averaged from five measurements.

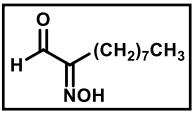

2-(hydroxyimino)decanal (1b). Reaction performed on 750 mg (4.81 mmol) of decanal. Flash chromatography was performed with a mixture of hexane/EtOAc in gradient from 30:1 to 8:1. White solid, 581 mg (3.14 mmol), 65 % yield, m.p. = 60-62 °C.

^{1}H-NMR (300 MHz, $CDCl_3$) δ 9.44 (s, 1H), 8.64 (bs, 1H) 2.59 – 2.34 (m, 2H), 1.53 – 1.39 (m, 2H), 1.26 (m, 10H), 0.87 (t, *J* = 6.7 Hz, 3H).

^{13}C$\{^1H\}$**-NMR** (75 MHz, $CDCl_3$) δ 191.3, 162.2, 32.2, 30.0, 29.5, 29.4, 25.8, 23.0, 22.2, 14.4. Data are in agreement to those reported in the literature[29].

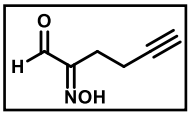

2-(hydroxyimino)-5-hexynal. Reaction performed on 940 mg (9.79 mmol) of 5-hexynal. Flash chromatography was performed with a mixture of hexane/Et_2O in gradient from 10:1 to 4:1. Yellow oil, 340 mg (2.72 mmol), 28 % yield.

^{1}H-NMR (300 MHz, DMSO-*d*$_6$) δ 13.06 (s, 1H); 9.40 (s, 1H); 2.76 (t, *J* = 7.6 Hz, 1H); 2.53 (t, *J* = 6.6 Hz 2H); 2.32 (td, *J* = 7.4, 2.6 Hz, 2H).

^{13}C$\{^1H\}$**-NMR** (75 MHz, DMSO-*d*$_6$) δ 190.9; 159.4; 82.6; 70.5; 69.4; 21.1; 14.7. Data are in agreement to those reported in the literature[40].

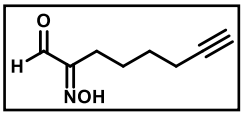

2-(hydroxyimino)-7-octynal. Reaction performed on 240 mg (1.94 mmol) of 7-octynal. Flash chromatography was performed with a mixture of hexane/EtOAc in gradient from 8:1 to 5:1. Yellow oil, 219 mg (1.43 mmol), 74 % yield.

^{1}H-NMR (300 MHz, $CDCl_3$) δ 9.46 (s, 1H); 8.66 (bs, 1H); 2.52 (t, *J* = 7.2 Hz, 2H); 2.20 (td, *J* = 7.0, 2.7 Hz, 2H); 1.94 (t, *J* = 2.7 Hz, 1H); 1.66 – 1.48 (m, 4H).

^{13}C$\{^1H\}$**-NMR** (75 MHz,$CDCl_3$) δ 191.0; 161.4; 84.1; 68.7; 28.4; 24.7; 21.4; 18.2. Data are in agreement to those reported in the literature[40].

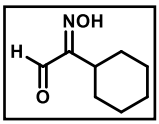

2-cyclohexyl-2-(hydroxyimino)ethanal (1j). Reaction performed on 400 mg (3.17 mmol) of 2-cyclohexylethanal. Flash chromatography was performed with a mixture of petroleum ether/Et_2O in gradient from 8:1 to 5:1. White solid, 374 mg (2.41mmol), 76 % yield, m.p. = 84-86 °C.

^{1}H-NMR (300 MHz, DMSO-*d*$_6$) δ 12.86 (s, 1H), 9.292 and 9.287 (s, 1H, *syn* and *anti* conformations), 3.10 – 2.70 (m, 1H), 1.99 – 1.52 (m, 5H), 1.42 – 1.37 (m, 2H), 1.21 – 1.15 (m, 3H).

^{13}C$\{^1H\}$**-NMR** (75 MHz, DMSO-*d*$_6$) δ 192.2, 161.4, 33.8, 26.9, 25.9, 25.5.

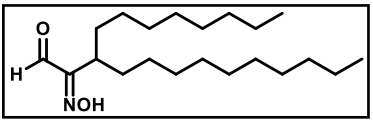

2-(hydroxyimino)-3-octyltridecanal (1i). Reaction performed on 350 mg (1.03 mmol) of 3-octyltridecanal. Flash chromatography was performed with a mixture of hexane/Et_2O in ratio 90:1. Gray solid, 210 mg (0.62 mmol), 60 % yield.

^{1}H-NMR (300 MHz, DMSO-*d*$_6$) δ : 12.8 (s, 1H); 9.34 (s, 1H); 3.06 (m, 1H); 1.68 (m, 2H); 1.46 (m, 2H); 1.19 (m, 28H), 0.839 (t, *J* = 6.5 Hz, 6H).

^{13}C{^{1}H}**-NMR** (75 MHz, DMSO-*d*$_6$) δ 192.2; 160.8; 34.4; 31.3; 31.3; 30.7; 29.0; 28.9; 28.9; 28.7; 28.7; 27.3; 22.12; 22.1; 13.9. Data are in agreement to those reported in the literature[31].

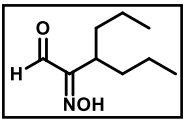

2-(hydroxyimino)-3-propylhexanal (1h). Reaction performed on 95 mg (0.67 mmol) of 3-propylhexanal. Flash chromatography was performed with a mixture of pentane/Et_2O in gradient from 15:1 to 10:1. Colourless oil, 36 mg (0.21 mmol), 32 % yield.

^{1}H-NMR (300 MHz, DMSO-*d*$_6$) δ 12.85 (s, 1H), 9.336 and 9.331 (s, 1H, *syn* and *anti* conformations), 3.20 – 2.99 (m, 1H), 1.74 – 1.62 (m, 2H), 1.50 – 1.31 (m, 2H), 1.20 – 0.96 (m, 4H), 0.79 (t, *J* = 7.3 Hz, 6H).

^{13}C{^{1}H}**-NMR** (75 MHz, DMSO-*d*$_6$) δ 192.4, 160.9, 33.9, 33.0, 20.6, 13.9.

ESI-HRMS (negative): calculated for $C_9H_{16}NO_2$ $[M-H]^-$, 170.11865; found 170.11887 ± 3.5 x 10^{-4} u, averaged from five measurements.

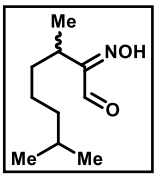

2-(hydroxyimino)-3,7-dimethyloctanal (1g). Reaction performed on 459 mg (2.94 mmol) of 3,7-dimethyloctanal. Flash chromatography was performed with a mixture of pentane/Et_2O in gradient from 15:1 to 5:1. Colourless oil, 434 mg (2.35 mmol), 80 % yield.

^{1}H NMR (300 MHz, DMSO-d_6) δ 12.83 (s, 1H), 9.32 (s, 1H). 3.20 – 3.01 (m, 1H), 1.80 – 1.58 (m, 1H), 1.42 (m, 2H), 1.13 – 1.03 (m, 7H), 0.83 – 0.74 (m, 6H).
^{13}C$\{^1H\}$ **NMR** (75 MHz, DMSO-d_6) δ 192.2, 161.7, 38.2, 32.2, 28.6, 27.2, 25.1, 22.4, 16.2.

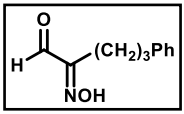

2-(hydroxyimino)-5-phenylpentanal (1e). Reaction performed on 795 mg (4.91 mmol) of 3,7-dimethyloctanal. Flash chromatography was performed with a mixture of pentane/Et_2O in gradient from 12:1 to 5:1. Colourless oil, 643 mg (3.37 mmol), 69 % yield.
^{1}H NMR (300 MHz, DMSO) δ 12.90 (s, 1H), 9.39 (s, 1H), 7.28 – 7.23 (m, 2H), 7.19 – 7.10 (m, 3H), 2.59 – 2.45 (m, 2H), 2.40 – 2.31 (m, 2H), 1.75 – 1.57 (m, 2H).
^{13}C$\{^1H\}$ **NMR** (75 MHz, DMSO) δ 191.9, 159.5, 141.5, 128.3, 128.1, 125.8, 35.2, 26.8, 21.2.

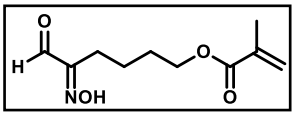

5-(hydroxyimino)-6-oxohexyl 2-methylprop-2-enoate (1f). Reaction performed on 829 mg (4.51 mmol) of 6-oxohexyl 2-methylprop-2-enoate. Flash chromatography was performed with a mixture of hexane/EtOAc in gradient from 30:1 to 8:1. Colourless oil, 575 mg (2.70 mmol), 60 % yield.
^{1}H-NMR (300 MHz, DMSO-d_6) δ 9.79 (s, 1H); 9.45 (s, 1H); 6.1 (m, 1H); 5.5 (m, 1H); 4.1 (t, 2H, J = 6.2 Hz); 2.5 (t, 2H, J = 7.5 Hz); 1.9 (m, 3H); 1.5-1.7 (m, 4H). Data are in agreement to those reported in the literature[31].

5.3.6 General procedure for Cu catalyzed azide-alkyne Huisgen cycloaddition

1.0 mmol of alkyne and 1.0 mmol of heptylazide are dissolved in 4 mL acetonitrile in a schlenk tube equipped with magnetic stirring.

Then, 0.23 mL (0.21 g, 2.0 mmol) of 2,6-lutidine and 0.35 mL (0.26 g, 2.0 mmol) of di*iso*propylethylamine are added and the solution is degassed through three freeze-pump-thaw cycles under Argon. 19 mg of CuI (0.10 mmol) is added under Ar. The reaction is stirred for 3 h at room temperature. Most of the CH_3CN is removed by rotary evaporation and the resulting residue is dissolved in 50 mL EtOAc. The organic phase is washed three times with 25 mL NH_4Cl (sat), then with 25 mL HCl 0.1 M, and finally with 25 mL distilled water. After drying over anhydrous sodium sulphate, the solvent is evaporated and the residue is purified by column chromatography on silica gel. Removal of residual copper ions was achieved by washing a dichloromethane solution of the product several times with EDTA 0.1 M, previously adjusted at pH 7.6 (10:1 organic phase/EDTA solution).

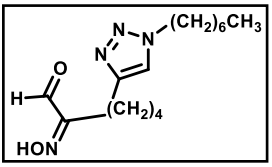

6-(1-heptyl-1H-1,2,3-triazol-4-yl)-2-(hydroxyimino)hexanal (1c). Reaction performed on 188 mg (1.23 mmol) of 2-(hydroxyimino)-7-octynal. White solid, 295 mg (1.00 mmol), 82 % yield, m.p. = 42-44 °C.

^{1}H-NMR (300 MHz, DMSO-*d*$_6$) δ : 12.89 (s, 1H), 9.38 (s, 1H), 7.79 (s, 1H), 4.25 (t, *J* = 7.1 Hz, 2H), 2.56 (t, *J* = 7.4 Hz, 2H), 2.35 (t, *J* = 7.4 Hz, 2H), 1.85 – 1.65 (m, 2H), 1.59 – 1.45 (m, 2H), 1.44 – 1.29 (m, 2H), 1.21 (m, 8H), 0.83 (t, *J* = 6.8 Hz, 3H).

^{13}C{^{1}H}**-NMR** (75 MHz, DMSO-*d*$_6$) δ δ 191.9, 159.7, 146.5, 121.6, 49.1, 31.1, 29.7, 29.1, 28.0, 25.8, 24.7, 24.6, 22.0, 21.0, 13.9. All analytical data are in accordance with literature reports.[40]

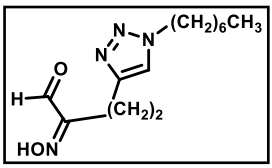

4-(1-heptyl-1H-1,2,3-triazol-4-yl)-2-(hydroxyimino)butanal (1d). Reaction performed on 96 mg (1.0 mmol) of 2-(hydroxyimino)-5-hexynal. Flash chromatography was performed using

hexane/EtOAc in ratio 1:1. White solid, 160 mg (0.60 mmol), 60 % yield, m.p. = 64-66 °C.
^{1}H-NMR (300 MHz, DMSO-*d*$_6$) δ 13.00 (s, 1H); 9.39 (s, 1H,); 7.86 (s, 1H); 4.27 (t, *J* = 7.0 Hz, 2H); 2.80 – 2.60 (m, 4H); 1.76 (m, *J* = 7.14 Hz, 2H); 1.24 (m, 8H); 0.85 (t, *J* = 6,48 Hz, 3H).
^{13}C$\{^{1}H\}$**-NMR** (75 MHz, DMSO-*d*$_6$) δ 191.5; 158.7; 145.5; 121.8; 49.1; 31.1; 29.7; 28.1; 25.8; 22.0; 21.6; 20.9; 13.9. All analytical data are in accordance with literature reports.[40]

5.3.7 General procedure for methylation of 2-(hydroxyimino)aldehydes

The 2-(hydroxyimino)aldehyde (1.3 mmol, 1.0 equiv) and K_2CO_3 (5.2 mmol, 4 equiv) are dissolved in 4 mL of acetone. The resulting suspension is stirred for 10 minutes, then DMS (dimethyl sulphate, 2.6 mmol, 2.0 equiv) is added dropwise. After 2.5 h, 25 mL of H_2O are added to the reaction mixture and stirred for 15 minutes, then the aqueous solution is extracted with diethyl ether (3 x 20 mL). The reunited organic layers are washed with saturated $NaHCO_3$ (1 x 40 mL) and brine (1 x 40 mL), dried over Na_2SO_4 and the solvent evaporated at reduced pressure. The crude is purified through a quick filtration over a pad of silica gel.

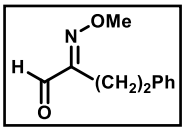

2-(methoxyimino)-4-phenylbutanal (1k). Reaction performed on 164 mg (0.93 mmol) of 2-(hydroxyimino)-4-phenylbutanal (**1a**). Flash chromatography was performed with a mixture of petroleum ether/Et_2O in ratio 30:1. Colourless liquid, 159 mg (0.83 mmol), 90 % yield.
^{1}H-NMR (300 MHz, DMSO-*d*$_6$) δ 9.32 (s, 1H), 7.28 – 7.24 (m, 2H), 7.20 – 7.11 (m, 3H), 4.05 (s, 3H), 2.77 – 2.54 (m, 4H).
^{13}C$\{^{1}H\}$**-NMR** (75 MHz, DMSO-*d*$_6$) δ 190.4, 158.6, 140.5, 128.3, 128.1, 126.2, 63.7, 30.7, 23.8.
ESI-HRMS (positive): calculated for $C_{11}H_{14}NO_2$ $[M+H]^+$, 192.1019; found 192.1021 ± 4.0 x 10^{-4} u, averaged from six measurements.

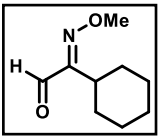

2-cyclohexyl-2-(methoxyimino)ethanal (1n). Reaction performed on 200 mg (1.29 mmol) of 2-cyclohexyl-2-(hydroxyimino)ethanal (**1j**). Flash chromatography was performed with a mixture of petroleum ether/Et_2O in ratio 50:1. White solid, 188 mg (1.11 mmol), 86 % yield, m.p. = 51-52 °C.

^{1}H-NMR (300 MHz, $CDCl_3$) δ 9.318 and 9.314 (s, 1H, *syn* and *anti* conformations), 4.08 (s, 3H), 3.19 – 2.68 (m, 1H), 1.90 – 1.68 (m, 5H), 1.51 – 1.47 (m, 2H), 1.27 – 1.22 (m, 3H).

^{13}C{^{1}H}**-NMR** (75 MHz, $CDCl_3$) δ 191.4, 162.1, 63.7, 35.1, 27.5, 26.3, 25.8.

ESI-HRMS (positive): calculated for $C_9H_{16}NO_2$ $[M+H]^+$, 170.1176; found 170.1177 ± 3.5 x 10^{-4} u, averaged from five measurements.

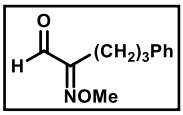

2-(methoxyimino)-5-phenylpentanal (1l). Reaction performed on 151 mg (0.79 mmol) of 2-(hydroxyimino)-5-phenylpentanal (**1e**). Flash chromatography was performed with a mixture of pentane/Et_2O in ratio 30:1. Colourless oil, 65 mg (0.32 mmol), 41 % yield.

^{1}H NMR (300 MHz, DMSO) δ 9.35 (s, 1H), 7.29 – 7.22 (m, 2H), 7.19 – 7.13 (m, 3H), 4.06 (s, 3H), 2.54 (m, 2H), 2.43 – 2.29 (m, 2H), 1.75 – 1.56 (m, 2H).

^{13}C{^{1}H} **NMR** (75 MHz, DMSO) δ 190.6, 159.2, 141.3, 128.3, 125.9, 63.6, 35.1, 26.7, 21.7.

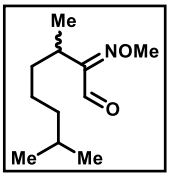

2-(methoxyimino)-3,7-dimethyloctanal (1m). Reaction performed on 120 mg (0.65 mmol) of 2-(hydroxyimino)-3,7-dimethyloctanal (**1g**). Flash chromatography was performed using pure petroleum ether followed by a mixture of petroleum ether/Et_2O in ratio 20:1. Colourless oil, 92 mg (0.46 mmol), 71 % yield.

^{1}H NMR (300 MHz, DMSO) δ 9.29 (d, J = 1.4 Hz, 1H), 4.05 (s, 3H), 3.16 – 2.97 (m, 1H), 1.63 (dt, J = 18.0, 8.9 Hz, 1H), 1.43 (td, J =

13.6, 6.8 Hz, 2H), 1.06 (t, *J* = 7.0 Hz, 7H), 0.79 (dd, *J* = 6.6, 3.5 Hz, 6H).
$^{13}C\{^1H\}$ NMR (75 MHz, DMSO) δ 191.0, 161.6, 63.7, 38.1, 32.2, 29.3, 27.2, 25.0, 22.6, 22.3, 16.2.

5.3.8 Synthesis of 2-((benzyloxy)imino)-2-cyclohexylethanal

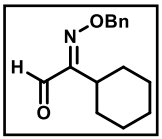

2-((benzyloxy)imino)-2-cyclohexylethanal (1o). In a round-bottom flask 96 mg (0.62 mmol, 1.0 equiv) of 2-cyclohexyl-2-(hydroxyimino)ethanal (**1j**) and 74 µL of benzyl bromide (106 mg, 0.62 mmol, 1.0 equiv) are dissolved in 3 mL of acetone, then 342 mg of K_2CO_3 (2.48 mmol, 4 equiv) are added slowly. After 1.5 h the crude is diluted with 20 mL of H_2O and extracted with diethyl ether (4 x 15 mL). The reunited organic layers are dried with Na_2SO_4 and the solvent is removed via evaporation at reduced pressure. The product is purified via flash chromatography using as eluant a mixture of petroleum ether/Et_2O in ratio 20:1. Light yellow solid, 147 mg (0.60 mmol), 97 % yield, m.p. = 38-39 °C.
^{1}H-NMR (300 MHz, DMSO-*d*$_6$) δ 9.278 and 9.274 (s, 1H, *syn* and *anti* conformations), 7.63 – 7.14 (m, 5H), 5.35 (s, 2H), 3.05 – 2.74 (m, 1H), 1.84 – 1.61 (m, 5H), 1.48 – 1.44 (m, 2H), 1.32 – 1.01 (m, 3H).
$^{13}C\{^1H\}$-NMR (75 MHz, DMSO-*d*$_6$) δ 190.9, 161.5, 136.7, 128.5, 128.2, 128.0, 77.3, 34.6, 26.9, 25.7, 25.4.
ESI-HRMS (positive): calculated for $C_{15}H_{20}NO_2$ $[M+H]^+$, 246.1489; found 246.1486 ± 3.5 x 10^{-4} u, averaged from six measurements.

5.3.9 General procedure for the photocyclization of 2-(hydroxyimino)aldehydes

The 2-(hydroxyimino)aldehyde or alkylated 2-(hydroxyimino)aldehyde (0.060 – 0.075 mmol, 1.0 equiv) is dissolved in the appropriate deuterated solvent (600 – 750 µL, C =

0.1 M) and placed in an NMR quartz tube. The sample is placed in the photoreactor (see section **1.1** of the supporting information) and irradiated with a 365 nm LED light source while thermostated at 25 °C with a cooling fan. Reaction completion is monitored with ^{1}H-NMR until disappearance of the aldehydic proton of the 2-(hydroxyimino)aldehyde.

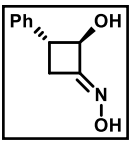

(±)-2-hydroxy-3-phenylcyclobutan-1-one oxime (2a). Reaction performed on 11 mg (0.062 mmol) of 2-(hydroxyimino)-4-phenylbutanal (**1a**). Conversion > 99 %, 99% yield, dr (*trans:cis*) = 1 : 0.8, isolated 11 mg as colourless oil, characterized without purification. Diastereomeric ratio determined via ^{1}H-NMR.

^{1}H-NMR (300 MHz, DMSO-*d*$_6$) δ 10.51 (s, 1H, *trans* diastereomer), 10.46 (s, 1H, *cis* diastereomer), 7.34 – 7.15 (m, 5H + 5H, both diastereomers), 6.05 (d, *J* = 8.0 Hz, 1H, *cis* diastereomer), 5.49 (d, *J* = 6.6 Hz, 1H, *trans* diastereomer), 5.07 – 4.96 (m, 1H, *trans* diastereomer), 4.63 (td, *J* = 7.8, 2.9 Hz, 1H, *cis* diastereomer), 3.58 (td, *J* = 8.7, 6.0 Hz, 1H, *trans* diastereomer), 3.23 (td, *J* = 9.4, 7.0 Hz, 1H, *cis* diastereomer), 3.07 (ddd, *J* = 16.1, 9.9, 2.9 Hz, 1H, *cis* diastereomer), 2.91 (ddd, *J* = 16.9, 9.1, 0.8 Hz, 1H, *trans* diastereomer), 2.79 (ddd, *J* = 16.9, 6.0, 2.8 Hz, 1H, *trans* diastereomer), 2.47 – 2.39 (m, 1H, *cis* diastereomer, partially overlapped with residual DMSO signal).

^{13}C{^{1}H}**-NMR** (75 MHz, DMSO-*d*$_6$) *trans* diastereomer: δ 158.5, 139.7, 128.6, 127.8, 126.0, 72.9, 41.2, 32.0; *cis* diastereomer: δ 157.2, 142.3, 128.4, 126.8, 126.4, 78.6, 45.3, 30.0.

ESI-HRMS (positive): calculated for $C_{10}H_{11}NO_2Na$ $[M+Na]^+$, 200.0682; found 200.0686 ± 4.5 x 10^{-4} u, averaged from five measurements.

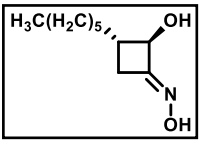

(±)-3-hexyl-2-hydroxycyclobutan-1-one oxime (2b). Reaction performed on 11 mg (0.062 mmol) of 2-(hydroxyimino)decanal (**1b**). Conversion > 99 %, 99% yield, dr (*trans:cis*) = 1 : 0.8, isolated 11

mg as colourless oil, characterized without purification. Diastereomeric ratio determined via ^{1}H-NMR.

^{1}H-NMR (300 MHz, DMSO-d_6) *trans* and *cis* diastereomers: δ 10.27 (s, 1H), 10.26 (s, 1H), 5.59 (d, J = 7.8 Hz, 1H), 5.42 (d, J = 7.2 Hz, 1H), 4.71 (dt, J = 7.2, 2.8 Hz, 1H), 4.20 (td, J = 7.5, 3.1 Hz, 1H), 2.71 (ddd, J = 15.9, 9.0, 3.1 Hz, 1H), 2.46 – 2.39 (m, 1H), 2.29 – 2.10 (m, 2H), 1.98 (dt, J = 12.2, 8.1 Hz, 1H), 1.91 – 1.80 (m, 1H), 1.31 – 1.14 (m, 20H), 0.91 – 0.78 (m, 6H).

^{13}C$_{\{^1H\}}$-NMR (75 MHz, DMSO-d_6) *trans* and *cis* diastereomers: δ 159.5, 157.9, 76.6, 71.5, 40.6, 35.7, 33.7, 31.3, 31.25, 30.8, 29.1, 28.9, 28.6, 28.4, 27.1, 26.9, 22.1, 14.0.

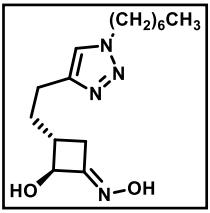

(±)-3-(2-(1-heptyl-1H-1,2,3-triazol-4-yl)ethyl)-2-hydroxycyclobutan-1-one oxime (2c). Reaction performed on 11 mg (0.037 mmol) of 6-(1-heptyl-1H-1,2,3-triazol-4-yl)-2-(hydroxyimino)hexanal (**1c**). Conversion > 99 %, 99% yield, isolated 11 mg as colourless oil, dr (*trans:cis*) = 1 : 0.8, characterized without purification. Diastereomeric ratio determined via ^{1}H-NMR.

^{1}H-NMR (300 MHz, DMSO-d_6) *trans* and *cis* diastereomers: δ 10.33 (s, 1H), 10.30 (s, 1H), 7.84 (s, 2H), 5.67 (d, J = 7.7 Hz, 1H), 5.53 (d, J = 7.2 Hz, 1H), 4.76 (dt, J = 7.2, 2.9 Hz, 1H), 4.35 – 4.31 (m, 1H), 4.27 (t, J = 7.1 Hz, 4H), 2.72 (ddd, J = 16.0, 9.1, 3.2 Hz, 1H), 2.62 (t, J = 7.6 Hz, 4H), 2.39 – 2.19 (m, 2H), 2.11 – 1.81 (m, 4H), 1.81 – 1.70 (m, 4H), 1.61 – 1.46 (m, 2H), 1.35 – 1.10 (m, 20H), 0.84 (t, J = 6.8 Hz, 6H).

^{13}C$_{\{^1H\}}$-NMR (75 MHz, DMSO-d_6) *trans* and *cis* diastereomers: δ 159.2, 157.7, 146.8, 146.4, 121.7, 121.6, 76.4, 71.5, 49.1, 40.2, 35.2, 33.4, 31.1, 30.7, 29.7, 28.9, 28.7, 28.0, 25.8, 23.2, 23.1, 22.0, 13.9, 13.9.

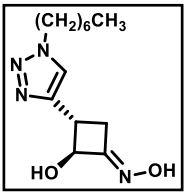

(±)-3-(1-heptyl-1H-1,2,3-triazol-4-yl)-2-hydroxycyclobutan-1-one oxime (2d). Reaction performed on 13 mg (0.045 mmol) of 4-(1-heptyl-1H-1,2,3-triazol-4-yl)-2-(hydroxyimino)butanal (**1d**). Conversion > 99 %, 99% yield, dr (*trans:cis*) = 1 : 0.8, isolated 13 mg as colourless oil, characterized without purification. Diastereomeric ratio determined via ^{1}H-NMR.

^{1}H-NMR (300 MHz, DMSO-*d*$_6$) *trans* and *cis* diastereomers: δ 10.52 (s, 1H), 10.50 (s, 1H), 8.02 (s, 1H), 7.85 (s, 1H), 6.04 (d, *J* = 8.1 Hz, 1H), 5.56 (d, *J* = 6.9 Hz, 1H), 4.98 (t, *J* = 7.0 Hz, 1H), 4.70 (td, *J* = 7.4, 2.9 Hz, 1H), 4.30 (t, *J* = 7.1 Hz, 4H), 3.69 (dd, *J* = 15.3, 7.9 Hz, 1H), 3.32 – 3.23 (m, *J* = 9.4, 7.2 Hz, 1H), 3.07 (ddd, *J* = 16.4, 10.1, 3.1 Hz, 1H), 2.94 – 2.86 (m, 4H), 2.53 – 2.43 (m, 1H), 1.85 – 1.70 (m, *J* = 14.0, 7.0 Hz, 4H), 1.35 – 1.11 (m, 14H), 0.85 (t, *J* = 6.8 Hz, 6H).

^{13}C{^{1}H}**-NMR** (75 MHz, DMSO-*d*$_6$) *trans* and *cis* diastereomers: δ 158.2, 157.1, 147.7, 144.8, 122.8, 121.7, 77.9, 72.2, 49.3, 49.2, 36.8, 33.3, 31.5, 31.1, 30.4, 29.8, 29.7, 28.1, 28.1, 25.8, 22.0, 13.9.

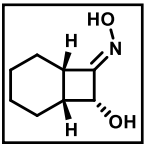

(±)-*Endo*-*cis*-(*E*)-8-hydroxybicyclo[4.2.0]octan-7-one oxime (2j). Reaction performed on 11 mg (0.062 mmol) of 2-cyclohexyl-2-(hydroxyimino)ethanal (**1j**). Conversion > 99 %, 99% yield, isolated 11 mg as thick colourless oil, characterized without purification.

^{1}H-NMR (300 MHz, DMSO-*d*$_6$) δ 9.93 (s, 1H), 5.37 (d, *J* = 6.6 Hz, 1H), 4.63 – 4.31 (m, 1H), 2.85 – 2.61 (m, 1H), 2.41 – 1.98 (m, 2H), 1.61 – 1.23 (m, 5H), 1.17 – 0.92 (m, 2H).

^{13}C{^{1}H}**-NMR** (75 MHz, DMSO-*d*$_6$) δ 160.6, 69.8, 36.9, 32.8, 23.2, 22.7, 22.1, 21.0.

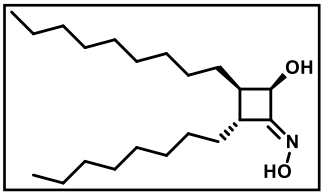

(±)-2-hydroxy-3-nonyl-4-octylcyclobutan-1-one oxime (2i). Please note that since the HIA **1i** possesses two different γ hydrogen, it is possible to also form the 2-decyl-3-heptyl-4-hydroxycyclobutan-1-one oxime regioisomer, the two being indistinguishable from one another through NMR analysis. Reaction performed on 10 mg (0.03 mmol) of 2-(hydroxyimino)-3-octyltridecanal (**1i**).Conversion > 99 %, 99% yield, isolated 11 mg as thick colourless oil, characterized without purification.

^{1}H-NMR (300 MHz, DMSO-d_6) δ 10.16 (s, 1H), 5.44 (d, J = 7.1 Hz, 1H), 4.02 (t, J = 6.3 Hz, 1H), 2.28 (td, J = 8.4, 5.1 Hz, 1H), 1.95 – 1.81 (m, 1H), 1.67 (dt, J = 13.7, 7.0 Hz, 1H), 1.55 – 1.39 (m, 3H), 1.31 – 1.19 (m, 26H), 0.85 (t, J = 6.4 Hz, 6H).

^{13}C$\{^{1}$H$\}$**-NMR** (75 MHz, DMSO-d_6) δ 159.9, 73.8, 45.8, 44.4, 33.7, 33.7, 31.3, 31.3, 30.5, 29.1, 29.0, 29.0, 28.9, 28.7, 28.6, 27.0, 26.9, 26.5, 26.5, 22.1, 13.9.

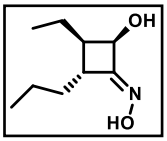

(±)-3-ethyl-2-hydroxy-4-propylcyclobutan-1-one oxime (2h). Reaction performed on 11 mg (0.064 mmol) of 2-(hydroxyimino)-3-propylhexanal (**1h**). Conversion > 99 %, 99% yield, isolated 11 mg as thick colourless oil, characterized without purification.

^{1}H-NMR (300 MHz, DMSO-d_6) tabulation referred to the major diastereomer: δ 10.18 (s, 1H), 5.47 (d, J = 7.1 Hz, 1H), 4.05 (t, J = 6.0 Hz, 1H), 2.31 (td, J = 8.4, 4.8 Hz, 1H), 1.97 – 1.81 (m, 1H), 1.68 – 1.22 (m, 6H), 0.95 – 0.79 (m, 6H).

^{13}C$\{^{1}$H$\}$**-NMR** (75 MHz, DMSO-d_6)) tabulation referred to the major diastereomer: δ 159.8, 73.5, 47.7, 44.0, 32.9, 26.5, 19.9, 14.1, 11.8.

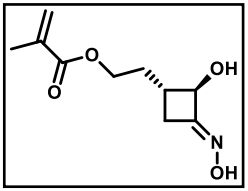

(±)-2-(2-hydroxy-3-(hydroxyimino)cyclobutyl)ethyl 2-methylprop-2-enoate (2f). Reaction performed on 13 mg (0.061 mmol) of 5-(hydroxyimino)-6-oxohexyl 2-methylprop-2-enoate (**1f**). Conversion > 99 %, 99% yield, isolated 13 mg as thick colourless oil, characterized without purification.

^{1}H NMR (300 MHz, DMSO-d_6) *trans* and *cis* diastereomers: δ 10.36 (s, 1H), 10.32 (s, 1H), 6.08 – 5.94 (m, 1H), 5.68 – 5.59 (m, 3H), 4.82 – 4.72 (m, 1H), 4.37 – 4.22 (m, 1H), 4.19 – 4.04 (m, 2H), 4.02 – 3.77 (m, 2H), 2.74 (ddd, J = 15.9, 8.7, 3.4 Hz, 1H), 2.44 – 2.22 (m, 2H), 2.16 – 1.46 (m, 11H), 1.18 – 0.48 (m, 4H).

^{13}C{^{1}H} **NMR** (75 MHz, DMSO-d_6) *trans* and *cis* diastereomers: δ 166.6, 166.6, 158.9, 157.7, 136.0, 136.0, 125.7, 125.6, 76.3, 71.4, 63.2, 63.1, 37.9, 32.5, 32.3, 30.8, 29.0, 27.9, 18.0.

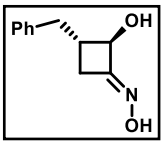

(±)-3-benzyl-2-hydroxycyclobutan-1-one oxime (2e). Reaction performed on 15 mg (0.078 mmol) of 5-(hydroxyimino)-6-oxohexyl 2-methylprop-2-enoate (**1e**). Conversion > 99 %, 99% yield, isolated 15 mg as thick colourless oil, characterized without purification.

^{1}H NMR (300 MHz, DMSO-d_6) *cis* and *trans* diastereomers: δ 10.39 (s, 1H), 10.34 (s, 1H), 7.30 – 7.14 (m, 10H), 5.74 – 5.52 (m, 2H), 4.82 (m, 1H), 4.36 (m, 1H), 2.98 – 2.84 (m, 2H), 2.75 – 2.53 (m, 4H), 2.32 – 2.21 (m, 3H), 2.03 (dd, J = 16.4, 8.2 Hz, 1H).

^{13}C{^{1}H} **NMR** (75 MHz, DMSO-d_6) *cis* and *trans* diastereomers: δ 158.9, 157.6, 140.7, 140.1, 128.8, 128.6, 128.3, 128.3, 125.9, 125.7, 76.1, 71.5, 41.5, 39.1, 37.2, 34.2, 30.6, 29.0.

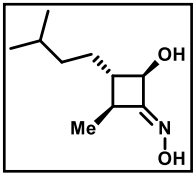

(±)-2-hydroxy-3-isopentyl-4-methylcyclobutan-1-one oxime (2g). Reaction performed on 10 mg (0.054 mmol) of 2-(hydroxyimino)-3,7-dimethyloctanal (**1g**). Conversion > 99 %, 99%

yield, isolated 10 mg as thick colourless oil, characterized without purification.

^{1}H NMR (300 MHz, DMSO-d_6) tabulation referred to the major (*2R,3S,4S,E*) diastereomer: δ 10.12 (s, 1H), 5.47 (d, J = 7.6 Hz, 1H), 4.01 (t, J = 6.6 Hz, 1H), 2.37 – 2.20 (m, 1H), 1.56 – 1.39 (m, 2H), 1.26 (d, J = 7.1 Hz, 3H), 1.25 – 1.00 (m, 3H), 0.84 (d, J = 6.6 Hz, 6H).

^{13}C$\{^1$H$\}$ **NMR** (75 MHz, DMSO) δ 160.7, 73.7, 48.6, 36.2, 30.8, 27.5, 22.5, 22.4, 17.0.

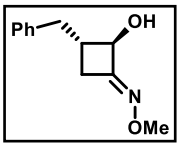

(±)-3-benzyl-2-hydroxycyclobutan-1-one O-methyl oxime (2l). Reaction performed on 34 mg (0.166 mmol) of 2-(methoxyimino)-5-phenylpentanal **(1l)**. Purification via flash chromatography using as eluant a mixture of pentane/CH_2Cl_2 in gradient from 4:1 to 1:1 followed by a mixture of pentane/CH_2Cl_2/Et_2O in gradient from 50:50:1 to 10:10:1. Colourless oil, 29 mg (0.141 mmol), 85 % yield as sum of *cis*/*trans* diastereomers, dr (*cis:trans*) = 1:1.3.

^{1}H NMR (600 MHz, CD_2Cl_2) *cis* diastereomer: δ 7.32 – 7.28 (m, 2H), 7.25 – 7.19 (m, 3H), 5.02 (ddd, *J* = 8.2, 6.8, 3.0 Hz, 1H), 3.86 (s, 3H), 3.08 (dd, *J* = 14.3, 6.0 Hz, 1H), 2.89 – 2.73 (m, 1H), 2.64 – 2.56 (m, 2H), 2.53 (ddd, *J* = 17.3, 4.7, 3.0 Hz, 1H), 2.36 (d, *J* = 6.6 Hz, 1H). *trans* diastereomer: δ 7.34 – 7.30 (m, 2H), 7.25 – 7.20 (m, 3H), 4.58 (td, *J* = 6.4, 3.2 Hz, 1H), 3.82 (s, 3H), 2.99 – 2.89 (m, 2H), 2.84 (dd, *J* = 14.1, 7.8 Hz, 1H), 2.51 – 2.44 (m, 1H), 2.33 (d, *J* = 6.9 Hz, 1H), 2.18 (dd, *J* = 16.7, 8.5 Hz, 1H).

^{13}C$\{^1$H$\}$ **NMR** (75 MHz, CD_2Cl_2) *cis* diastereomer: δ 157.9 , 139.1, 128.2, 128.0, 125.6, 76.1 61.1, 41.5, 39.1, 29.4. *trans* diastereomer: δ 159.5, 139.7, 128.4, 127.9, 125.8, 71.9, 61.2, 36.8, 33.6, 30.7.

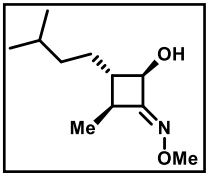

2-hydroxy-3-((3-methyl)-1-butyl)-4-methylcyclobutan-1-one O-methyl oxime (2m). Reaction performed on 27 mg (0.136 mmol) of 2-(hydroxyimino)-3,7-dimethyloctanal (**1m**). Purification via flash chromatography using as eluant a mixture of CH_2Cl_2/Et_2O in gradient from 100:1 to 30:1. Colourless oil, 24 mg (0.121 mmol), 89 % yield as sum of *trans*/*cis* diastereomers, dr (*trans:cis*) = 2 : 1.

^{1}H NMR (300 MHz, CD_2Cl_2) *trans* diastereomer: δ 4.24 (m, 1H), 3.79 (s, 3H), 2.71 (d, *J* = 6.4 Hz, 1H), 2.46 (p, *J* = 7.2 Hz, 1H), 1.68 – 1.54 (m, *J* = 7.2 Hz, 4H), 1.35 (d, *J* = 6.0 Hz, 3H), 1.23 – 1.28 (m, 2H), 0.90 (d, *J* = 6.6 Hz, 6H). *cis* diastereomer: δ 4.37 (dd, *J* = 6.3, 2.4 Hz, 1H), 3.72 (s, 3H), 2.99 (d, *J* = 2.5 Hz, 1H), 2.27 (dt, *J* = 13.8, 6.9 Hz, 1H), 1.61 – 1.59 (m, 1H), 1.57 – 1.45 (m, 2H), 1.20 – 1.11 (m, 6H), 0.90 (d, *J* = 6.6 Hz, 6H).

^{13}C{^{1}H} **NMR** (75 MHz, CD_2Cl_2) *trans* diastereomer: δ 161.6, 74.0, 61.1, 48.6, 40.2, 36.0, 30.8, 27.6 , 21.8, 21.8, 16.3. *cis* diastereomer: δ 161.7, 75.7 , 61.2, 47.1, 37.8, 36.0, 31.0, 27.5, 21.8 , 15.8.

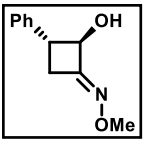

(±)-(*E*)-2-hydroxy-3-phenylcyclobutan-1-one O-methyl oxime (2k). Reaction performed on 19 mg (0.099 mmol) of 2-(methoxyimino)-4-phenylbutanal (**1k**). Purification via flash chromatography using as eluant CH_2Cl_2 followed by CH_2Cl_2/Et_2O in gradient from 50:1 to 10:1. Colourless oil, 18 mg (0.094 mmol), 95 % yield as sum of *cis*/*trans* diastereomers, dr (*E-trans:E-cis:Z-trans:Z-cis*) = 1 : 0.6 : 0.12 : 0.04.

^{1}H-NMR (300 MHz, DMSO-d_6) *E-trans* diastereomer: δ 7.32 – 7.24 (m, 2H), 7.22 – 7.15 (m, 3H), 5.62 (d, *J* = 6.5 Hz, 1H), 5.11 – 4.98 (m, 1H), 3.77 (s, 3H), 3.60 (td, *J* = 8.8, 5.8 Hz, 1H), 2.93 (ddd, *J* = 17.2, 9.3, 1.1 Hz, 1H), 2.78 (ddd, *J* = 17.2, 5.8, 2.9 Hz, 1H); *E-cis* diastereomer: δ 7.35 – 7.27 (m, 4H), 7.27 – 7.17 (m, 1H), 6.16 (d, *J* = 7.8 Hz, 1H), 4.65 (td, *J* = 7.6, 3.0 Hz, 1H), 3.76 (s, 3H), 3.24 (td, *J* = 9.5, 7.2 Hz, 1H), 3.05 (ddd, *J* = 16.2, 9.9, 2.9 Hz, 1H), 2.58 –

2.41 (m, 1H); *Z-trans* diastereomer: δ 7.36 – 7.11 (m, 5H), 5.52 (d, *J* = 6.9 Hz, 1H), 5.08 – 4.94 (m, 1H), 3.72 (s, 3H), 3.58 (dd, *J* = 16.4, 8.4 Hz, 1H), 3.02 – 2.81 (m, 2H); *Z-cis* diastereomer: δ 7.48 – 7.14 (m, 5H), 6.07 (d, *J* = 7.9 Hz, 1H), 4.65 (td, *J* = 7.7, 3.2 Hz, 1H), 3.71 (s, 3H), 3.24 (td, *J* = 10.0, 7.5 Hz, 1H), 2.90 (ddd, *J* = 16.2, 10.0, 3.0 Hz, 1H), 2.62 – 2.49 (m, 1H).

$^{13}C\{^1H\}$-NMR (75 MHz, DMSO-*d*$_6$) *E-trans* diastereomer: δ 160.2, 139.3, 128.6, 127.9, 126.1, 72.7, 61.1, 41.2, 32.3; *E-cis* diastereomer: δ 158.8, 141.9, 128.4, 126.8, 126.6, 78.4, 61.0, 45.1, 30.3; *Z-trans* diastereomer: δ 158.6, 139.1, 128.8, 127.8, 126.1, 72.4, 61.1, 40.3, 33.0.

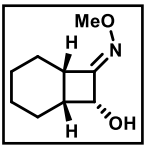

(±)-*Endo-cis*-(*E*)-8-hydroxybicyclo[4.2.0]octan-7-one O-methyl oxime (2n). Reaction performed on 30 mg (0.18 mmol, C = 0.3 M) of 2-cyclohexyl-2-(methoxyimino)ethanal (**1n**). Purification via chromatography over neutral Al_2O_3 using as eluant CH_2Cl_2/CH_3OH in ratio 70:1. Thick colourless oil, 28 mg (0.14 mmol), 93 % yield.

^{1}H-NMR (300 MHz, DMSO-*d*$_6$) δ 5.51 (d, *J* = 6.5 Hz, 1H), 4.53 (dd, *J* = 7.7, 6.6 Hz, 1H), 3.67 (s, 3H), 2.87 – 2.67 (m, 1H), 2.36 – 2.06 (m, 2H), 1.67 – 1.19 (m, 5H), 1.13 – 0.92 (m, 2H).

$^{13}C\{^1H\}$-NMR (75 MHz, DMSO-*d*$_6$) δ 162.3, 69.6, 61.1, 37.3, 32.6, 23.3, 22.6, 22.0, 21.0.

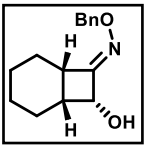

(±)-*Endo-cis*-(*E*)-8-hydroxybicyclo[4.2.0]octan-7-one O-benzyl oxime (2o). Reaction performed on 20 mg (0.082 mmol) of 2-((benzyloxy)imino)-2-cyclohexylethanal (**1o**). Purification via flash chromatography using as eluant CH_2Cl_2/Et_2O in gradient from 10:1 to 8:1. Light yellow oil, 19 mg (0.078 mmol), 95 % yield. Scale-up reaction performed on 265 mg (1.08 mmol) of 2-((benzyloxy)imino)-2-cyclohexylethanal (**1o**) in 4.3 mL of MeOH (C = 0.25 M) and 13 h reaction time. After flash chromatography 242 mg (0.99 mmol) of **2o** were obtained, 91 % yield.

^{1}H-NMR (300 MHz, DMSO-d_6) δ 7.48 – 7.05 (m, 5H), 5.55 (bs, 1H), 4.95 (s, 2H), 4.56 (d, J = 7.0 Hz, 1H), 2.81 (dd, J = 10.7, 4.3 Hz, 1H), 2.35 – 2.06 (m, 2H), 1.67 – 1.21 (m, 5H), 1.19 – 0.69 (m, 2H).
^{13}C{^{1}H}-NMR (75 MHz, DMSO-d_6) δ 163.0, 138.4, 128.2, 127.6, 127.5, 74.8, 69.7, 37.2, 32.6, 23.2, 22.6, 21.9, 21.0.
ESI-HRMS (positive): calculated for $C_{15}H_{20}NO_2$ $[M+H]^+$, 246.1489; found 246.1490 ± 4.0 x 10^{-4} u, averaged from five measurements.

5.3.10 General Procedure for the Synthesis of Enals

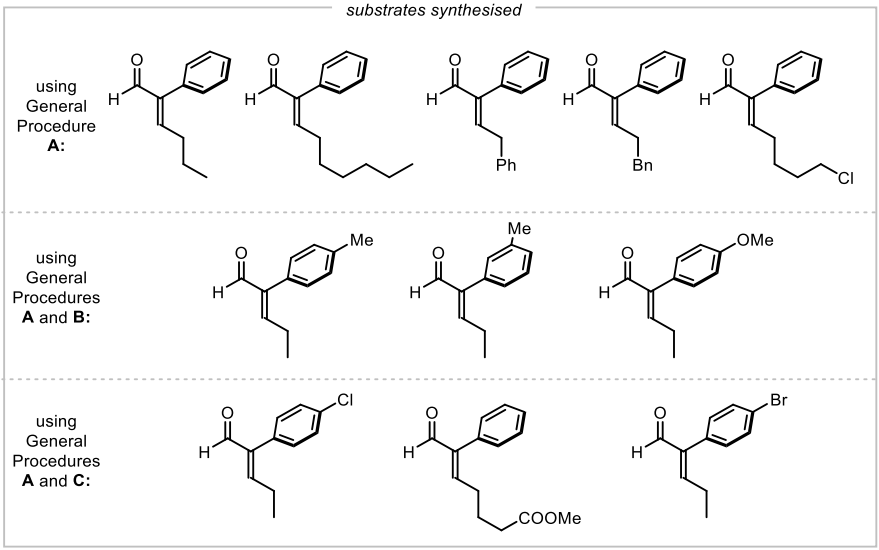

Figure 5.3 The enal substrates used in this study.

Pent-2-enal and 2-phenyl-pent-2enal are commercially available and were used without prior purification. Enals **5i–m** were prepared by aldol condensation from 2-phenyl acetaldehyde and butanal, heptenal, 2-phenyl acetaldehyde, hydrocinnamaldehyde and 5-chloro-pentanal respectively following general procedure **A**

described below. Substrates **5n, 5o, 5q** were prepared by a two-step sequence, starting from the corresponding styrene, following general procedure **B**, followed by aldol condensation using general procedure **A**. Enals **5p, 5r** and **5s** were prepared from the corresponding alcohol using general procedure **C** followed by general procedure **A**. The general procedures are based on reported protocols and were slightly modified.[118–120] All known products matched the spectroscopic data reported in literature.[97,98]

General Procedure A:

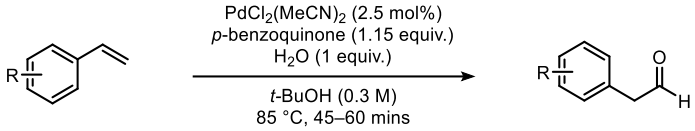

To a stirred solution of $PdCl_2(MeCN)_2$ (2.5 mol%) and benzoquinone (1.15 equiv.) in *t*-BuOH (0.3 M) was added distilled H_2O (1 equiv.) and the requisite styrene derivative (1 equiv.). The resulting mixture was stirred at 85 °C for 45–60 minutes (until consumption of starting material judged by TLC analysis). The solvent was removed under reduced pressure and the residue dissolved in CH_2Cl_2. The organic solution was washed once with water, brine, and then dried over anhydrous magnesium sulphate, filtered, and concentrated *in vacuo*. The aldehyde was further purified by vacuum distillation before use in the next step.

General Procedure B:

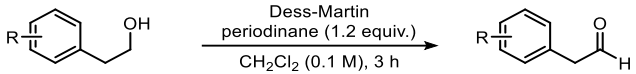

To a stirring solution of alcohol (1 equivs.) in DCM (0.1 M), Dess-Martin periodinane (1.2 equivs.) was added under argon. After 3h stirring, the reaction was quenched with saturated aqueous solutions of $NaHCO_3$ and $Na_2S_2O_3$ (20 mL). After 30 min, the resulting mixture was extracted with DCM (2 x 25 mL). The combined organic layers were washed with brine, dried over

$MgSO_4$, filtered, evaporated under reduced pressure, and purified by column chromatography (eluent: hexane/EtOAc 10:1) to give the corresponding aldehyde (yields ranging from 40% to 60%) as a colourless oil. The crude aldehyde was of sufficient purity and used for the next step without further purification.

General Procedure C:

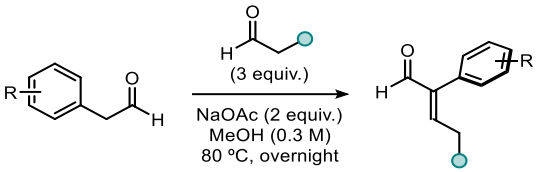

To a stirred solution of 2-aryl acetaldehyde (1 equiv.) in MeOH (0.3 m) was added the corresponding aldehyde (3 equiv.) and NaOAc (2 equiv.) and the resulting mixture was heated under reflux overnight. The MeOH was evaporated under reduced pressure and the residue suspended in a minimal amount of Et_2O. The organic solution was washed twice with brine, dried over anhydrous magnesium sulphate, filtered, and concentrated *in vacuo*. The residue was purified by column chromatography on silica (hexane/EtOAc) to afford the enal product.

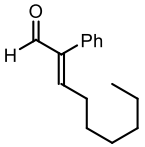

2-phenylnonen-2-enal

Synthesised according to General Procedure **A** using 2-phenyl-acetaldehyde and heptanaldehyde. The crude mixture was purified by flash column chromatography on silica gel (hexane/CH_2Cl_2 9:1 to 7:3) to afford product in 31% yield as a colourless oil.

HRMS (ESI$^+$) $C_{15}H_{20}O$ $[M+Na]^+$: found xxxx, required xxxx (ppm).

^{1}H NMR (500 MHz, CDCl3) δ 9.68 (s, 1H), 7.52 – 7.37 (m, 3H), 7.13 – 7.06 (m, 2H), 6.68 (d, J = 10.8, 1H), 3.59 – 3.45 (m, 1H), 1.33 (d, J = 8.3 Hz, 3H).

^{13}C NMR (126 MHz, CDCl3) δ 193.76, 156.71, 143.94, 132.66, 129.41, 128.21, 127.89, 31.51, 29.78, 28.94, 28.77, 22.51, 14.02.

(5-phenyl)2-phenylpent-2-enal

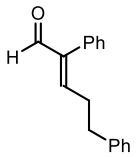

Synthesised according to General Procedure **A** using 2-phenyl-acetaldehyde and hydrocinnamaldehyde. The crude mixture was purified by flash column chromatography on silica gel (hexane/CH_2Cl_2 9:1 to 7:3) to afford product in 31% yield as a colourless oil.

^{1}H NMR (500 MHz, CDCl3) δ 9.60 (s, 1H), 7.40 – 7.27 (m, 5H), 7.21 (m, 1H), 7.17 – 7.09 (m, 2H), 7.10 – 7.00 (m, 2H), 2.82 (m, 2H), 2.74 – 2.64 (m, 2H).

^{13}C NMR (126 MHz, CDCl3) δ 193.72, 154.90, 144.64, 140.42, 132.55, 129.45, 128.70, 128.53, 128.38, 128.13, 126.51, 34.96, 31.52.

(7-chloro)-2-phenyheptan-2-enal

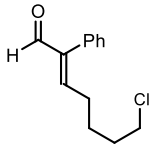

Synthesised according to General Procedure **A** using 2-phenyl-acetaldehyde and heptaldehyde. The crude mixture was purified by flash column chromatography on silica gel (hexane/CH_2Cl_2 8:2) to afford product in 38% yield as a colourless oil.

HRMS (ESI$^+$) $C_{15}H_{20}O$ $[M+Na]^+$: found 239.1512, required 239.1411 (ppm).

^{1}H NMR (500 MHz, CDCl3) δ 9.65 (s, 1H), 7.46 – 7.35 (m, 2H), 7.22 – 7.10 (m, 2H), 3.51 (t, J = 6.4 Hz, 2H), 2.43 (q, J = 7.5 Hz, 2H), 1.84 – 1.76 (m, 2H), 1.70 (dd, J = 8.5, 7.1 Hz, 2H), 0.90 (d, J = 7.0 Hz, 1H).

^{13}C NMR (126 MHz, CDCl3) δ 191.60, 147.21, 145.19, 130.54, 128.23, 128.65, 128.45, 38.41, 32.45, 30.60, 29.11, 29.05, 22.89.

Methyl (*E*)-7-oxo-6-phenylhept-5-enoate

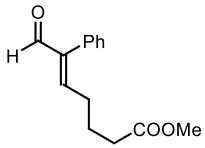

Synthesised according to General Procedures **A** using 2-phenyl-acetaldehyde and methyl-5-oxopentanoate. The crude mixture was purified by flash column chromatography on silica gel (hexane/CH_2Cl_2 8:2 to 7:3) to afford product in 45% yield as a colourless oil.

HRMS (ESI+) $C_{14}H_{16}O_3$ [M+Na]+: found: 255.0990, required 255.0992 (0.8 ppm).
^{1}H NMR (300 MHz, $CDCl_3$) δ_H: 9.62 (s, 1H), 7.43 – 7.31 (m, 3H), 7.22 – 7.08 (m, 2H), 6.69 (t, *J* = 7.5 Hz, 1H), 3.63 (s, 3H), 2.41 (q, *J* = 7.5 Hz, 2H), 2.31 (t, *J* = 7.4 Hz, 2H), 1.84 (p, *J* = 7.5 Hz, 2H).
^{13}C NMR (75 MHz, $CDCl_3$) δ 193.49, 173.32, 154.53, 144.65, 132.36, 129.37, 128.31, 128.07, 51.63, 33.32, 29.04, 23.97.

5.3.11 Catalysts Synthesis

Aminocatalysts **A, B** and **F** were purchased from Sigma Aldrich and used as received. Aminocatalysts **C**, **D** and **E** were synthesized from *trans*-4-Hydroxy-*L*-proline following a reported 5-step route described below.[3] All the intermediates S1-S4 matched the spectroscopic characterization reported in literature.[121] The characterization data for catalyst **E** is reported below.

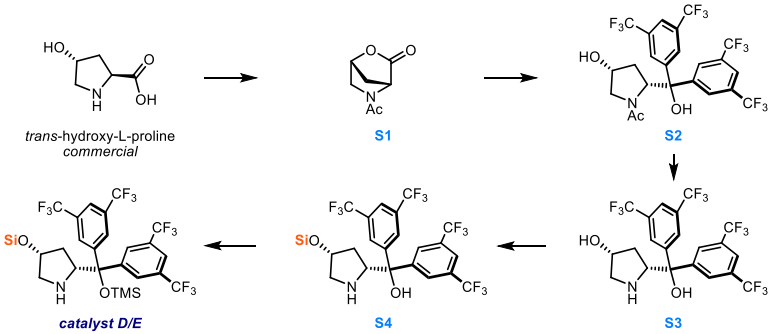

Scheme 5.1 Synthetic route to catalysts **D** and **E**.

(1*R*,4*R*)-5-Acetyl-2-oxa-5-azabicyclo[2.2.1]heptan-3-one (S1)

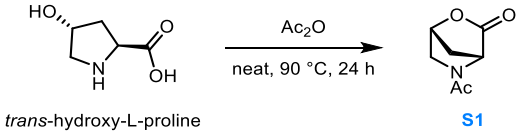

A suspension of *trans*-4-hydroxy-*L*-proline (10.0 g, 76 mmol) in acetic anhydride (50 mL, 534 mmol) was stirred at 90 °C for 24 h.

Upon completion, the reaction mixture was cooled to room temperature and concentrated under reduced pressure. *i*-PrOH (50 mL) was added under rapid stirring and the resulting mixture was stored in the freezer at –20 °C for 16 h. The resulting white precipitate was filtered off and washed with hexane (3 x 25 mL). Drying under vacuum afforded lactone **S1** (7.1 g, 60%) as a white solid, which was sufficiently pure to be taken on to the next step.

1-((2*R*,4*R*)-2-(Bis(3,5-bis(trifluoromethyl)phenyl)(hydroxy)methyl)-4-hydroxypyrrolidin-1-yl)ethan-1-one (S2)

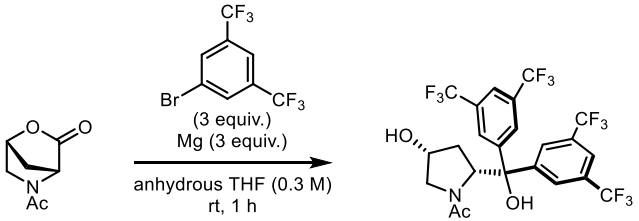

S1 S2

In an oven-dried two-necked round bottom flask, equipped with a septum and condenser, Mg turnings (3.3 g, 137 mmol) were stirred under vacuum for 30 minutes. Anhydrous THF (60 mL) was added, followed by one crystal of I_2. 1-Bromo-3,5-bis(trifluoromethyl)benzene (25.2 mL, 137 mmol) was added dropwise, maintaining a controlled exothermic reaction while the colour changed gradually from red-brown to grey. After the solution cooled to room temperature, lactone **S1** (7.1 g, 46 mmol) was added in one portion, and the reaction stirred for 1 h. The mixture was cooled to 0 °C and carefully quenched with aqueous HCl (1 N, 100 mL). The mixture was extracted with CH_2Cl_2 (3 x 50 mL) and the combined organic layers washed once with brine, dried over anhydrous magnesium sulphate, filtered, and then concentrated *in vacuo* to afford prolinol **S2** as a dark brown oil which was sufficiently pure to be taken on to the next step.

(3*R*,5*R*)-5-(bis(3,5-bis(trifluoromethyl)phenyl)(hydroxy)methyl)-pyrrolidin-3-ol (S3)

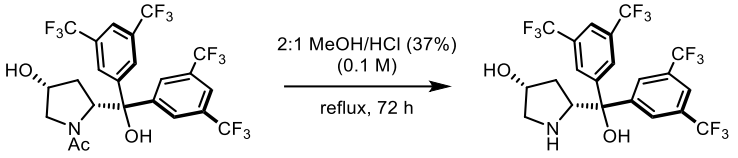

S2 S3

A suspension of prolinol **S2** (2.80 g, 4.80 mmol) and conc. HCl (37% in water, ca. 12 M, 15 mL) in MeOH (30 mL) was heated to reflux for 72 h. Excess MeOH removed *in vacuo* and the remaining solution was neutralized by careful addition of saturated aqueous Na_2CO_3. Addition was continued with frequent testing of the solution with pH indicator paper until a pH of ~10 was measured. The mixture was then extracted with CH_2Cl_2 (3 x 25 mL). The combined organic layers were washed once with brine, dried over anhydrous magnesium sulphate, filtered and concentrated in vacuo to afford a brown foam. The crude product was purified by column chromatography on silica (hexane/EtOAc 1:1) to afford prolinol **S3** (1.90 g, 72%) as a light brown foam.

Bis(3,5-bis(trifluoromethyl)phenyl)((2*R*,4*R*)-4-(((2,3-dimethylbutan-2-yl)dimethylsilyl)oxy)pyrrolidin-2-yl)methanol (S4)

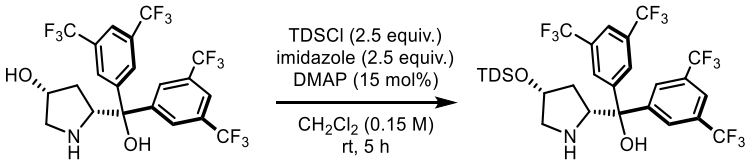

S3 S4

To a rapidly stirred solution of prolinol **S3** (3.30 g, 6.10 mmol), imidazole (1.04 g, 15.2 mmol), and DMAP (112 mg, 0.91 mmol) in CH_2Cl_2 (40 mL) was added TDSCl (2.94 g, 15.24 mmol) dropwise at room temperature. The solution was stirred at room temperature for 5 h, before H_2O (30 mL) was added. The mixture was extracted with CH_2Cl_2 (3 x 50 mL), and the combined organic layers were

washed once with brine, dried over anhydrous magnesium sulphate, filtered, and concentrated *in vacuo* to afford crude prolinol **S4** as a light brown oil which was sufficiently pure to be taken on to the next step.

(2*R*,4*R*)-2-(Bis(3,5-bis(trifluoromethyl)phenyl)((trimethylsilyl)oxy)-methyl)-4-(((2,3-dimethylbutan-2-yl)dimethylsilyl)oxy)pyrrolidine (catalyst E)

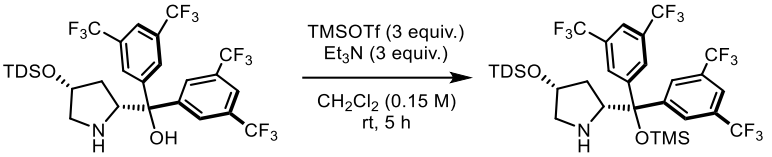

S4 *catalyst E*

To a solution of prolinol **S4** (4.17 g, 6.10 mmol) and triethylamine (2.6 mL, 18.29 mmol) in CH_2Cl_2 (40 mL) was added TMSOTf (3.3 mL, 18.29 mmol) dropwise at 0 °C under strong stirring. The resulting solution was stirred at 23 °C for 5 h. The reaction was quenched with H_2O and extracted with CH_2Cl_2 (3 x 50 mL). The organic layer was washed with brine, dried over anhydrous magnesium sulphate, filtered, and concentrated *in vacuo* to afford a brown oil. Purification by silica gel column chromatography (hexane/Et_2O 98:2) to afford catalyst **E** (3.46 g, 75% over two steps) as a pale-yellow oil.

HRMS (ESI$^+$) $C_{32}H_{42}F_{12}NO_2Si_2$ $[M+H]^+$: found 756.2588, required 756.2557 (+4.1 ppm).

^{1}H NMR (500 MHz, $CDCl_3$) δ_H: 7.98 (s, 2H), 7.84 (s, 2H), 7.80 (s, 2H), 4.21 (ddd, J = 7.0, 4.0, 1.1 Hz, 1H), 3.99 (dd, J = 9.4, 7.4 Hz, 1H), 2.90 (dd, J = 11.7, 5.9 Hz, 1H), 2.42 (dd, J = 11.7, 4.8 Hz, 1H), 1.88 (dt, J = 13.8, 7.2 Hz, 1H), 1.49 (p, J = 6.9 Hz, 1H), 1.30 (ddd, J = 13.1, 9.5, 5.9 Hz, 1H), 0.77 (d, J = 6.9 Hz, 6H), 0.71 (d, J = 2.9 Hz, 6H), -0.02 (d, J = 1.8 Hz, 6H), -0.07 (s, 9H).

^{13}C NMR (126 MHz, $CDCl_3$) δ_C: 148.3, 146.2, 131.8 (q, $^2J_{CF}$ = 33 Hz), 131.3 (q, $^2J_{CF}$ = 33 Hz), 128.9 (d, $^3J_{CF}$ = 2.5 Hz), 128.1 (d, $^3J_{CF}$ = 2.5 Hz), 123.4 (dd, $^1J_{CF}$ = 272.1, 14.4 Hz), 122.0 (m, overlapped

signals), 82.1, 72.2, 64.5, 55.8, 37.9, 34.2, 24.8, 20.3, 20.3, 18.6, 18.5, 2.0, –2.71.
^{19}F NMR (471 MHz, $CDCl_3$) δ_F: -62.83 (s, 6F), -62.89 (s, 6F).

5.3.12 General Procedures for the asymmetric γ-perfluoroalkylation of enals

General Procedure A: γ-fluoroalkyation using liquid or solid perfluoroalkyl iodides

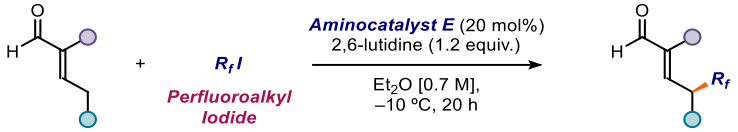

To an oven-dried 8 mL vial, equipped with a Teflon septum screw cap and a magnetic stirring bar, were added, sequentially, aminocatalyst **E** (40 μmol, 20 mol%), degassed Et_2O (300 μL, 0.7 M), enal **5** (600 μmol, 3 equiv.), 2,6-lutidine (240 μmol, 1.2 equiv.), and perfluoroalkyl iodide **6** (200 μmol, 1 equiv.). The vial was purged with argon before being capped and sealed with parafilm and placed in the photoreactor set-up with the LED irradiance fixed at 100 mW/cm^2. The reaction was stirred at –10 °C for 18 hours, before subjection of the mixture to silica gel column chromatography (silica pre-treated with triethylamine, elution solvent pre-cooled to <10 °C). The enantiomeric excess of the product was determined by conversion of the aldehyde product to the corresponding 2,4-dinitrophenyl hydrazone prior to chiral UPC^2 analysis. The purified γ-perfluoroalkyl enal **7** was dissolved in 1 mL of CH_2Cl_2 and 1 mL of MeOH then 2,4-dinitrophenyl hydrazine hydrochloride (1.5 equiv) and 3 drops of concentrated HCl were added. The mixture was stirred for 10 minutes, then the solvents evaporated and the crude purified with preparative TLC on silica gel (hexane/EtOAc 9:1). **Notes**: if the enal **5** appeared of an intense yellow colour, instead of colourless or very pale yellow, it was dissolved in unstabilized Et_2O, filtered on a pad of activated

charcoal and the solvent removed under reduced pressure. If the radical precursor **6** appeared pink/purple for the presence of I_2, it was washed with a saturated solution of $Na_2S_2O_3$ and dried over $MgSO_4$ prior to use.

General Procedure B: γ-trifluoromethylation of enals (gas reagent)

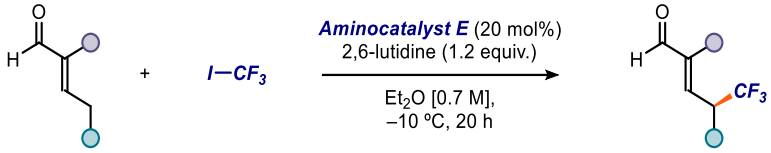

An argon-purged Schlenk tube, equipped with a rubber septum and a magnetic stirring bar, was cooled in a dry-ice/acetone bath to –78 °C. Under a gentle flow of Argon, trifluoromethyl iodide (1 equiv.) was condensed in the tared Schlenk tube using a rubber tube fitted with an 18-gauge needle (see Figure **5.3**). Et_2O (300 μL), 2,6-lutidine (1.2 equiv.), enal (3 equiv.), aminocatalyst **E** (20 mol%) and DMSO (25 μL) were added sequentially, and the tube sealed with parafilm. The Schlenk tube was removed from the cooling bath and transferred to the pre-cooled photoreactor. The remainder of the procedure follows the instructions described in General Procedure A.

Figure 5.4 Setting up the trifluoromethylation reaction. Left: general setup used to condense CF_3I gas in the Schlenk tube. Right: zoom of the reactor cooled to condense the CF_3I.

(*S*,*E*)-4-(Perfluorobutyl)-2-phenylpent-2-enal (7a)

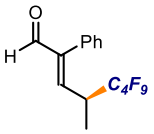

Synthesized according to General Procedure A using phenylpent-2-enal **5a** (96 mg, 600 µmol) and perfluorobutyl iodide (69 mg, 200 µmol). The crude mixture was purified by flash column chromatography on silica gel (hexane/CH_2Cl_2 8:2) to afford product **7a** (54 mg, 72% yield) as a colourless oil. The enantiomeric ratio of the product was determined by UPC^2 analysis on a Daicel Chiralpak IE column (eluent: CO_2/*i*-PrOH = 90:10; flow rate 2 mL/min, λ = 211 nm; τ_{minor} = 4.3 min, τ_{major} = 4.5 min), 93:7 er.

$[\alpha]_D^{20}$ = -56.1 (c=0.5, CH_3Cl)

^{1}H NMR (500 MHz, $CDCl_3$) δ_H: 9.68 (s, 1H), 7.55 – 7.35 (m, 3H), 7.13 – 7.08 (m, 2H), 6.64 (d, J = 10.4 Hz, 1H), 3.49 – 3.39 (m, 1H), 1.30 (d, J = 6.9 Hz, 3H).

^{13}C{^{1}H} NMR (126 MHz, $CDCl_3$) δ_C: 192.6, 146.4, 145.9, 131.4, 128.7 (2C), 128.7, 36.9, 13.0.

^{19}F NMR (471 MHz, $CDCl_3$) δ_F: –81.0 (t, J = 10.3 Hz, 3F), –115.5 – –120.0 (m, 2F), –120.3 – –122.8 (m, 2F), –124.6 – –127.1 (m, 2F).

HRMS (ESI+) $C_{15}H_{11}F_9O$ [M+Na]+: found: 401.0553, required 401.0558 (–1.2 ppm).

(*S*,*E*)-4-(Perfluoroisopropyl)-2-phenylpent-2-enal (7b)

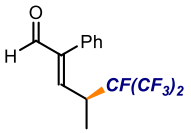

Synthesized according to General Procedure A using phenylpent-2-enal **5a** (96 mg, 600 µmol) and heptafluoro-2-iodopropane (28.5 µL, 200 µmol). The crude mixture was purified by flash column chromatography on silica gel (hexane/CH_2Cl_2 8:2) to afford product **7b** (47 mg, 71% yield) as a colourless oil. The enantiomeric ratio of the product was determined by UPC² analysis on a Daicel Chiralpak IE column (eluent: CO_2/*i*-PrOH = 90:10; flow rate 2 mL/min, λ = 211 nm: τ_{minor} = 4.5 min, τ_{major} = 4.7 min), 88:12 er.

$[\alpha]_D^{20}$ = -17.0 (c=0.5, CH_3Cl)

^{1}H NMR (500 MHz, $CDCl_3$) δ_H: 9.68 (s, 1H), 7.52 – 7.37 (m, 3H), 7.13 – 7.06 (m, 2H), 6.68 (d, J = 10.8, 1H), 3.59 – 3.45 (m, 1H), 1.33 (d, J = 8.3 Hz, 3H).

$^{13}C\{^1H\}$ NMR (126 MHz, $CDCl_3$) δ_C: 192.7, 146.8, 146.2, 131.2, 128.8, 128.7, 128.3, 35.4, 14.5.

^{19}F NMR (471 MHz, $CDCl_3$) δ_F: –73.1 (m, 6F), –178.4 (m, 1F).

HRMS (ESI+) $C_{14}H_{11}F_7O$ [M+Na]+: found 351.0581, required 351.0590 (–2.6 ppm).

(*S*,*E*)-4-(Perfluoropropyl)-2-phenylpent-2-enal (7c)

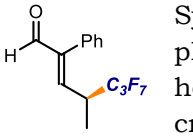

Synthesized according to General Procedure A using phenylpent-2-enal **5a** (96 mg, 600 µmol) and heptafluoro-1-iodopropane (28.5 µL, 200 µmol). The crude mixture was purified by flash column chromatography on silica gel (hexane/CH_2Cl_2 8:2) to afford product **7c** (39 mg, 60% yield) as a colourless oil. The enantiomeric ratio of the product was determined by UPC² analysis on a Daicel Chiralpak IE column (eluent: CO_2/*i*-PrOH = 90:10; flow rate 2 mL/min, λ = 375 nm: τ_{minor} = 6.3 min, τ_{major} = 6.6 min), 92:8 er.

$[\alpha]_D^{20}$ = +11.3 (c=0.5, CH_3Cl)
^1H NMR (500 MHz, $CDCl_3$) δ_H: 9.68 (s, 1H), 7.52 – 7.34 (m, 3H), 7.14 – 7.07 (m, 2H), 6.63 (d, J = 10.4 Hz, 1H), 3.53 – 3.33 (m, 1H), 1.30 (d, J = 6.9 Hz, 3H).
$^{13}C\{^1H\}$ NMR (126 MHz, $CDCl_3$) δ_C: 192.7, 146.4, 145.9, 131.4, 128.8, 128.7, 128.7, 36.7, 13.0.
^{19}F NMR (471 MHz, $CDCl_3$) δ_F: –80.8 (m, 3F), –116.1 – –120.9 (m, 2F), –123.5 – –126.8 (m, 2F).
HRMS (ESI$^+$) $C_{14}H_{11}F_7O$ $[M+Na]^+$: found 351.0592; required: 351.0590 (+0.6 ppm).

(*S*,*E*)-4-(Perfluoropentyl)-2-phenylpent-2-enal (7d)

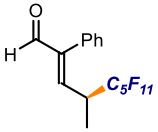

Synthesized according to General Procedure A using phenylpent-2-enal **5a** (96 mg, 600 µmol) and perfluoropentyl iodide (79 mg, 200 µmol). The crude mixture was purified by flash column chromatography on silica gel (hexane/CH_2Cl_2 8:2) to afford product **7d** (63 mg, 74% yield) as a colourless oil. The enantiomeric ratio of the product was determined by UPC^2 analysis on a Daicel Chiralpak IE column (eluent: CO_2/*i*-PrOH = 90:10; flow rate 2 mL/min, λ = 350 nm: τ_{minor} = 5.8 min, τ_{major} = 6.0 min), 89:11 er.
$[\alpha]_D^{20}$ = -40.7 (c=0.5, CH_3Cl)
^1H NMR (500 MHz, $CDCl_3$) δ_H: 9.68 (s, 1H), 7.52 – 7.35 (m, 3H), 7.13 – 7.08 (m, 2H), 6.64 (d, *J* = 10.5 Hz, 1H), 3.52 – 3.40 (m, 1H), 1.30 (d, *J* = 6.9 Hz, 3H).
$^{13}C\{^1H\}$ NMR (126 MHz, $CDCl_3$) δ_C: 192.6, 146.4, 145.9, 131.4, 128.7, 128.7, 128.7, 37.0, 13.0.
^{19}F NMR (471 MHz, $CDCl_3$) δ_F: –80.8 (m, 3F), –115.4 – –119.5 (m, 2F), –119.7 – –121.8 (m, 2F), –122.8 (m, 2F), –125.4 – –127.0 (m, 2F).
HRMS (ESI$^+$) $C_{16}H_{11}F_{11}O$ $[M+Na]^+$: found: 451.0511, required 451.0526 (–3.3 ppm).

(*S*,*E*)-4-(Perfluorohexyl)-2-phenylpent-2-enal (7e)

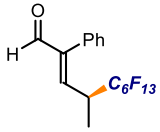

Synthesized according to General Procedure A using phenylpent-2-enal **5a** (96 mg, 600 µmol) and perfluorohexyl iodide (89 mg, 200 µmol). The crude mixture was purified by flash column chromatography on silica gel (hexane/CH_2Cl_2 8:2) to afford product **7e** (67 mg, 70% yield) as a white solid. The enantiomeric ratio of the product was determined by UPC² analysis on a Daicel Chiralpak IE column (eluent: CO_2/*i*-PrOH = 90:10; flow rate 2 mL/min, λ = 211 nm: τ_{minor} = 4.0 min, τ_{major} = 4.1 min), 91:9 er.
$[\alpha]_D^{20}$ = +22.3 (c=0.5, CH_3Cl)
^{1}H NMR (500 MHz, $CDCl_3$) δ_H: 9.68 (s, 1H), 7.47 – 7.37 (m, 3H), 7.13 – 7.07 (m, 2H), 6.64 (d, *J* = 10.5 Hz, 1H), 3.47 – 3.38 (m, 1H), 1.30 (d, *J* = 7.0 Hz, 3H).
$^{13}C\{^1H\}$ NMR (126 MHz, $CDCl_3$) δ_C: 192.6, 146.4, 145.9, 131.4, 128.7, 128.7, 128.7, 37.0, 13.0.
^{19}F NMR (471 MHz, $CDCl_3$) δ_F: –80.8 (m, 3F), –115.1 – –119.4 (m, 2F), –119.6 – –121.6 (m, 2F), –122.0 (m, 2F), –122.8 (m, 2F), –126.0 – –126.3 (m, 2F).
HRMS (ESI⁺) $C_{17}H_{11}F_{13}O$ $[M+H]^+$: found: 479.0685, required 479.0675 (+2.1 ppm).

(*S*,*E*)-4-(Perfluorooctyl)-2-phenylpent-2-enal (7f)

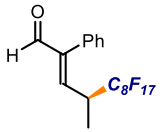

Synthesized according to General Procedure A using phenylpent-2-enal **5a** (96 mg, 600 µmol) and heptadecafluoro-1-iodooctane (53.5 µL, 200 µmol). The crude mixture was purified by flash column chromatography on silica gel (hexane/CH_2Cl_2 85:15) to afford product **7f** (65 mg, 56% yield) as a white solid. The enantiomeric ratio of the product was determined by UPC² analysis on a Daicel Chiralpak IB column (eluent: CO_2/EtOH = 97:3; flow rate 2 mL/min, λ = 375 nm. τ_{minor} = 3.3 min, τ_{major} = 3.5 min), 89:11 er.
$[\alpha]_D^{20}$ = +5.0 (c=0.5, CH_3Cl)
^{1}H NMR (500 MHz, $CDCl_3$) δ_H: 9.68 (s, 1H), 7.55 – 7.36 (m, 3H), 7.15 – 7.05 (m, 2H), 6.64 (d, *J* = 10.5 Hz, 1H), 3.51 – 3.38 (m, 1H), 1.30 (d, *J* = 7.0 Hz, 3H).

^{13}C NMR (126 MHz, $CDCl_3$) δ_C: 192.6, 146.43 145.9, 131.4, 128.7, 128.7, 128.7, 37.0, 13.0.
^{19}F NMR (471 MHz, $CDCl_3$) δ_F: –80.8 (t, *J* = 10.3 Hz, 3F), –115.3 – –119.3 (m, 2F), –119.4 – –121.5 (m, 2F), –121.6 – –122.0 (m, 6F), –122.7 (m, 2F), –126.1 (m, 2F).
HRMS (ESI$^+$) $C_{19}H_{11}F_{17}O$ $[M+Na]^+$: found 601.0431, required 601.0427 (–0.7 ppm).

(*S*,*E*)-4-(Perfluorodecyl)-2-phenylpent-2-enal (7g)

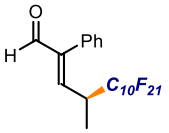

Synthesized according to General Procedure A using phenylpent-2-enal **5a** (96 mg, 600 µmol) and perfluorodecyl iodide (129 mg, 200 µmol). The crude mixture was purified by flash column chromatography on silica gel (hexane/CH_2Cl_2 8:2) to afford product **7g** (84 mg, 62% yield) as a white solid. The enantiomeric excess of the product was determined by chiral HPLC analysis on a Daicel Chiralpak IC-3 column (eluent: *n*-hexane/*i*-PrOH 80:20; flow rate 1 mL/min, λ = 254 nm: τ_{minor} = 13.3 min, τ_{major} = 17.0 min), 86:14 er.
$[\alpha]_D^{20}$ = -81.1 (c=0.5, CH_3Cl)
^{1}H NMR (500 MHz, $CDCl_3$) δ_H: 9.69 (s, 1H), 7.51 – 7.35 (m, 3H), 7.10 (m, 2H), 6.64 (d, *J* = 10.4 Hz, 1H), 3.52 – 3.40 (m, 1H), 1.30 (d, *J* = 6.8 Hz, 3H).
^{13}C{^{1}H} NMR (126 MHz, $CDCl_3$) δ_C: 192.6, 146.4, 145.9, 131.4, 128.7, 128.7, 128.7, 37.0, 13.1.
^{19}F NMR (471 MHz, $CDCl_3$) δ_F: –80.8 (t, *J* = 9.5 Hz, 3F), –115.6 – –119.2 (m, 2F), –119.6 – –121.5 (m, 2F), –121.9 (m, 10F), –122.7 (m, 2F), –126.2 (m, 2F).
HRMS (ESI$^+$) $C_{21}H_{11}F_{21}O$ $[M+Na]^+$: found 701.0374, required 701.0367 (+1.0 ppm).

Ethyl (S,E)-2,2-difluoro-3-methyl-6-oxo-5-phenylhex-4-enoate (7h)

Synthesized according to General Procedure A using phenylpent-2-enal **5a** (96 mg, 600 µmol) and ethyl 2,2-difluoro-2-iodoacetate

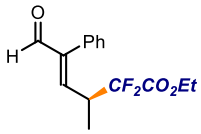

(50.0 mg, 200 µmol). The crude mixture was purified by flash column chromatography on silica gel (hexane/CH_2Cl_2 3:2) to afford product **7h** (37.9 mg, 67 % yield) as a colourless oil. The enantiomeric excess of the product was determined by chiral UPC^2 analysis on a Daicel Chiralpak IC-3 column (eluent: *n*-hexane/*i*-PrOH 80:20; flow rate 1 mL/min, λ = 254 nm: τ_{minor} = 2.2 min, τ_{major} = 2.1 min), 88:12 er.

$[\alpha]_D^{20}$ = -81.1 (c=0.5, CH_3Cl)

^{1}H NMR (500 MHz, $CDCl_3$) δ_H: 9.69 (s, 1H), 7.49 – 7.33 (m, 3H), 7.18 – 7.12 (m, 2H), 6.65 (d, *J* = 10.6 Hz, 1H), 4.38 – 4.22 (m, 2H), 3.53 – 3.36 (m, 1H), 1.31 (t, *J* = 7.2 Hz, 3H), 1.23 (d, *J* = 6.9 Hz, 3H).

$^{13}C\{^1H\}$ NMR (126 MHz, $CDCl_3$) δ_C: 193.0, 163.3, 148.0, 146.3, 131.6, 129.0, 128.6, 117.6, 115.6, 113.6, 63.1, 38.8, 29.7, 13.9, 13.1.

^{19}F NMR (471 MHz, $CDCl_3$) δ_F: -62.75 – -63.13 (m, 1F), -108.83 – -115.21 (m, 1F).

HRMS (ESI$^+$) $C_{15}H_{16}F_2O_3$ $[M+Na]^+$: found 305.0973, required 305.0960 (+4.3 ppm).

(S,E)-1,1,2,2-tetrafluoro-2-((1,1,2,2-tetrafluoro-3-methyl-6-oxo-5-phenylhex-4-en-1-yl)oxy)ethane-1-sulfonyl fluoride (7i)

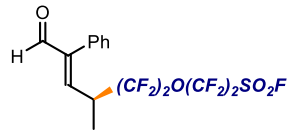

Synthesized according to General Procedure A using phenylpent-2-enal **5a** (96 mg, 600 µmol) and 1,1,2,2-tetrafluoro-2-(1,1,2,2-tetrafluoro-2-iodoethoxy)ethane-1-sulfonyl fluoride (85.2 mg, 200 µmol). The crude mixture was purified by flash column chromatography on silica gel (hexane/CH_2Cl_2 8:2) to afford product **7h** (36.4 mg, 40 % yield) as a colourless oil. The enantiomeric excess of the product was determined by chiral UPC^2 analysis on a Daicel Chiralpak IE column (eluent: *n*-hexane/*i*-PrOH 80:20; flow rate 2 mL/min, λ = 360 nm: τ_{minor} = 4.2 min, τ_{major} = 4.4 min), 84:16 er.

$[\alpha]_D^{20}$ = -81.1 (c=0.5, CH_3Cl)

^{1}H NMR (400 MHz, $CDCl_3$) δ_H: 9.70 (s, 1H), 7.51 – 7.36 (m, 3H), 7.17 – 7.07 (m, 2H), 6.63 (d, *J* = 10.5 Hz, 1H), 3.40 (dtq, *J* = 17.5, 10.5, 6.9 Hz, 1H), 1.32 (d, *J* = 6.9 Hz, 4H).
^{13}C{^{1}H} NMR (101 MHz, $CDCl_3$) δ_C: 192.6, 146.0, 131.2, 128.8, 128.7, 128.7, 36.4, 36.2, 36.2, 36.0, 29.7, 13.1.
^{19}F NMR (471 MHz, $CDCl_3$) δ_F: -81.99 (m, 2F), -83.00 – -85.33 (m, 2F), -112.20 (m, 2F), -118.52 – -123.09 (m, 2F).
HRMS (ESI$^+$) $C_{15}H_{11}F_9O_4S$ $[M+Na]^+$: found 481.0126, required 481.0127 (+0.2 ppm).

(*S*,*E*)-4-(Perfluorobutyl)-pent-2-enal 2,4-dinitrophenyl hydrazone (7x)

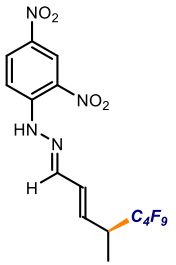

Synthesized according to General Procedure A using pent-2-enal **5x** (600 µmol, 50.5 mg) and perfluorobutyl iodide **6a** (69.2 mg, 200 µmol). To the crude mixture were added 1 mL of MeOH, 2,4-dinitrophenyl hydrazine hydrochloride (164.2 mg, 700 µmol) and 3 drops of concentrated HCl. After 10 minutes of stirring the solvents were evaporated and the crude mixture purified by flash column chromatography on silica gel (hexane/EtOAc 9:1) to afford product **7x** (30.2 mg, 50% yield) as an orange solid. The enantiomeric excess of the product was determined by UPC^2 analysis on a Daicel Chiralpak IE column (eluent: CO_2/IPA = 90:10; flow rate 2 mL/min, λ = 355 nm: τ_{minor} = 4.4 min, τ_{major} = 4.6 min), 50:50 er.
^{1}H NMR (400 MHz, $CDCl_3$) δ_H: 9.16 (d, *J* = 2.6 Hz, 1H), 8.36 (dd, *J* = 9.6, 2.6 Hz, 1H), 7.97 (d, *J* = 9.6 Hz, 1H), 7.82 (d, *J* = 9.1 Hz, 1H), 6.53 (dd, *J* = 15.7, 9.1 Hz, 1H), 6.16 (dd, *J* = 15.9, 8.6 Hz, 1H), 3.34 – 3.18 (m, 1H), 1.39 (d, *J* = 6.9 Hz, 3H).
^{13}C NMR (101 MHz, $CDCl_3$) δ_C: 150.3, 147.9, 144.6, 138.5, 136.8, 130.1, 130.0, 123.4, 116.7, 40.5, 30.9, 29.7, 13.0, 12.7.
^{19}F NMR (376 MHz, $CDCl_3$) δ_F: -81.01 (tt, *J* = 9.7, 3.1 Hz, 3F), -114.33 – -119.44 (m, 2F), -119.61 – -122.70 (m, 2F), -123.89 – -128.29 (m,2F).

HRMS (ESI+) $C_{15}H_{11}F_9N_4O_4$ $[M+Na]^+$: found 505.0531, required 505.0529 (+0.5 ppm).

(4*S*,7R,11R,*E*)-4-(Perfluorobutyl)-3,7,11,15-tetramethylhexadec-2-enal (7z)

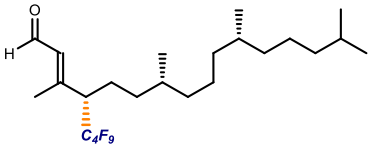

Synthesized according to General Procedure A using (7R,11R,E)-3,7,11,15-tetramethylhexadec-2-enal **5z** (300 µmol, 88.4 mg) and perfluorobutyl iodide **6a** (34.6 mg, 100 µmol). The crude mixture was purified by flash column chromatography on silica gel (pentane/CH_2Cl_2 8:2) to afford product **7z** (66.0 mg, 64% yield as a 1.5:1 mixture of *E* and *Z*) as a colourless oil. The enantiomeric excess of the product was determined by UPC² analysis on a Daicel Chiralpak IE column (eluent: CO_2/IPA = 90:10; flow rate 1 mL/min, λ = 360 nm: *Z* isomer: τ_{minor} = 5.8 min, τ_{major} = 5.9 min; *E* isomer: τ_{minor} = 6.4 min, τ_{major} = 6.8 min), *Z* isomer: 50:50 er; *E* isomer: 50:50 er.

^{1}H NMR (400 MHz, $CDCl_3$) δ_H: δ 10.09 (d, *J* = 7.6 Hz, 1H), 5.99 (d, *J* = 6.2 Hz, 1H), 2.99 – 2.83 (m, 1H), 2.21 (s, 3H), 2.02 – 1.83 (m, 1H), 1.84 – 1.65 (m, 1H), 1.53 (dq, *J* = 13.2, 6.6 Hz, 2H), 1.35 – 1.00 (m, 15H), 1.01 – 0.76 (m, 12H).

^{13}C NMR (101 MHz, $CDCl_3$) δ_C: 190.4, 190.4, 154.1, 154.1, 154.0, 153.9, 132.7, 132.7, 51.9, 51.7, 51.5, 51.3, 39.4, 37.4, 37.3, 37.3, 37.3, 36.6, 36.6, 34.0, 33.9, 33.7, 33.6, 32.8, 32.7, 32.6, 32.6, 32.5, 29.7, 28.0, 24.8, 24.4, 24.3, 22.7, 22.6, 22.5, 22.4, 19.7, 19.7, 19.6, 19.6, 19.3, 19.2, 14.8.

^{19}F NMR (376 MHz, $CDCl_3$) δ_F: -80.54 – -80.79 (m, 3F), -110.27 – -115.24 (m, 2F), -119.80 – -122.76 (m, 2F), -124.24 – -126.79 (m, 2F).

HRMS (ESI+) $C_{24}H_{37}F_9O$ $[M+Na]^+$: found 535.2601, required 535.2593 (+1.6 ppm).

(*S*,*E*)-4-(Perfluorobutyl)-3-phenylpent-2-enal (7y)

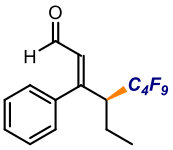

Synthesized according to General Procedure A using 3-phenylhex-2-enal (48.1 mg, 300 μmol) and perfluorobutyl iodide (34.6 mg, 100 μmol) The crude mixture was purified by flash column chromatography on silica gel (hexane/CH_2Cl_2 8:2) to afford product **7y** (12.4 mg, 31 % yield) as a colourless oil. The enantiomeric excess of the product was determined by UPC² analysis on a Daicel Chiralpak IE column (eluent: CO_2/MeOH = 90:10; flow rate 1 mL/min, λ = 360 nm: τ_{minor}= 7.2 min, τ_{major} = 7.4 min), 64:36 er.

$[\alpha]_D^{20}$ = -8.0 (c=0.5, CH_3Cl)

^{1}H NMR (400 MHz, $CDCl_3$) δ_H: δ 9.45 (d, *J* = 7.6 Hz, 1H), 7.54 – 7.38 (m, 3H), 7.38 – 7.26 (m, 2H), 6.37 (d, *J* = 7.6 Hz, 1H), 3.48 (m, 1H), 1.51 (d, *J* = 7.2 Hz, 3H).

$^{13}C\{^1H\}$ NMR (101 MHz, $CDCl_3$) δ_C: 192.8, 159.1, 136.8, 131.9, 129.6, 128.9, 128.6, 44.5, 44.3, 44.1.

^{19}F NMR (376 MHz, $CDCl_3$) δ_F: -81.01 (m, 3F), -108.15 – -117.95 (m, 2F), -120.86 (m, 2F), -125.76 – -126.22 (m, 2F).

HRMS (ESI⁺) $C_{15}H_{11}F_9O$ $[M+Na]^+$: found 401.0548, required 401.0558 (+2.7 ppm).

(*S*,*E*)-4-(Perfluorobutyl)-2-phenylhex-2-enal (7h)

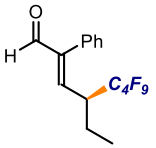

Synthesized according to General Procedure A using 2-phenylhex-2-enal **5b** (105 mg, 600 μmol) and perfluorobutyl iodide (69.2 mg, 200 μmol) The crude mixture was purified by flash column chromatography on silica gel (hexane/EtOAc 8:2) to afford product **7h** (49 mg, 62% yield) as a colourless oil. The enantiomeric excess of the product was determined by UPC² analysis on a Daicel Chiralpak IE column (eluent: CO_2/*i*-PrOH = 90:10; flow rate 2 mL/min, λ = 360 nm: τ_{minor}= 6.1 min, τ_{major} = 6.3 min), 91:9 er.

$[\alpha]_D^{20}$ = -8.0 (c=0.5, CH_3Cl)

^{1}H NMR (500 MHz, $CDCl_3$) δ_H: 9.72 (s, 1H), 7.48 – 7.35 (m, 3H), 7.11 (m, 2H), 6.54 (dd, J = 10.8, 2.0 Hz, 1H), 3.37 – 3.20 (m, 1H), 1.94 (m, 1H), 1.65 (m, 1H), 0.86 (t, J = 7.5 Hz, 3H).
^{13}C{^{1}H} NMR (126 MHz, $CDCl_3$) δ_C: 192.5, 172.3, 148.2, 144.0, 131.2, 129.1, 128.9, 128.9, 51.9, 41.4, 30.3, 22.4.
^{19}F NMR (376 MHz, $CDCl_3$) δ_F: –81.1 (m, 3F), –114. 5 – –116.5 (m, 2F), –120.2 – –122.0 (m, 2F), –126.0 (m, 2F).
HRMS (ESI$^+$) $C_{16}H_{13}F_9O$ [M+Na]$^+$: found 415.0715, required 415.0706 (+2.2 ppm).

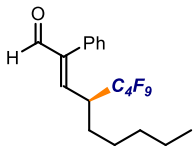

(*S*,*E*)-4-(Perfluorobutyl)-2-phenylnon-2-enal (7i)
Synthesized according to General Procedure A using 2-phenylnon-2-enal **5c** (130 mg, 600 µL) and perfluorobutyl iodide (69.2 mg, 200 µL). The crude mixture was purified by flash column chromatography on silica gel (hexane/CH_2Cl_2 8:2) to afford product **7i** (65 mg, 75% yield) as a colourless oil. The enantiomeric excess of the product was determined by UPC^2 analysis on a Daicel Chiralpak IE column (eluent: CO_2/*i*-PrOH = 90:10; flow rate 2 mL/min, λ = 211 nm: τ_{minor} = 4.4 min, τ_{major} = 4.6 min), 90:10 er.
$[\alpha]_D^{20}$ = -13.3 (c=0.5, CH_3Cl)
^{1}H NMR (500 MHz, $CDCl_3$) δ_H: 9.71 (s, 1H), 7.48 – 7.34 (m, 3H), 7.19 – 7.04 (m, 2H), 6.54 (dd, *J* = 10.8, 1.8 Hz, 1H), 3.43 – 3.30 (m, 1H), 3.46 – 3.32 (m, 1H), 1.91 – 1.80 (m, 1H), 1.62 (m, 1H), 1.38 – 1.01 (m, 6H), 0.84 (t, *J* = 7.3 Hz, 3H).
^{13}C{^{1}H} NMR (126 MHz, $CDCl_3$) δ_C: 192.9, 147.6, 145.9, 131.7, 129.2, 128.7 (2C), 42.0, 31.5, 27.2, 26.2, 22.5, 14.0.
^{19}F NMR (376 MHz, $CDCl_3$) δ_F: –81.1 (m, 3F), –113. 9 – –116.5 (m, 2F), –119.4 – –123.0 (m, 2F), –126.0 (m, 2F).
HRMS (ESI$^+$) $C_{19}H_{19}F_9O$ [M+Na]$^+$: found 457.1198, required 457.1184 (+2.9 ppm).

(*S*,*E*)-7-Chloro-4-(perfluorobutyl)-2-phenylhept-2-enal (7j)

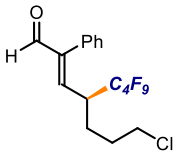

Synthesized according to General Procedure A using 7-chloro-2-phenylhept-2-enal **5d** (134 mg, 600 µL) and perfluorobutyl iodide (69.2 mg, 200 µL). The crude mixture was purified by flash column chromatography on silica gel (hexane/CH_2Cl_2 8:2) to afford product **7j** (36 mg, 41% yield) as a colourless oil. The enantiomeric excess of the product was determined by UPC² analysis on a Daicel Chiralpak IE column (eluent: CO_2/*i*-PrOH = 90:10; flow rate 2 mL/min, λ = 360 nm: τ_{minor} = 4.6 min, τ_{major} = 4.8 min), 88:12 er.

$[\alpha]_D^{20}$ = -4.1 (c=0.5, CH_3Cl)

^{1}H NMR (500 MHz, $CDCl_3$) δ_H: 9.72 (s, 1H), 7.51 – 7.35 (m, 3H), 7.13 – 7.08 (m, 2H), 6.56 (dd, *J* = 10.7, 1.5 Hz, 1H), 3.45 – 3.27 (m, 3H), 2.05 (m, 1H), 1.82 – 1.70 (m, 2H), 1.60 – 1.48 (m, 1H).

^{13}C{^{1}H} NMR (126 MHz, $CDCl_3$) δ_C: 192.5, 147.8, 144.6, 131.4, 129.0, 128.9 (2C), 43.9, 41.5, 29.4, 24.8.

^{19}F NMR (376 MHz, $CDCl_3$) δ_F: –81.0 (m, 3F), –112.9 – –116.6 (m, 2F), –118.9 – –122.7 (m, 2F), –125.0– –127.1 (m, 2F).

HRMS (ESI⁺) $C_{17}H_{14}ClF_9O$ $[M+Na]^+$: found 463.0483, required 463.0482 (+0.2 ppm).

Methyl (*S*,*E*)-7-oxo-6-phenyl-4-(perfluorobutyl)hept-5-enoate (7k)

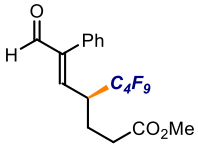

Synthesized according to General Procedure A using methyl (*E*)-7-oxo-6-phenylhept-5-enoate **5e** (139 mg, 600 µL) and nonafluoro-1-iodobutane (34.6 µL, 200 µmmol). The crude mixture was purified by flash column chromatography on silica gel (hexane/CH_2Cl_2 8:2) to afford product **7k** (54 mg, 59% yield) as a colourless oil. The enantiomeric excess of the product was determined by UPC² analysis on a Daicel Chiralpak IB column (eluent: CO_2/MeOH = 90:10; flow rate 2 mL/min, λ = 375 nm: τ_{minor} = 4.2 min, τ_{major} = 4.4 min), 93:7 er.

^{1}H NMR (500 MHz, $CDCl_3$) δ_H: 9.71 (s, 1H), 7.45 – 7.39 (m, 3H), 7.12 – 7.07 (m, 2H), 6.52 (dd, *J* = 10.9, 1.8 Hz, 1H), 3.55 (s, 3H),

3.54 – 3.48 (m, 1H), 2.34 – 2.26 (m, 1H), 2.26 – 2.20 (m, 1H), 2.19 – 2.10 (m, 1H), 1.95 – 1.84 (m, 1H).
$^{13}C\{^{1}H\}$ NMR (126 MHz, $CDCl_3$) δ 192.5, 172.3, 148.2, 144.0, 131.2, 129.1, 128.9, 128.9, 51.9, 41.4 (t, $^{2}J_{CF}$ = 21.5 Hz), 30.3, 22.4.
^{19}F NMR (376 MHz, $CDCl_3$) δ_F: –81.0, –114.8 – –115.6 (m), –120.0 – –122.2 (m), –125.9 – –126.1 (m).
HRMS (ESI$^+$) $C_{18}H_{15}F_9O_3$ $[M+Na]^+$: found 473.0771, required 473.0770 (+0.2 ppm)

(*S*,*E*)-4-(Perfluorobutyl)-2,5-diphenylpent-2-enal (7l)

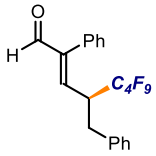

Synthesized according to General Procedure A using 2,5-diphenylpent-2-enal **5g** (142 mg, 600 µL) and nonafluoro-1-iodobutane (34.6 µL, 200 µL). The crude mixture was purified by flash column chromatography on silica gel (hexane/CH_2Cl_2 8:2) to afford product **7l** (54 mg, 59% yield) as a colourless oil. The enantiomeric excess of the product was determined by UPC^2 analysis on a Daicel Chiralpak IE column (eluent: CO_2/*i*-PrOH = 90:10; flow rate 2 mL/min, λ = 211 nm: τ_{minor}= 4.7 min, τ_{major}= 4.9 min), 90:10 er.
$[\alpha]_D^{20}$ = +31.2 (c=0.5, CH_3Cl)
^{1}H NMR (500 MHz, $CDCl_3$) δ_H: 9.63 (s, 1H), 7.27 – 7.23 (m, 4H), 7.22 – 7.10 (m, 2H), 7.00 – 6.93 (m, 2H), 6.54 (dd, *J* = 10.9, 2.1 Hz, 1H), 6.35 – 6.29 (m, 2H), 3.60 – 3.46 (m, 1H), 3.30 (dd, *J* = 13.6, 3.2 Hz, 1H), 2.78 (dd, *J* = 13.6, 10.8 Hz, 1H).
$^{13}C\{^{1}H\}$ NMR (126 MHz, $CDCl_3$) δ_C: 192.6, 148.2, 143.9, 135.9, 131.0, 129.7, 128.9, 128.7, 128.4, 128.2, 127.4, 44.6, 33.5.
^{19}F NMR (376 MHz, $CDCl_3$) δ_F: –81.0 (m, 3F), –112.5 – –117.6 (m, 2F), –118.6 – –123.2 (m, 2F), –125.7 – –126.3 (m, 2F).
HRMS (ESI$^+$) $C_{21}H_{15}F_9O$ $[M+Na]^+$: found 477.0871, required 477.0871 (+0.0 ppm).

(*S*,*E*)-4-(Perfluorobutyl)-2,4-diphenylbut-2-enal (7m)

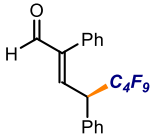

Synthesized according to General Procedure A using 2,4-diphenylbut-2-enal **5f** (133 mg, 600 µL) and nonafluoro-1-iodobutane (34.6 µL, 600 µL). The crude mixture was purified by flash column chromatography on silica gel (hexane/CH_2Cl_2 8:2) to afford product **7m** (55 mg, 62% yield) as a colourless oil. The enantiomeric excess of the product was determined by UPC^2 analysis on a Daicel Chiralpak OJ column (eluent: CO_2/MeCN = 90:10; flow rate 2 mL/min, λ = 350 nm: τ_{minor} = 2.7 min, τ_{major} = 2.9 min), 89:11 er.

$[\alpha]_D^{20}$ = +44.5 (c=0.5, CH_3Cl)

^{1}H NMR (500 MHz, $CDCl_3$) δ_H: 9.74 (s, 1H), 7.44 – 7.36 (m, 6H), 7.24 – 7.19 (m, 2H), 7.13 – 7.03 (m, 2H), 7.02 – 6.96 (d, 10.5 Hz, 1H), 4.44 (m, 1H).

^{13}C{^{1}H} NMR (126 MHz, $CDCl_3$) δ_C: 192.5, 146.3, 143.7, 131.2, 129.3, 129.3, 129.0, 128.9, 128.9, 128.6, 127.8, 47.7.

^{19}F NMR (376 MHz, $CDCl_3$) δ_F: –81.1 (m, 3F), –111.8 – –115.9 (m, 2F), –121.0 (m, 2F), –126.0 (m, 2F).

HRMS (ESI$^+$) $C_{20}H_{13}F_9O$ $[M+Na]^+$: found 463.0715, required 463.0727 (–2.6 ppm).

(*S*,*E*)-4-(Perfluorobutyl)-2-(*m*-tolyl)pent-2-enal (7n)

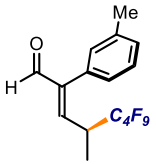

Synthesized according to General Procedure A using 2-(*m*-tolyl)pent-2-enal (600 µmol, 105 mg) and perfluorobutyl iodide (69.2 mg, 200 µmol). The crude mixture was purified by flash column chromatography on silica gel (hexane/CH_2Cl_2 8:2) to afford product **7n** (37 mg, 47% yield) as a colourless oil. The enantiomeric excess of the product was determined by UPC^2 analysis on a Daicel Chiralpak IE column (eluent: CO_2/IPA = 90:10; flow rate 2 mL/min, λ = 360 nm, τ_{minor} = 4.3 min, τ_{major} = 4.4 min), 90:10 er.

$[\alpha]_D^{20}$ = -15.9 (c=0.5, CH_3Cl)

^{1}H NMR (500 MHz, $CDCl_3$) δ_H: 9.67 (s, 1H), 7.32 (t, *J* = 7.5 Hz, 1H), 7.21 (d, *J* = 7.7 Hz, 1H), 6.92 – 6.87 (m, 2H), 6.62 (dd, *J* = 10.4,

2.2 Hz, 1H), 3.52 – 3.38 (m, 1H), 2.38 (s, 3H), 1.29 (d, *J* = 6.9 Hz, 3H).
^{13}C NMR (126 MHz, $CDCl_3$) δ_C: 192.9, 146.4, 146.2, 138.6, 131.5, 129.6, 129.5, 128.8, 125.9, 37.0, 21.6, 13.2.
^{19}F NMR (282 MHz, $CDCl_3$) δ_F: -81.0 (m, 3F), -115.5 – -119.7 (m, 2F), -120.2 – -123.1 (m, 2F), -126.1 (m, 2F).
HRMS (ESI$^+$) $C_{16}H_{13}F_9O$ $[M+Na]^+$: found 415.0715, required 415.0720 (–1.2 ppm)

(*S*,*E*)-4-(Perfluorobutyl)-2-(*p*-tolyl)pent-2-enal (7o)

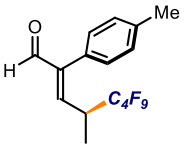

Synthesized according to General Procedure A using 2-(*p*-tolyl)pent-2-enal (600 µmol, 105 mg, 3 eq.) and perfluorobutyl iodide (69.2 mg, 200 µmol. The crude mixture was purified by flash column chromatography on silica gel (hexane/CH_2Cl_2 8:2) to afford product **7o** (50 mg, 64% yield) as a colourless oil. The enantiomeric excess of the product was determined by UPC^2 analysis on a Daicel Chiralpak IE column (eluent: CO_2/IPA = 90:10; flow rate 2 mL/min, λ = 360 nm: τ_{minor} = 4.4 min, τ_{major} = 4.6 min), 90:10 er.
$[\alpha]_D^{20}$ = +21.0 (c=0.5, CH_3Cl)
^{1}H NMR (500 MHz, $CDCl_3$) δ_H: 9.67 (s, 1H), 7.26 – 7.21 (m, 2H), 7.02 – 6.96 (m, 2H), 6.61 (dd, *J* = 10.4, 2.1 Hz, 1H), 3.51 – 3.42 (m, 1H), 2.39 (s, 3H), 1.29 (d, *J* = 7.0 Hz, 3H).
^{13}C NMR (126 MHz, $CDCl_3$) δ_C: 192.9, 146.2, 145.9, 138.6, 129.5, 128.6, 128.3, 37.0, 21.4, 13.2
^{19}F NMR (282 MHz, $CDCl_3$) δ -81.0 (m, 3F), -115.2 – -119.9 (m, 2F), -120.3 – -122.9 (m, 2F), 125.0 – -126.9 (m, 2F).
HRMS (ESI$^+$) $C_{16}H_{13}F_9O$ $[M+Na]^+$: found 415.0731, required 415.0715 (+3.8 ppm).

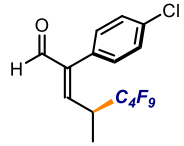

(*S*,*E*)-4-(Perfluorobutyl)-2-(*p*-chlorophenyl)pent-2-enal (7p)

Synthesized according to General Procedure A using 2-(*p*-chlorophenyl)pent-2-enal (0.6 mmol,

117 mg, 3 eq.) and perfluorobutyl iodide (69.2 mg, 0.2 mmol). The crude mixture was purified by flash column chromatography on silica gel (hexane/CH_2Cl_2 8:2) to afford product **7p** (50 mg, 61% yield) as a colourless oil. The enantiomeric excess of the product was determined UPC^2 analysis on a Daicel Chiralpak IE column (eluent: CO_2/IPA = 90:10; flow rate 2 mL/min, λ = 211 nm: τ_{minor} = 4.6 min, τ_{major} = 4.9 min), 92:8 er.

$[\alpha]_D^{20}$ = -46.3 (c=0.5, CH_3Cl)

^{1}H NMR (500 MHz, $CDCl_3$) δ_H: 9.66 (s, 1H), 7.42 (d, *J* = 8.7 Hz, 2H), 7.05 (d, *J* = 8.6 Hz, 2H), 6.65 (dd, *J* = 10.5, 2.2 Hz, 1H), 3.41 (m, 1H), 1.30 (d, *J* = 6.9 Hz, 3H).

^{13}C NMR (126 MHz, $CDCl_3$) δ_C: 192.4, 147.1, 145.0, 135.1, 130.3, 129.8, 129.2, 37.1, 13.2.

^{19}F NMR (282 MHz, $CDCl_3$) δ_F: -80.4 – -81.1 (m, 3F), -115.4 – -119.8 (m, 2F), -119.9 – -123.1 (m, 2F), -125.1 – -127.0 (m, 2F).

HRMS (ESI$^+$) $C_{15}H_{10}ClF_9O$ $[M+Na]^+$: found 435.0169, required 435.0174 (–1.1 ppm).

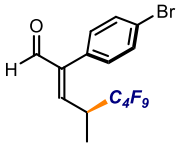

(*S*,*E*)-4-(Perfluorobutyl)-2-(*p*-bromophenyl)pent-2-enal (7q)

Synthesized according to General Procedure A using 2-(*p*-bromophenyl)pent-2-enal (600 µmol, 96 mg) and perfluorobutyl iodide (69.2 mg, 200 µmol). The crude mixture was purified by flash column chromatography on silica gel (hexane/CH_2Cl_2 8:2) to afford product **7q** (31.2 mg, 56% yield) as a colourless oil. The enantiomeric excess of the product was determined by UPC^2 analysis on a Daicel Chiralpak IE column (eluent: CO_2/IPA = 90:10; flow rate 1 mL/min, λ = 211 nm: τ_{minor} = 6.6 min, τ_{major} = 6.9 min), 89:11 er.

^{1}H NMR (400 MHz, $CDCl_3$) δ_H: 9.66 (s, 1H), 7.64 – 7.52 (m, 2H), 7.02 – 6.94 (m, 2H), 6.65 (dd, *J* = 10.5, 2.1 Hz, 1H), 3.53 – 3.31 (m, 1H), 1.30 (d, *J* = 6.9 Hz, 3H).

^{13}C NMR (126 MHz, $CDCl_3$) δ 192.3, 147.0 (d, J = 5.1 Hz), 145.0 (d, J = 1.8 Hz), 132.2, 130.6, 130.3, 77.4, 37.1 (dd, J = 23.7, 21.1 Hz), 13.1 (t, J = 4.8 Hz).
^{19}F NMR (376 MHz, $CDCl_3$) δ -81.1 (m, 3F), -115.7 – -119.6 (m, 2F), -120.4 – -122.7 (m, 2F), -126.2 (m, 2F).
HRMS (ESI$^+$) $C_{15}H_{10}BrF_9O$ $[M+Na]^+$: found 478.9656, required 478.9664 (–1.6 ppm).

(*S*,*E*)-4-(Perfluorobutyl)-2-(*p*-methoxyphenyl)pent-2-enal (7r)

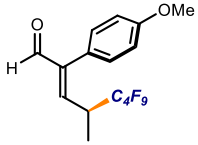

Synthesized according to General Procedure A using 2-(*p*-methoxyphenyl)pent-2-enal (600 μmmol, 114 mg) and perfluorobutyl iodide (69.2 mg, 200 μmol). The crude mixture was purified by flash column chromatography on silica gel (hexane/CH_2Cl_2 7:3) to afford product **7r** (42 mg, 51% yield) as a colourless oil. The enantiomeric excess of the product was determined by UPC^2 analysis on a Daicel Chiralpak IE column (eluent: CO_2/IPA = 90:10; flow rate 2 mL/min, λ = 211 nm: τ_{minor} = 4.5 min, τ_{major} = 4.8 min), 90:10 er.
$[\alpha]_D^{20}$ = -40.1 (c=0.5, CH_3Cl)
^{1}H NMR (400 MHz, $CDCl_3$) δ_H: 9.66 (s, 1H), 7.07 – 7.00 (m, 2H), 7.00 – 6.90 (m, 2H), 6.59 (dd, J = 10.5, 2.1 Hz, 1H), 3.84 (s, 3H), 3.56 – 3.44 (m, 1H), 1.30 (d, J = 7.1 Hz, 3H).
^{13}C NMR (101 MHz, $CDCl_3$) δ_C: 193.2, 160.0, 146.3, 145.6, 130.2, 123.5, 114.4, 54.9, 37.2, 13.2.
^{19}F NMR (376 MHz, $CDCl_3$) δ_F: -81.0 (m, 3F), -115.4 – -119.5 (m, 2F), -119.9 – -123.1 (m, 2F), -125.2 – -126.9 (m, 2F).
HRMS (ESI$^-$) $C_{16}H_{13}F_9O_2$ $[M]^-$: found 408.0783, required 408.0777 (+1.5 ppm).

(*S*,*E*)-4-(Trifluoromethyl)-2-phenylpent-2-enal (7j)

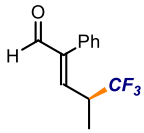

Synthesized according to General Procedure B using phenylpent-2-enal (600 μmol, 96 mg) and trifluoromethyl iodide (39.8 mg, 200 μmol). The crude mixture was purified by flash column chromatography

on silica gel (hexane/CH_2Cl_2 8:2) to afford product **7j** (31.2 mg, 56% yield) as a colourless oil. The enantiomeric excess of the product was determined by UPC² analysis on a Daicel Chiralpak IE column (eluent: CO_2/IPA = 90:10; flow rate 2 mL/min, λ = 360 nm. τ_{minor} = 5.3 min, τ_{major} = 5.5 min), 87:13 er.
$[\alpha]_D^{20}$ = -12.3 (c=0.5, CH_3Cl)
^{1}H NMR (400 MHz, $CDCl_3$) δ 9.69 (s, 1H), 7.50 – 7.38 (m, 3H), 7.14 (m, 2H), 6.57 (d, *J* = 10.4 Hz, 1H), 3.43 – 3.24 (m, 1H), 1.26 (d, *J* = 7.0 Hz, 3H).
^{13}C NMR (101 MHz, $CDCl_3$) δ_C: 192.7, 146.7, 146.4, 131.4, 129.0, 128.7, 127.8, 38.7, 13.8.
^{19}F NMR (282 MHz, $CDCl_3$) δ_F: –71.6 (m, 3F).
HRMS (ESI⁺) $C_{12}H_{11}F_3O$ $[M+Na]^+$: found 251.0654, required 251.0654 (+0.0 ppm).

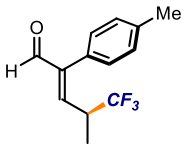

(*S*,*E*)-4-(Trifluoromethyl)-2-(*p*-tolyl)pent-2-enal (7k)

Synthesized according to General Procedure B using phenylpent-2-enal (600 µmol, 96 mg) and trifluoromethyl iodide (39.8 mg, 200 µmol) as reaction partners. The crude mixture was purified by flash column chromatography on silica gel (hexane/CH_2Cl_2 8:2) to afford product **7k** (21 mg, 43% yield) as a colourless oil. The enantiomeric excess of the product was determined by UPC² analysis on a Daicel Chiralpak IE column (eluent: CO_2/IPA = 90:10; flow rate 2 mL/min, λ = 360 nm: τ_{minor} = 5.4 min, τ_{major} = 5.7 min), 86:14 er.
$[\alpha]_D^{20}$ = -17.4 (c=0.5, CH_3Cl)
^{1}H NMR (400 MHz, $CDCl_3$) δ_H: 9.67 (s, 1H), 7.25 – 7.22 (m, 2H), 7.05 – 7.00 (m, 2H), 6.54 (d, *J* = 10.4 Hz, 1H), 3.41 – 3.29 (m, 1H), 2.39 (s, 3H), 1.26 (d, *J* = 6.9 Hz, 3H).
^{13}C NMR (126 MHz, $CDCl_3$) δ_C: 192.9, 146.7, 146.2, 146.2, 138.6, 129.4, 128.9, 38.8, 21.4, 13.8.
^{19}F NMR (376 MHz, $CDCl_3$) δ_F: -71.5 (d, *J* = 8.1 Hz, 3F).

HRMS (ESI+) $C_{13}H_{13}F_3O$ [M+Na]+: found 265.0815, required 265.0811 (+1.5 ppm).

(*S*,*E*)-4-(Trifluoromethyl)-2-phenylnon-2-enal (7l)

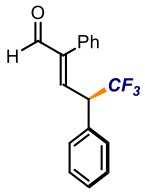

Synthesized according to General Procedure B using phenylpent-2-enal (600 μmol, 96 mg) and trifluoromethyl iodide (30.9 mg, 200 μmol). The crude mixture was purified by flash column chromatography on silica gel (hexane/Et_2O 98:2) to afford product **7l** (29 mg, 36% yield) as a colourless oil. The enantiomeric excess of the product was determined by UPC^2 analysis on a Daicel Chiralpak IE column (eluent: CO_2/IPA = 90:10; flow rate 2 mL/min, λ = 360 nm. τMajor = 5.84 min, τMinor = 5.66 min.) 85:15 e.r.

HRMS (ESI): m/z calculated for $[C_{17}H_{13}O_1F_3Na]^+$ $[M]^+$: 313.0816; found: 313.0811. (+1.6 ppm)

^{1}H NMR (500 MHz, $CDCl_3$) δ 9.76 (s,1), 7.40 (m 6H), 7.24 (m, 1H), 7.07 – 6.98 (m, 3H), 4.37 (dq, J = 10.6, 8.7 Hz, 1H).

^{13}C NMR (126 MHz, $CDCl_3$) δ 192.68, 147.14, 144.02, 133.42, 131.38, 129.39, 129.22, 129.12, 129.02, 128.97, 128.88, 128.76, 128.66, 49.69.

^{19}F NMR (376 MHz, $CDCl_3$) δ -68.57(d, J = 8.7 Hz)

5.4 NOESY contacts relevant to the determination of the relative configuration of CBOs 2j, 2n and 2o.

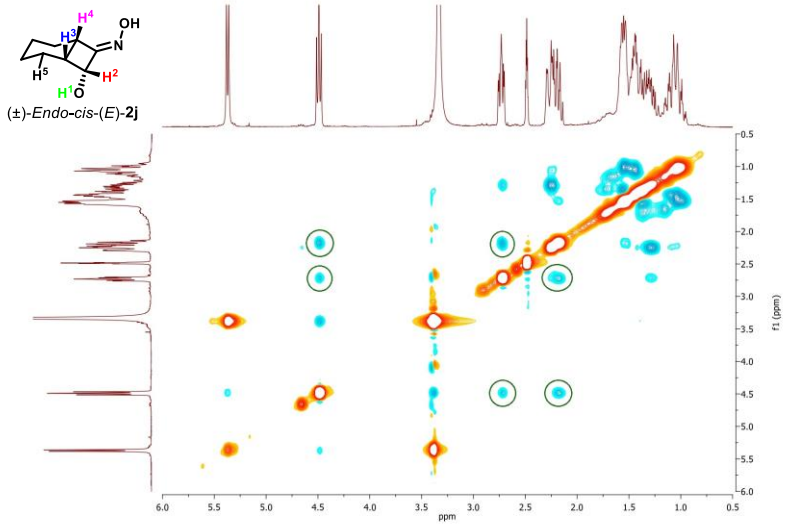

Figure 5.5 NOESY contacts between cyclobutane ring protons of CBO (±)-*Endo-cis*-(*E*)-**2j.**

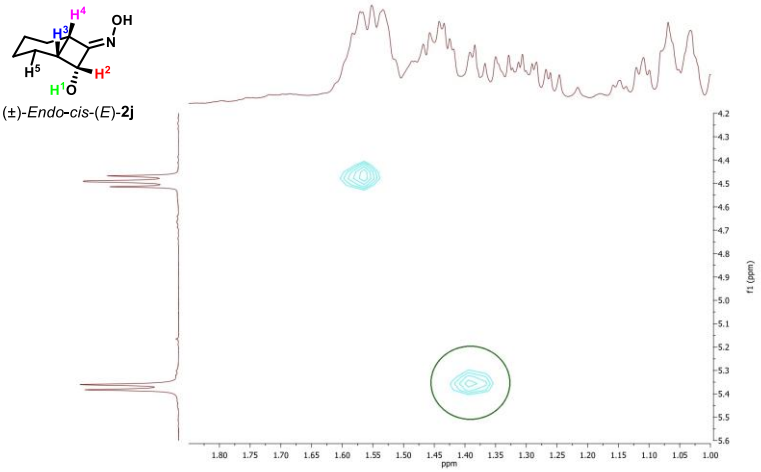

Figure 5.6 NOESY contacts between alcoholic and alkylic protons of CBO (±)-*Endo-cis-*(*E*)-**2j.**

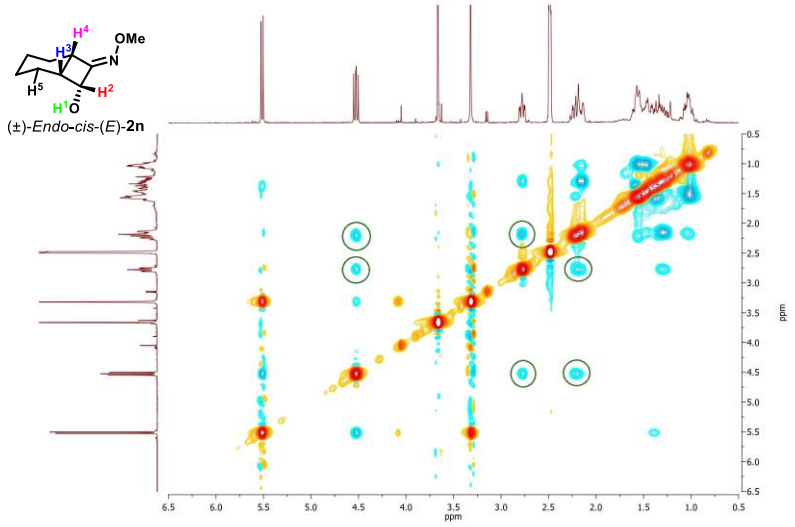

Figure 5.7 NOESY contacts between cyclobutane ring protons of CBO (±)-*Endo-cis-*(*E*)-**2n.**

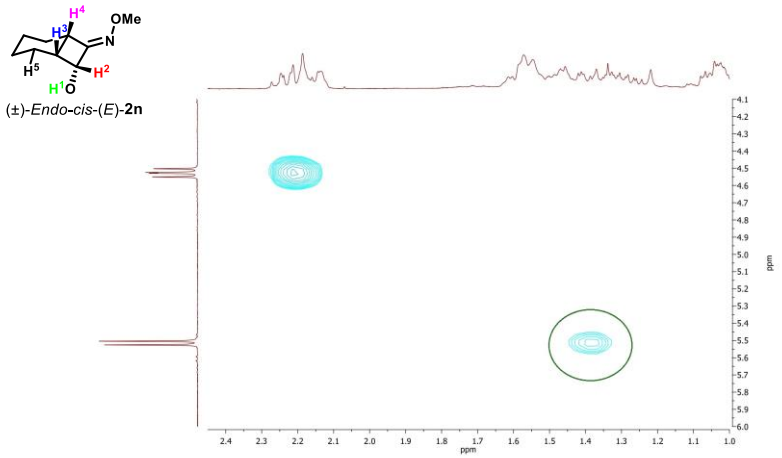

Figure 5.8 NOESY contacts between alcoholic and alkylic protons of CBO (±)-*Endo-cis-*(*E*)-**2n.**

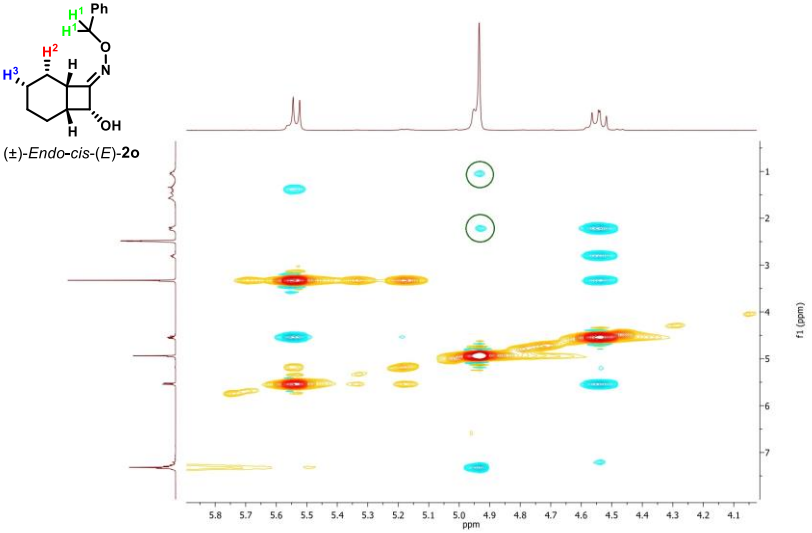

Figure 5.9 NOESY contacts between benzylic and alkylic protons of CBO (±)-*Endo-cis-*(*E*)-**2o.**

5.5 Molecular Dynamics

5.5.1 Methods

The simulation box consists of a single oxime molecule surrounded by 163 solvent molecules. Different oxime isomers were here considered: *cis-endo-E*-**2j**, *cis-endo-Z*-**2j**, *cis-exo-E*-**2j**, *cis-exo-E*-**2j** as well as a *cis-endo-E*-**2i** CBOs. Simulations are carried out using leap-frog algorithm with a time-step of 0.5 fs. UFF force field is adopted for the purpose.[122] Long range electrostatic interactions are considered using PME method while a cut-off scheme with cut-off distance 1 nm is applied for Van der Waals interactions. Initial configuration minimization is carried out using conjugate gradient method; further MD simulations lasting 90 ns were performed for each system in order to guarantee equilibrium. Canonical ensembles (NVT) are obtained through V-rescale thermostat with coupling constant τ_T=0.1 ps and reference temperature 298.15 K. Periodic boundary conditions were applied in the three spatial directions. Data were collected during 30000000 step lasting simulations (20000000 in the case of DCM).

5.5.2 Discussion

In order to better highlight the crucial role of the solvent polarity in oxime double bond isomerization, the radial distribution functions (RDFs) of DCM chlorine with respect to the oxime oxygen for both *cis-endo-E*-**2j** and *cis-endo-Z*-**2j** isomers is reported in Figure **5.10**. In the case of DCM solvent, we did not observe the appreciable differences between the two curves as in the case of DMSO solvent (Figure **2.13a**). The lower intensity of the radial distribution functions in Figure **5.11** suggests a weaker interaction of the alcoholic OH group with the DMSO.

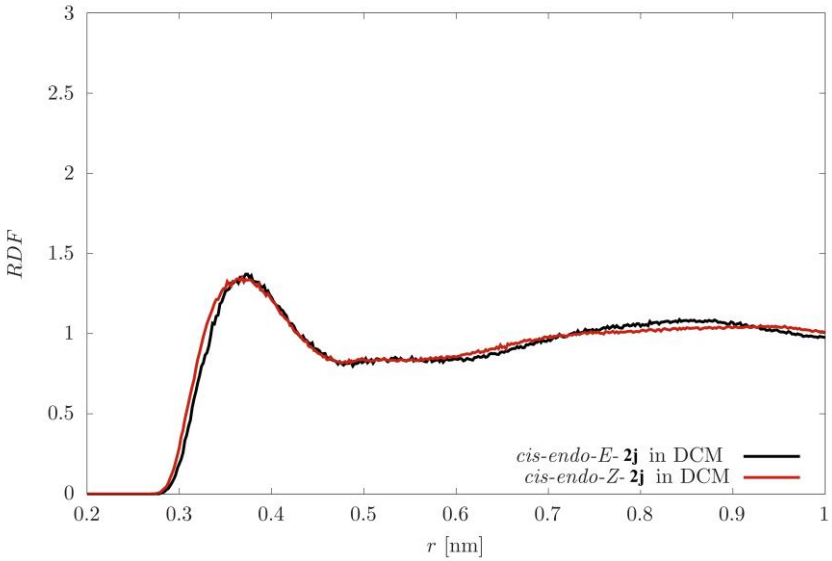

Figure 5.10 Radial distribution functions related to the interaction between CBO oxime oxygen and chlorine in DCM solvent.

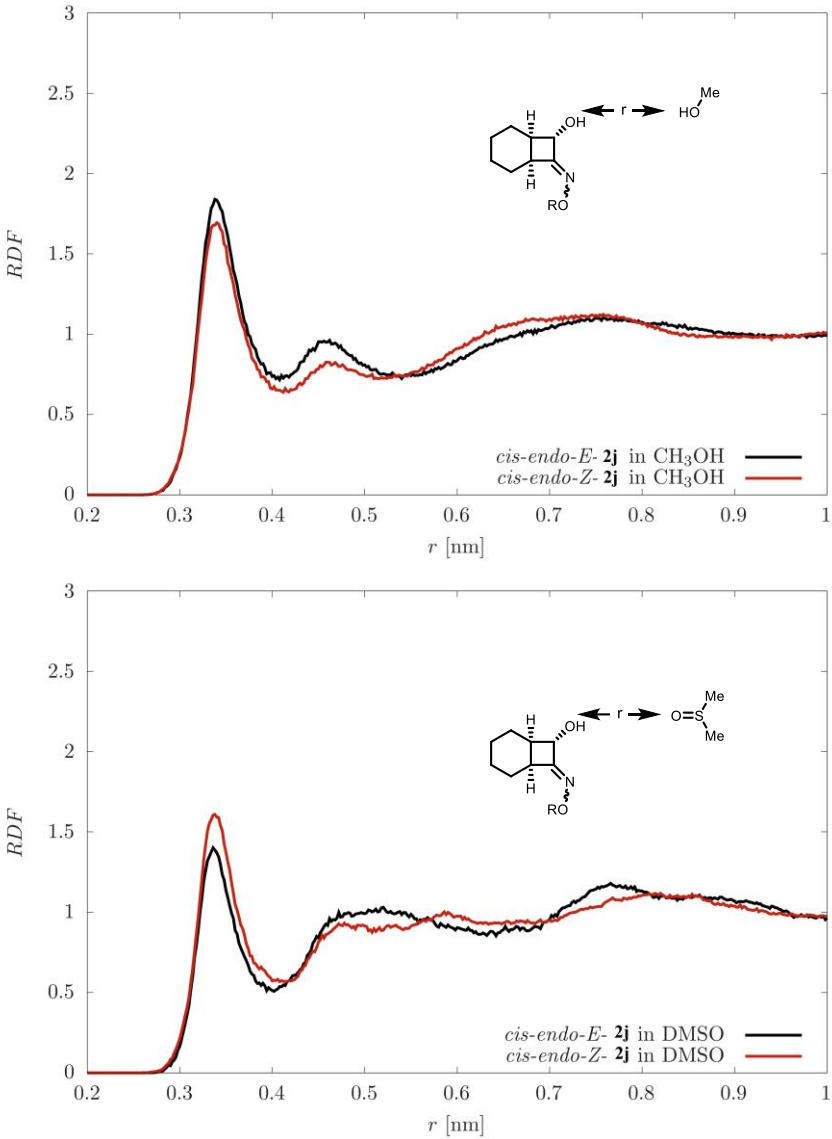

Figure 5.11 Radial distribution functions related to the interaction between CBO alcoholic oxygen and oxygen in DMSO and methanol.

In Figure **5.13**, distribution function of the dihedral angle θ (defined by atoms 24-21-8-5, Figure **5.12**) related to alcoholic OH group rotating around the oxygen-carbon bond of *cis-endo-E*-**2j** is reported. This distribution suggests that the most probable dihedral angles correspond to the conformations (θ = –89 and θ = 156), which have the alcoholic OH group near to the alkylic H (20, Figure 5.12). This observation is compatible with the observed contact in the NOESY experiment in Figure **5.6** and the distance distribution function reported in Figure **5.14**.

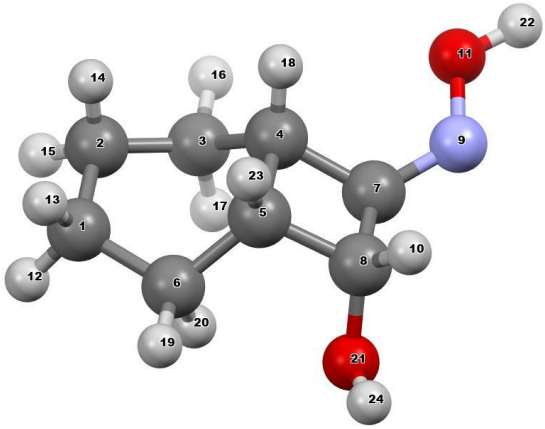

Figure 5.12 Snapshot of *cis-endo-E*-**2j** isomer with dihedral angle (defined by atoms 24-21-8-5) corresponding to □ = –95° in Figure **5.8.**

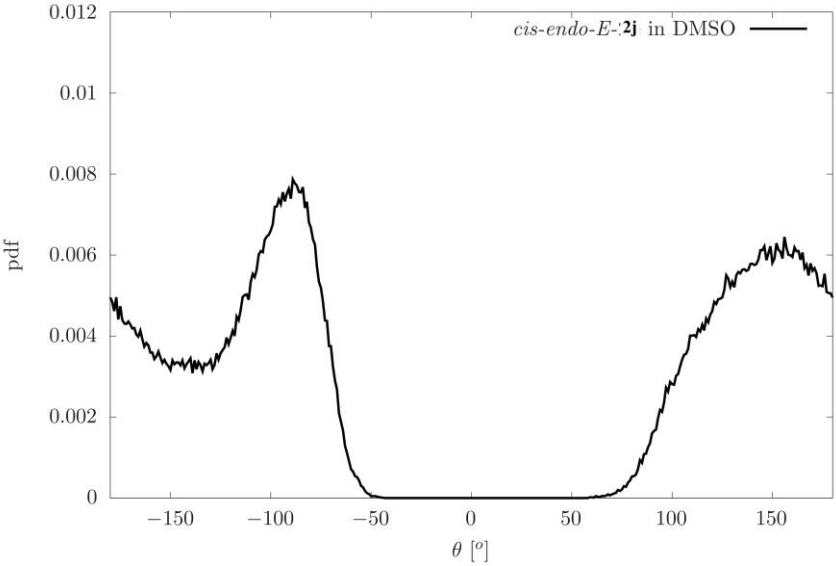

Figure 5.13 Distribution function of the dihedral angle θ (defined by atoms 24-21-8-5 in Figure **5.7**) related to alcoholic OH group rotating around the oxygen-carbon bond of *cis-endo-E*-**2j**. θ = 0 corresponds to *syn* conformation. Positive angles define the counterclockwise rotation of the OH group.

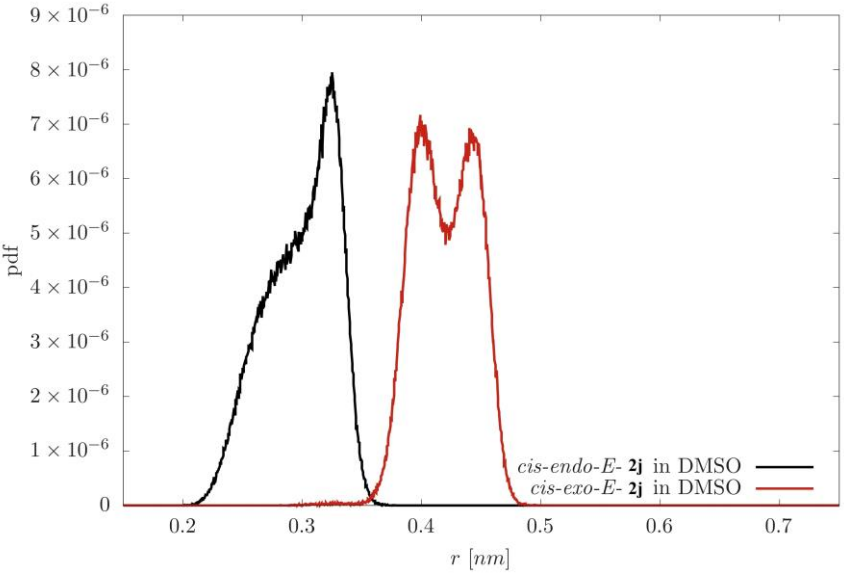

Figure 5.14 Distance distribution function between alcoholic H (atom 24 in Figure **5.7**) and alkylic hydrogen (atom 20 in Figure **5.7**) of *cis-endo-E-***2j** and *cis-exo-E-***2j** isomers in DMSO.

5.6 IRMPD

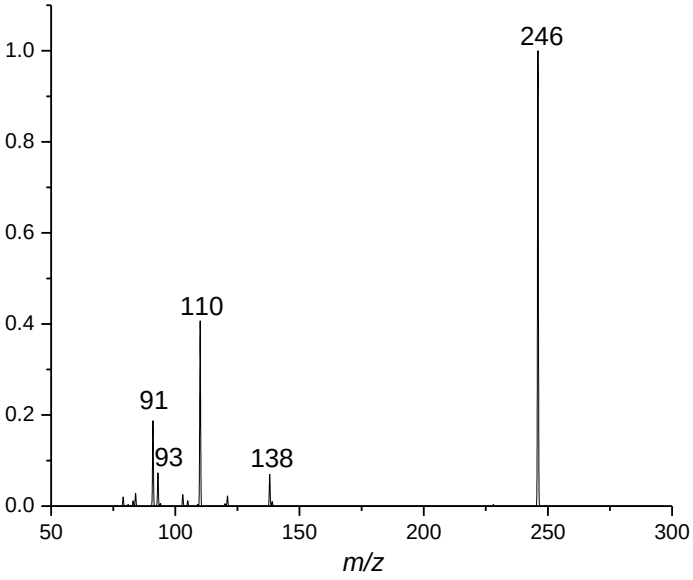

Figure 5.15 Photofragmentation mass spectrum recorded under irradiation of $[\mathbf{2o}+H]^+$ at 869 cm^{-1}. Main fragments are at *m/z* 138 (**1**+H-$PhCH_2OH$), 110 (138 -CO), 93 (110 -NH_3) and 91 (93 -H_2).

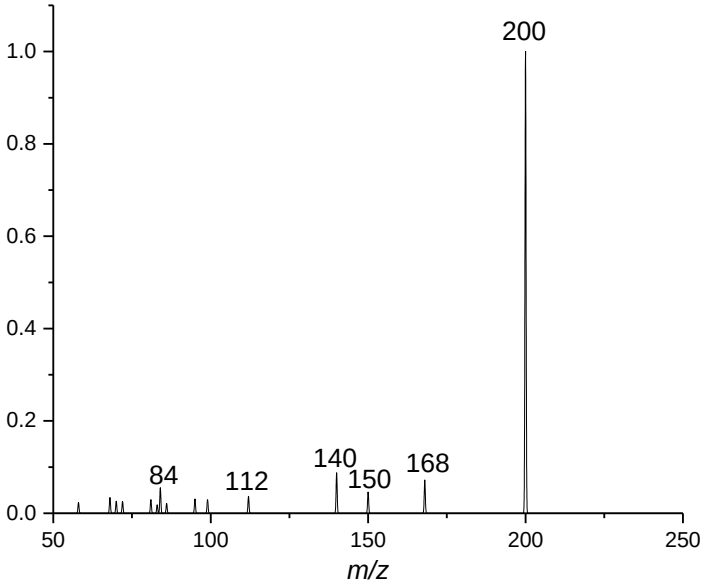

Figure 5.16 Photofragmentation mass spectrum recorded under irradiation of [*cis*-**2m** +H]$^+$ at 1460 cm^{-1}. Main fragments are at *m/z* 168 (**2**+H - CH_3OH), 150 (168 -H_2O), 140 (168 -CO), 112 (140 -C_2H_4) and 84 (112 - C_2H_4).

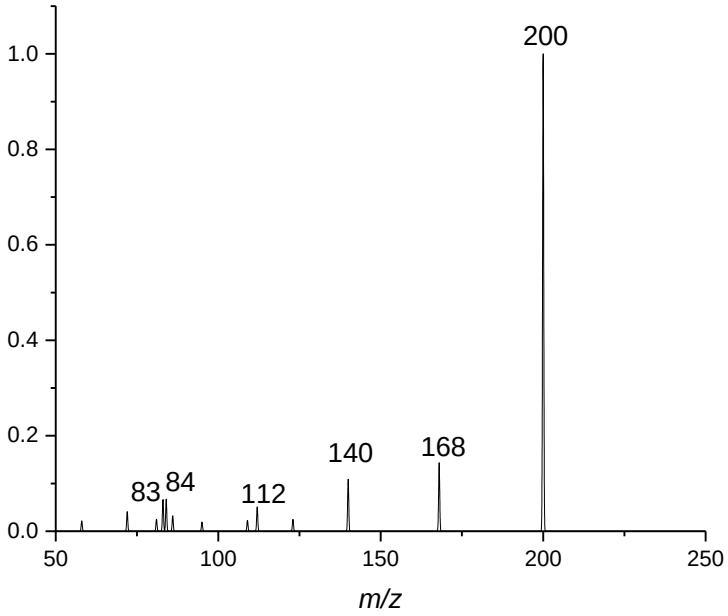

Figure 5.17 Photofragmentation mass spectrum recorded under irradiation of [*trans*-**2m**+H]$^+$ at 1454 cm^{-1} of [**3**+H]$^+$. Main fragments are at *m/z* 168 (**3**+H - CH_3OH), 140 (168 -CO), 112 (140 -C_2H_4), 84 (112 - C_2H_4) and 83 (112 -CH_3NH_2).

5.7 CID spectra

Collision induced dissociation (CID) on the deprotonated forms [M-H]⁻ with collision energy (CE) 30 V.

(*E*)-2-(Hydroxyimino)-4-phenylbutanal **1a** ($C_{10}H_{11}NO_2$)

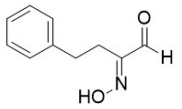

(*E*)-2-(hydroxyimino)-4-phenylbutanal
Chemical Formula: $C_{10}H_{11}NO_2$
Exact Mass: 177,0790

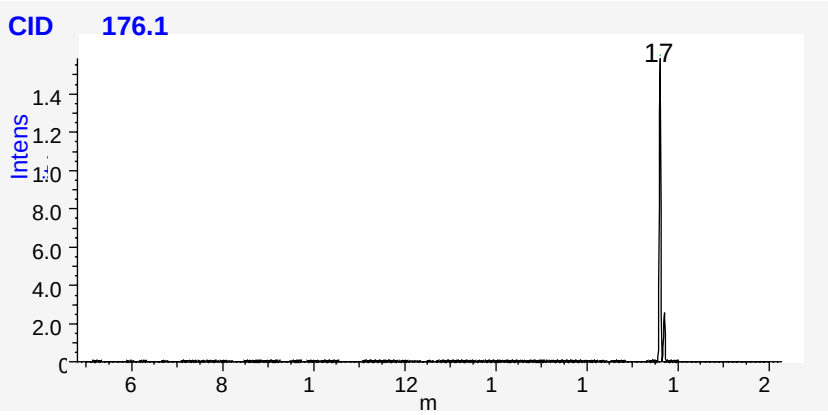

(*E*)-2-(Hydroxy)-3-phenylcyclobutan-1-one oxime **2a** ($C_{10}H_{11}NO_2$)

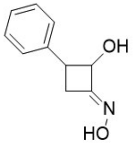

(*E*)-2-hydroxy-3-phenylcyclobutan-1-one oxime
Chemical Formula: $C_{10}H_{11}NO_2$
Exact Mass: 177,0790

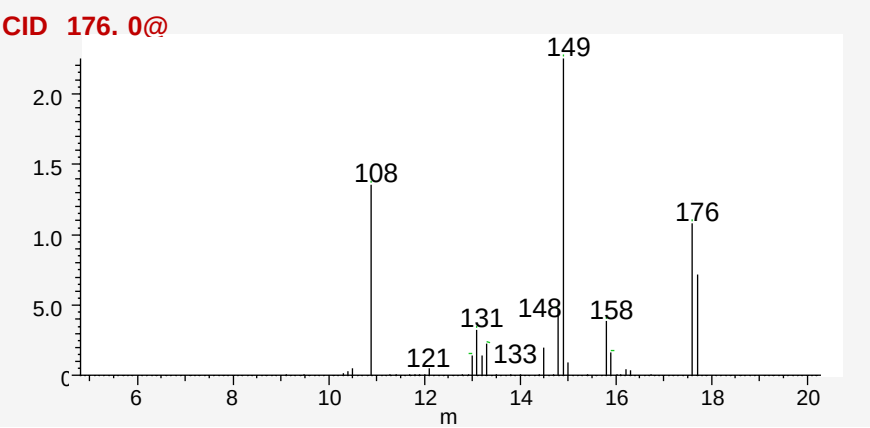

Collision induced dissociation (CID) were carried on the protonated forms $[M+H]^+$ with collision energy 12 V.

(*E*)-2-((Benzyloxy)imino-2-cyclohexylethanal **1j** ($C_{15}H_{19}NO_2$)

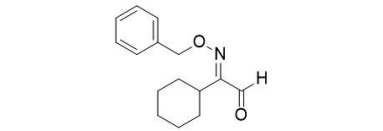

(*E*)-2-((benzyloxy)imino)-2-cyclohexylacetaldehyde
Chemical Formula: $C_{15}H_{19}NO_2$
Exact Mass: 245,1416

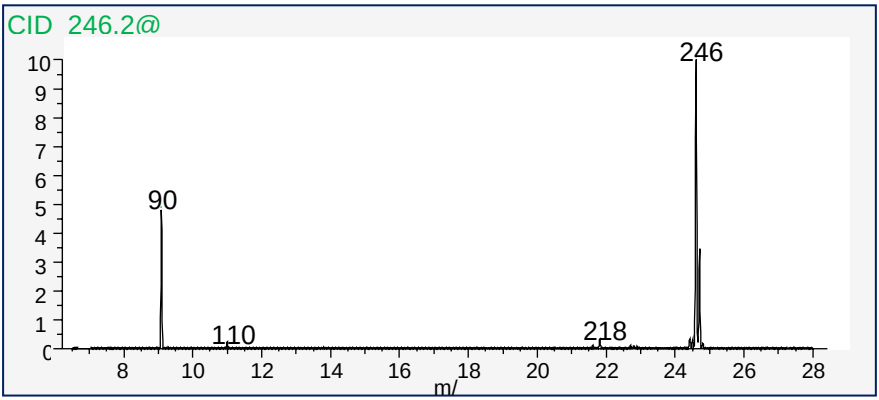

(*E*)-8-Hydroxybicyclo[4.2.0]octan-7-one *O*-benzyloxime **2j** ($C_{15}H_{19}NO_2$)

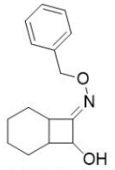

(*E*)-8-hydroxybicyclo[4.2.0]octan-7-one *O*-benzyl oxime
Chemical Formula: $C_{15}H_{19}NO_2$
Exact Mass: 245,1416

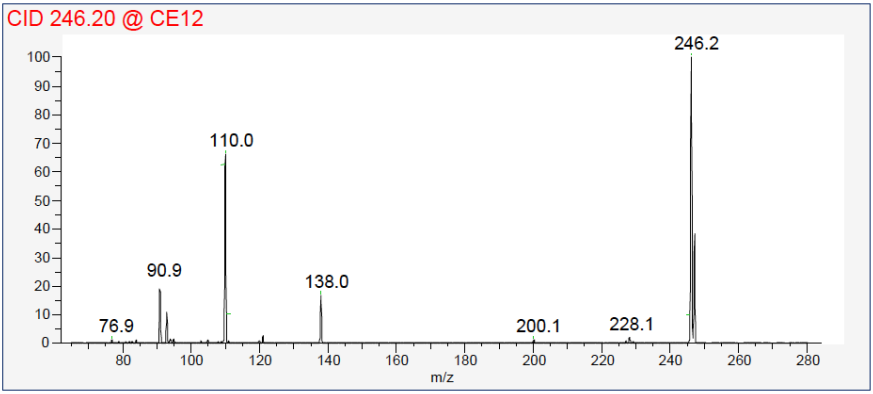

5.8 HPLC and UPC² traces

compound (±)-**2m** (a) and (4R)-**2m** (b)

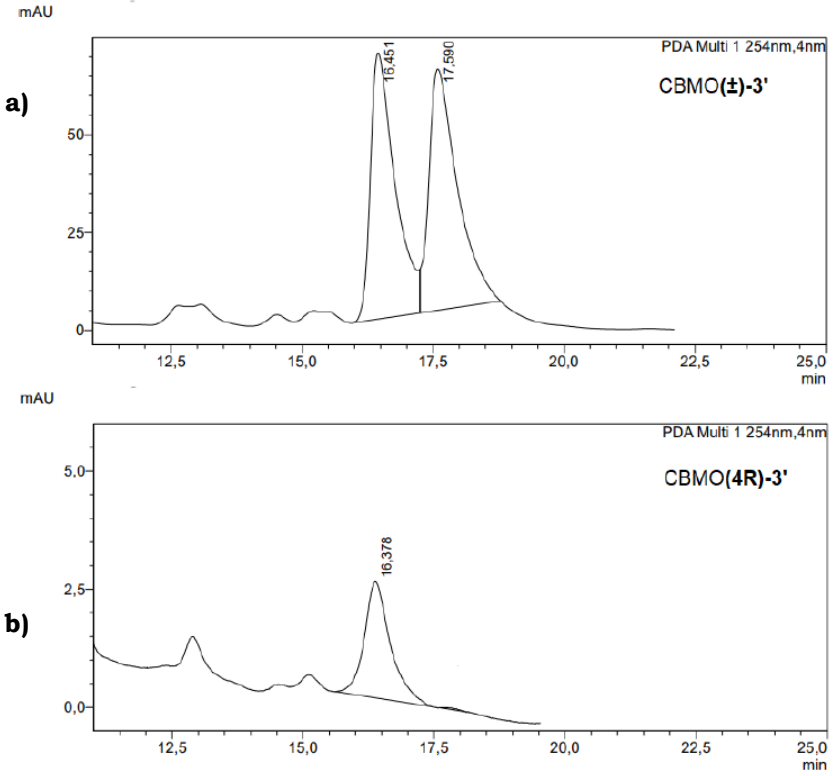

PDA Ch1 254nm

Peak#	Ret. Time	Area	Height	Conc.	Unit	Mark	Name
1	16,378	85250	2457	99,365		M	
2	17,667	544	15	0,635		M	
Total		85795	2472				

7a - UPC² analysis on a Daicel Chiralpak IE column (eluent: CO_2/*i*-PrOH = 90:10; flow rate 2 mL/min, λ = 211 nm; τ_{minor} = 4.3 min, τ_{major} = 4.5 min), 93:7 er.

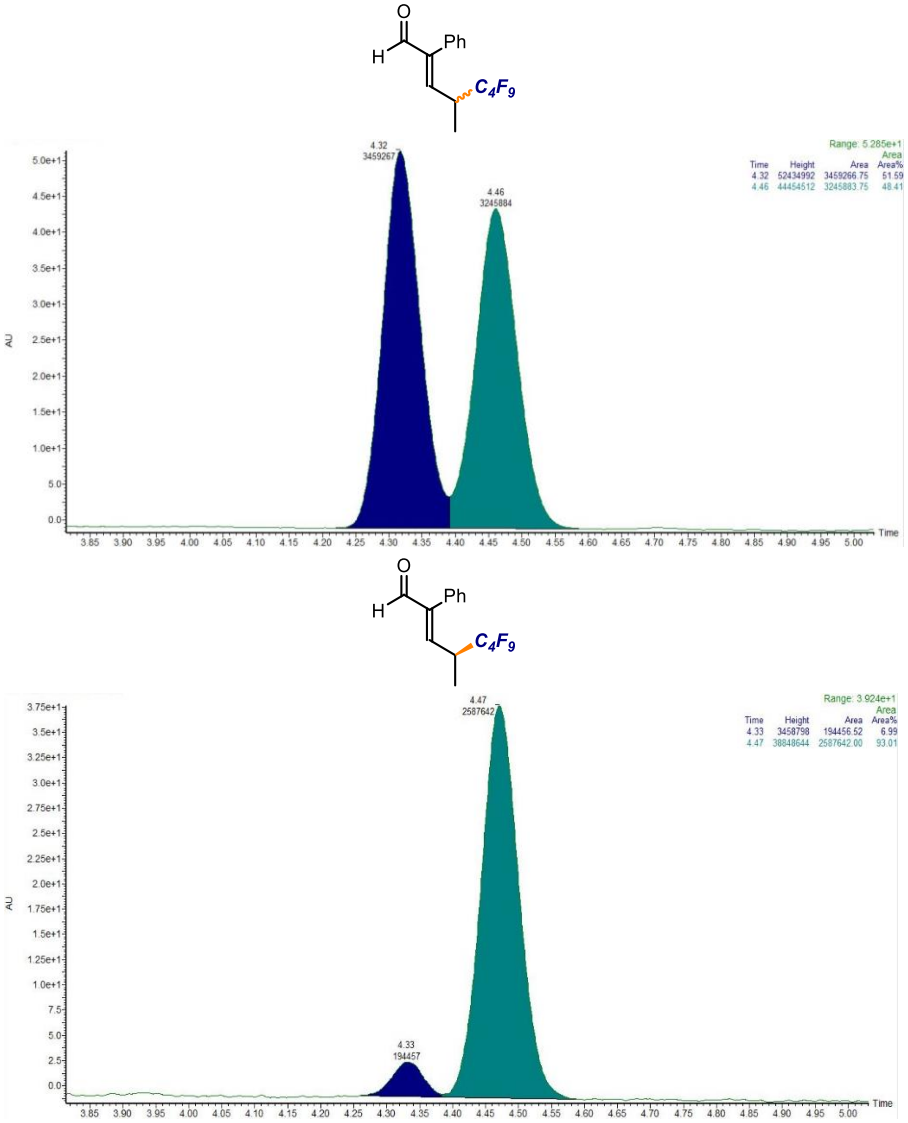

7b - UPC² analysis on a Daicel Chiralpak IE column (eluent: CO_2/*i*-PrOH = 90:10; flow rate 2 mL/min, λ = 211 nm: τ_{minor} = 4.5 min, τ_{major} = 4.7 min), 88:12 er.

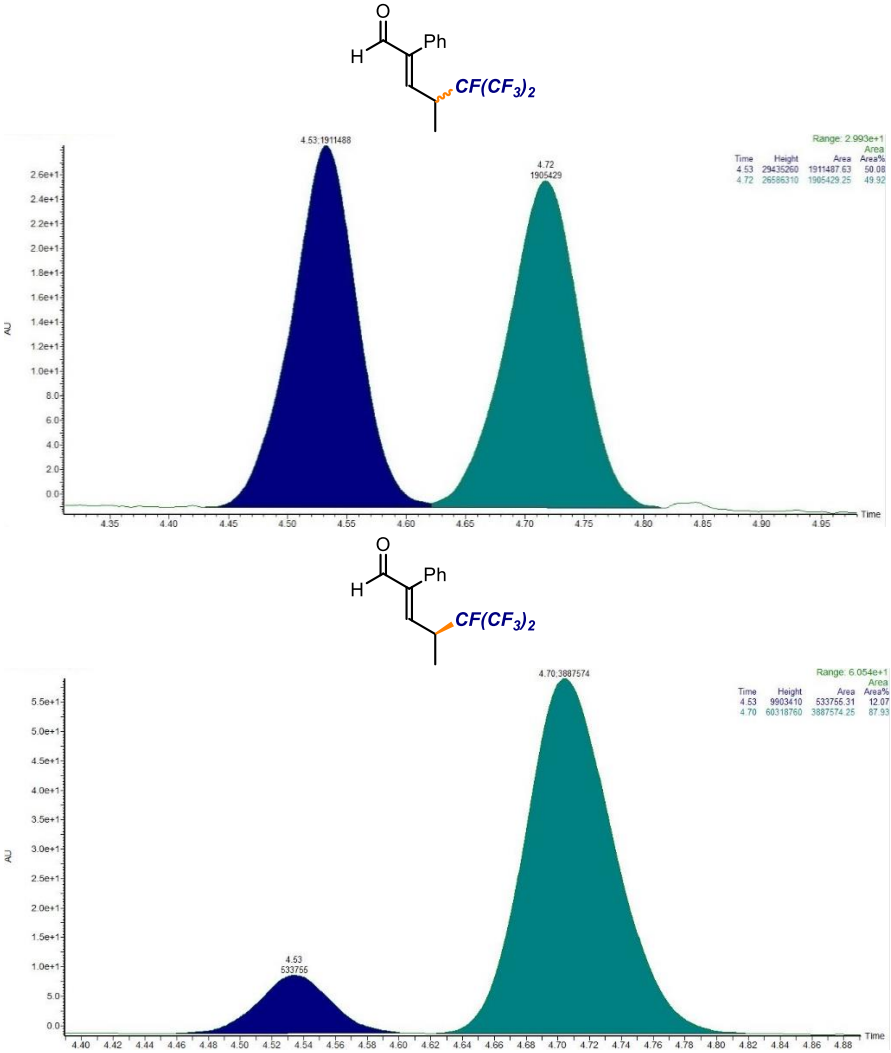

7c - UPC² analysis on a Daicel Chiralpak IE column (eluent: CO_2/*i*-PrOH = 90:10; flow rate 2 mL/min, λ = 375 nm: τ_{minor} = 6.3 min, τ_{major} = 6.6 min), 89:11 er.

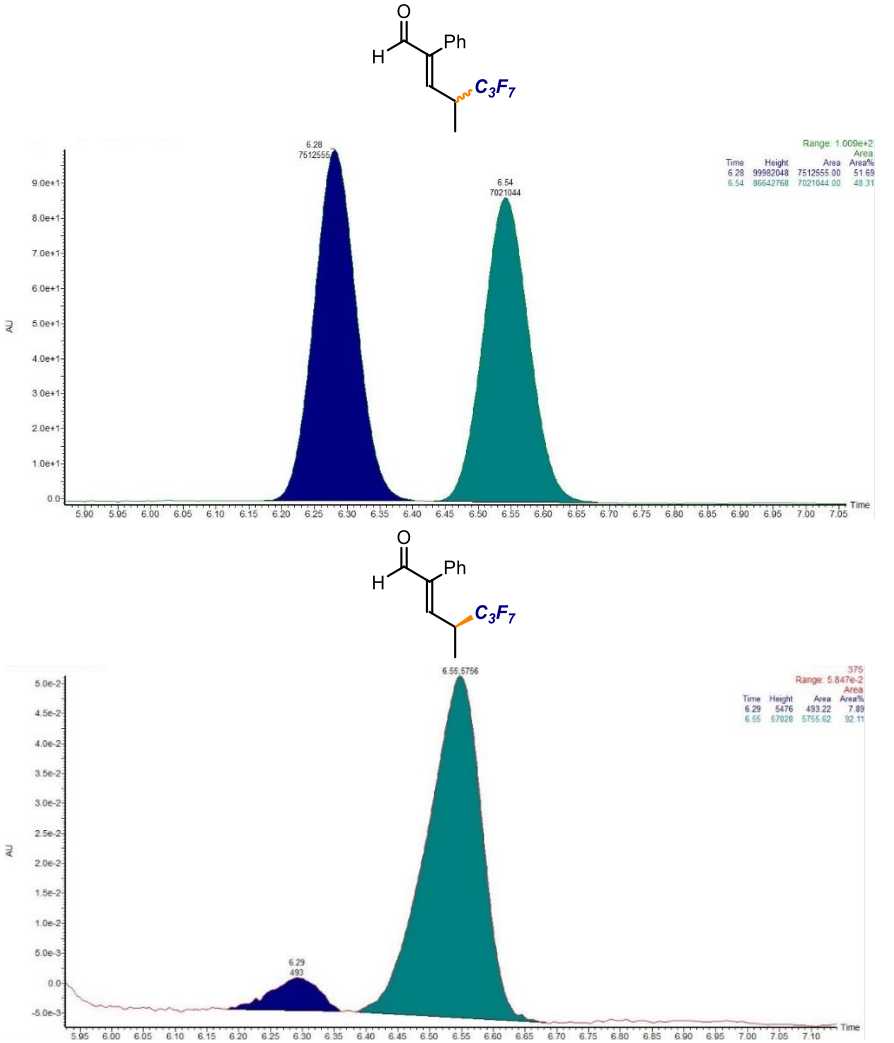

7d - UPC² analysis on a Daicel Chiralpak IE column (eluent: CO_2/*i*-PrOH = 90:10; flow rate 2 mL/min, λ = 350 nm: τ_{minor} = 5.8 min, τ_{major} = 6.0 min), 92:8 er.

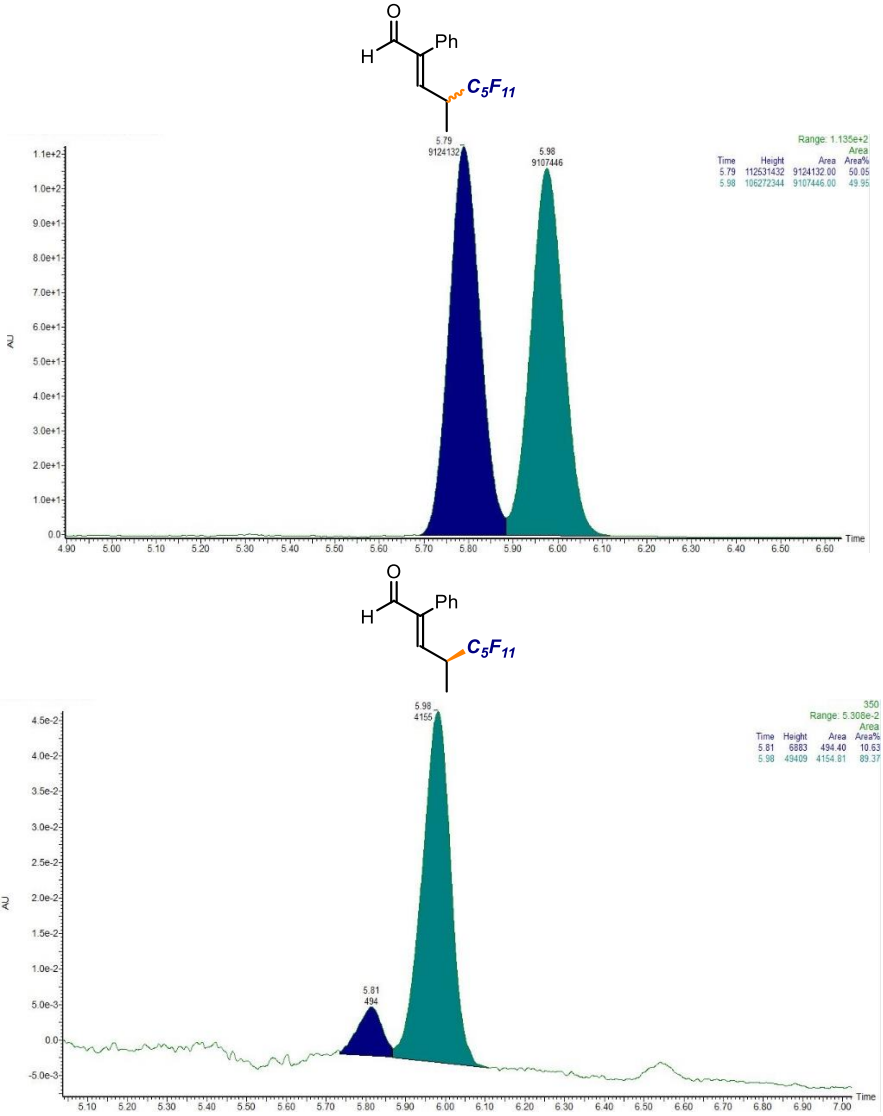

7e - UPC² analysis on a Daicel Chiralpak IE column (eluent: CO_2/*i*-PrOH = 90:10; flow rate 2 mL/min, λ = 211 nm: τ_{minor} = 4.0 min, τ_{major} = 4.1 min), 91:9 er.

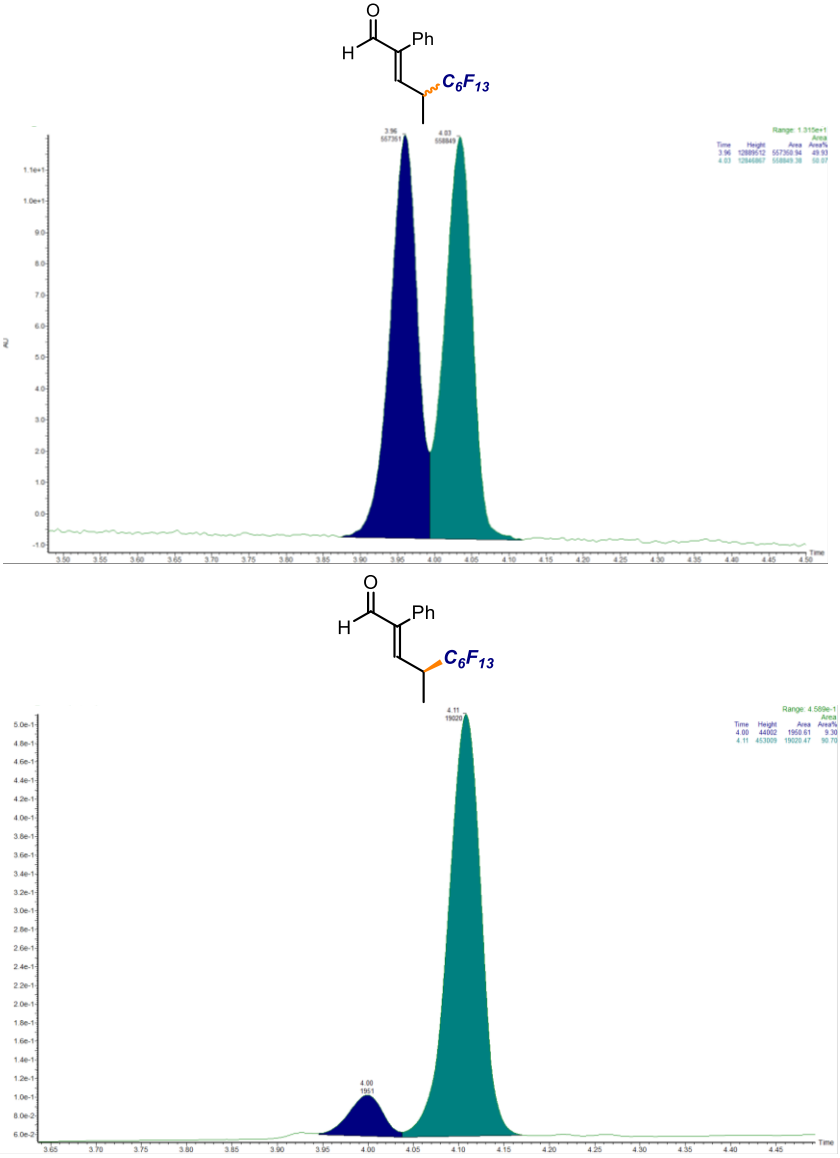

7f - UPC² analysis on a Daicel Chiralpak IE column (eluent: CO_2/*i*-PrOH = 90:10; flow rate 2 mL/min, λ = 211 nm: τ_{minor} = 4.0 min, τ_{major} = 4.1 min), 89:11 er.

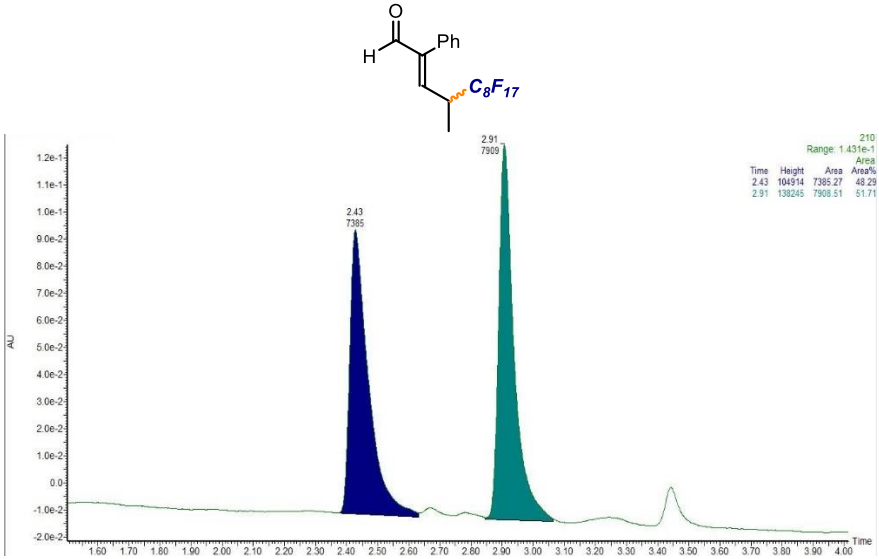

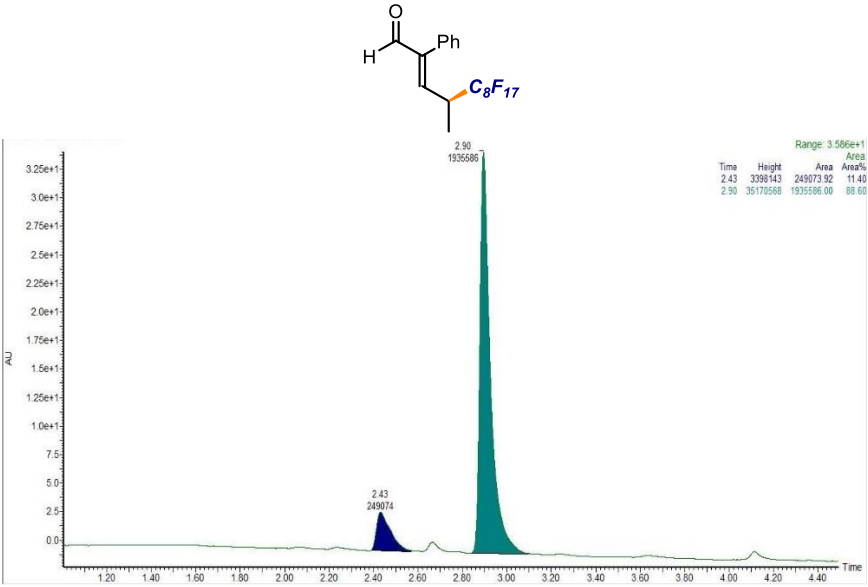

7g - Chiral HPLC analysis on a Daicel Chiralpak IC-3 column (eluent: *n*-hexane/*i*-PrOH 80:20; flow rate 1 mL/min, λ = 254 nm: τ_{minor} = 13.3 min, τ_{major} = 17.0 min), 86:14 er.

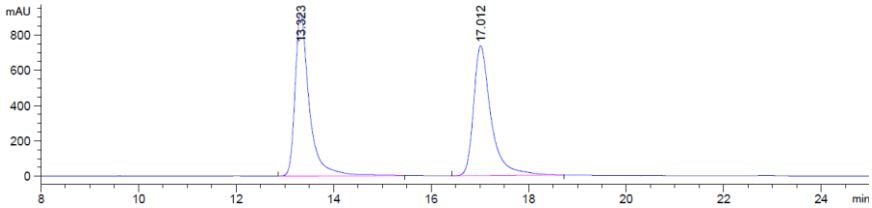

Peak #	RetTime [min]	Type	Width [min]	Area [mAU*s]	Height [mAU]	Area %
1	13.323	BV	0.2998	1.87222e4	922.55328	50.5785
2	17.012	BV	0.3657	1.82939e4	734.15399	49.4215

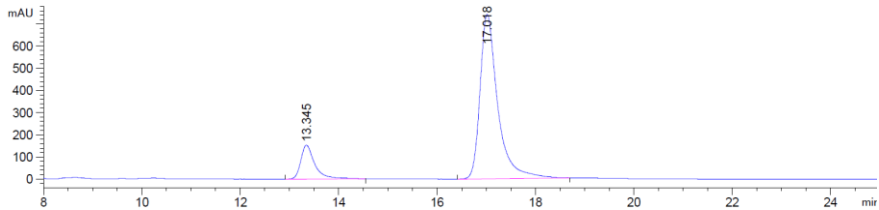

Peak #	RetTime [min]	Type	Width [min]	Area [mAU*s]	Height [mAU]	Area %
1	13.345	BB	0.2878	3003.66333	153.13341	13.9692
2	17.018	BB	0.3717	1.84983e4	742.44879	86.0308

7h - UPC² analysis on a Daicel Chiralpak IC-3 column (eluent: *n*-hexane/*i*-PrOH 80:20; flow rate 1 mL/min, λ = 254 nm: τ_{minor} = 2.2 min, τ_{major} = 2.1 min), 88:12 er.

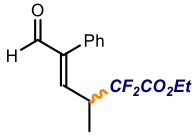

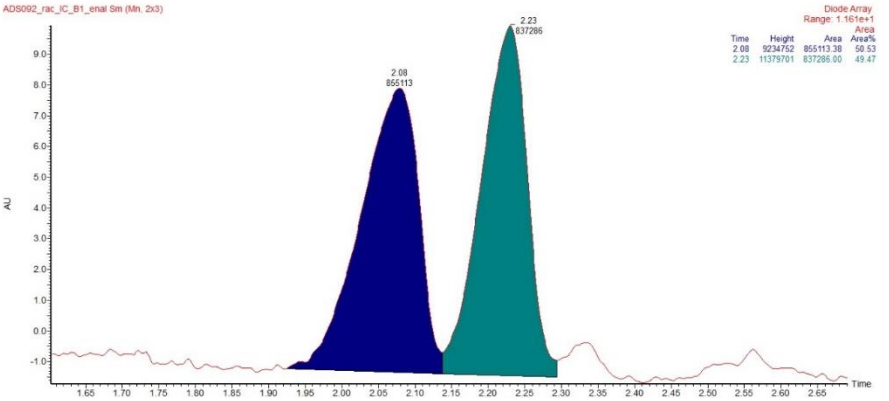

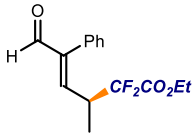

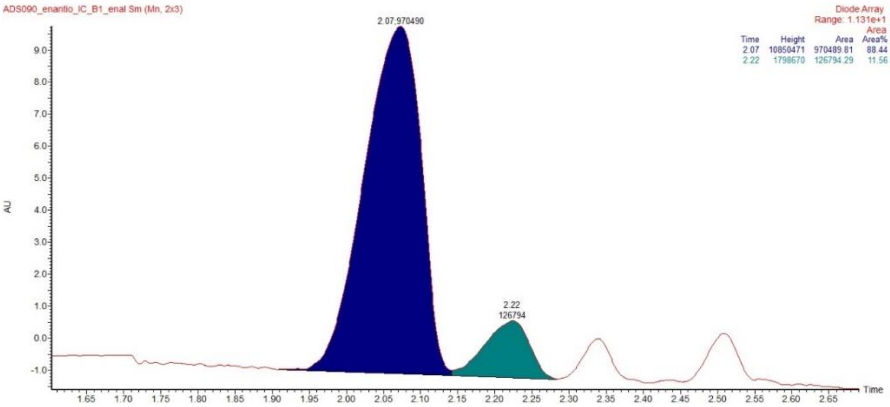

7i - UPC2 analysis on a Daicel Chiralpak IE column (eluent: n-hexane/i-PrOH 80:20; flow rate 2 mL/min, λ = 360 nm: τminor = 4.2 min, τmajor = 4.4 min), 84:16 er.

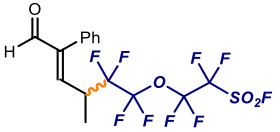

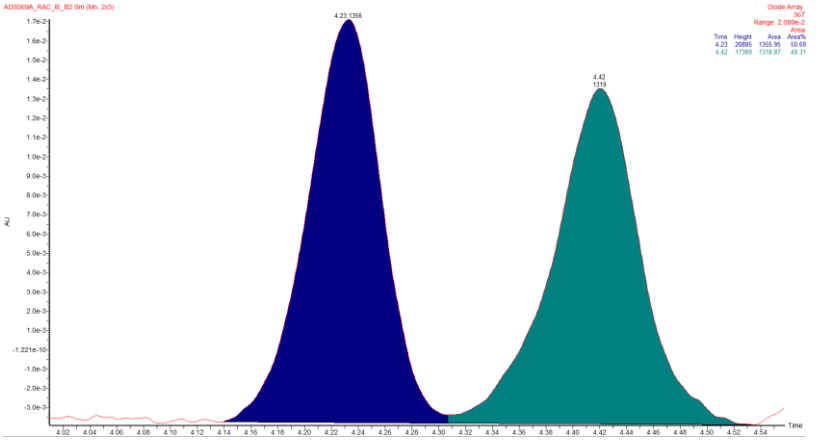

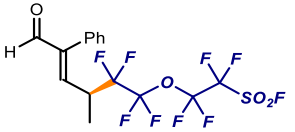

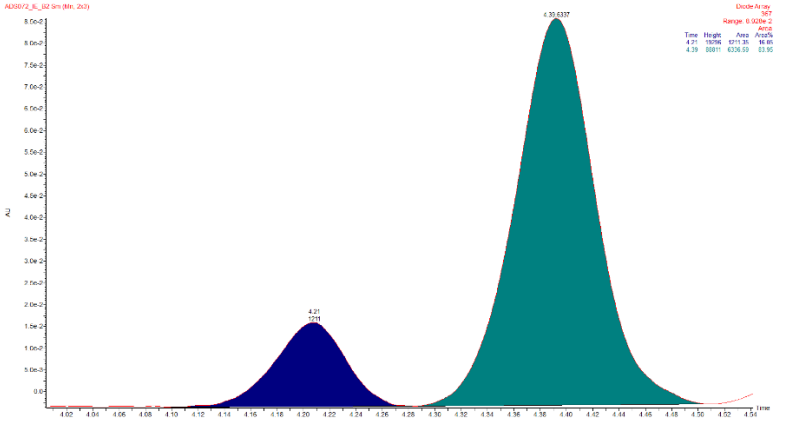

7x - UPC² analysis on a Daicel Chiralpak IE column (eluent: CO_2/IPA = 90:10; flow rate 2 mL/min, λ = 355 nm: τ_{minor} = 4.4 min, τ_{major} = 4.6 min), 50:50 er.

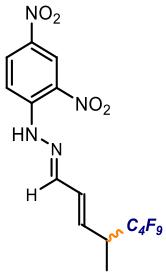

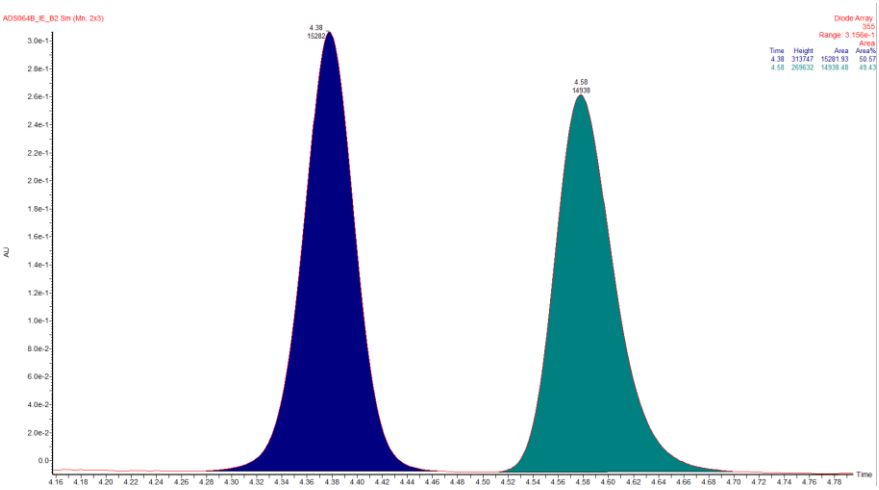

7y - UPC² analysis on a Daicel Chiralpak IE column (eluent: CO_2/MeOH = 90:10; flow rate 1 mL/min, λ = 360 nm: τ_{minor}= 7.2 min, τ_{major} = 7.4 min), 64:36 er.

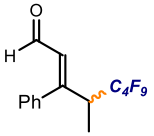

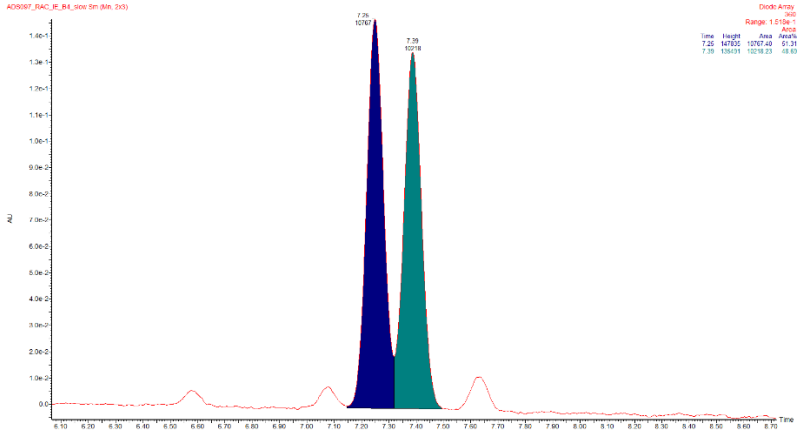

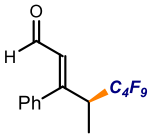

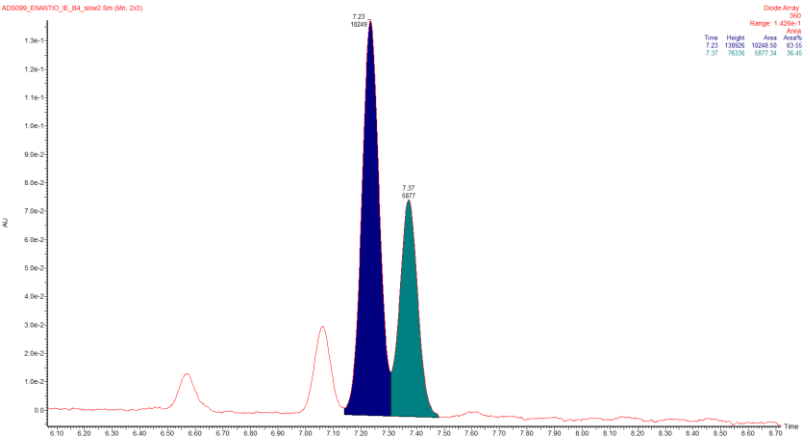

7z - UPC² analysis on a Daicel Chiralpak IE column (eluent: CO_2/IPA = 90:10; flow rate 1 mL/min, λ = 360 nm: *Z* isomer: τ_{minor} = 5.8 min, τ_{major} = 5.9 min; *E* isomer: τ_{minor} = 6.4 min, τ_{major} = 6.8 min), *Z* isomer: 50:50 er; *E* isomer: 50:50 er.

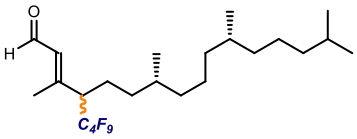

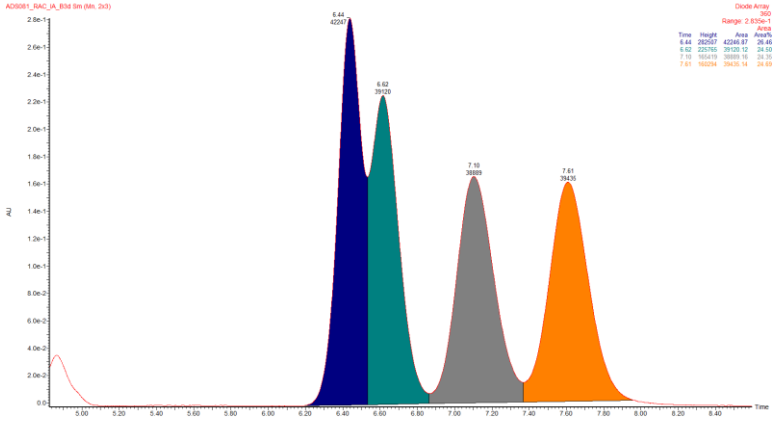

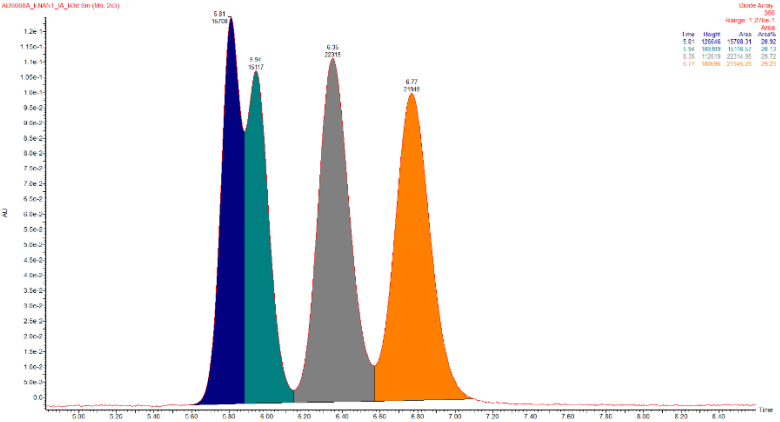

7m - UPC² analysis on a Daicel Chiralpak IE column (eluent: CO_2/*i*-PrOH = 90:10; flow rate 2 mL/min, λ = 211 nm, τ_{minor} = 6.1 min, τ_{major} = 6.3 min), 91:9 er.

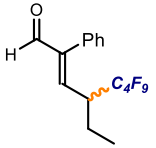

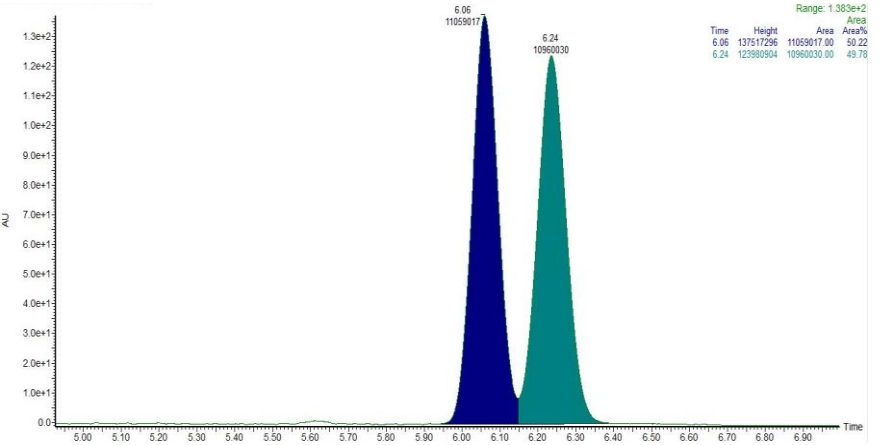

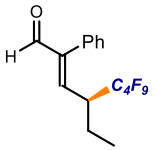

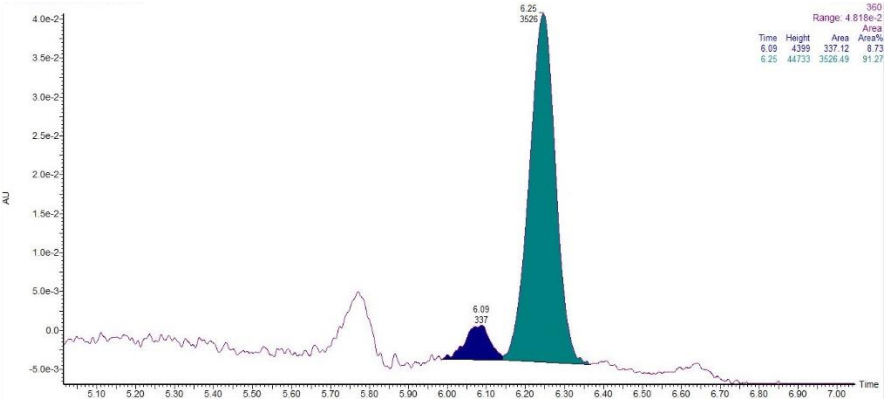

7n - UPC² analysis on a Daicel Chiralpak IE column (eluent: CO_2/*i*-PrOH = 90:10; flow rate 2 mL/min, λ = 211 nm, τ_{minor} = 4.4 min, τ_{major} = 4.6 min), 90:10 er.

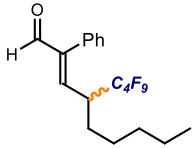

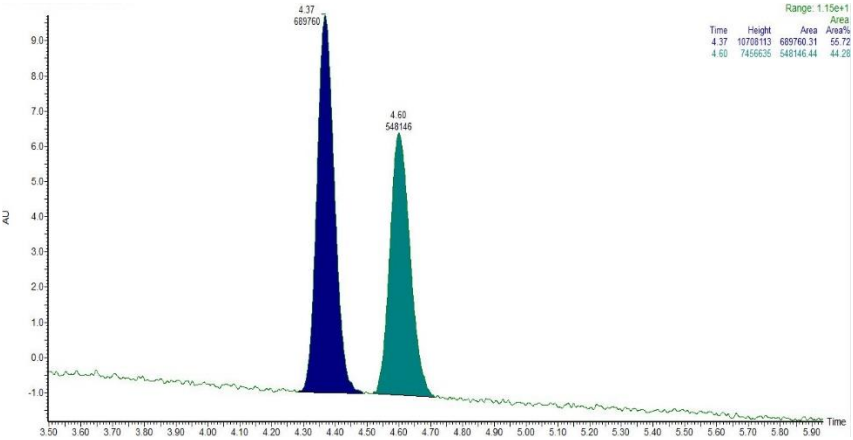

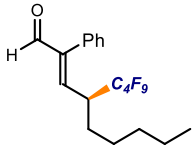

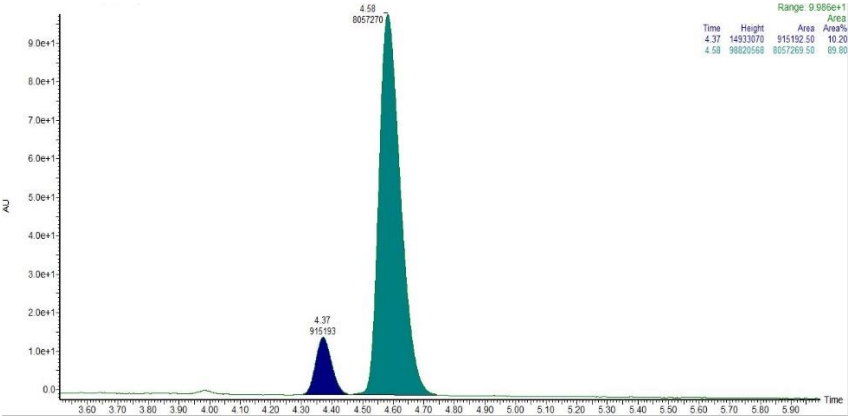

7o - UPC² analysis on a Daicel Chiralpak IE column (eluent: CO_2/*i*-PrOH = 90:10; flow rate 2 mL/min, λ = 360 nm, τ_{minor} = 4.6 min, τ_{major} = 4.8 min), 88:12 er.

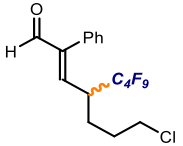

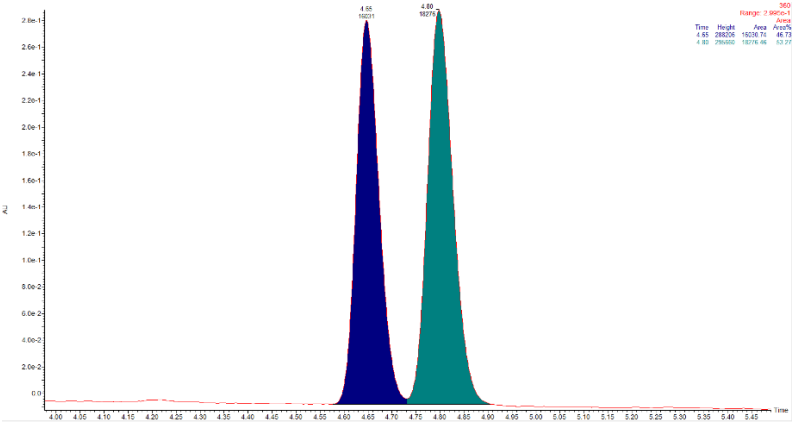

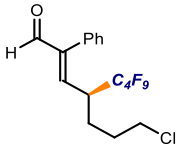

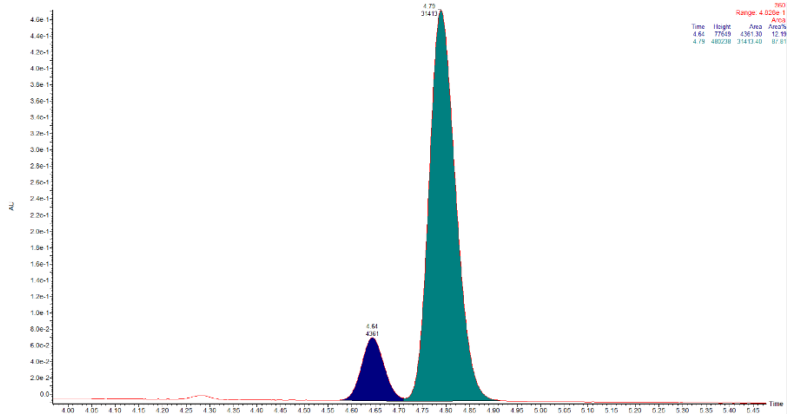

7p - UPC² analysis on a Daicel Chiralpak IE column (eluent: CO_2/*i*-PrOH = 90:10; flow rate 2 mL/min, λ = 211 nm, τ_{minor} = 4.2 min, τ_{major} = 4.4 min), 93:7 er.

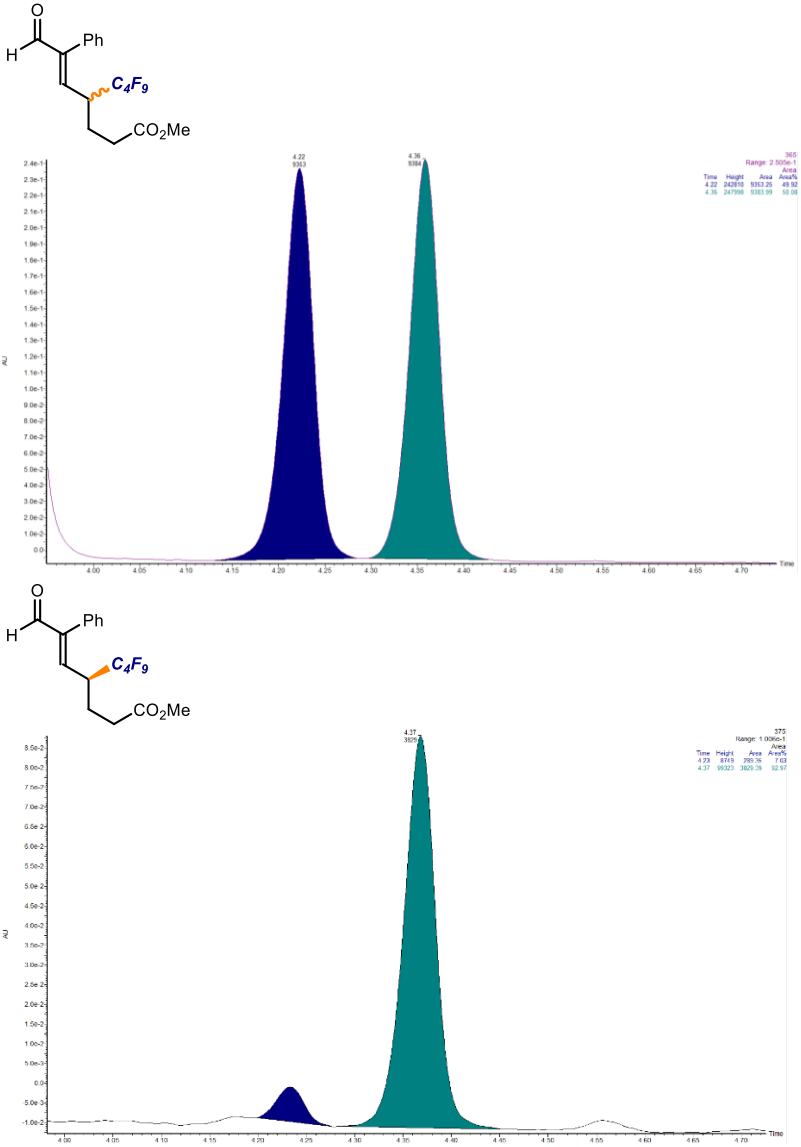

7q - UPC² analysis on a Daicel Chiralpak IE column (eluent: CO_2/*i*-PrOH = 90:10; flow rate 2 mL/min, λ = 211 nm, τ_{minor} = 4.7 min, τ_{major} = 4.9 min), 90:10 er.

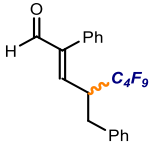

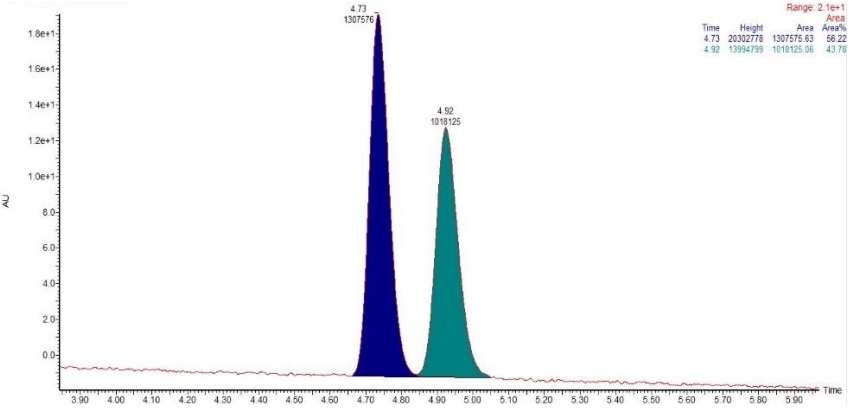

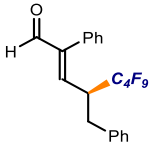

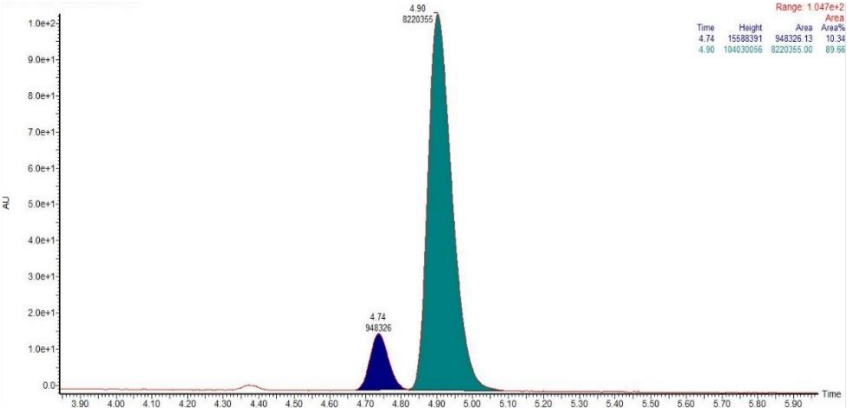

7r - UPC² analysis on a Daicel Chiralpak IE column (eluent: CO_2/*i*-PrOH = 90:10; flow rate 2 mL/min, λ = 350 nm, τ_{minor} = 2.7 min, τ_{major} = 2.9 min), 89:11 er.

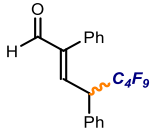

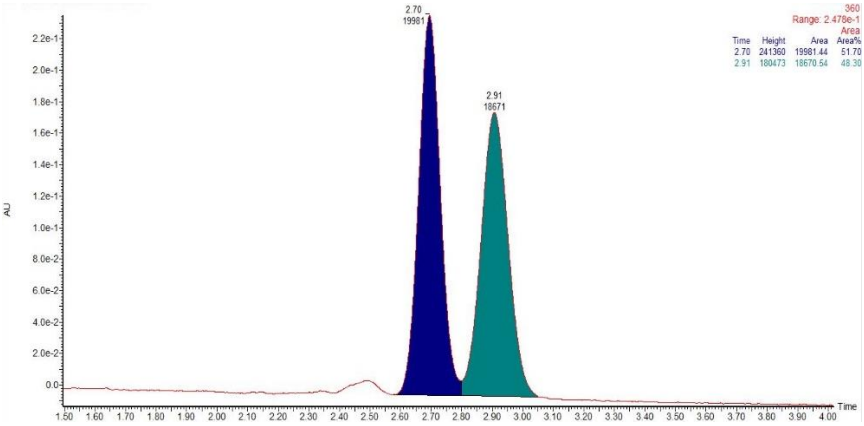

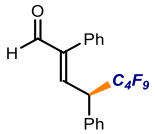

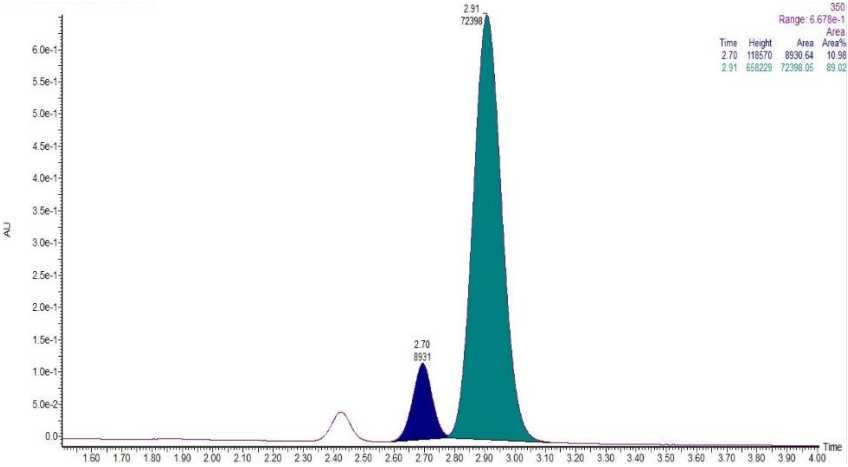

7s - UPC^2 analysis on a Daicel Chiralpak IE column (eluent: CO_2/*i*-PrOH = 90:10; flow rate 2 mL/min, λ = 360 nm, τ_{minor} = 4.3 min, τ_{major} = 4.4 min), 90:10 er.

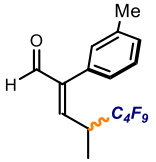

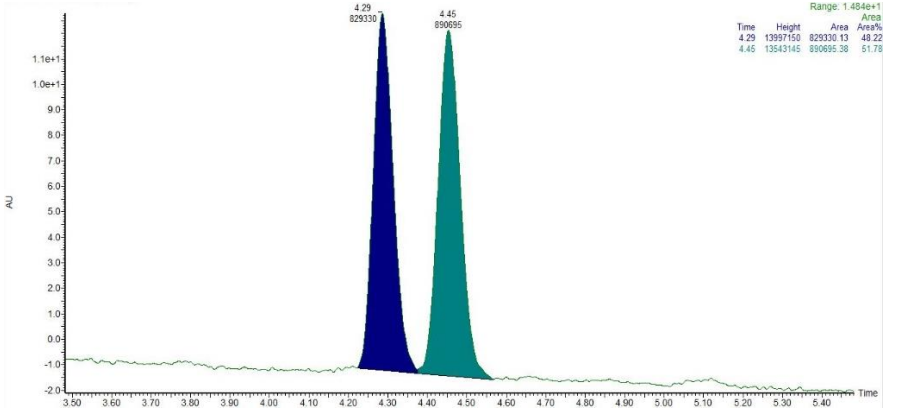

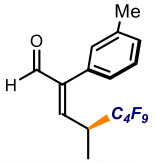

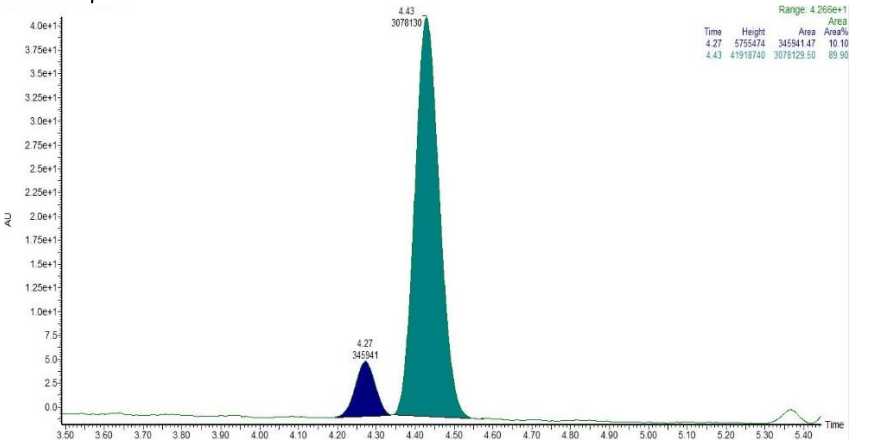

7t - UPC² analysis on a Daicel Chiralpak IE column (eluent: CO_2/*i*-PrOH = 90:10; flow rate 2 mL/min, λ = 211 nm, τ_{minor} = 4.4 min, τ_{major} = 4.6 min), 90:10 er.

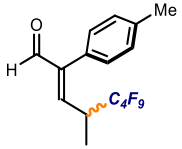

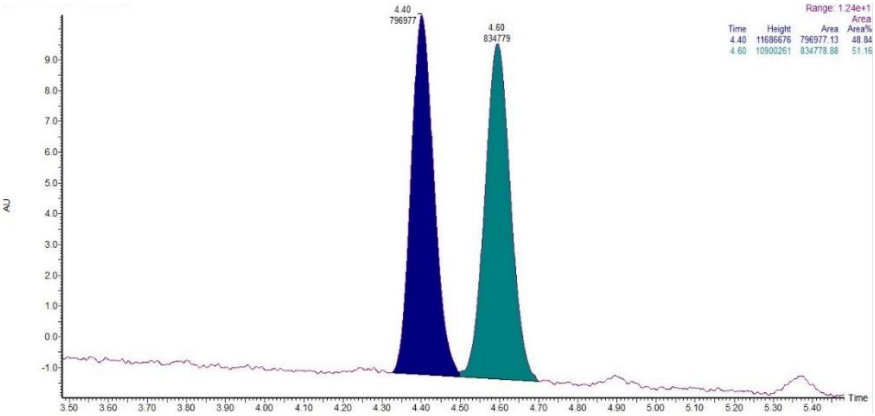

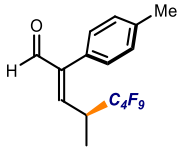

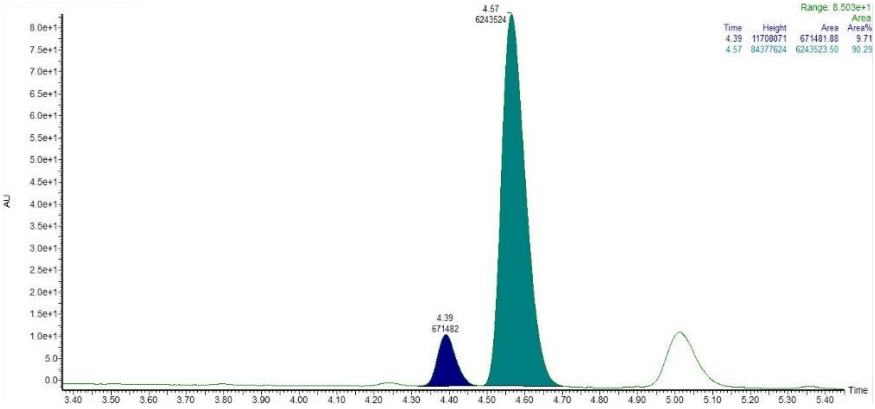

7u - UPC² analysis on a Daicel Chiralpak IE column (eluent: CO_2/*i*-PrOH = 90:10; flow rate 2 mL/min, λ = 211 nm, τ_{minor} = 4.6 min, τ_{major} = 4.9 min), 92:8 er.

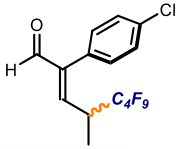

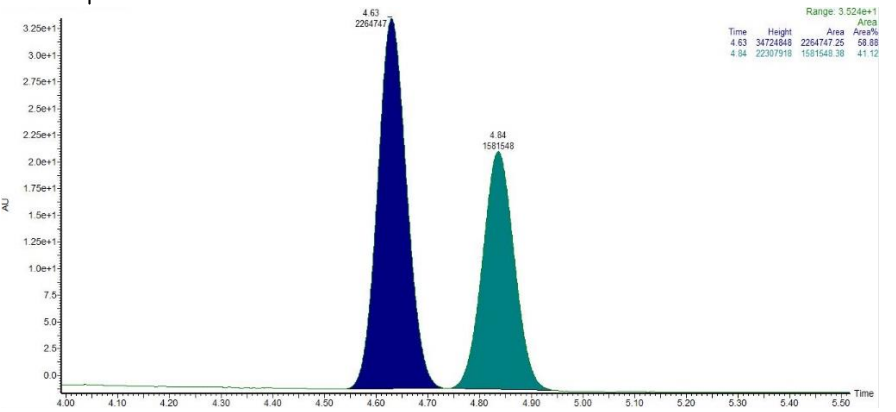

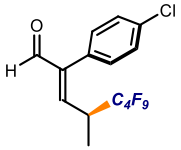

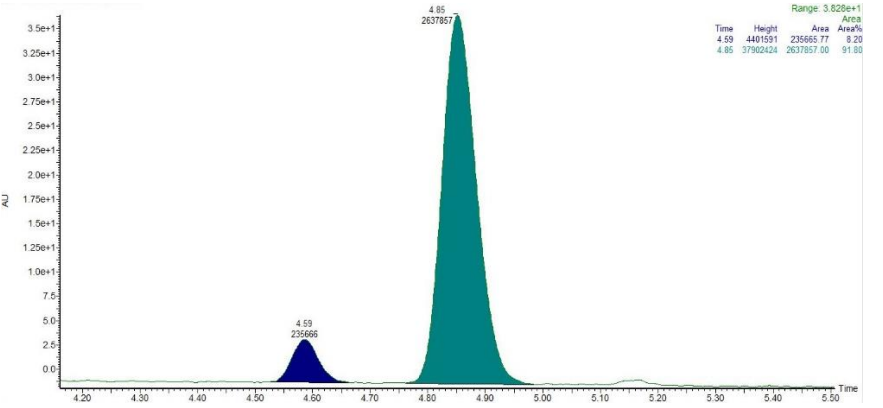

7v - UPC² analysis on a Daicel Chiralpak IE column (eluent: CO_2/*i*-PrOH = 90:10; flow rate 2 mL/min, λ = 211 nm, τ_{minor} = 6.6 min, τ_{major} = 7.0 min), 89:11 er.

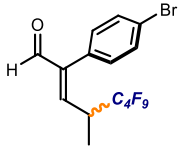

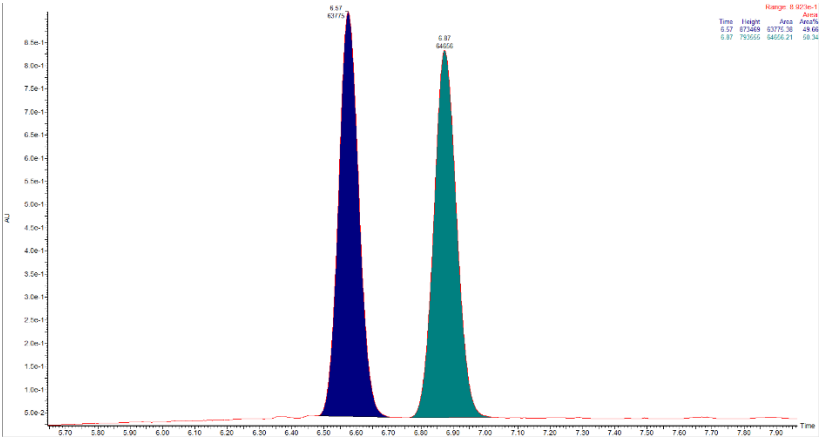

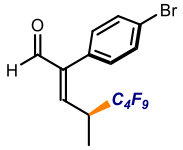

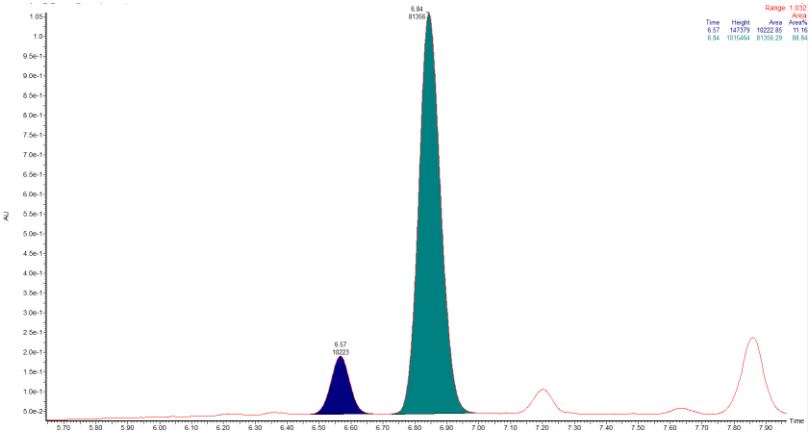

7w - UPC² analysis on a Daicel Chiralpak IE column (eluent: CO_2/*i*-PrOH = 90:10; flow rate 2 mL/min, λ = 211 nm, τ_{minor} = 4.5 min, τ_{major} = 4.8 min), 90:10 er.

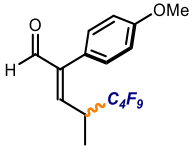

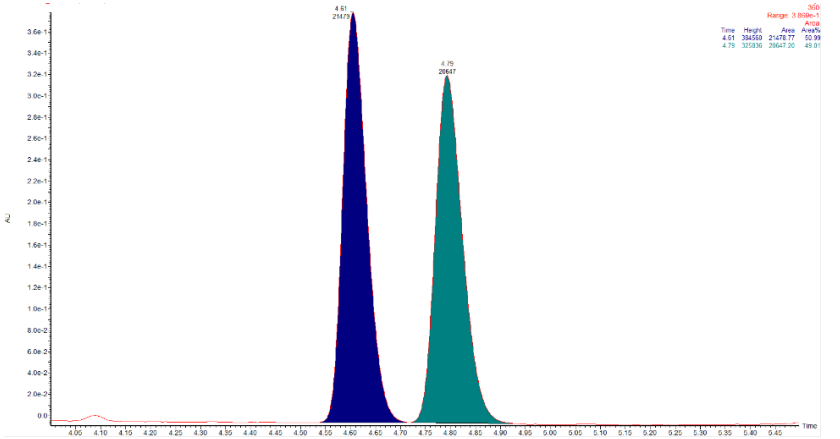

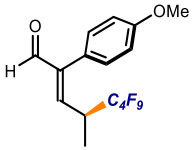

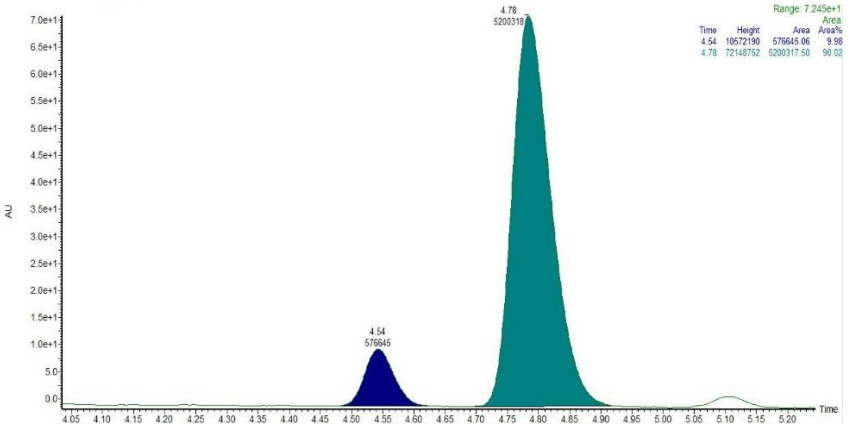

7j - UPC² analysis on a Daicel Chiralpak IE column (eluent: CO_2/*i*-PrOH = 90:10; flow rate 2 mL/min, λ = 211 nm: τ_{minor} = 5.3 min, τ_{major} = 5.5 min), 87:13 er.

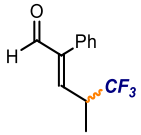

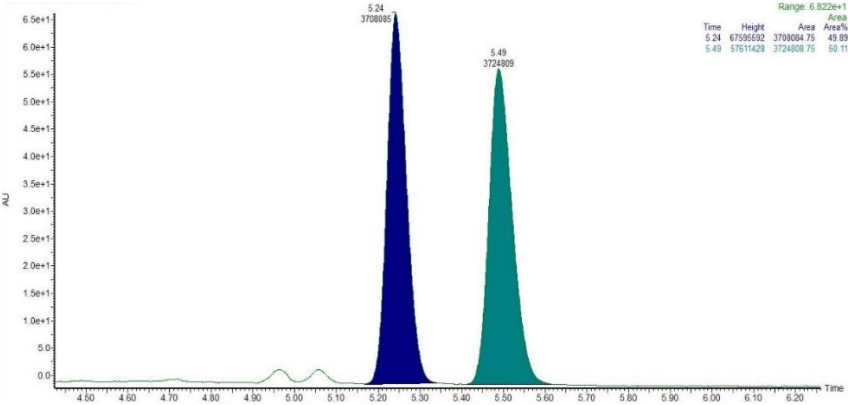

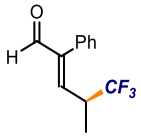

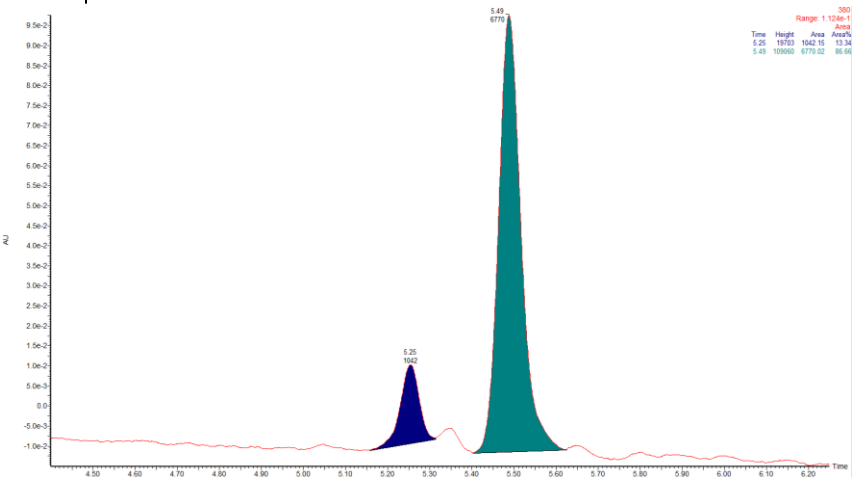

7k - UPC² analysis on a Daicel Chiralpak IE column (eluent: CO_2/*i*-PrOH = 90:10; flow rate 2 mL/min, λ = 211 nm: τ_{minor} = 5.3 min, τ_{major} = 5.5 min), 87:13 er.

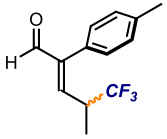

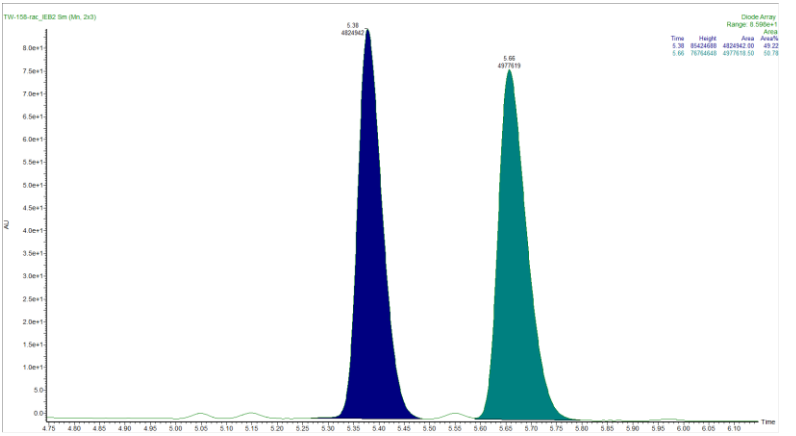

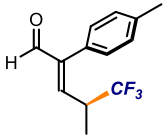

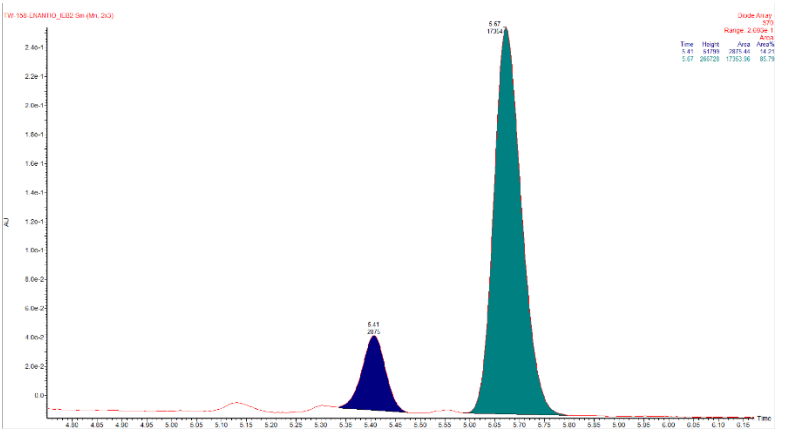

71 - UPC² analysis on a Daicel Chiralpak IB column (eluent: CO_2/*i*-PrOH = 90:10; flow rate 2 mL/min, λ = 211 nm: τ_{minor} = 5.66 min, τ_{major} = 5.84 min), 87:13 er.

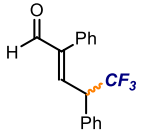

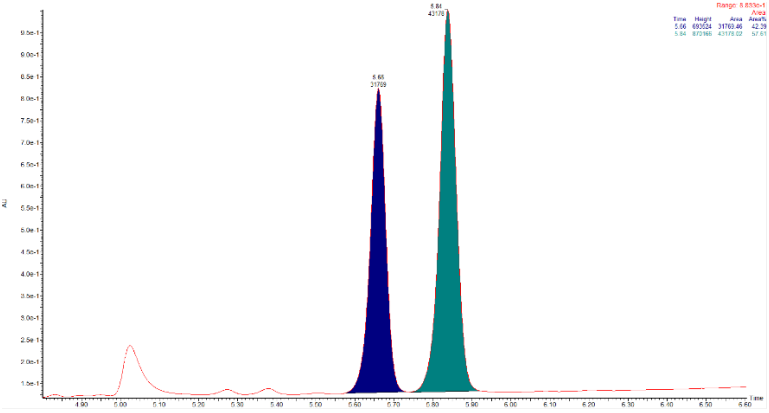

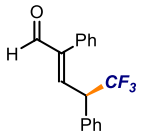

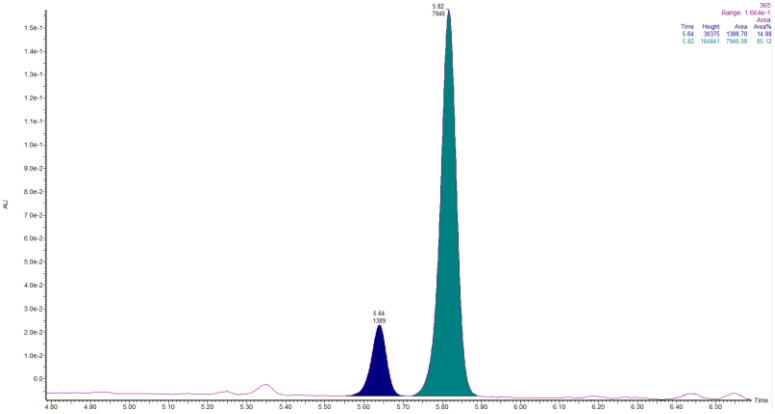

5.9 NMR Spectra

^{1}H-NMR (300 MHz, DMSO-d_6)

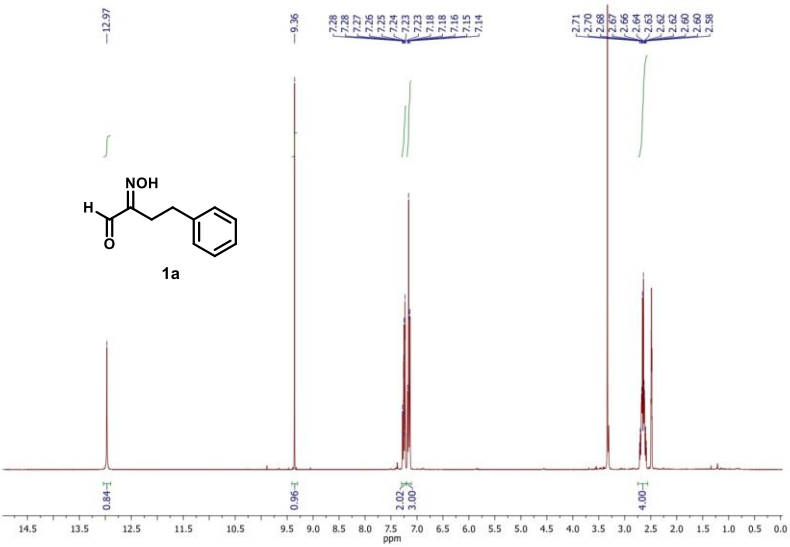

^{13}C{^{1}H}-NMR (75 MHz, DMSO-d_6)

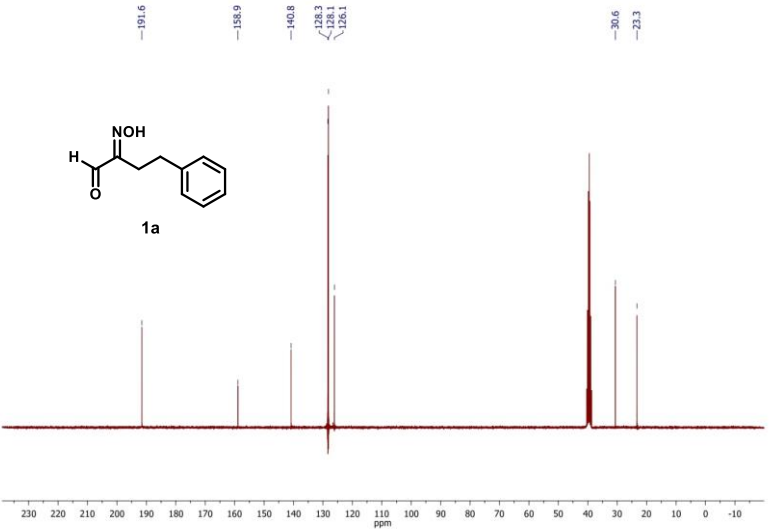

^{1}H-NMR (300 MHz, DMSO-d_6)

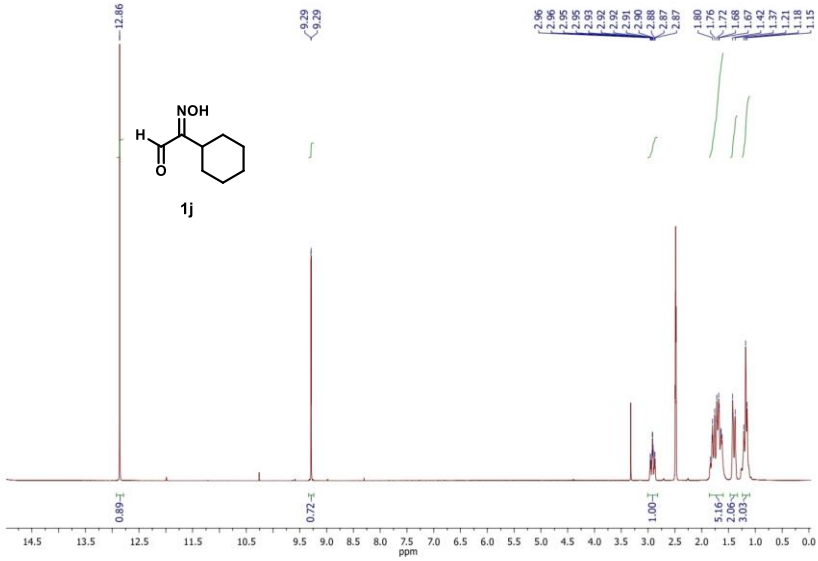

^{13}C{^{1}H}-NMR (75 MHz, DMSO-d_6)

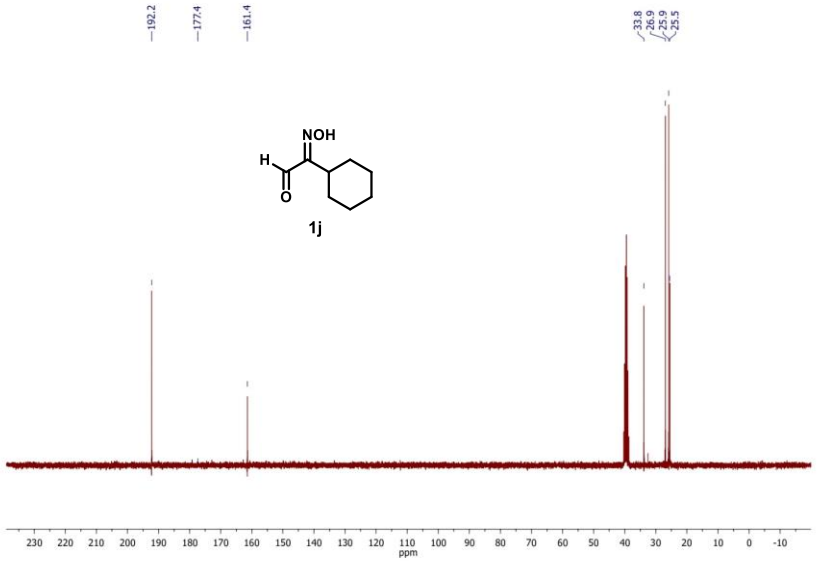

^{1}H-NMR (300 MHz, DMSO-d_6)

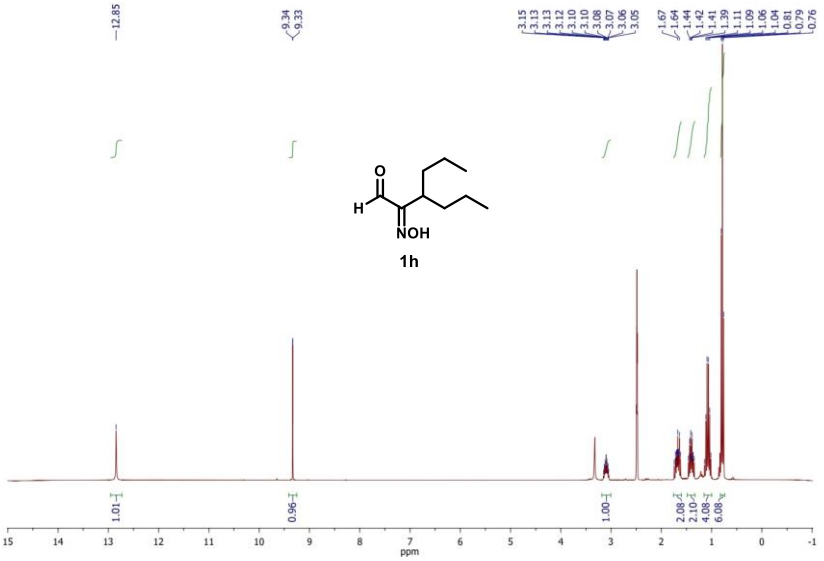

^{13}C{^{1}H}-NMR (75 MHz, DMSO-d_6)

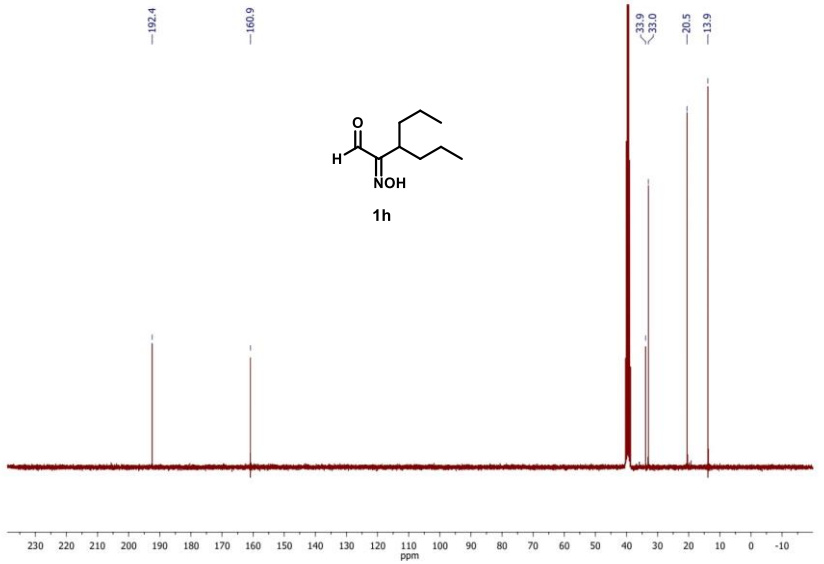

^{1}H-NMR (300 MHz, DMSO-d_6)

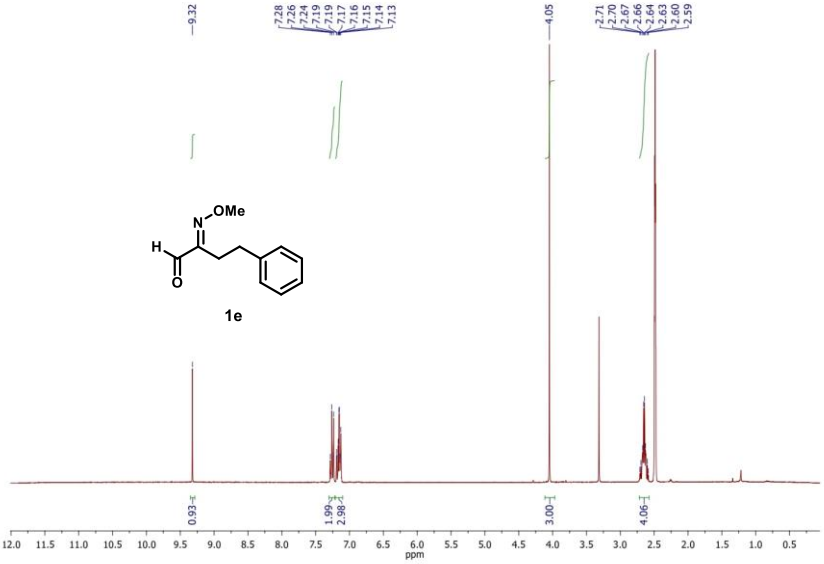

^{13}C{^{1}H}-NMR (75 MHz, DMSO-d_6)

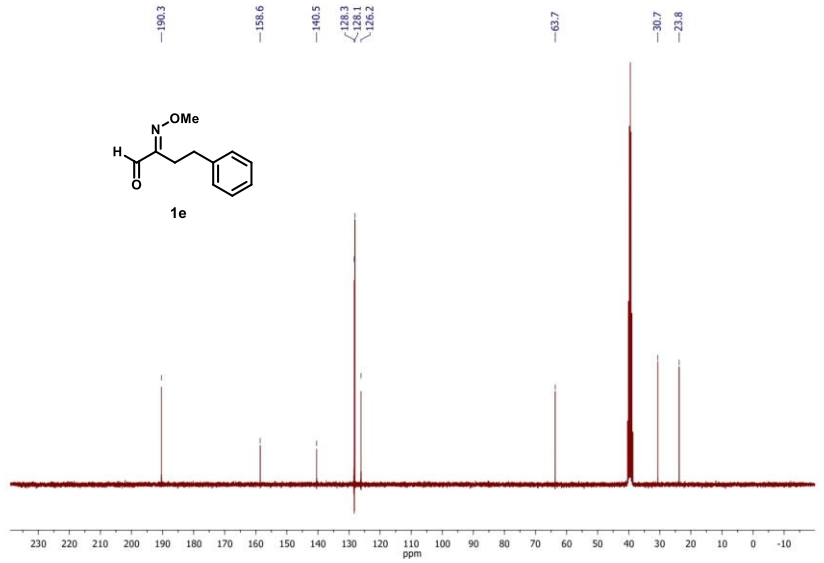

^{1}H-NMR (300 MHz,$CDCl_3$)

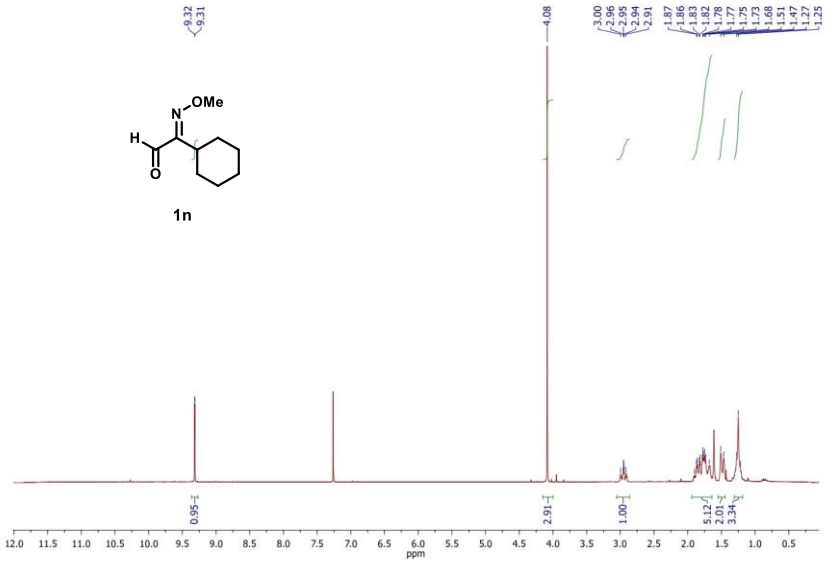

^{13}C{^{1}H}-NMR (75 MHz, $CDCl_3$)

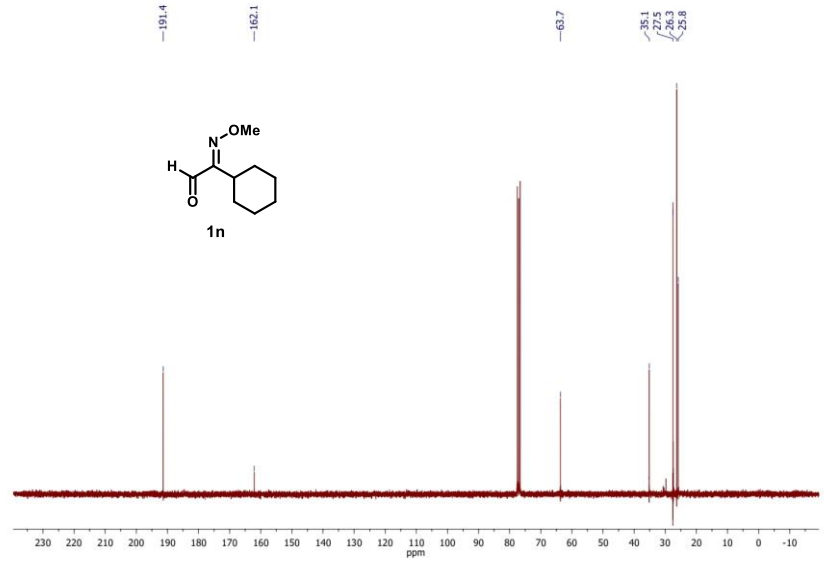

^{1}H-NMR (300 MHz, DMSO-d_6)

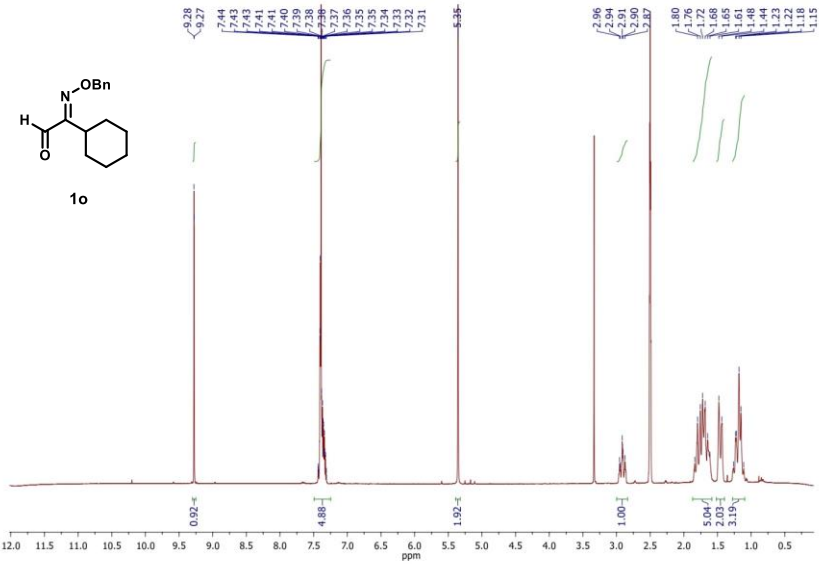

^{13}C{^{1}H}-NMR (75 MHz, DMSO-d_6)

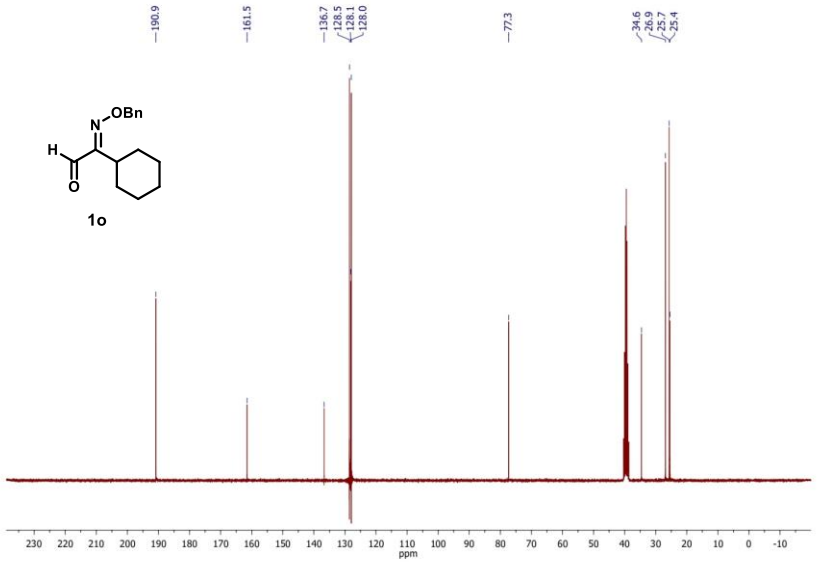

^{1}H-NMR (300 MHz, DMSO-d_6)

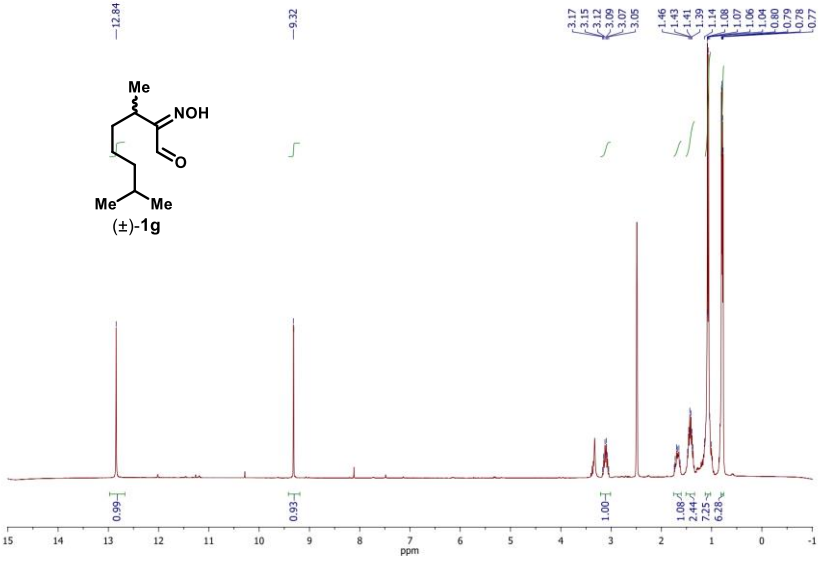

^{13}C{^{1}H}-NMR (75 MHz, DMSO-d_6)

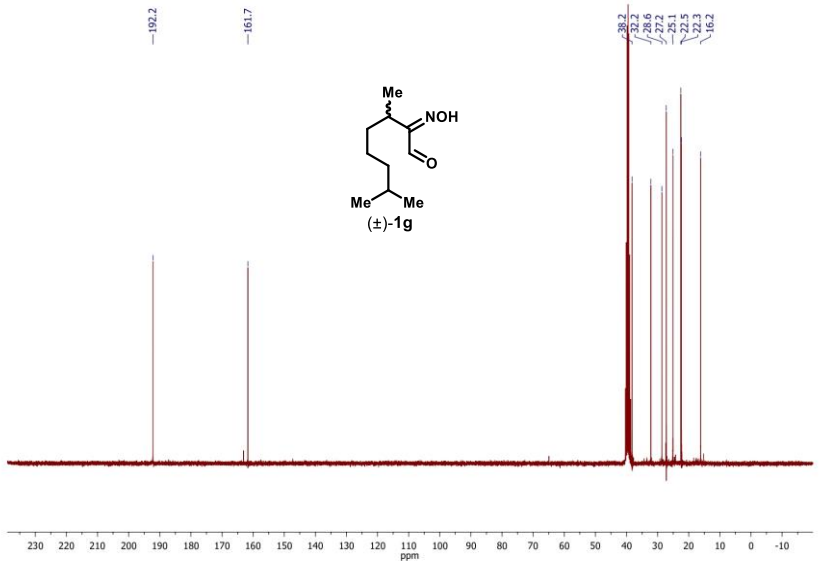

^{1}H-NMR (300 MHz, DMSO-d_6)

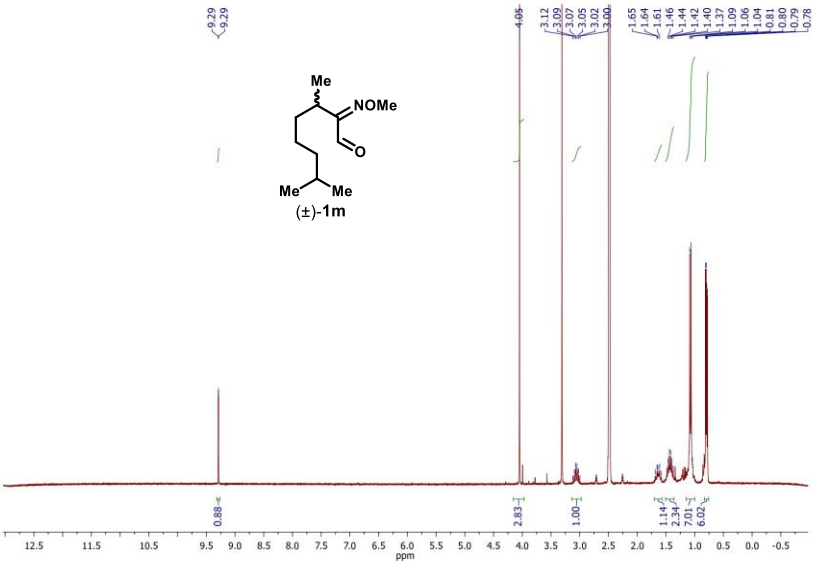

^{13}C{^{1}H}-NMR (75 MHz, DMSO-d_6)

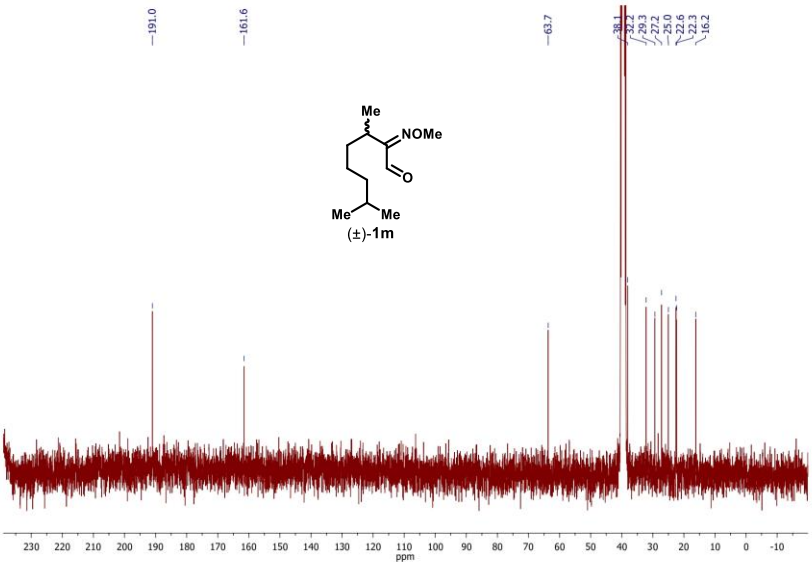

^{1}H-NMR (300 MHz, DMSO-d_6)

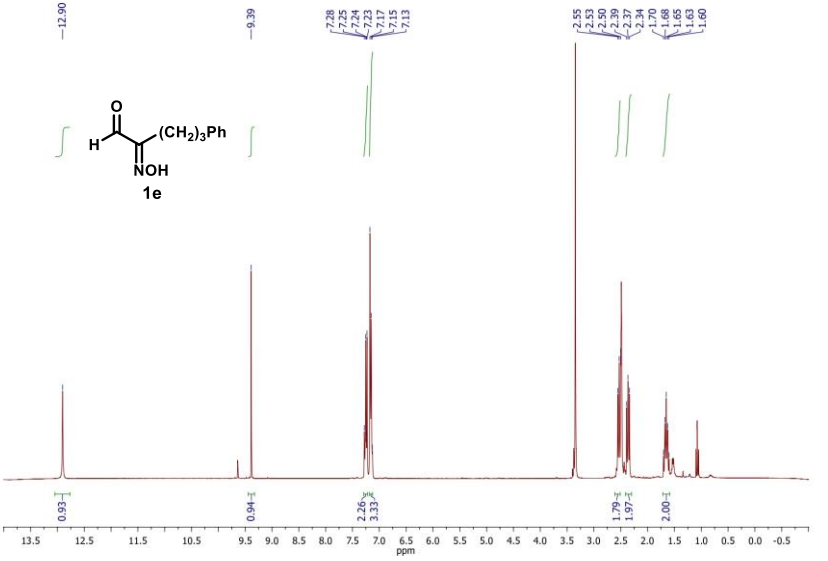

^{13}C{^{1}H}-NMR (75 MHz, DMSO-d_6)

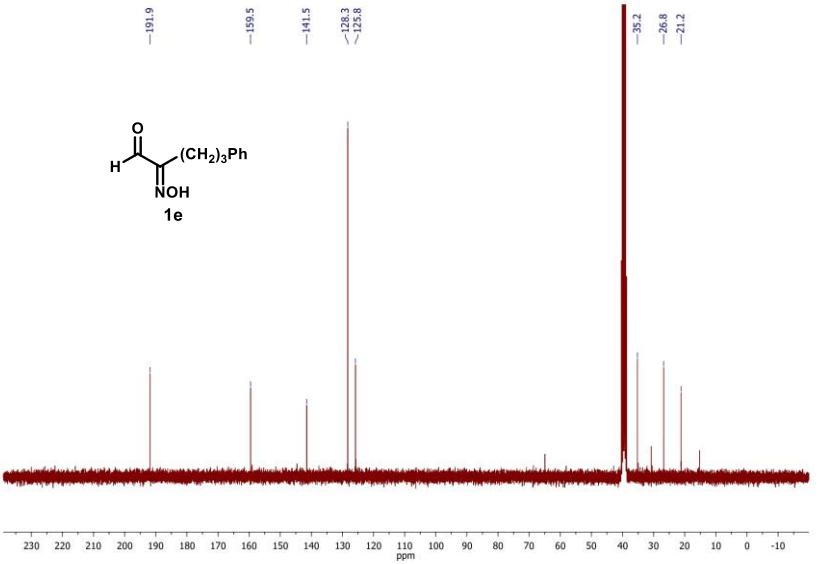

^{1}H-NMR (300 MHz, DMSO-d_6)

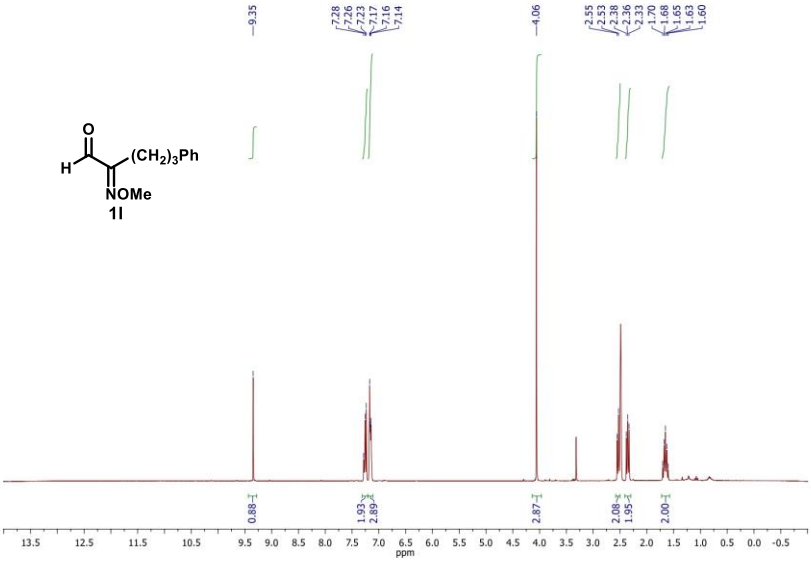

^{13}C{^{1}H}-NMR (75 MHz, DMSO-d_6)

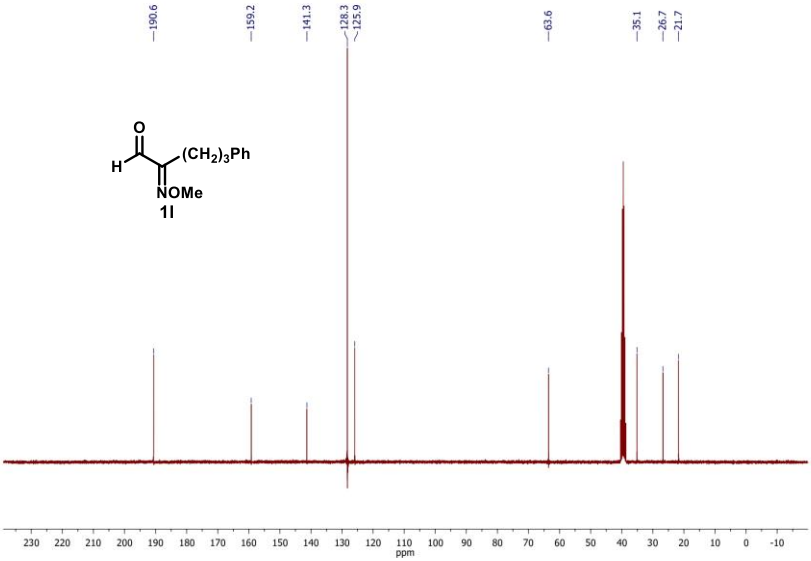

^{1}H-NMR (300 MHz, DMSO-d_6)

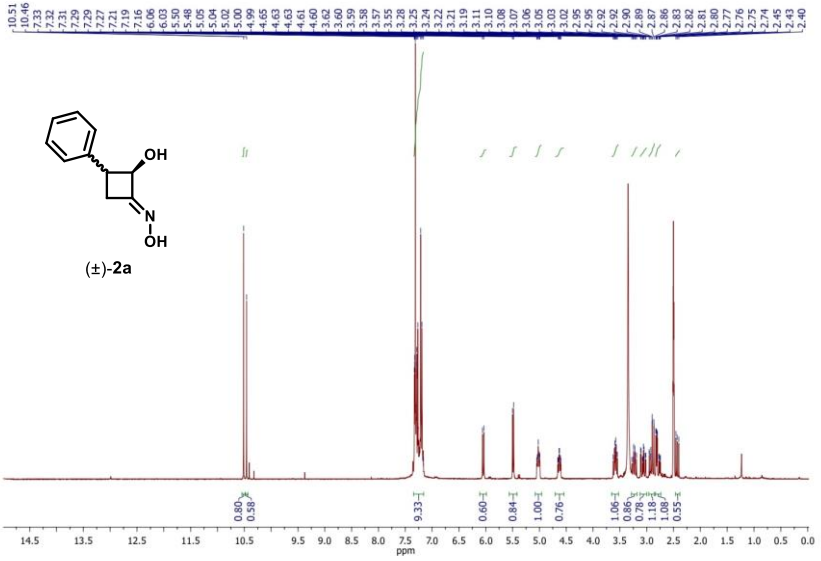

^{13}C{^{1}H}-NMR (75 MHz, DMSO-d_6)

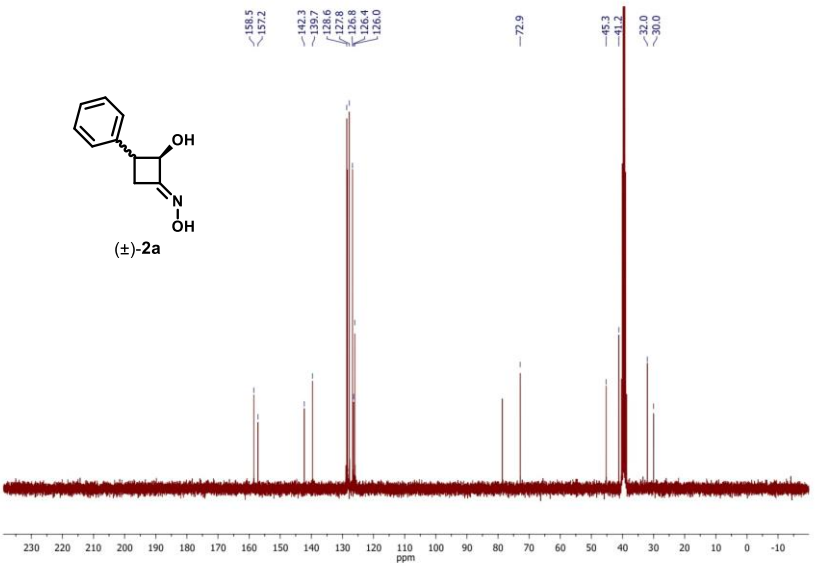

NOESY (300 MHz, DMSO-d_6)

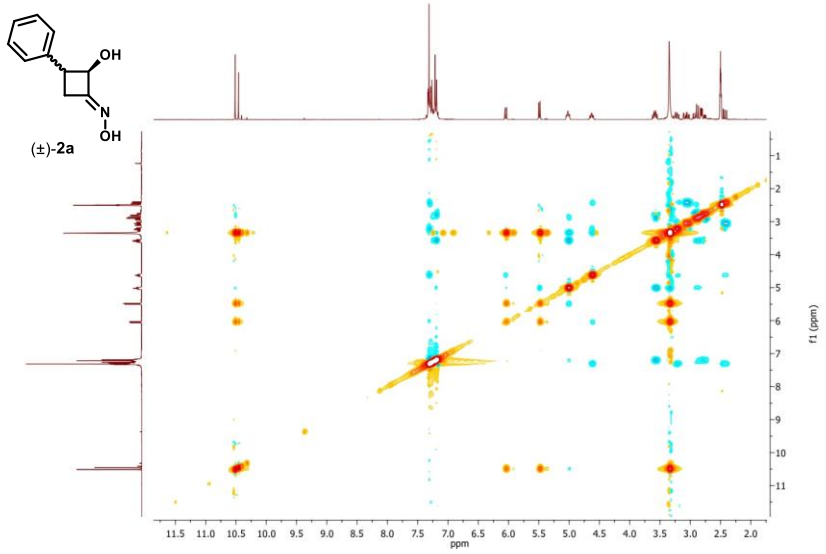

HSQC (300 MHz, DMSO-d_6)

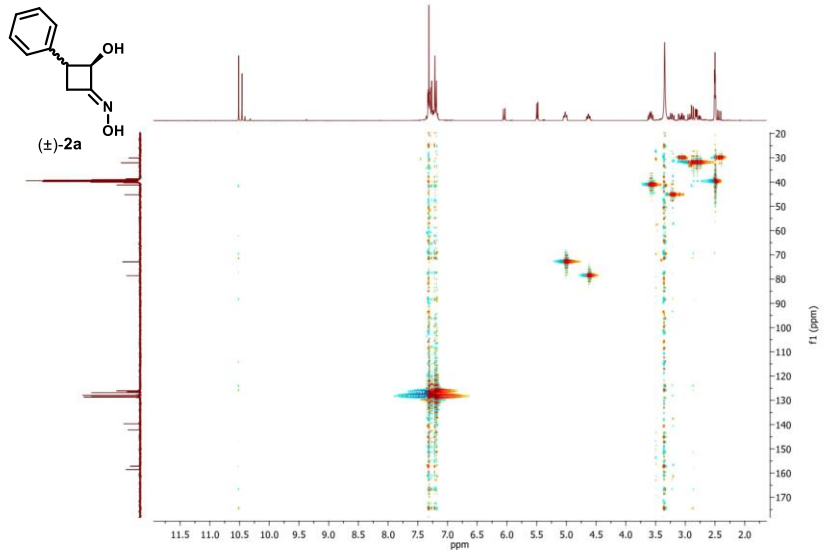

^{1}H-NMR (300 MHz, DMSO-*d*$_6$)

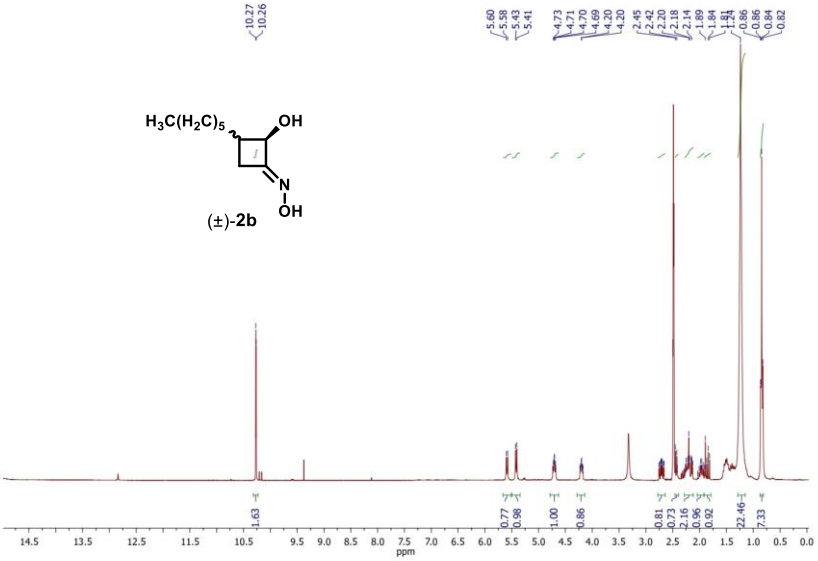

^{13}C{^{1}H}-NMR (75 MHz, DMSO-*d*$_6$)

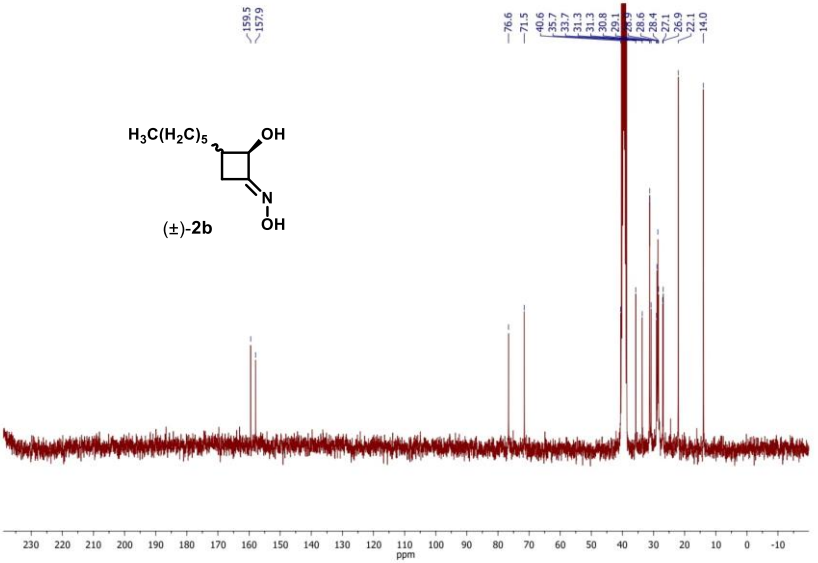

^{1}H-NMR (300 MHz, DMSO-d_6)

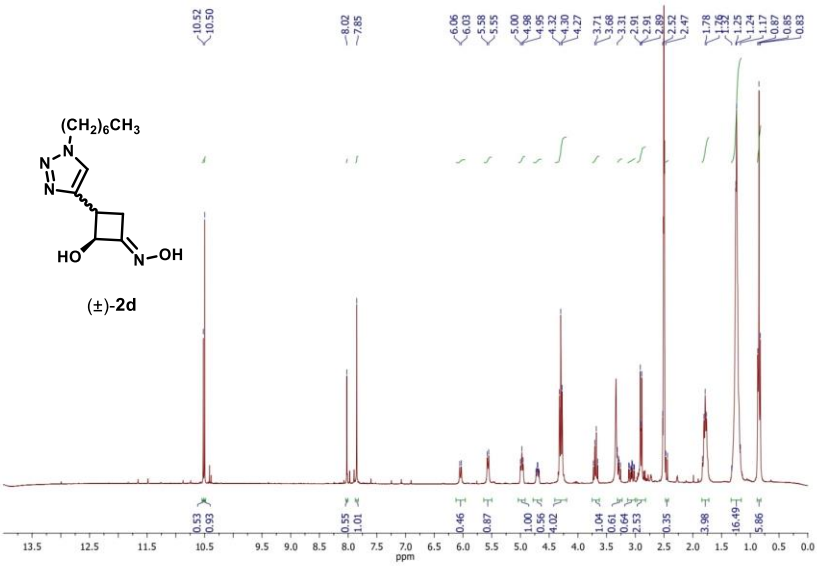

^{13}C{^{1}H}-NMR (75 MHz, DMSO-d_6)

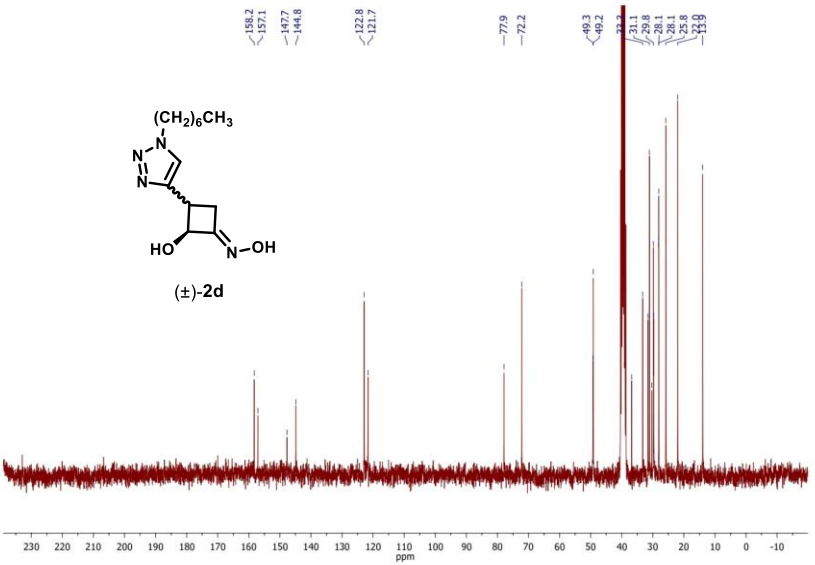

DEPT-135 (75 MHz, DMSO-d_6)

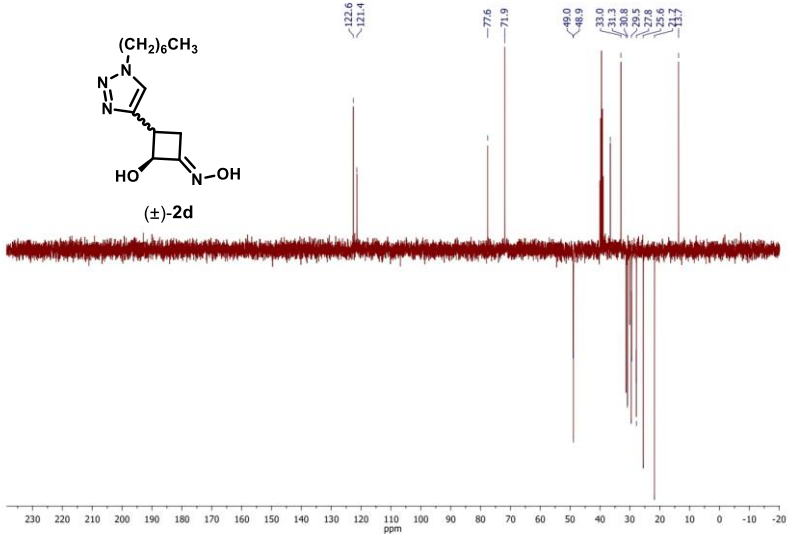

COSY-45 (300 MHz, DMSO-d_6)

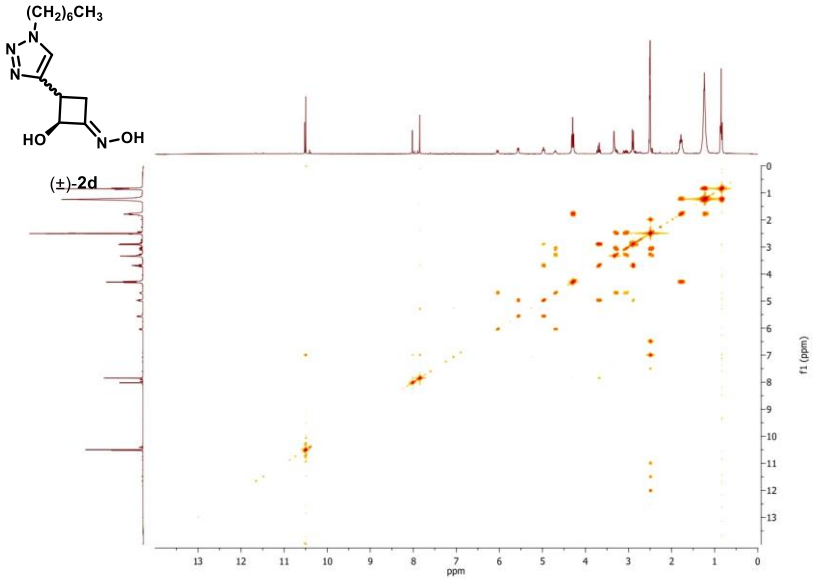

HSQC (300 MHz, DMSO-d_6)

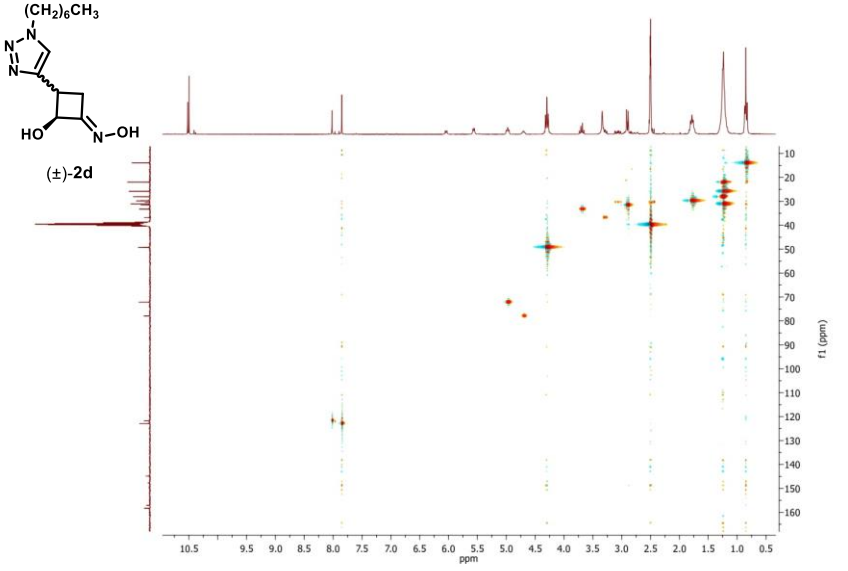

^{1}H-NMR (300 MHz, DMSO-d_6)

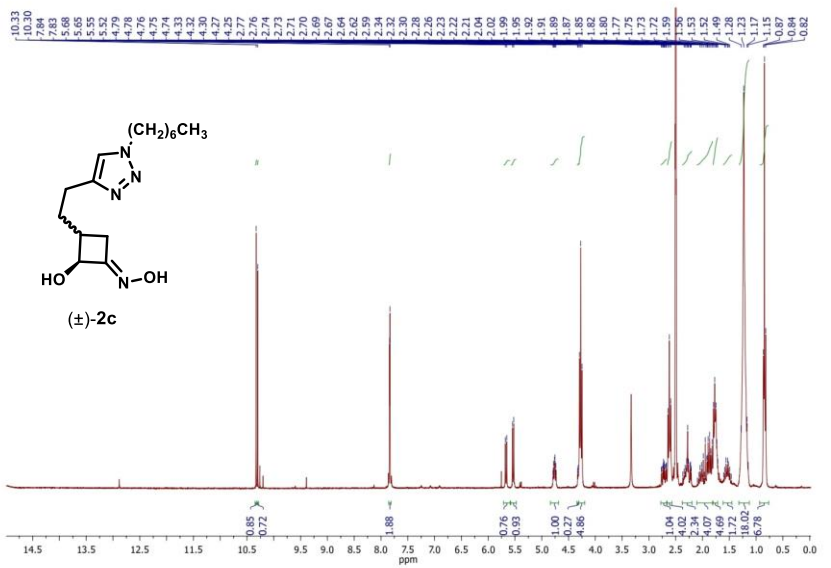

$^{13}C\{^{1}H\}$-NMR (75 MHz, DMSO-*d*$_6$)

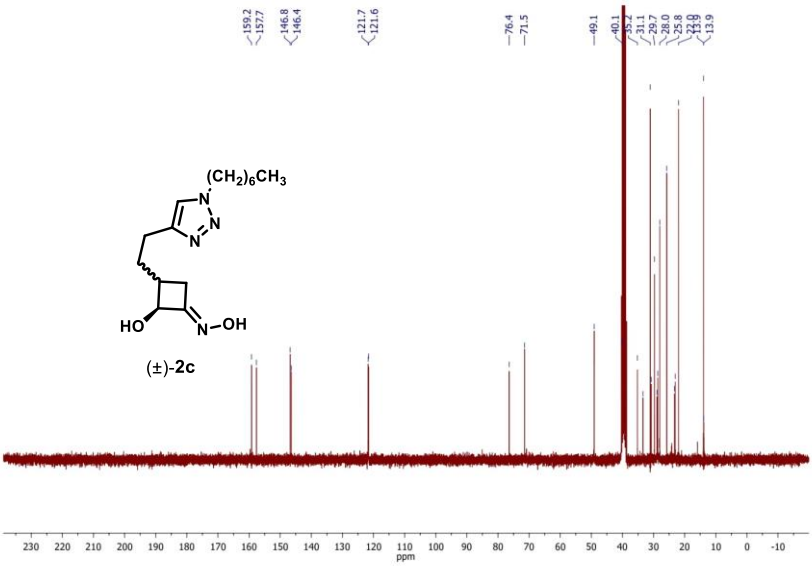

DEPT-135 (75 MHz, DMSO-*d*$_6$)

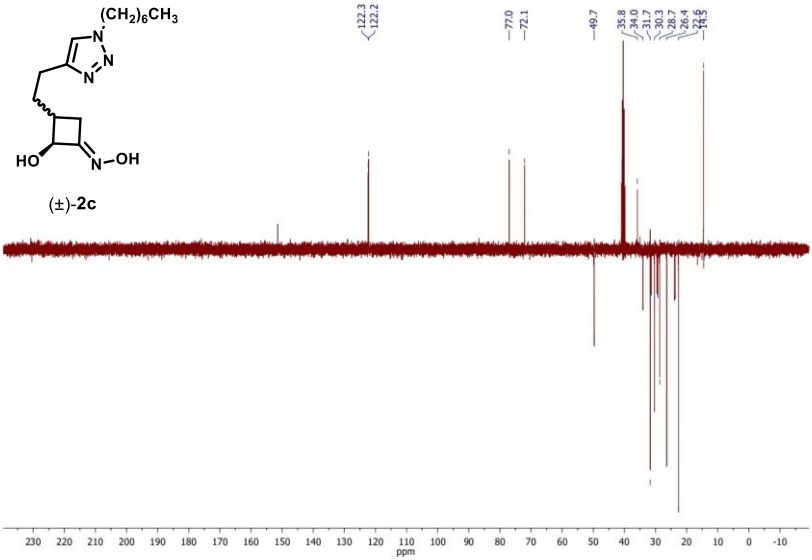

HSQC (300 MHz, DMSO-d_6)

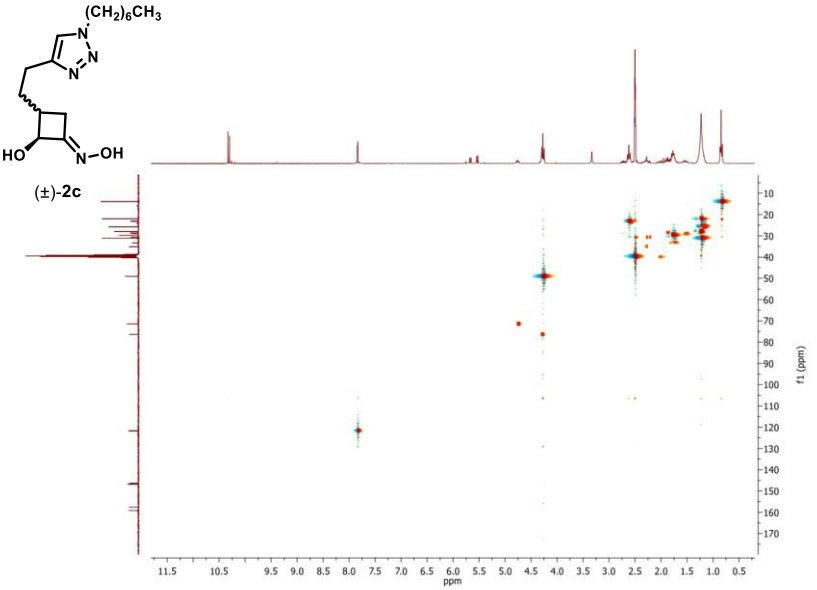

HMBC (300 MHz, DMSO-d_6)

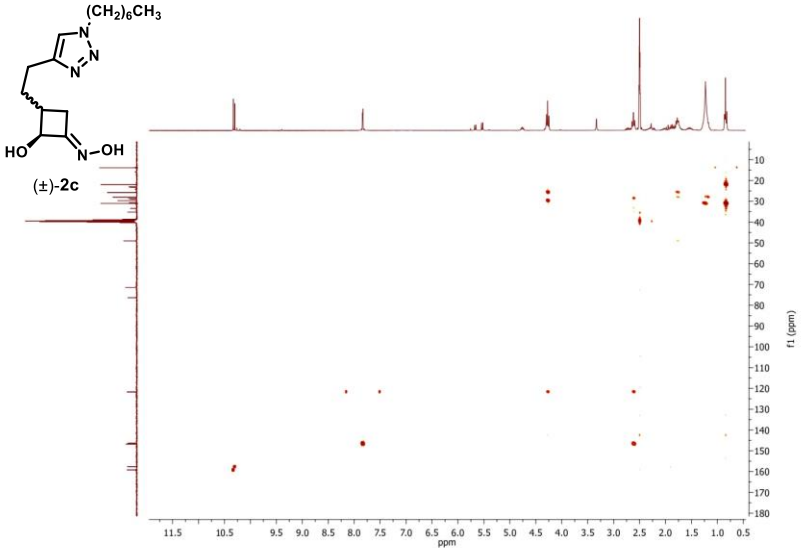

^{1}H-NMR (300 MHz, DMSO-d_6)

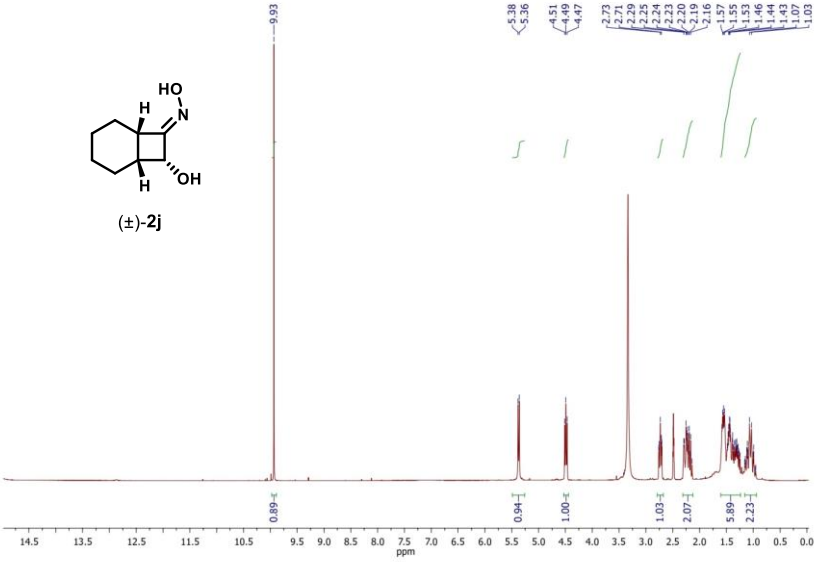

^{1}H-NMR (300 MHz, DMSO-d_6)

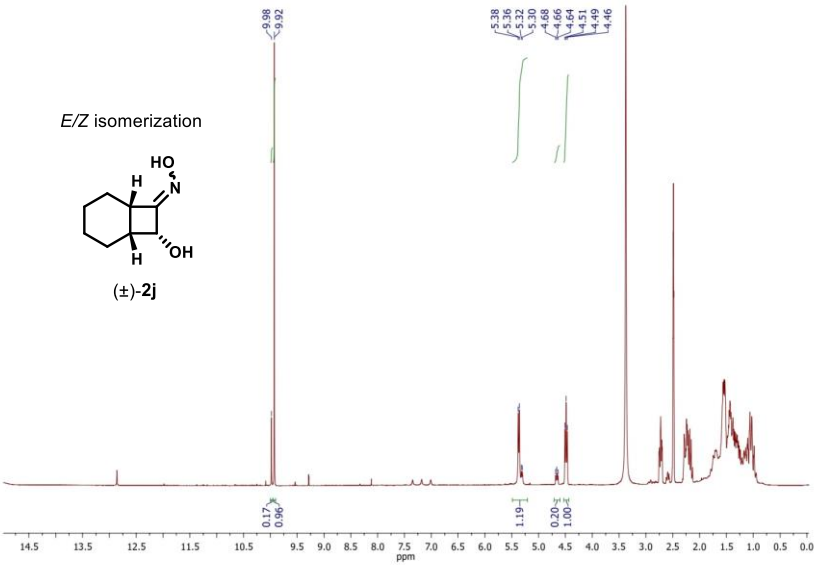

$^{13}C\{^{1}H\}$-NMR (75 MHz, DMSO-d_6)

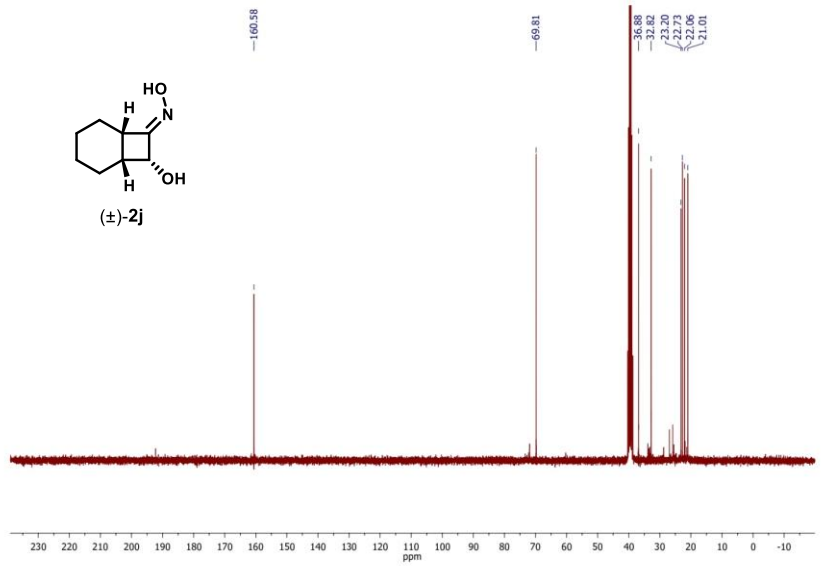

NOESY (300 MHz, DMSO-d_6)

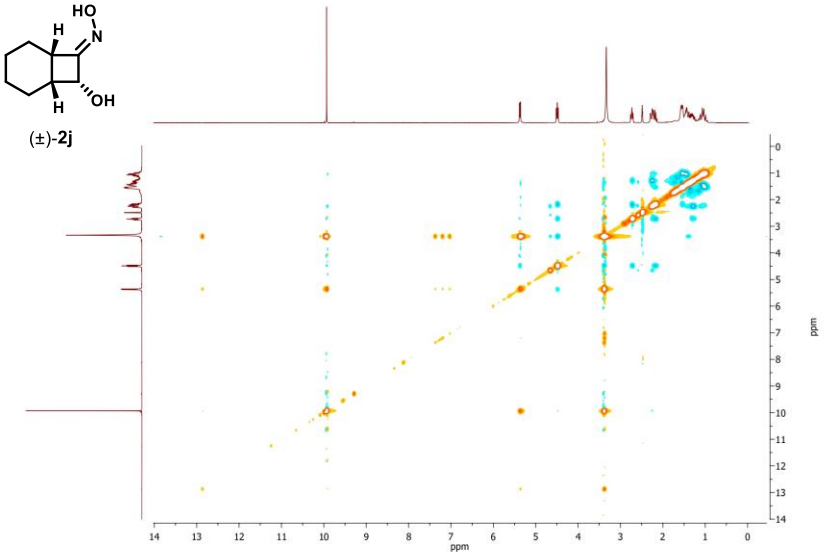

^{1}H-NMR (300 MHz, DMSO-d_6)

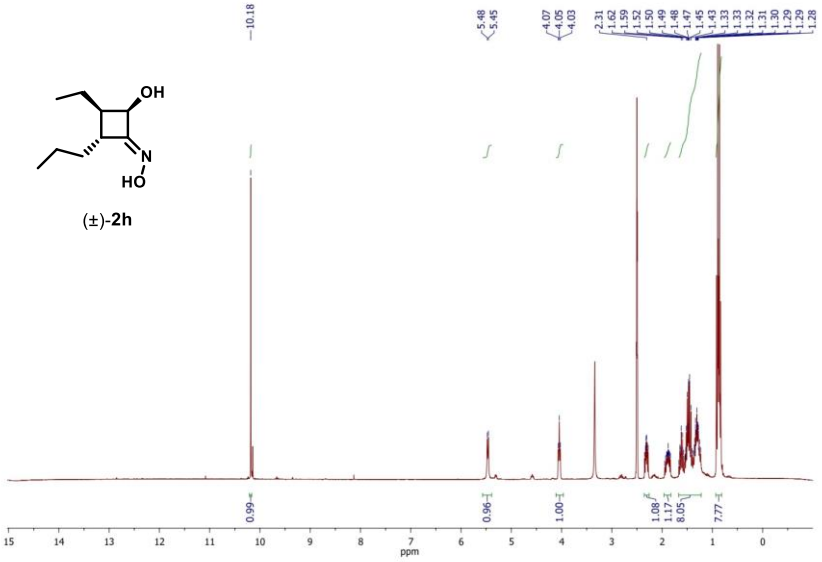

^{13}C{^{1}H}-NMR (75 MHz, DMSO-d_6)

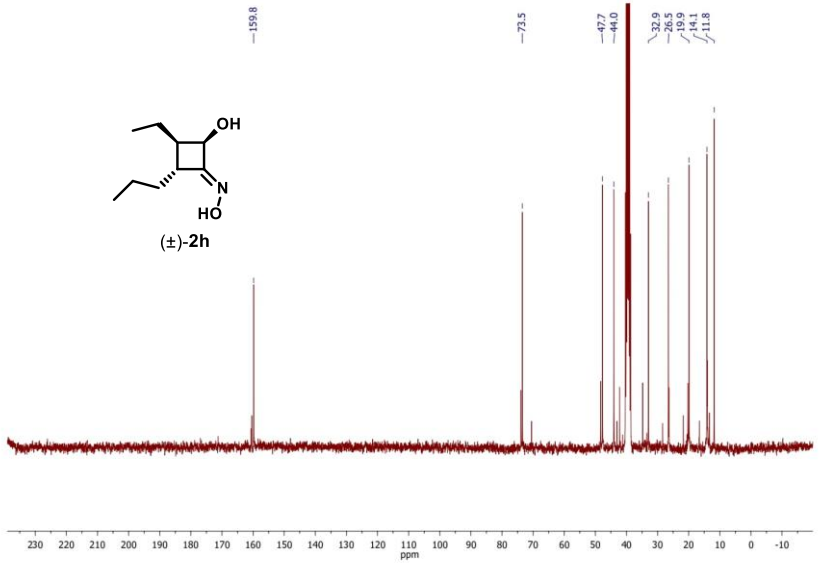

^{1}H-NMR (300 MHz, DMSO-d_6)

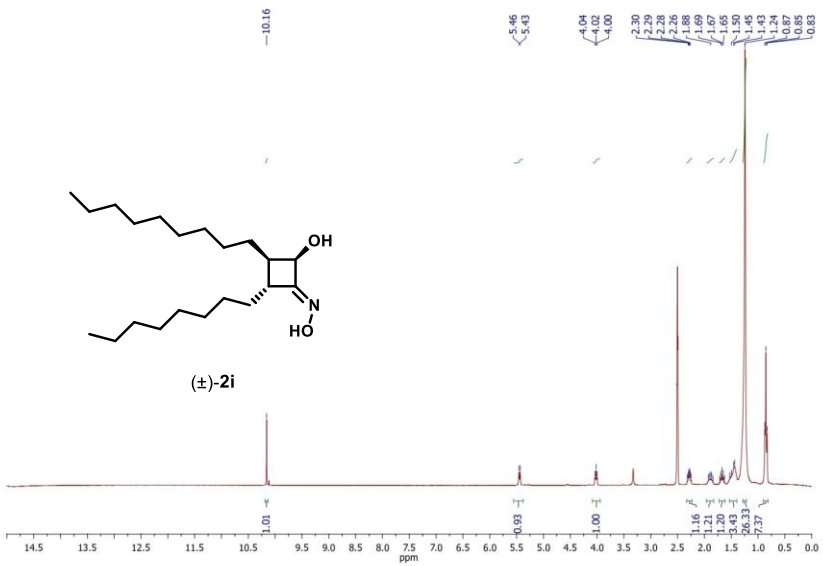

^{13}C{^{1}H}-NMR (75 MHz, DMSO-d_6)

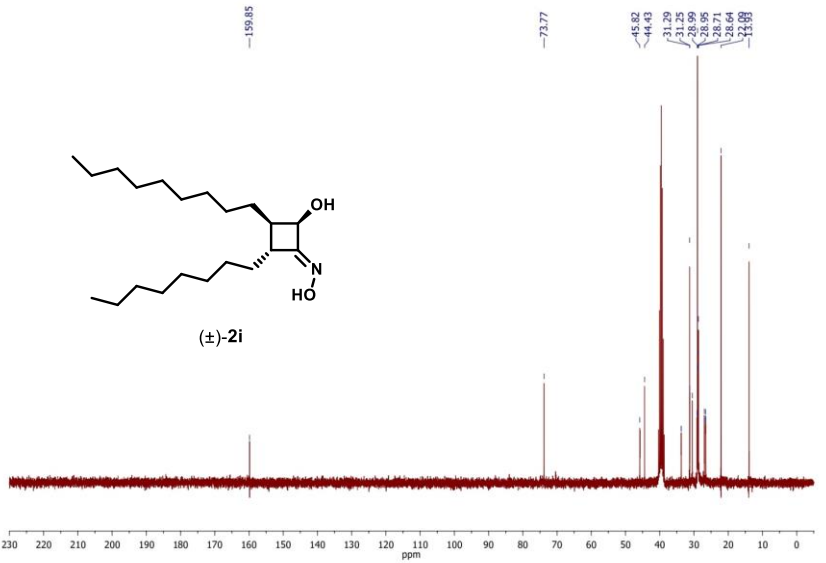

^{1}H-NMR (300 MHz, DMSO-d_6)

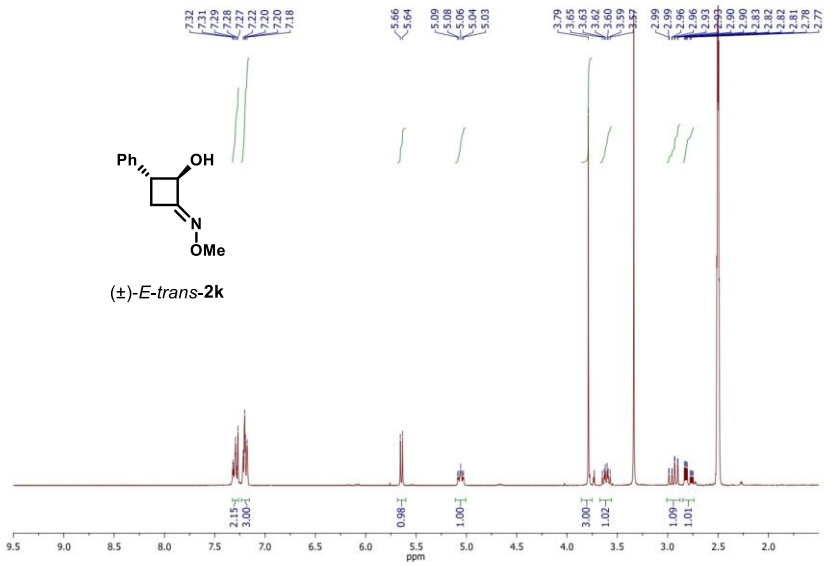

^{13}C{^{1}H}-NMR (75 MHz, DMSO-d_6)

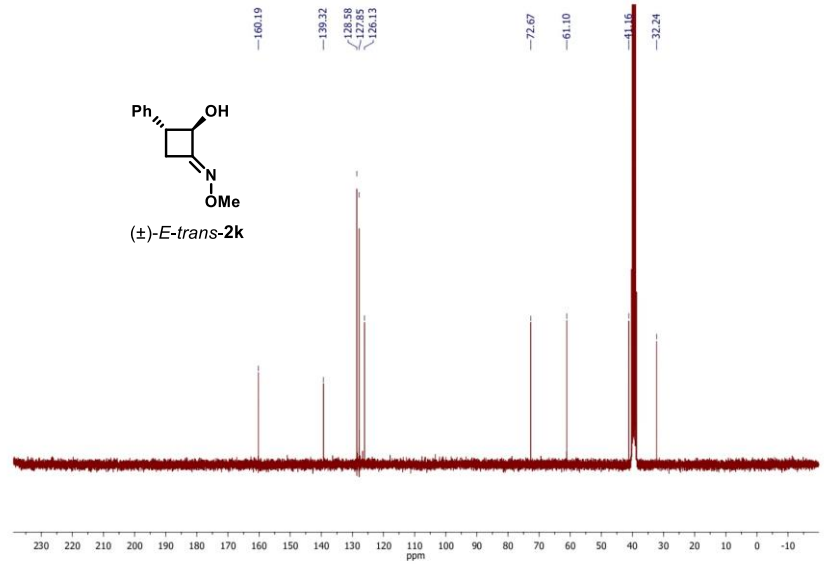

COSY-45 (300 MHz, DMSO-d_6)

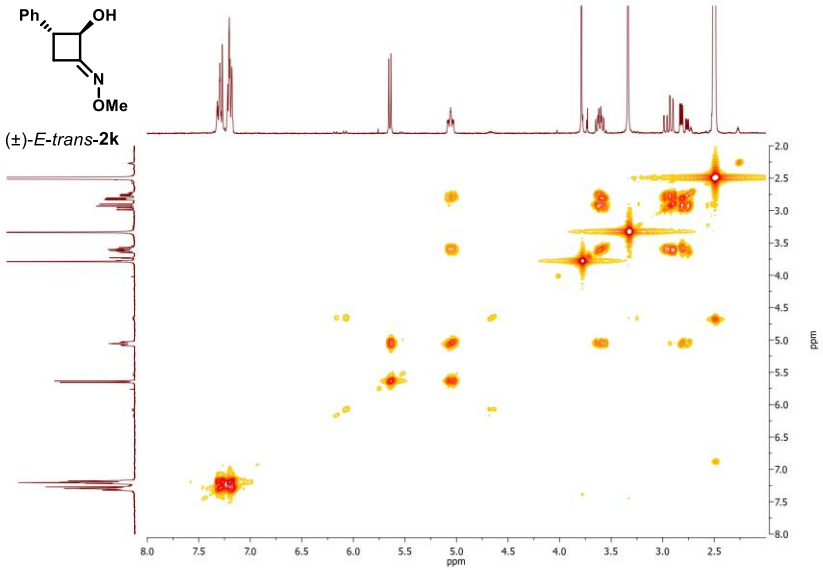

NOESY (300 MHz, DMSO-d_6)

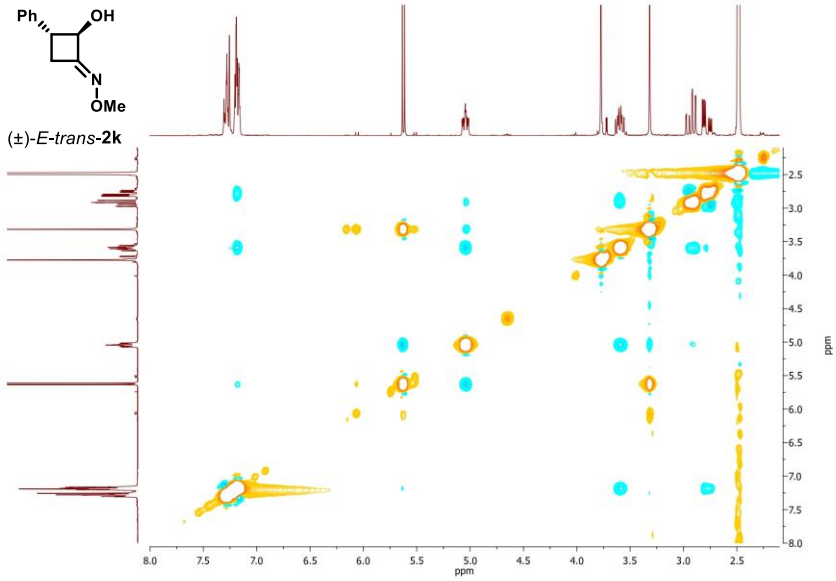

HSQC (300 MHz, DMSO-d_6)

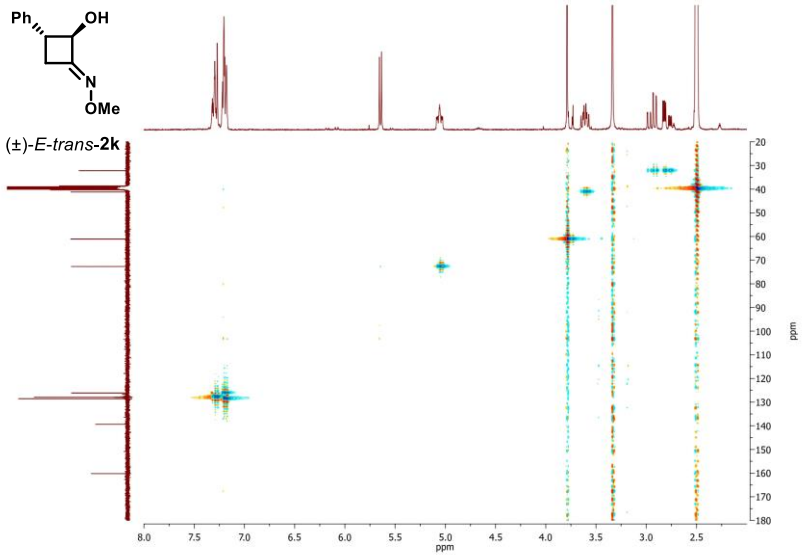

HMBC (300 MHz, DMSO-d_6)

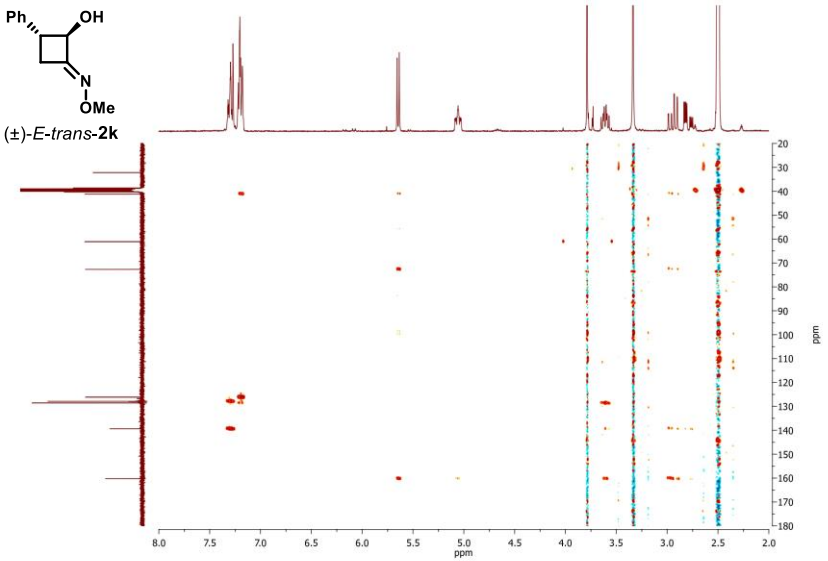

^{1}H-NMR (300 MHz, DMSO-d_6)

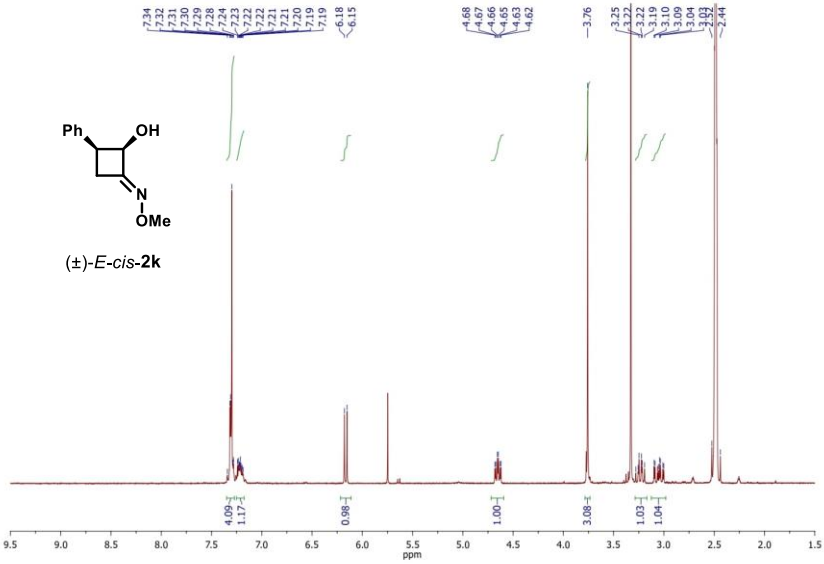

^{13}C{^{1}H}-NMR (75 MHz, DMSO-d_6)

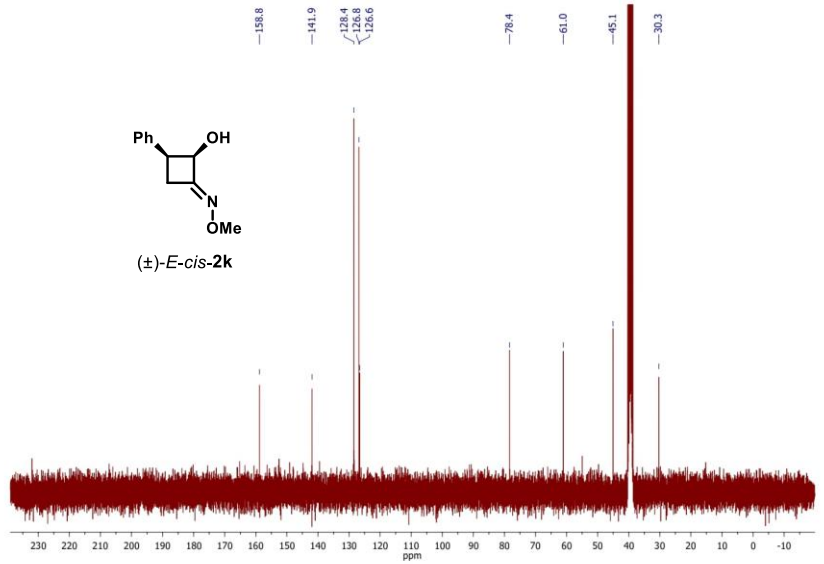

COSY-45 (300 MHz, DMSO-d_6)

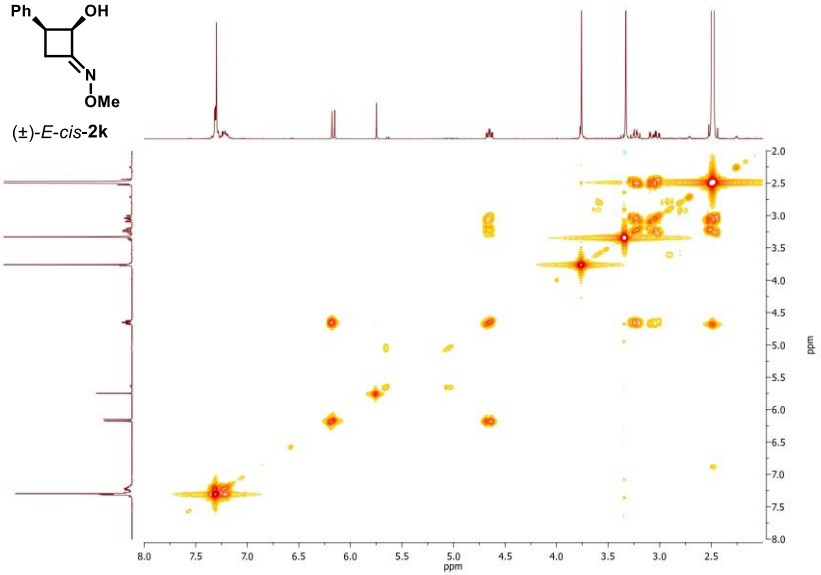

NOESY (300 MHz, DMSO-d_6)

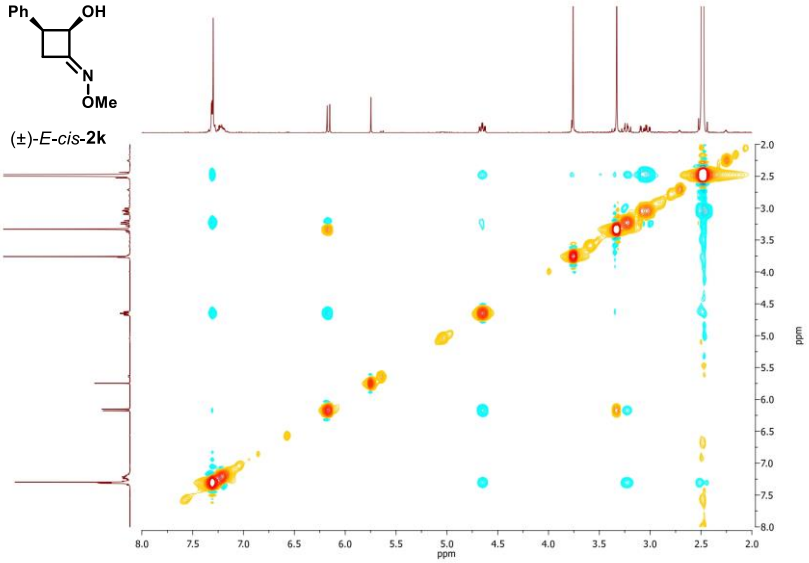

HSQC (300 MHz, DMSO-d_6)

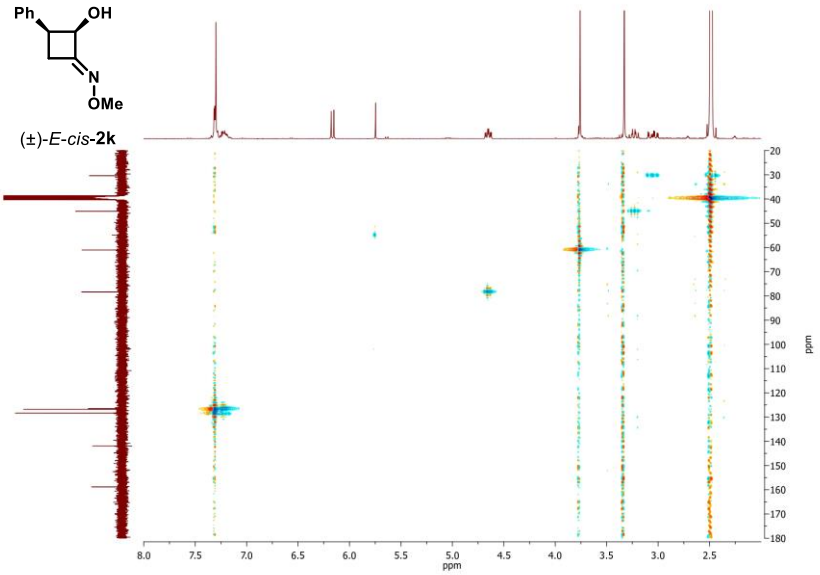

HMBC (300 MHz, DMSO-d_6)

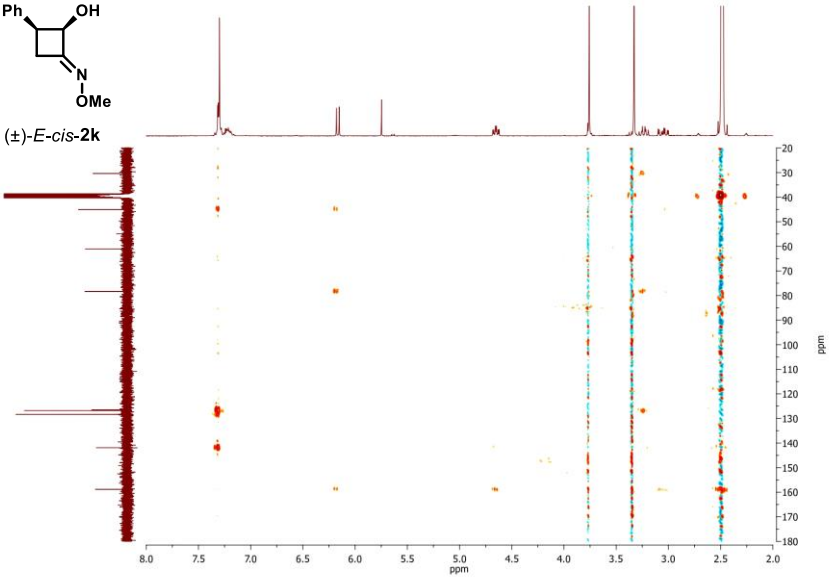

^{1}H-NMR (300 MHz, DMSO-d_6)

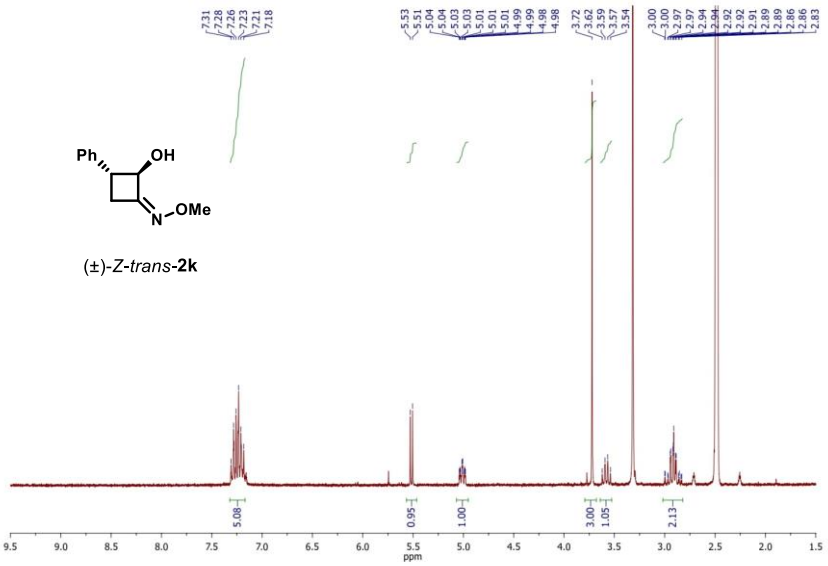

^{13}C{^{1}H}-NMR (75 MHz, DMSO-d_6)

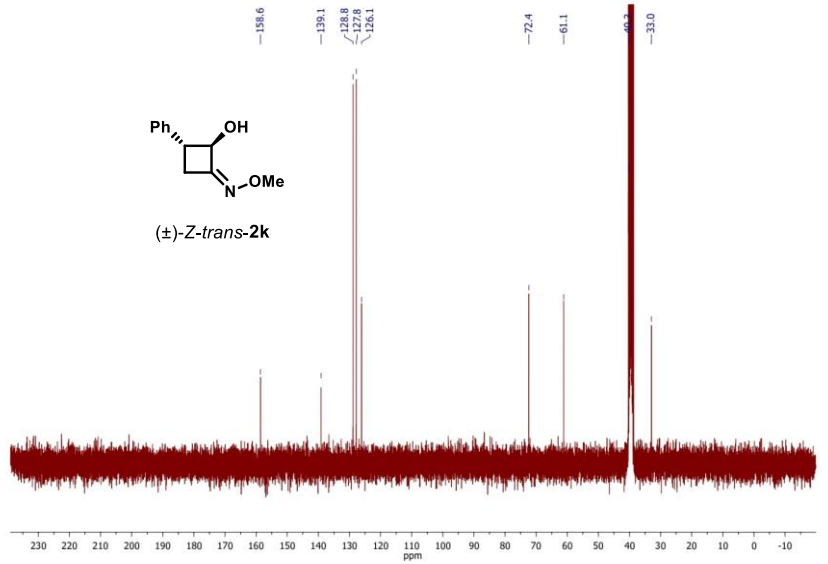

^{1}H-NMR (300 MHz, DMSO-d_6)

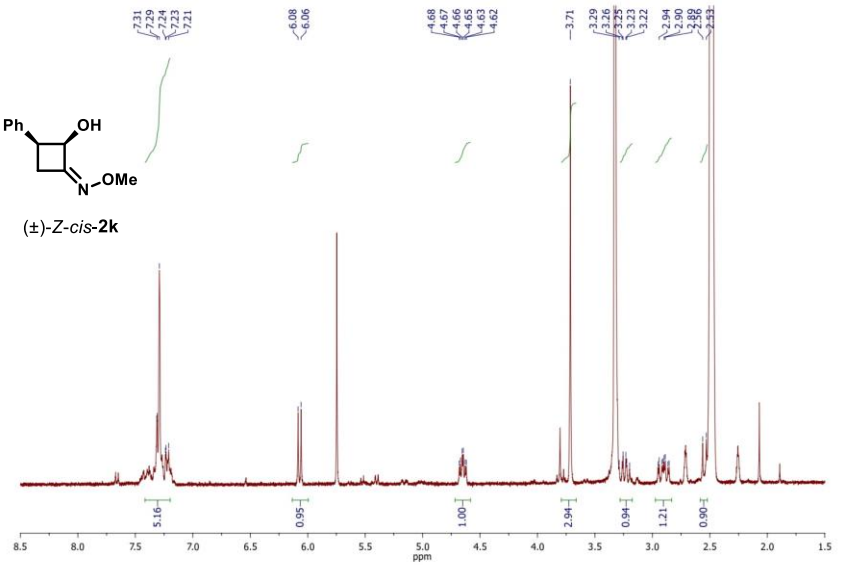

(±)-*Z-cis*-**2k**

^{1}H-NMR (300 MHz, DMSO-d_6)

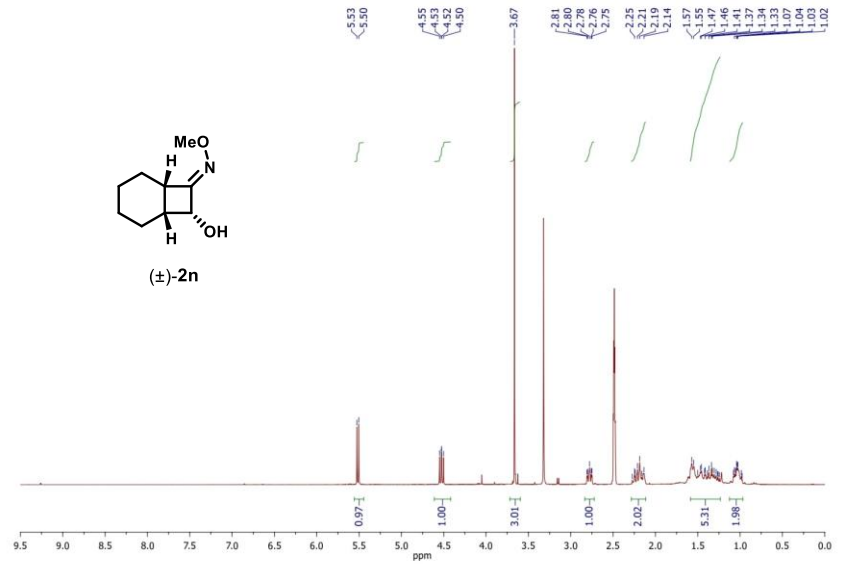

(±)-**2n**

$^{13}C\{^{1}H\}$-NMR (75 MHz, DMSO-d_6)

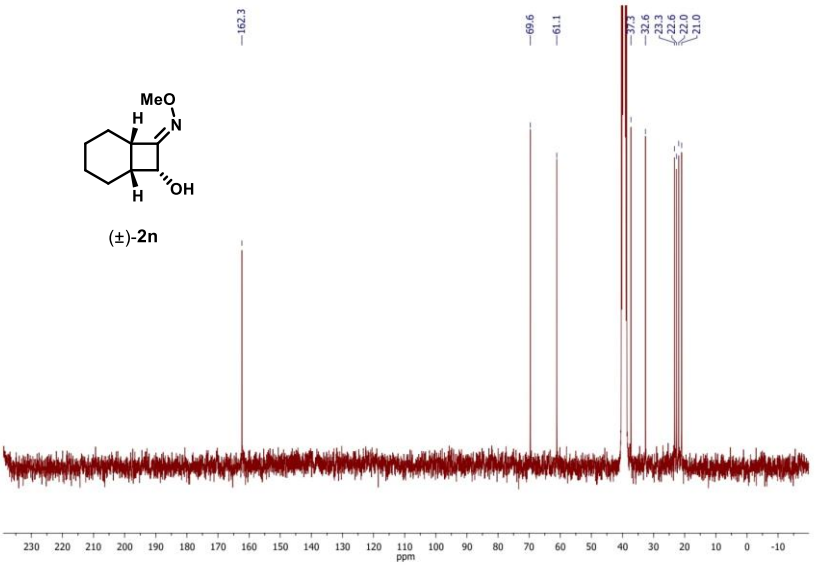

NOESY (300 MHz, DMSO-d_6)

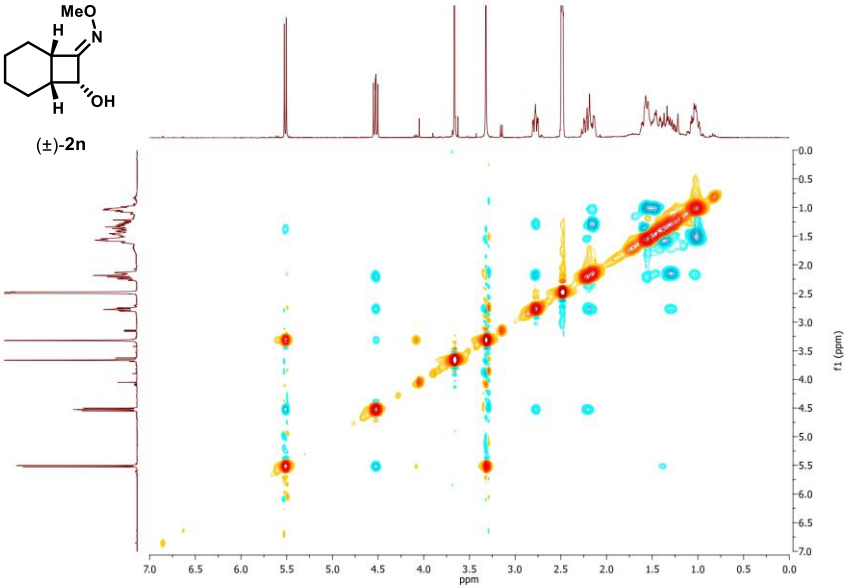

HSQC (300 MHz, DMSO-d_6)

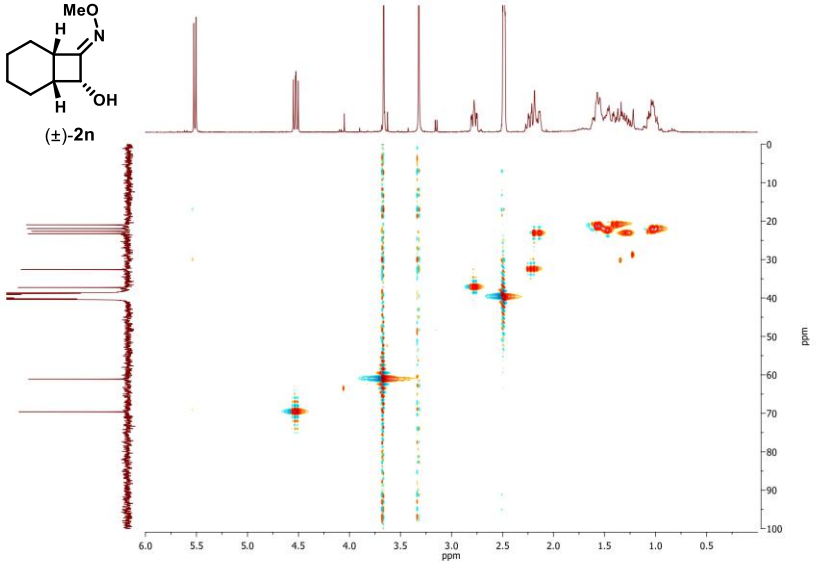

HMBC (300 MHz, DMSO-d_6)

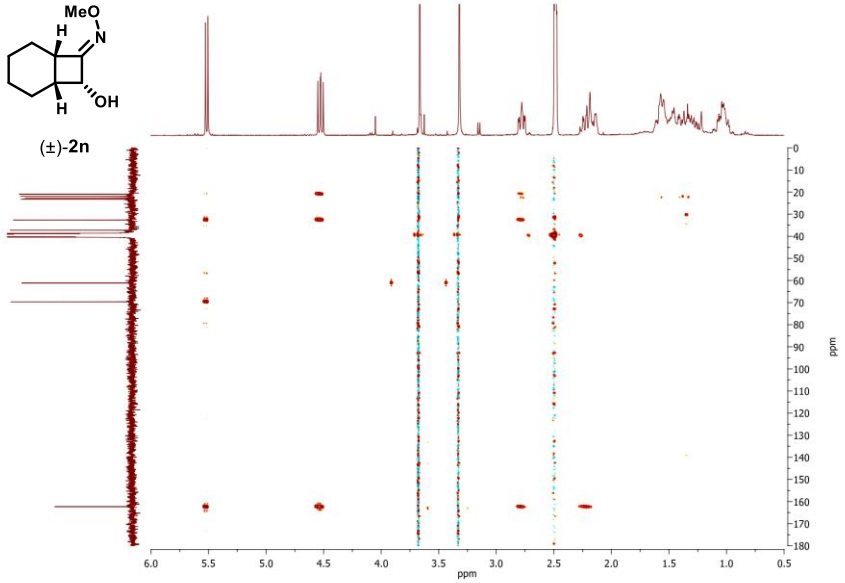

^{1}H-NMR (300 MHz, DMSO-d_6)

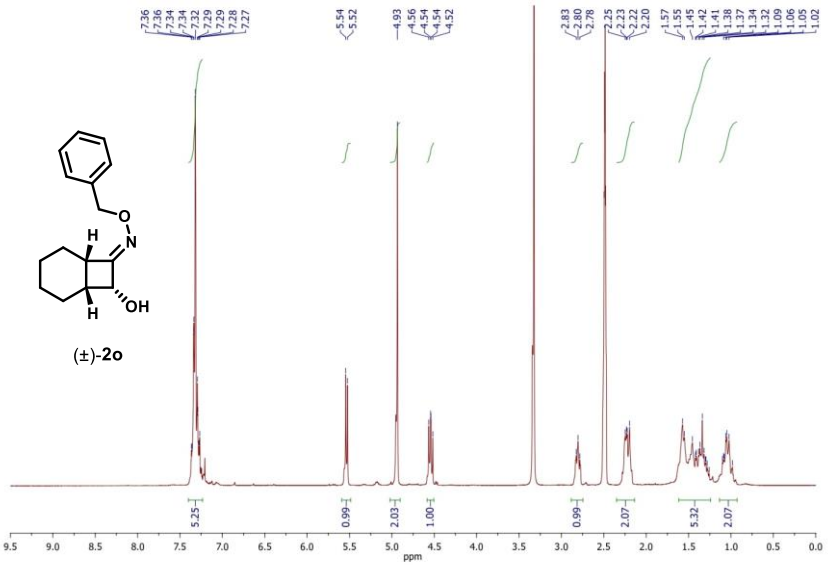

^{13}C{^{1}H}-NMR (75 MHz, DMSO-d_6)

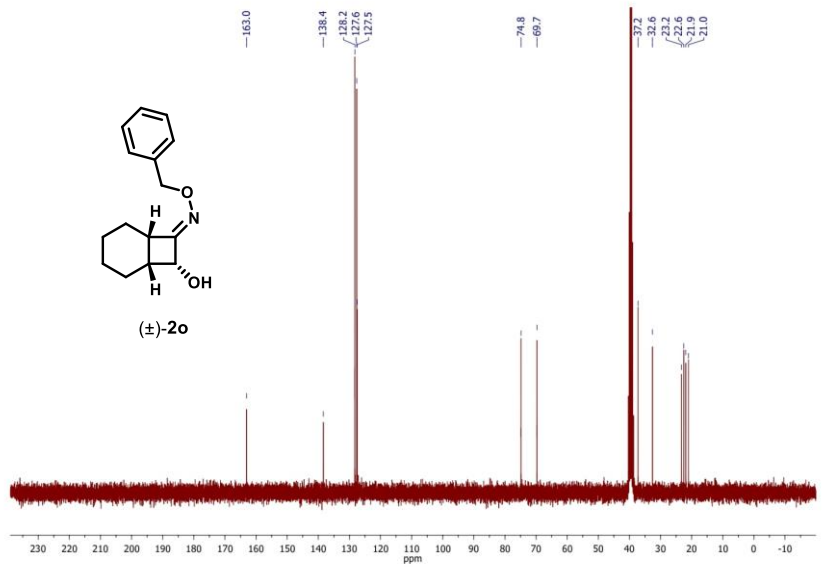

NOESY (300 MHz, DMSO-*d*6)

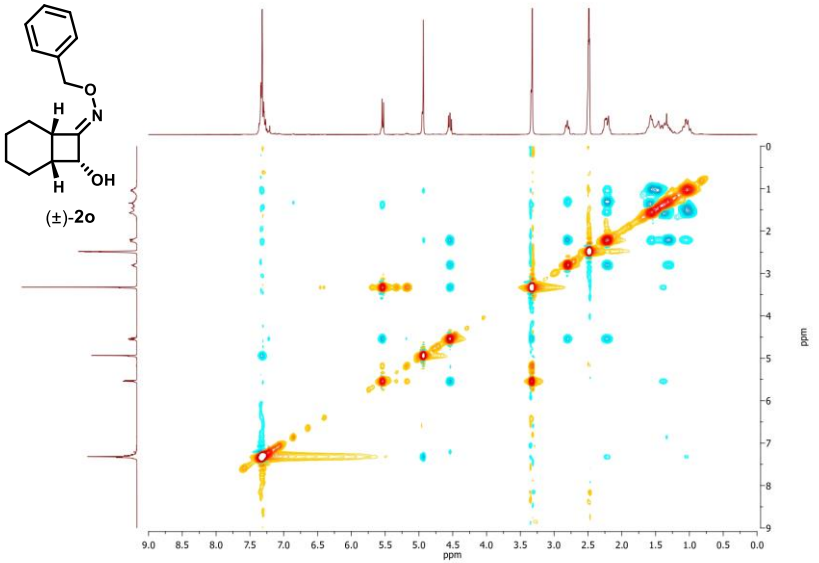

HSQC (300 MHz, DMSO-*d*6)

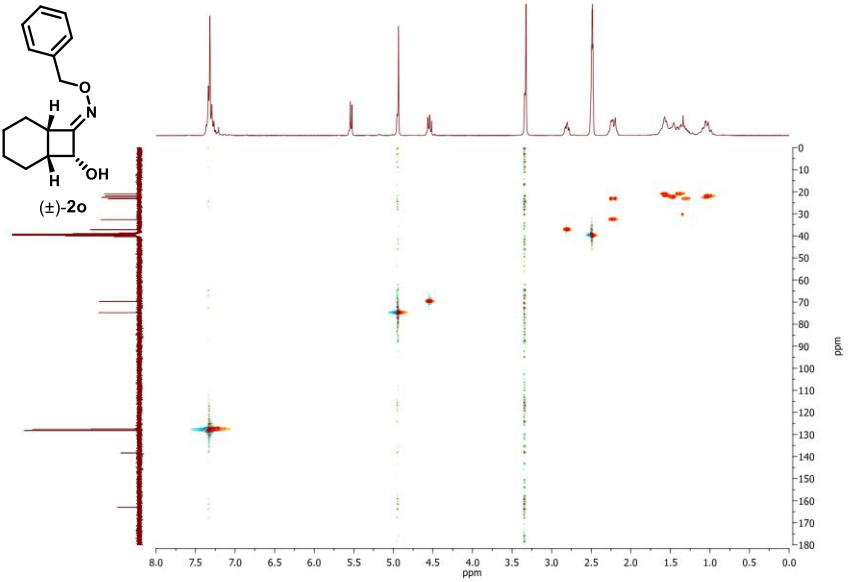

^{1}H-NMR (300 MHz, DMSO-d_6)

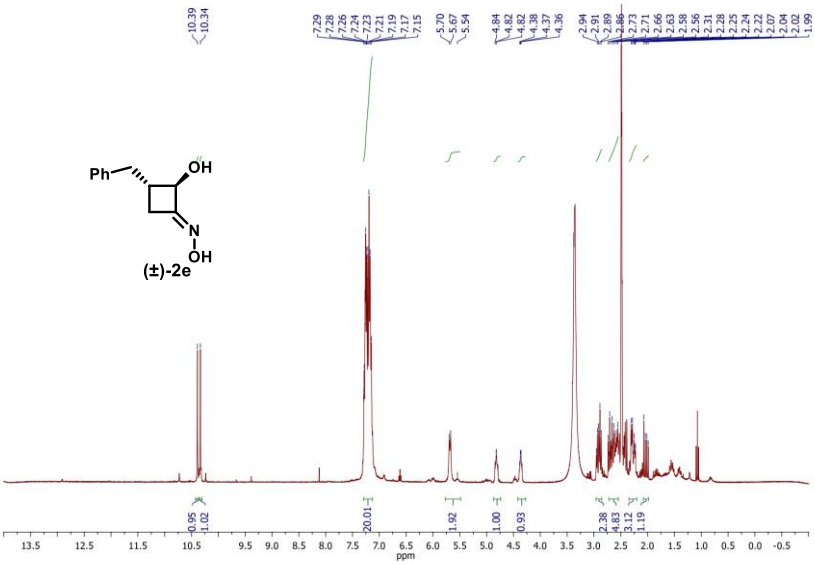

^{13}C{^{1}H}-NMR (75 MHz, DMSO-d_6)

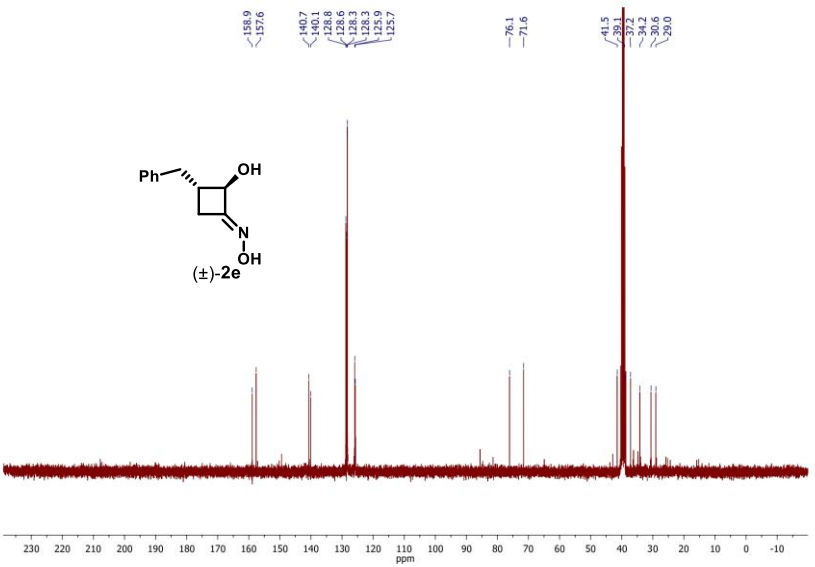

^{1}H-NMR (300 MHz, DMSO-d_6)

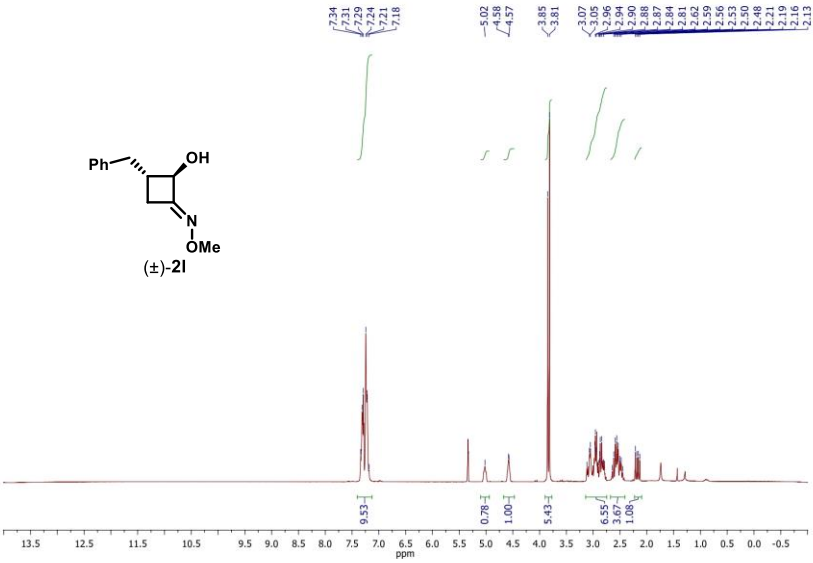

^{13}C{^{1}H}-NMR (75 MHz, DMSO-d_6)

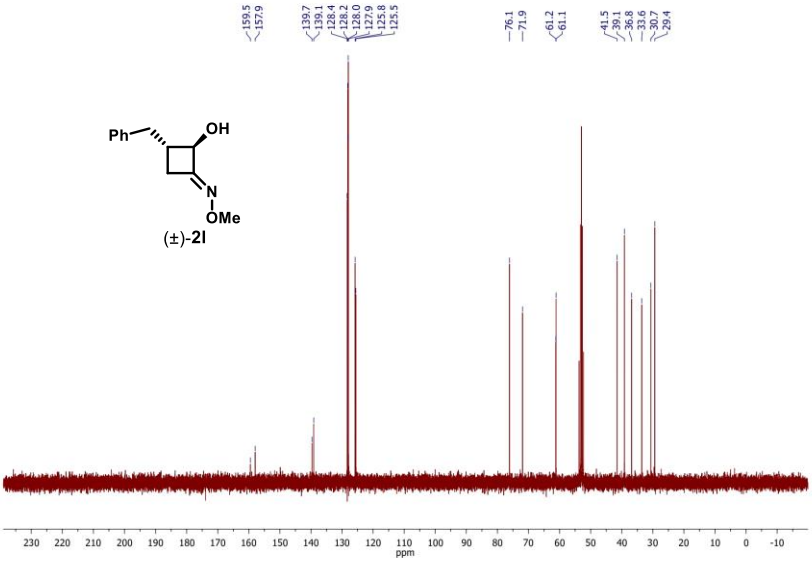

^{1}H-NMR (300 MHz, DMSO-d_6)

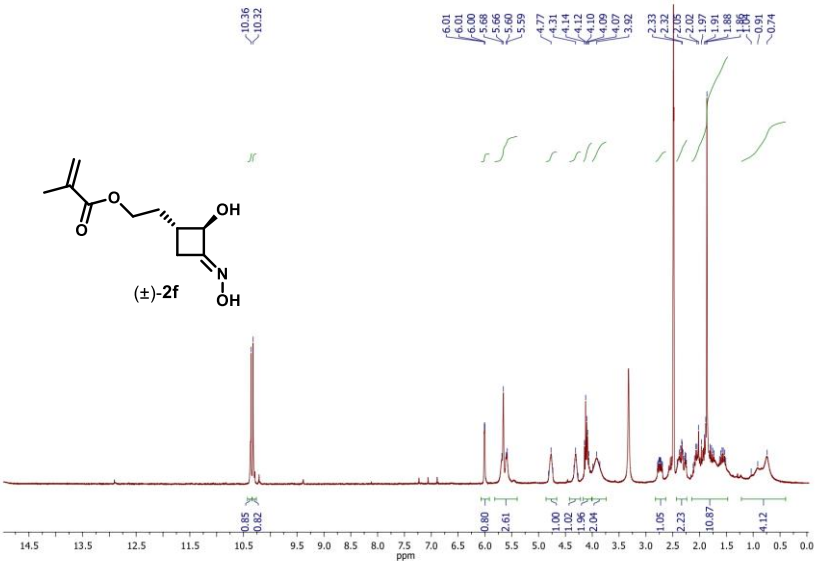

^{13}C{^{1}H}-NMR (75 MHz, DMSO-d_6)

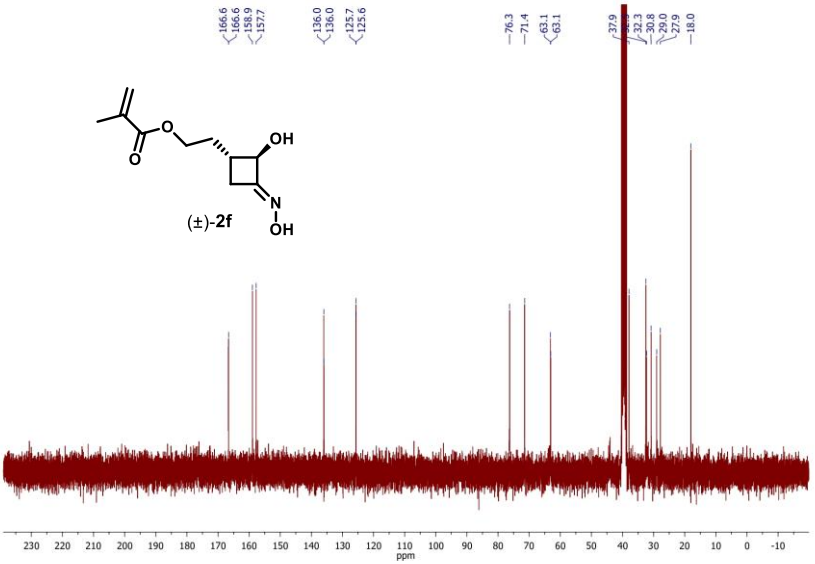

^{1}H-NMR (300 MHz, DMSO-d_6)

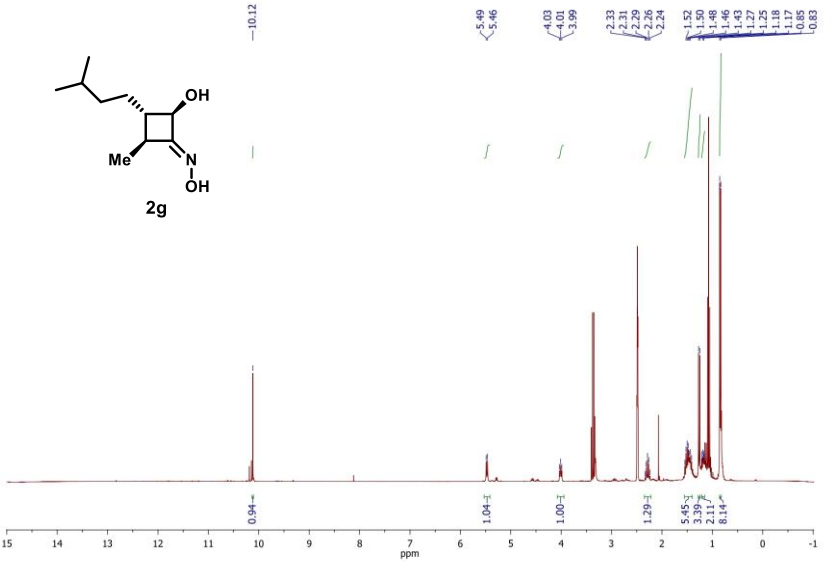

^{13}C{^{1}H}-NMR (75 MHz, DMSO-d_6)

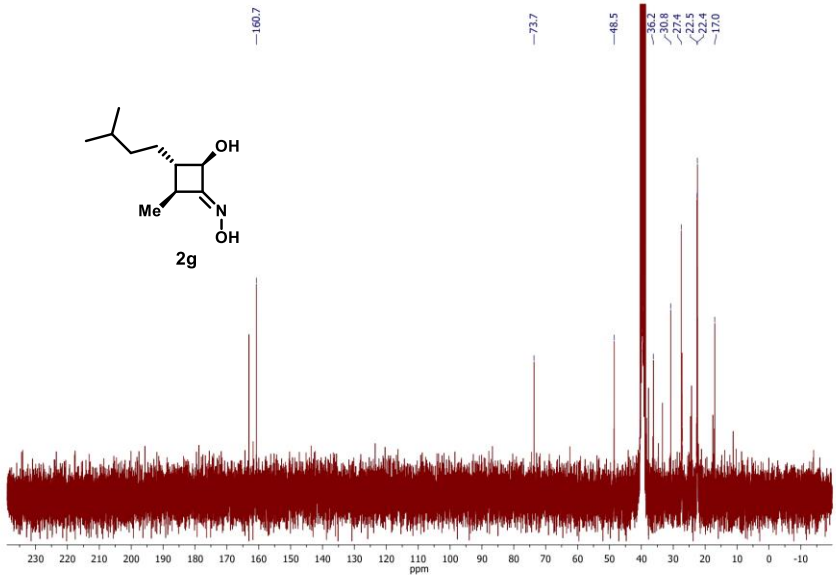

^{1}H-NMR (300 MHz, CD_2Cl_2)

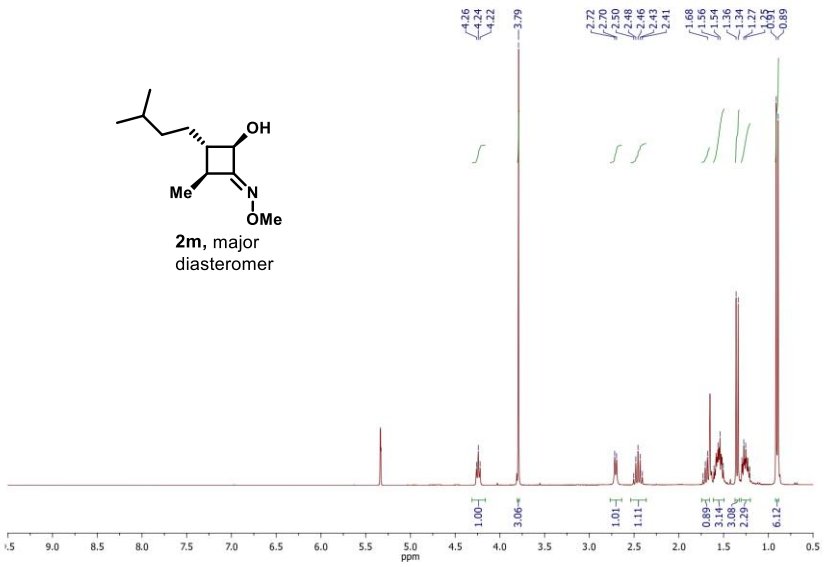

2m, major diasteromer

^{13}C{^{1}H}-NMR (75 MHz, CD_2Cl_2)

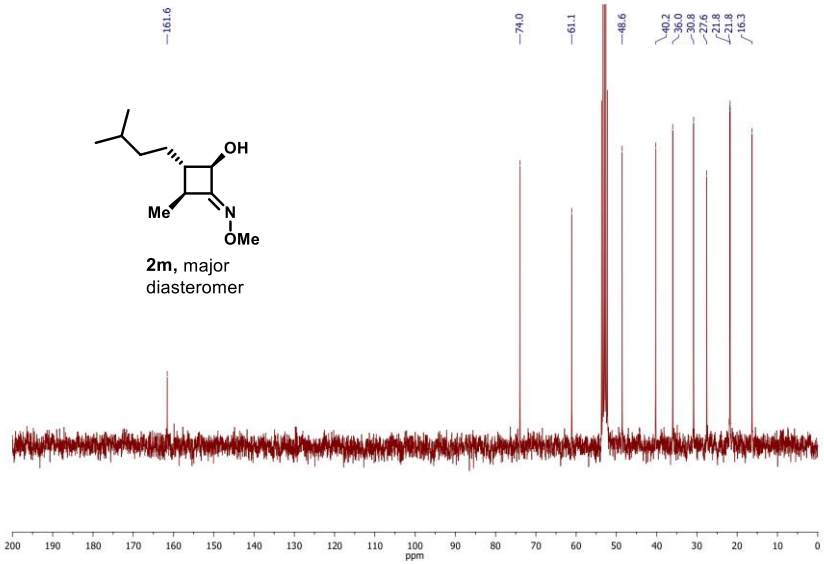

2m, major diasteromer

NOESY (300 MHz, CD_2Cl_2)

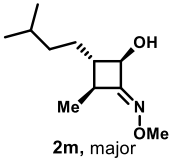

2m, major diasteromer

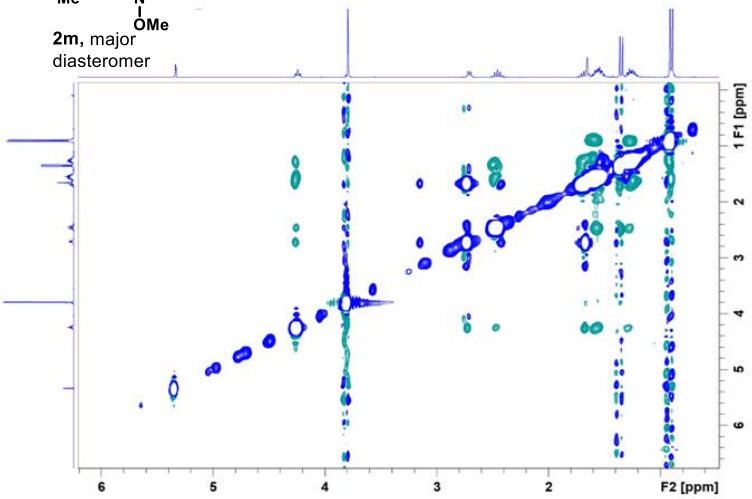

HSQC (300 MHz, CD_2Cl_2)

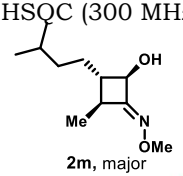

2m, major diasteromer

^{1}H-NMR (300 MHz, CD_2Cl_2)

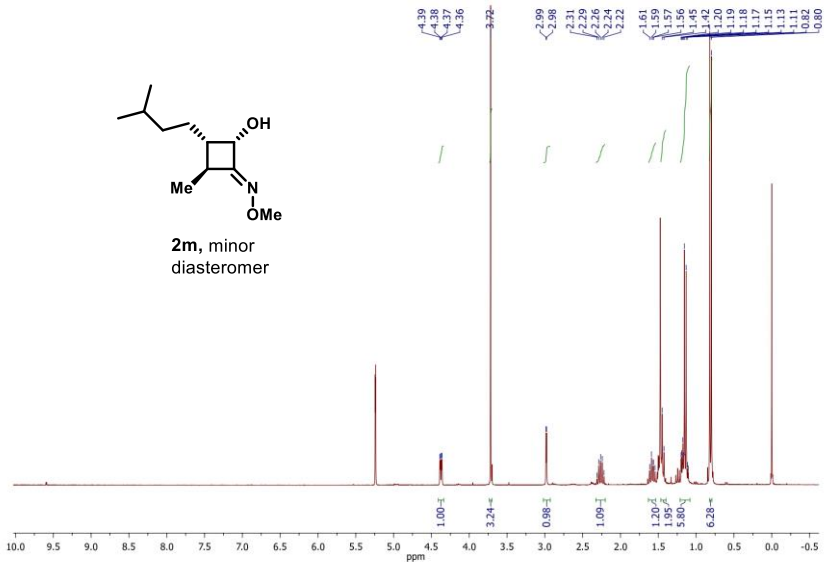

^{13}C{^{1}H}-NMR (75 MHz, CD_2Cl_2)

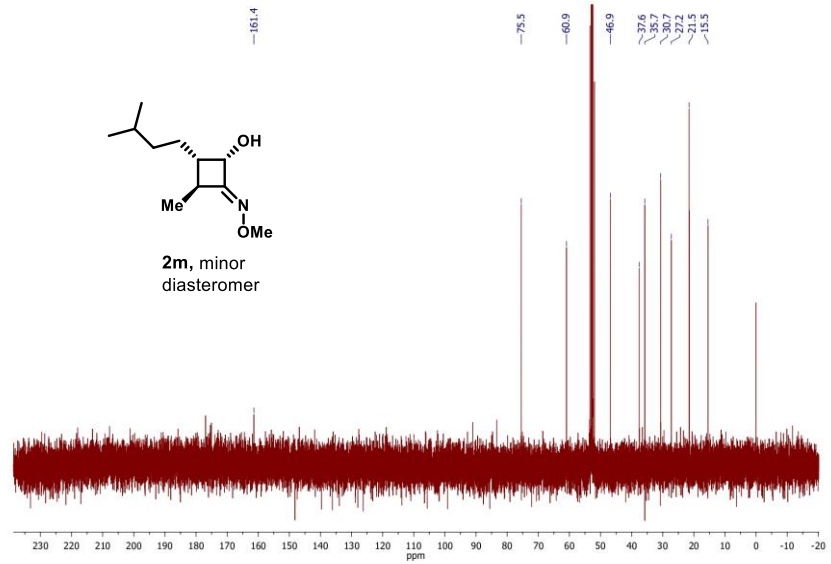

NOESY (300 MHz, CD_2Cl_2)

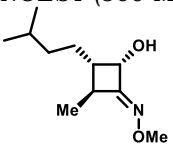

2m, minor diasteromer

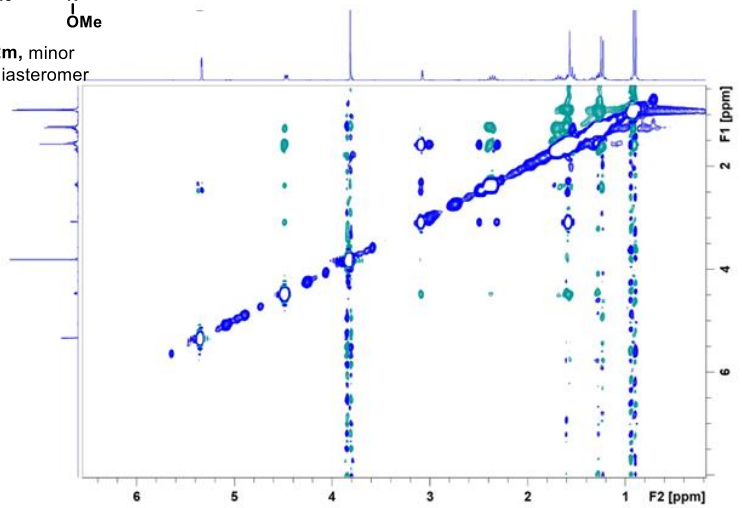

HSQC (300 MHz, CD_2Cl_2)

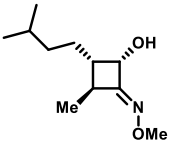

2m, minor diasteromer

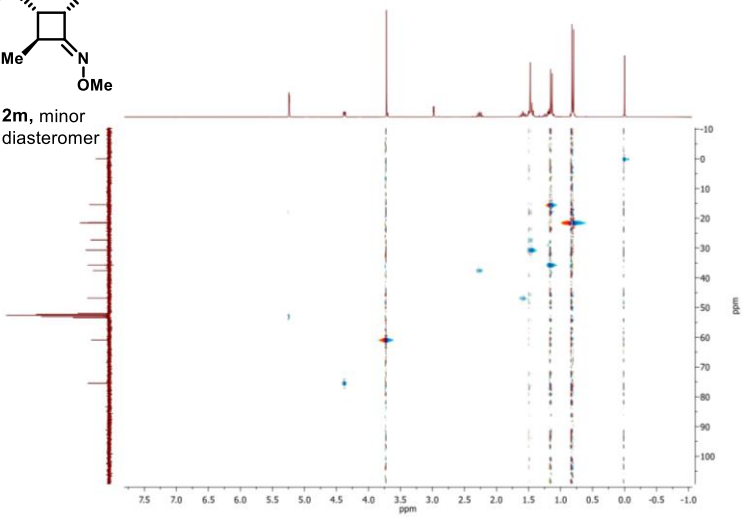

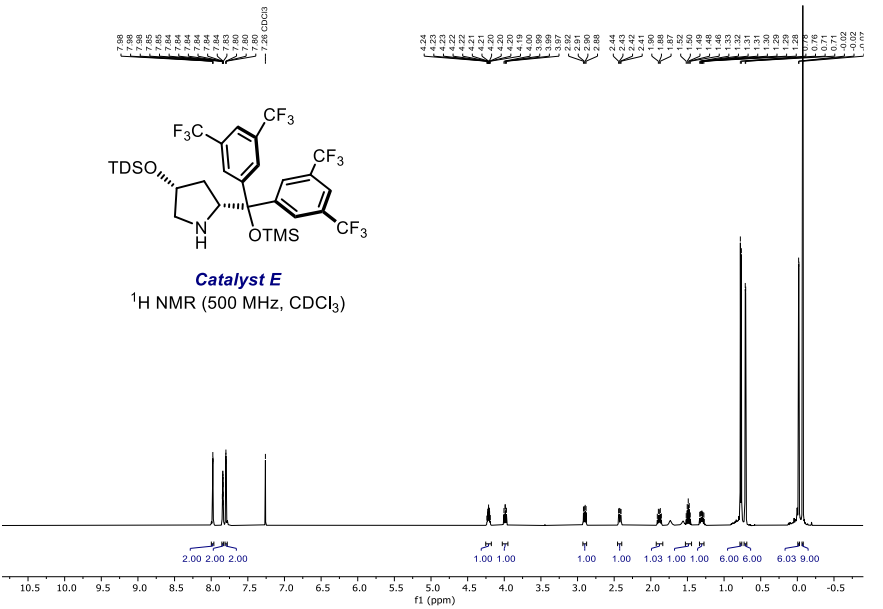

Catalyst E

^{1}H NMR (500 MHz, $CDCl_3$)

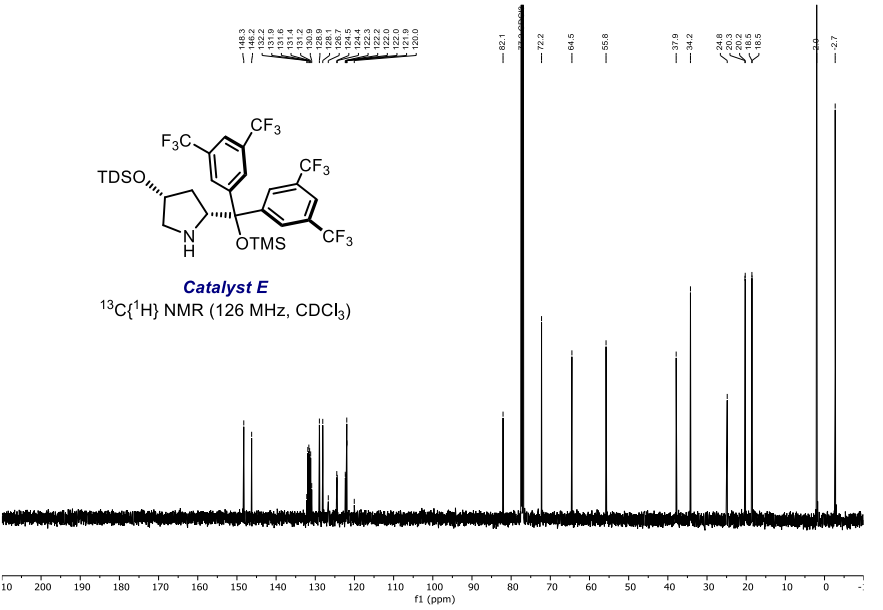

Catalyst E

^{13}C{^{1}H} NMR (126 MHz, $CDCl_3$)

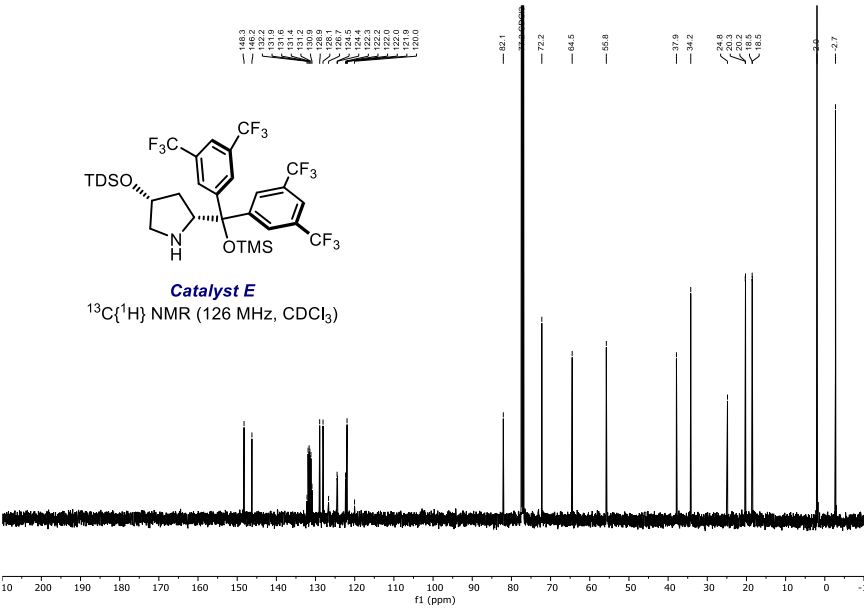

Catalyst E

$^{13}C\{^{1}H\}$ NMR (126 MHz, $CDCl_3$)

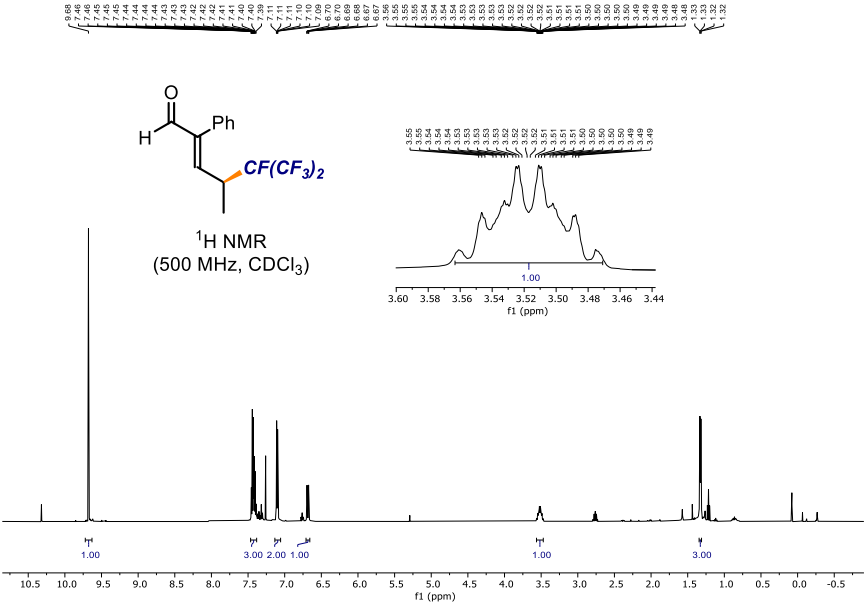

^{1}H NMR

(500 MHz, $CDCl_3$)

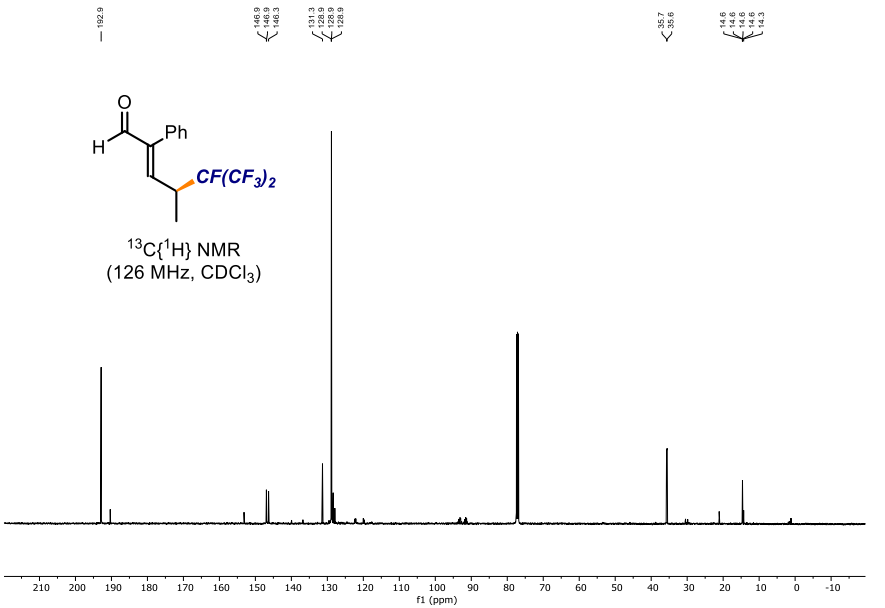
192.9
146.9
146.9
146.3
131.3
129.9
129.0
128.9
35.7
35.6
14.6
14.6
14.6
14.5
14.3
O
H
Ph
CF(CF3)2
13C{1H} NMR
(126 MHz, CDCl3)
f1 (ppm)

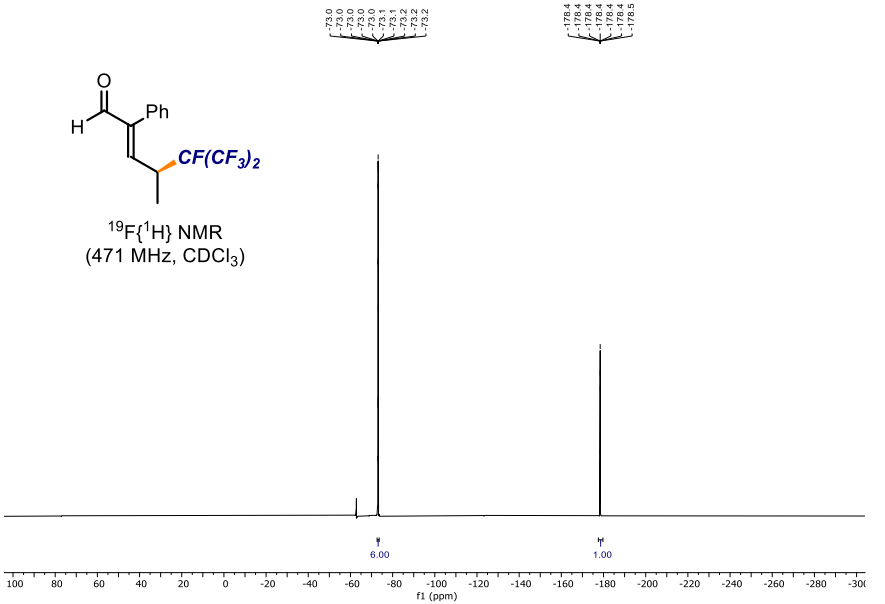
-73.0
-73.0
-73.0
-73.0
-73.0
-73.1
-73.1
-73.2
-73.2
-73.2
-178.4
-178.4
-178.4
-178.4
-178.4
-178.4
-178.5
O
H
Ph
CF(CF3)2
19F{1H} NMR
(471 MHz, CDCl3)
6.00
1.00
f1 (ppm)

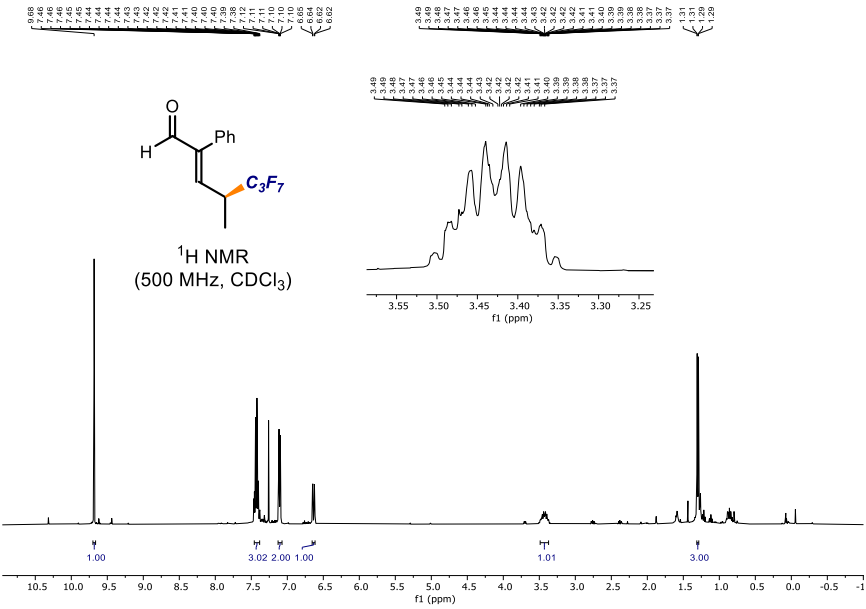
O
H
Ph
C_3F_7
^{1}H NMR
(500 MHz, $CDCl_3$)
f1 (ppm)

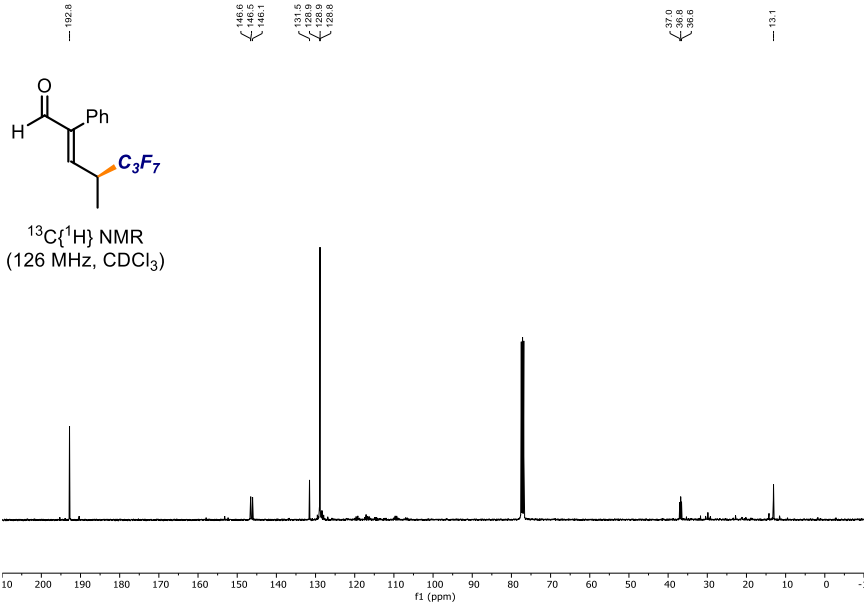
O
H
Ph
C_3F_7
^{13}C{^{1}H} NMR
(126 MHz, $CDCl_3$)
f1 (ppm)

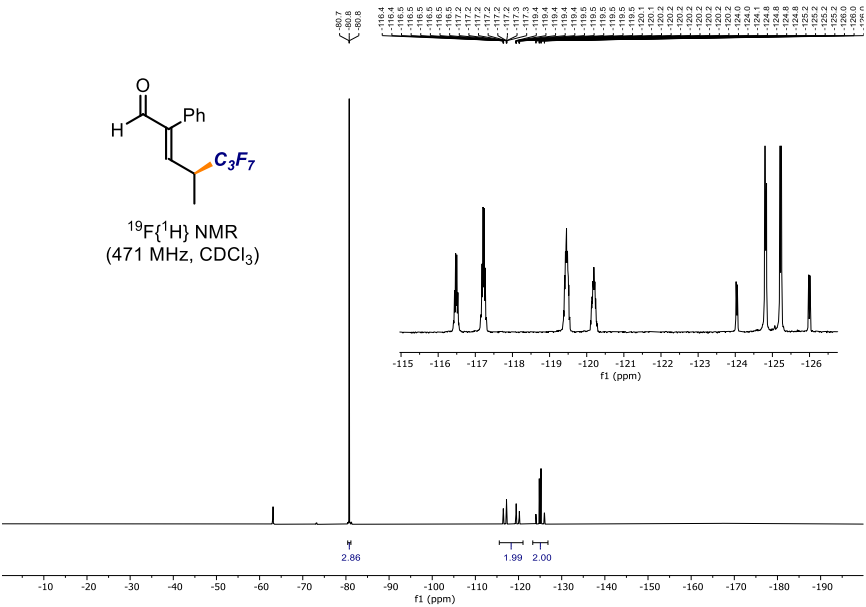
O
H
Ph
C_3F_7
$^{19}F\{^1H\}$ NMR
(471 MHz, $CDCl_3$)
f1 (ppm)

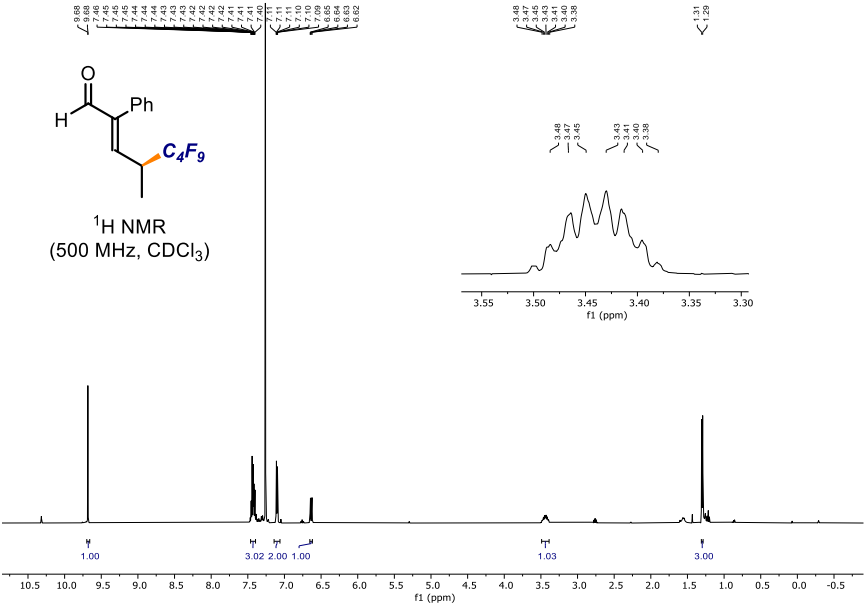
O
H
Ph
C_4F_9
^1H NMR
(500 MHz, $CDCl_3$)
f1 (ppm)

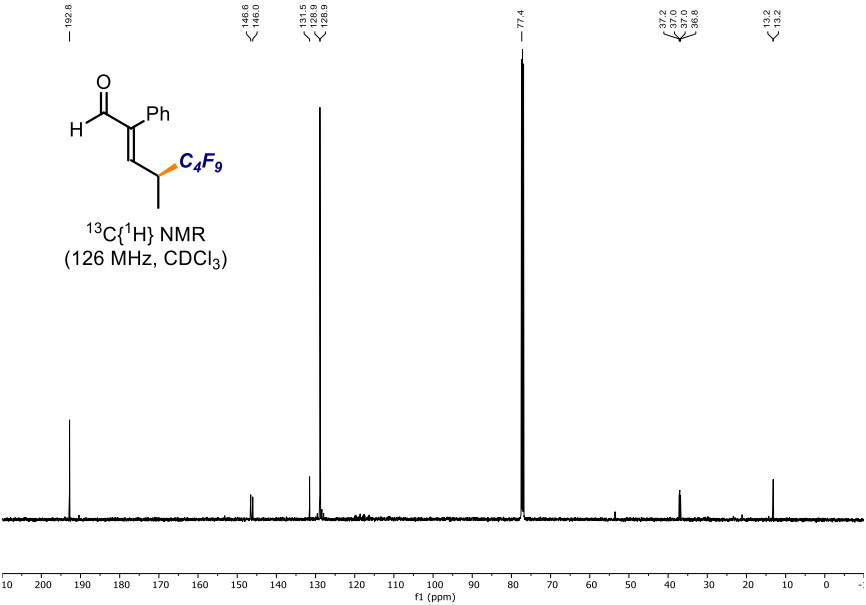
192.8
146.6
146.0
131.5
128.8
128.6
128.9
77.4
37.2
37.0
37.0
36.8
13.2
13.2
O
H
Ph
C4F9
13C{1H} NMR
(126 MHz, CDCl3)
f1 (ppm)

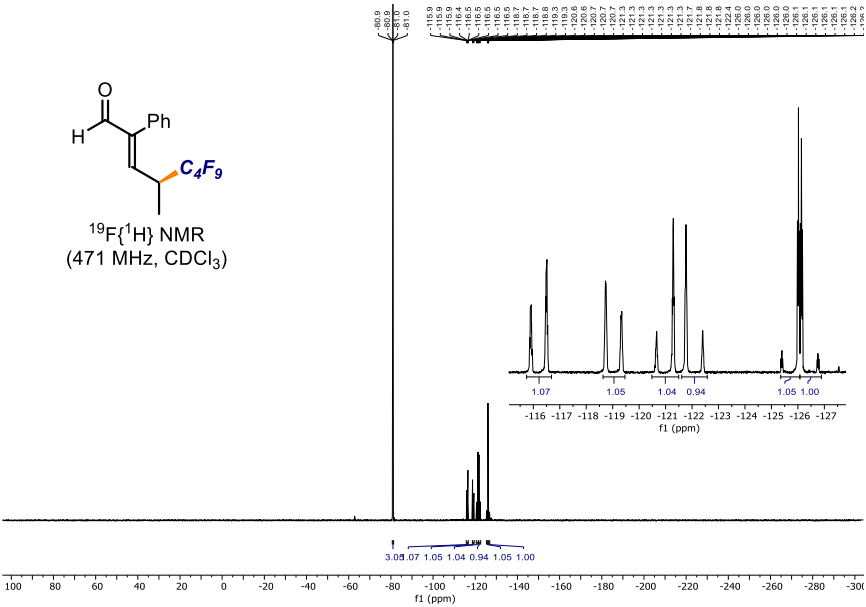
O
H
Ph
C4F9
19F{1H} NMR
(471 MHz, CDCl3)
1.07
1.05
1.04
0.94
1.05
1.00
3.05
1.07
1.05
1.04
0.94
1.05
1.00
f1 (ppm)

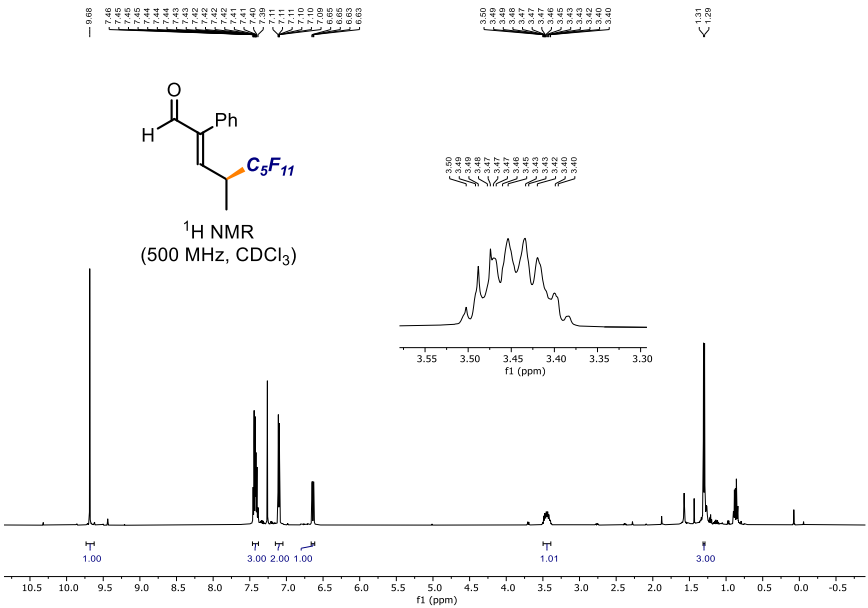
O
H
Ph
C5F11
1H NMR
(500 MHz, CDCl3)
f1 (ppm)

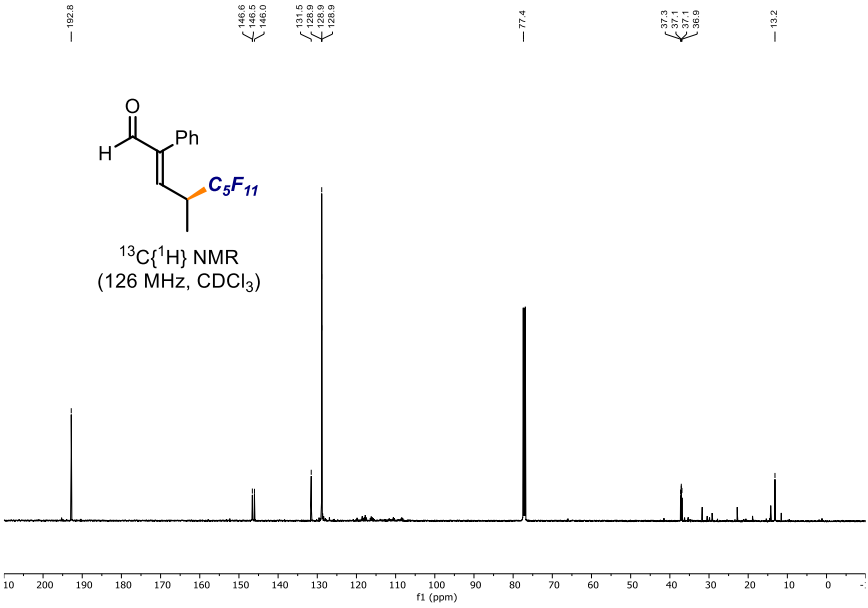
O
H
Ph
C5F11
13C{1H} NMR
(126 MHz, CDCl3)
f1 (ppm)

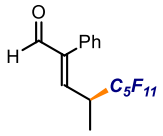

$^{19}F\{^1H\}$ NMR
(471 MHz, $CDCl_3$)

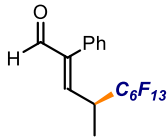

^1H NMR
(500 MHz, $CDCl_3$)

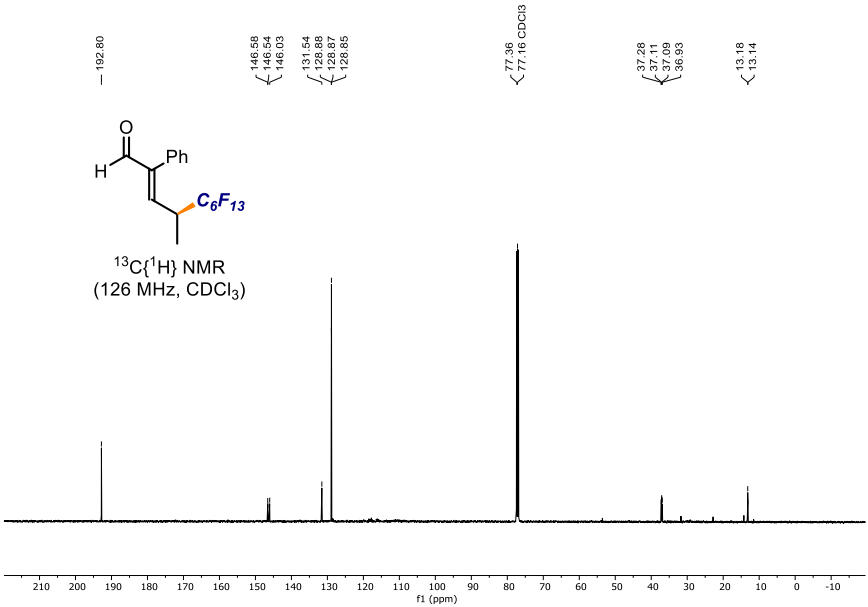

$^{13}C\{^{1}H\}$ NMR
(126 MHz, $CDCl_3$)

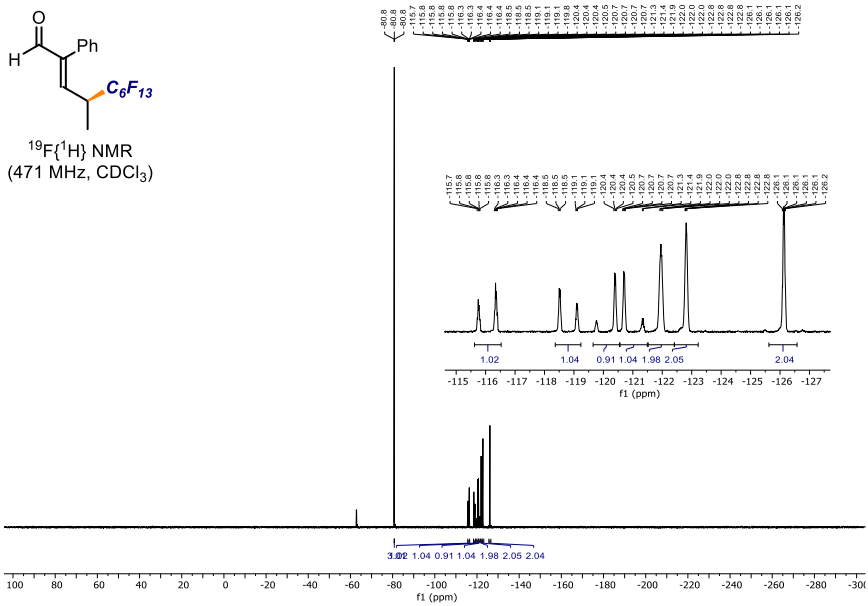

$^{19}F\{^{1}H\}$ NMR
(471 MHz, $CDCl_3$)

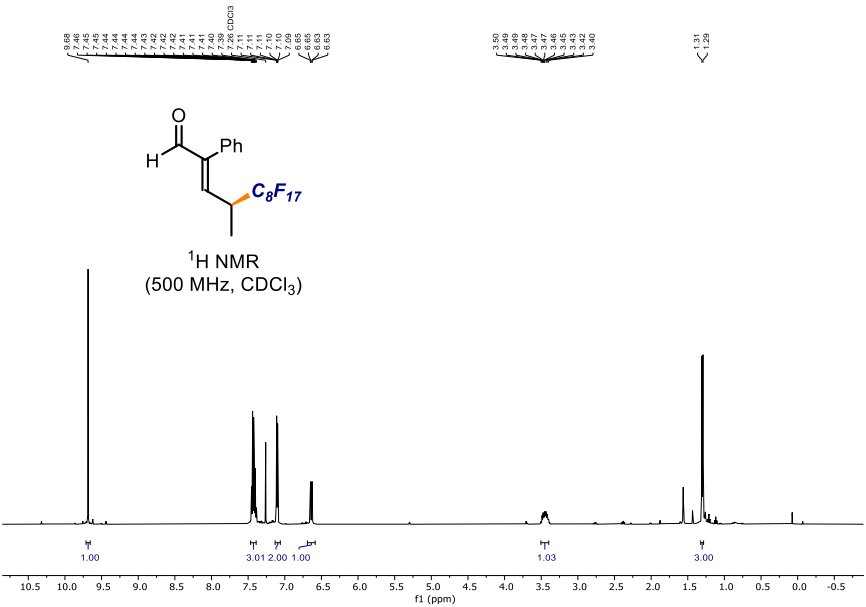
9.68
7.46
7.45
7.45
7.44
7.44
7.44
7.43
7.42
7.42
7.42
7.42
7.41
7.41
7.41
7.40
7.39
7.39 CDCl3
7.11
7.11
7.11
7.10
7.09
6.66
6.65
6.65
6.63
3.50
3.49
3.49
3.48
3.48
3.47
3.47
3.46
3.46
3.45
3.43
3.42
3.40
1.31
1.29
O
H
Ph
C8F17
1H NMR
(500 MHz, CDCl3)
1.00
3.01
2.00
1.00
1.03
3.00
f1 (ppm)

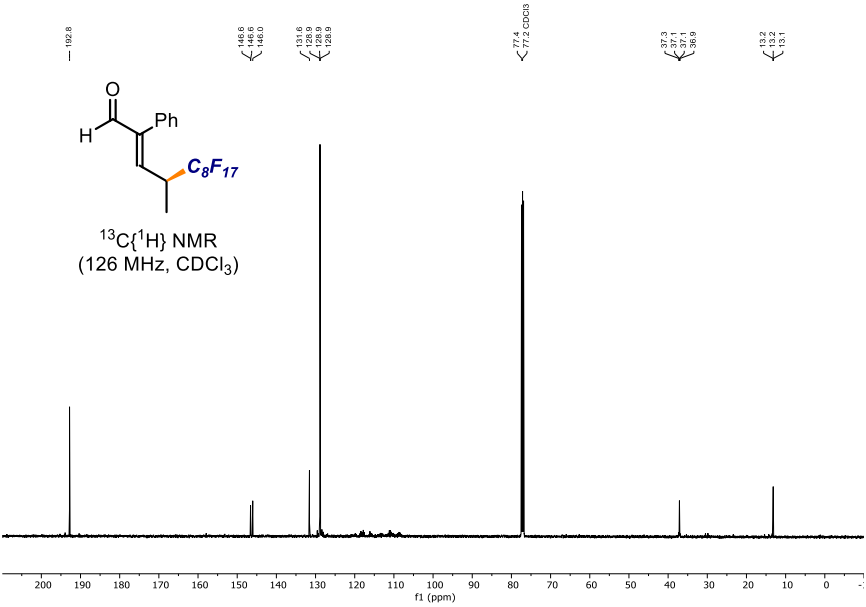
192.8
146.6
146.6
146.0
131.6
128.9
128.9
128.9
77.4
77.2 CDCl3
37.3
37.1
37.1
36.9
13.2
13.2
13.1
O
H
Ph
C8F17
13C{1H} NMR
(126 MHz, CDCl3)
f1 (ppm)

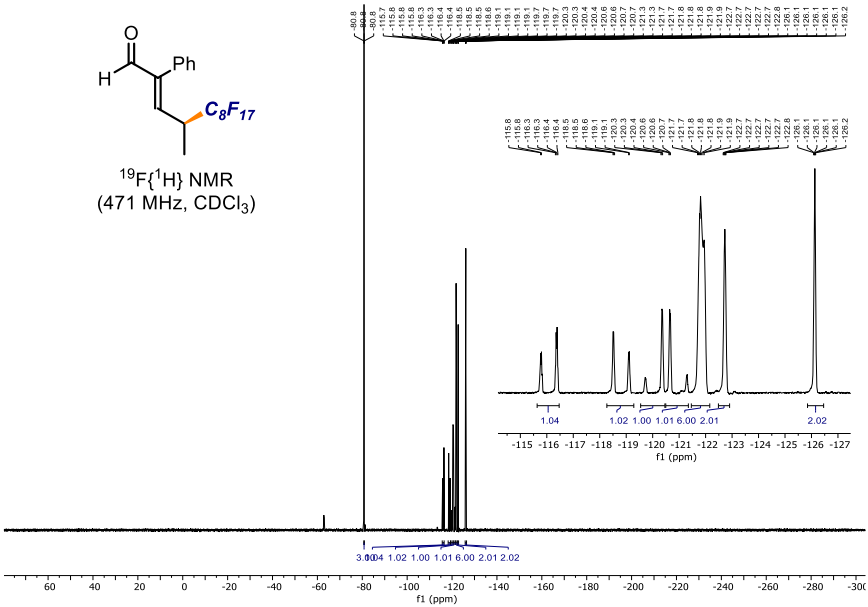
O
H
Ph
C8F17
19F{1H} NMR
(471 MHz, CDCl3)
f1 (ppm)

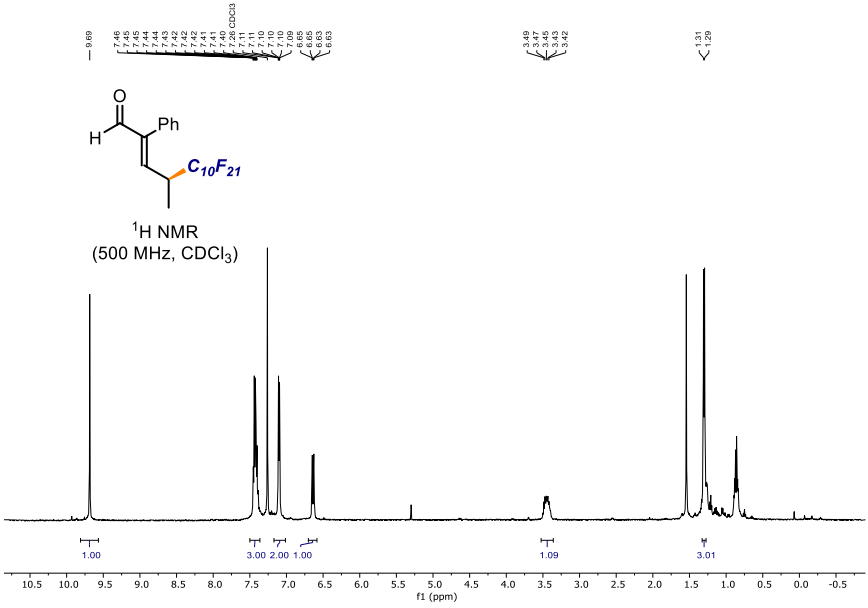
O
H
Ph
C10F21
1H NMR
(500 MHz, CDCl3)
f1 (ppm)

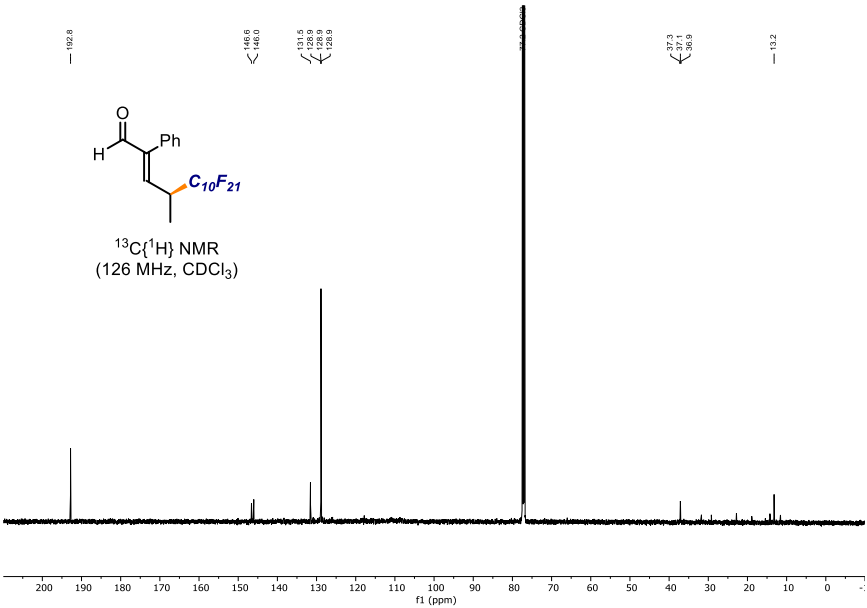

$^{13}C\{^{1}H\}$ NMR
(126 MHz, $CDCl_3$)

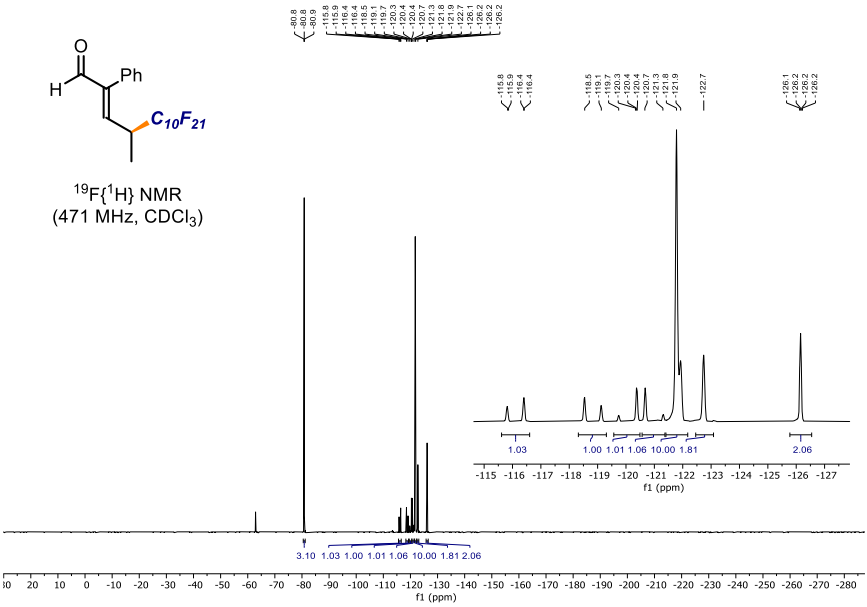

$^{19}F\{^{1}H\}$ NMR
(471 MHz, $CDCl_3$)

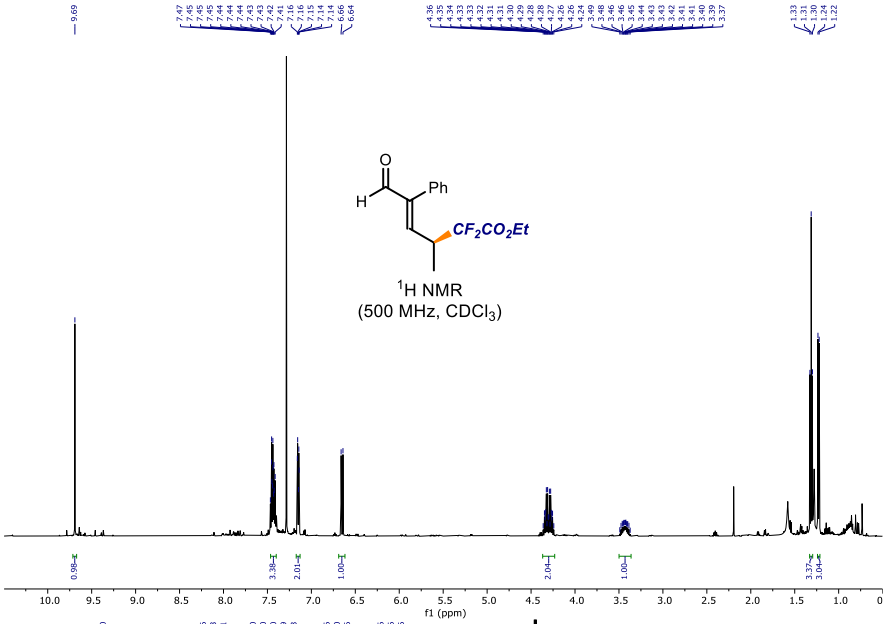
O
H
Ph
CF2CO2Et
1H NMR
(500 MHz, CDCl3)
f1 (ppm)

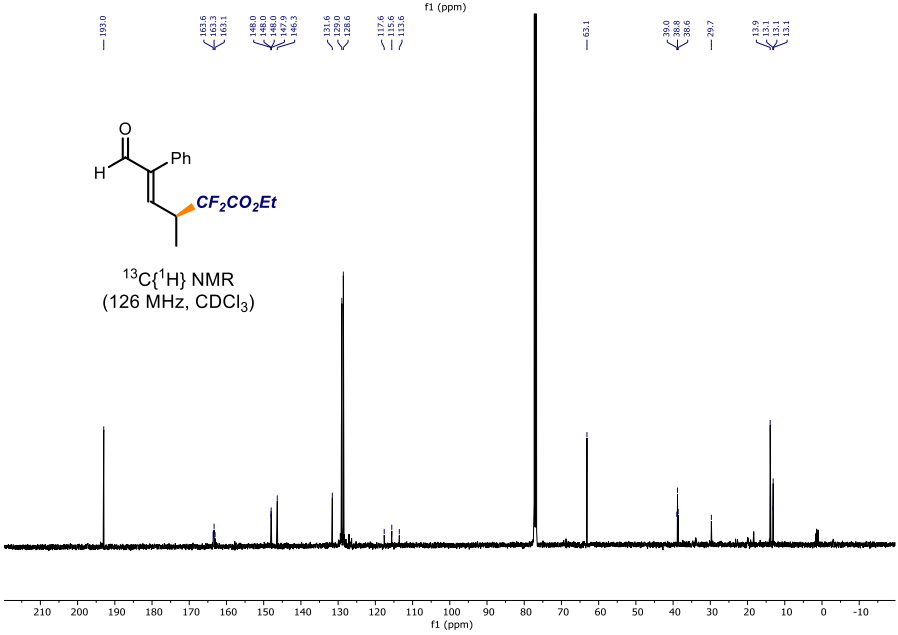
O
H
Ph
CF2CO2Et
13C{1H} NMR
(126 MHz, CDCl3)
f1 (ppm)

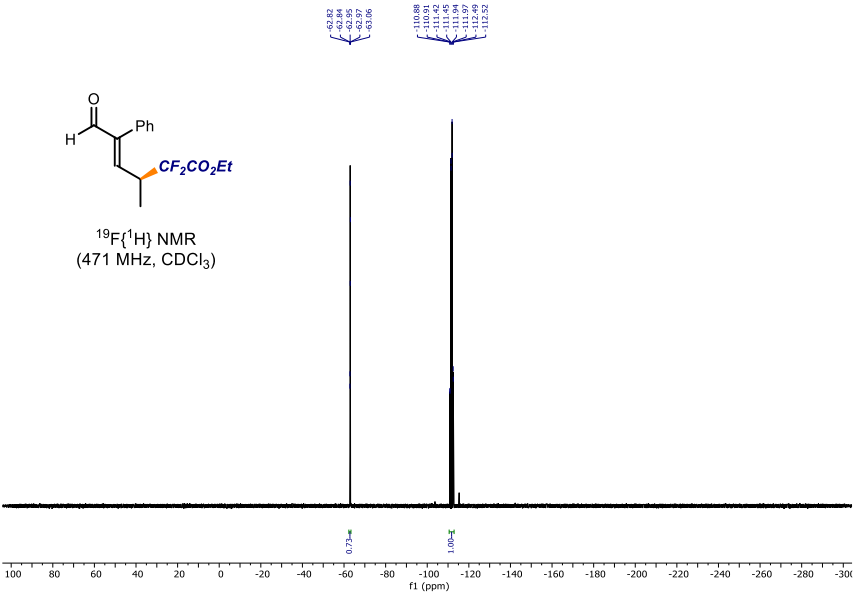
-62.82
-62.84
-62.95
-62.97
-63.06
-110.88
-110.91
-111.42
-111.45
-111.94
-111.97
-112.49
-112.52
O
H
Ph
CF2CO2Et
19F{1H} NMR
(471 MHz, CDCl3)
0.73
1.00
f1 (ppm)

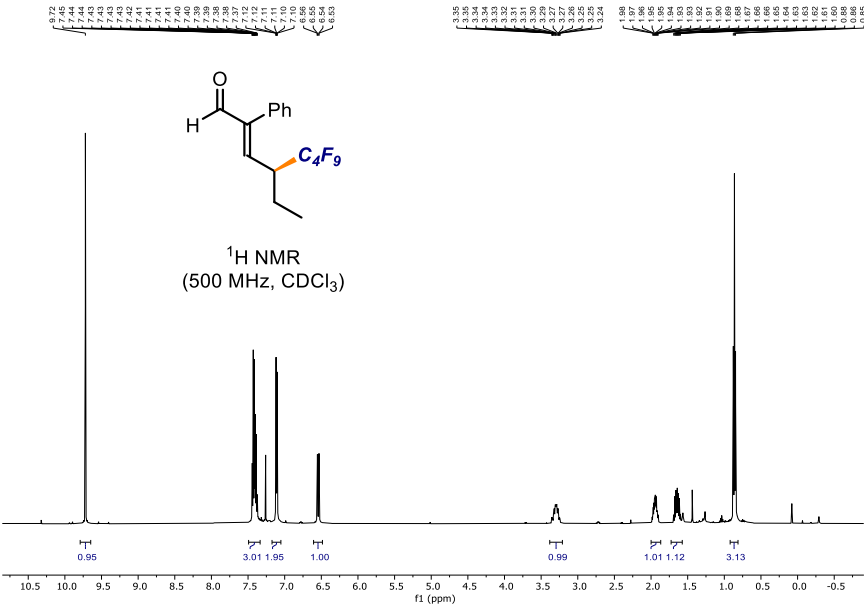
O
H
Ph
C4F9
1H NMR
(500 MHz, CDCl3)
0.95
3.01
1.95
1.00
0.99
1.01
1.12
3.13
f1 (ppm)

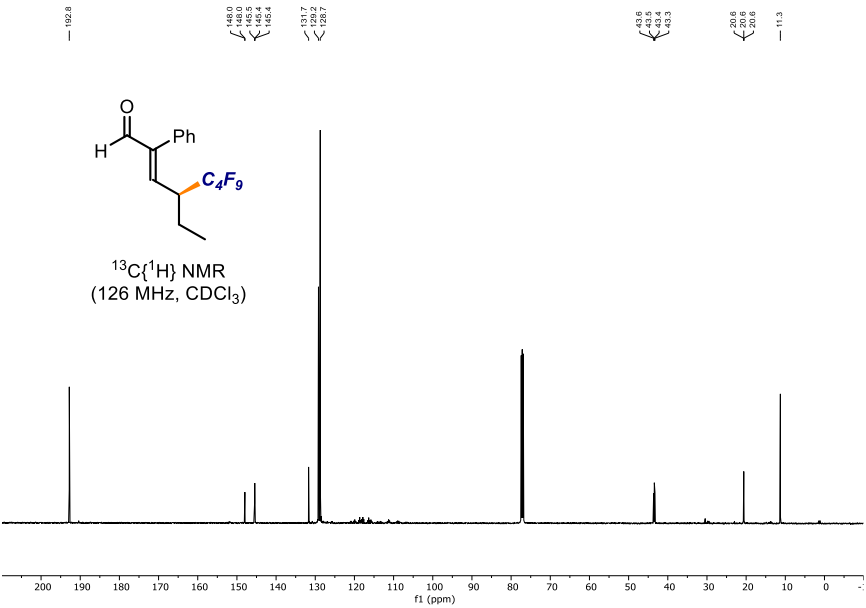
O
H
Ph
C4F9
13C{1H} NMR
(126 MHz, CDCl3)
f1 (ppm)

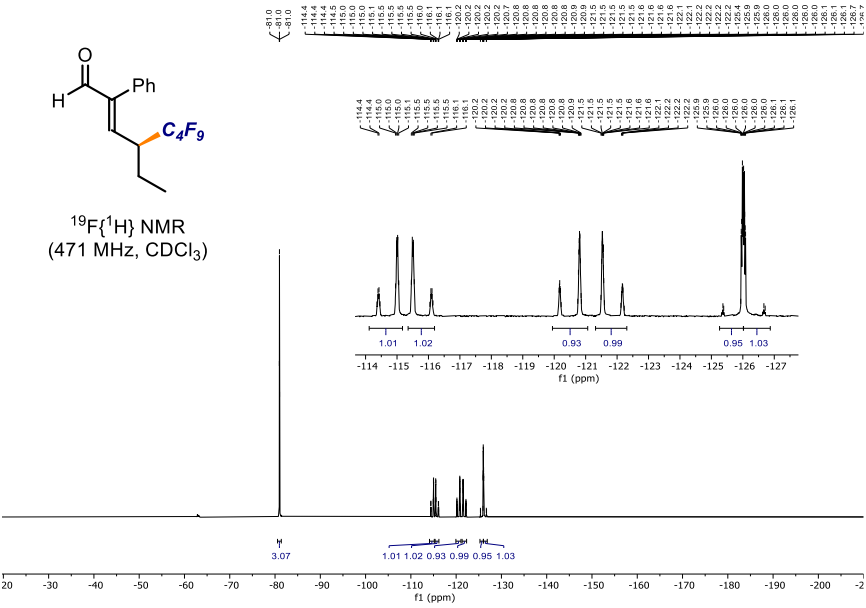
O
H
Ph
C4F9
19F{1H} NMR
(471 MHz, CDCl3)
1.01
1.02
0.93
0.99
0.95
1.03
3.07
1.01 1.02 0.93 0.99 0.95 1.03
f1 (ppm)

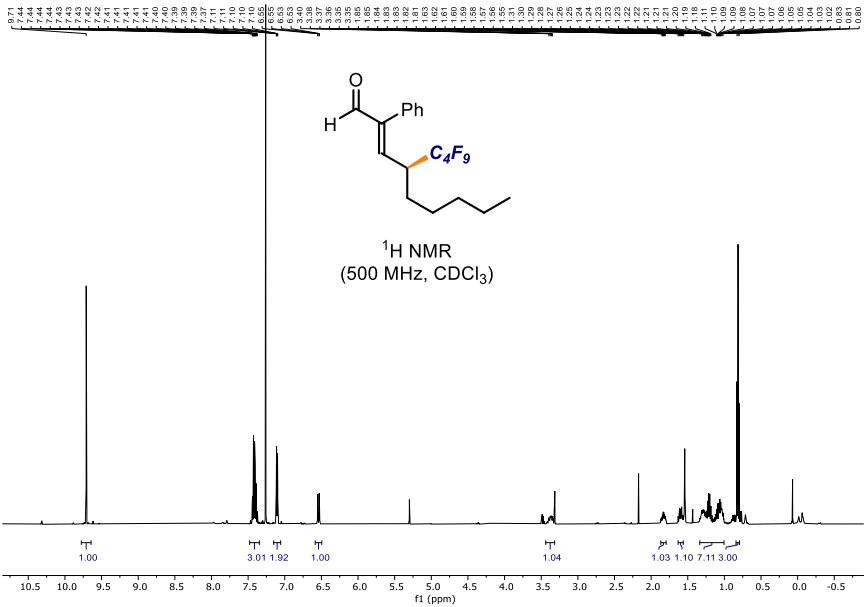
O
H
Ph
C4F9
1H NMR
(500 MHz, CDCl3)
1.00
3.01
1.92
1.00
1.04
1.03
1.10
7.11
3.00
f1 (ppm)

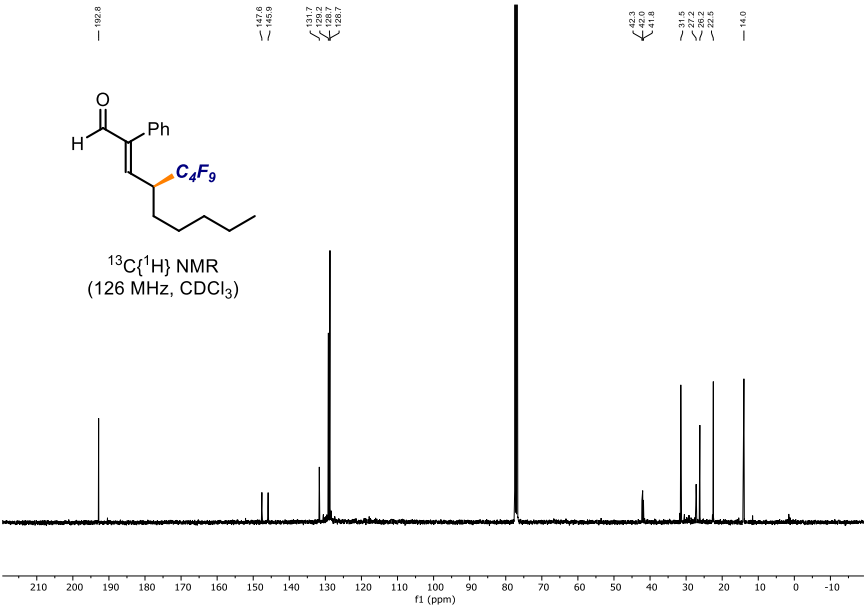
O
H
Ph
C4F9
13C{1H} NMR
(126 MHz, CDCl3)
f1 (ppm)

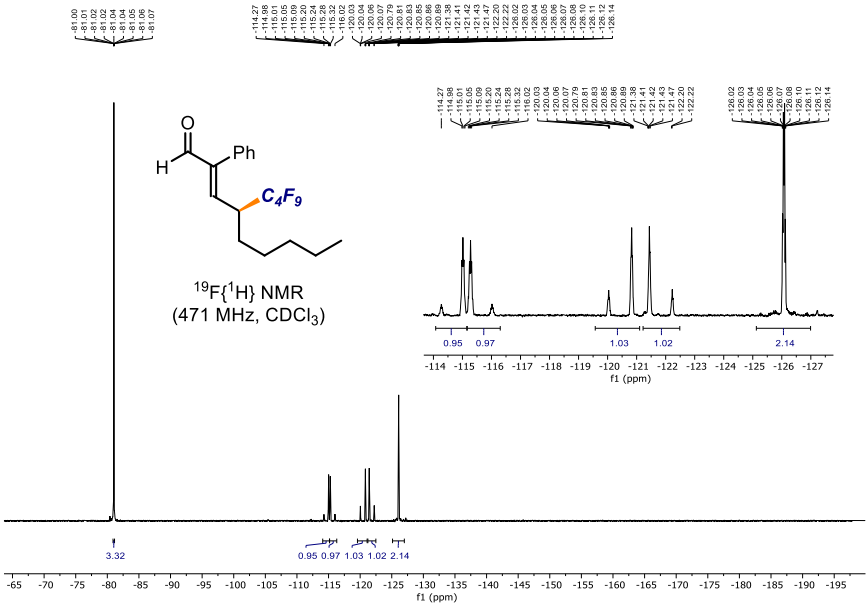
O
H
Ph
C_4F_9
$^{19}F\{^1H\}$ NMR
(471 MHz, $CDCl_3$)
0.95 0.97 1.03 1.02 2.14
f1 (ppm)
3.32
0.95 0.97 1.03 1.02 2.14
f1 (ppm)

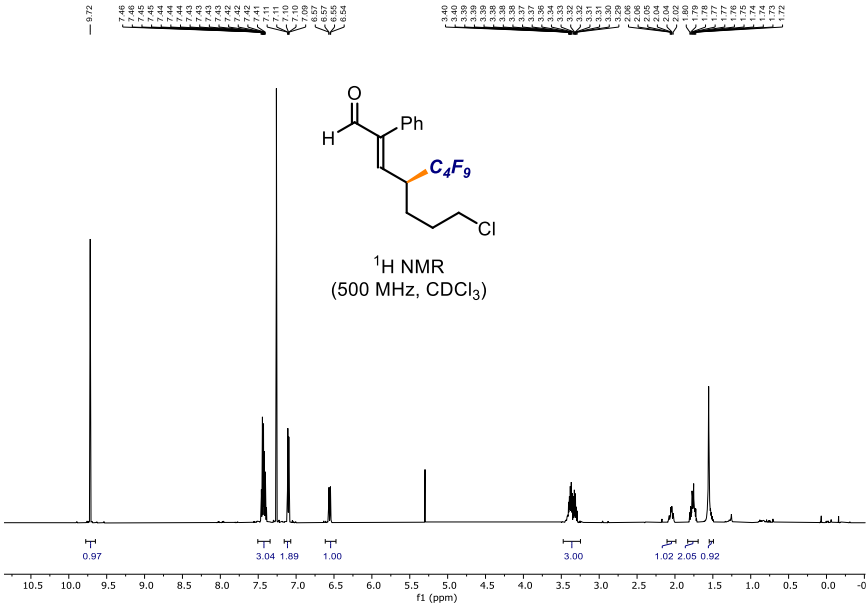
O
H
Ph
C_4F_9
Cl
^1H NMR
(500 MHz, $CDCl_3$)
0.97
3.04 1.89
1.00
3.00
1.02 2.05 0.92
f1 (ppm)

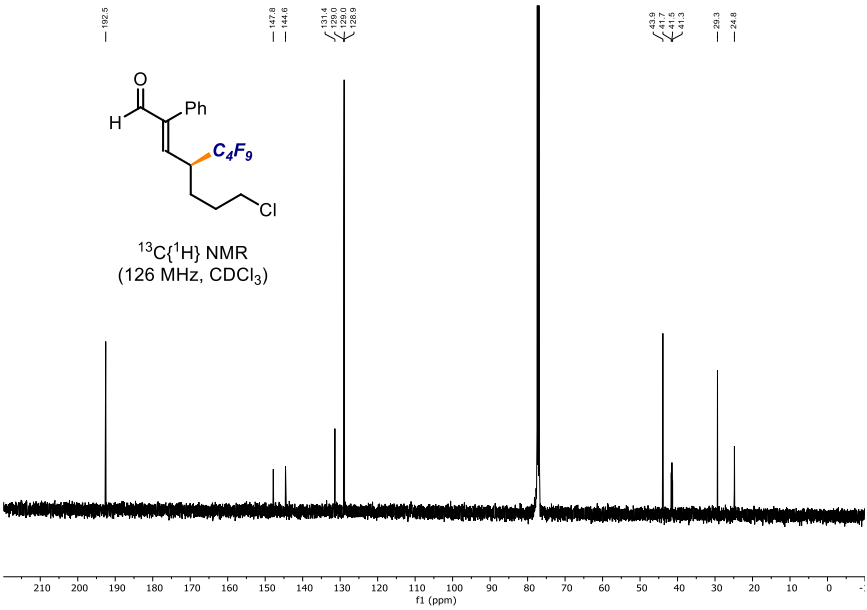
192.5
147.8
144.6
131.4
130.0
129.0
128.9
43.9
41.7
41.5
41.3
29.3
24.8
O
H
Ph
C4F9
Cl
13C{1H} NMR
(126 MHz, CDCl3)
f1 (ppm)

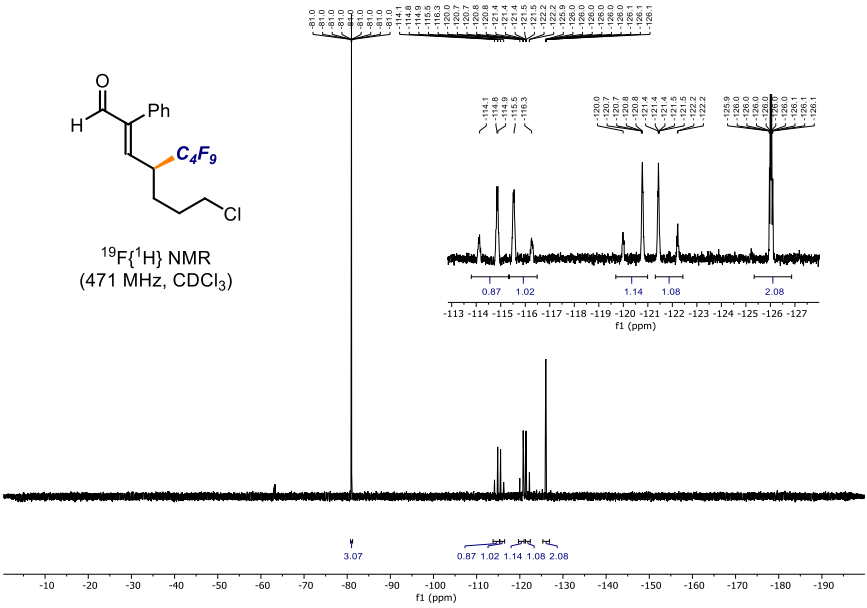
O
H
Ph
C4F9
Cl
19F{1H} NMR
(471 MHz, CDCl3)
0.87
1.02
1.14
1.08
2.08
3.07
f1 (ppm)

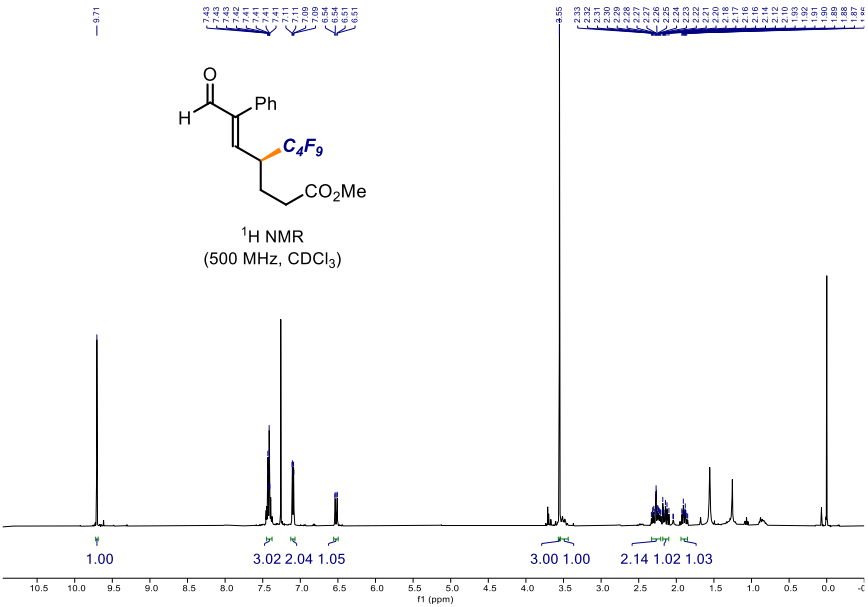
9.71
7.43
7.43
7.43
7.42
7.41
7.41
7.41
7.41
7.11
7.11
7.11
7.09
6.54
6.54
6.51
8.55
2.33
2.32
2.31
2.30
2.29
2.28
2.27
2.26
2.25
2.24
2.23
2.22
2.21
2.20
2.18
2.17
2.16
2.15
2.14
2.12
2.10
2.03
1.92
1.91
1.90
1.89
1.88
1.87
O
H
Ph
C4F9
CO2Me
1H NMR
(500 MHz, CDCl3)
1.00
3.02 2.04 1.05
3.00 1.00
2.14 1.02 1.03
f1 (ppm)

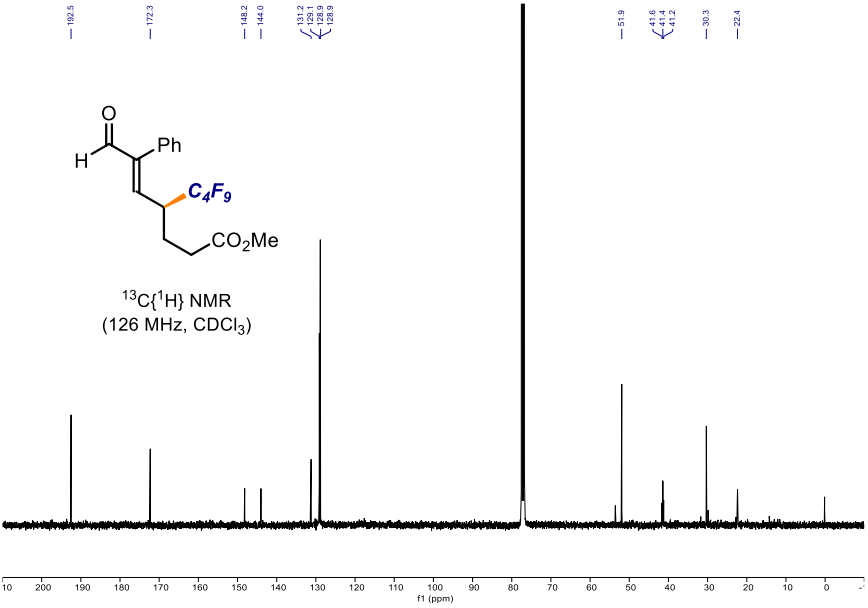
182.5
172.3
148.2
144.0
131.2
129.1
128.9
128.9
51.9
41.6
41.4
41.2
30.3
22.4
O
H
Ph
C4F9
CO2Me
13C{1H} NMR
(126 MHz, CDCl3)
f1 (ppm)

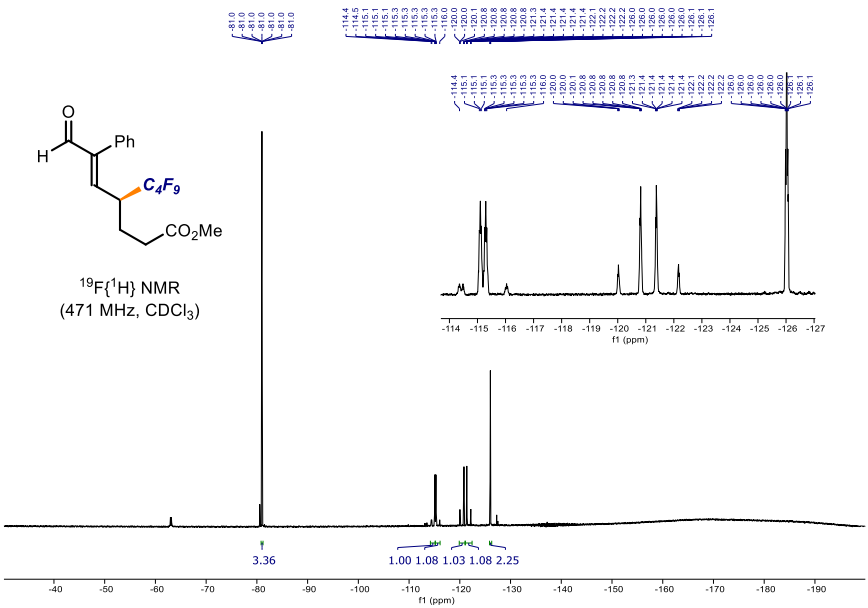
O
H
Ph
C_4F_9
CO_2Me
$^{19}F\{^1H\}$ NMR
(471 MHz, $CDCl_3$)
3.36
1.00 1.08 1.03 1.08 2.25
f1 (ppm)

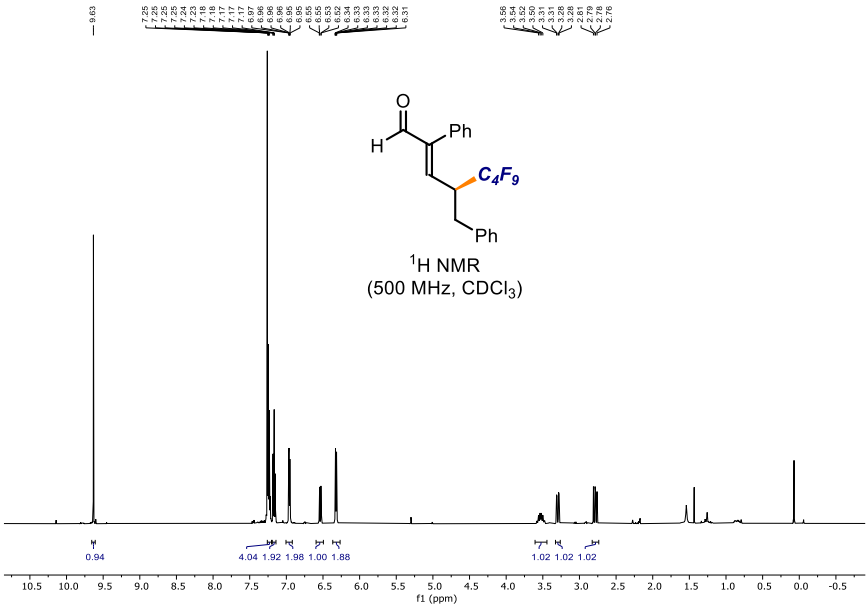
O
H
Ph
C_4F_9
Ph
^1H NMR
(500 MHz, $CDCl_3$)
0.94
4.04 1.92 1.98 1.00 1.88
1.02 1.02 1.02
f1 (ppm)

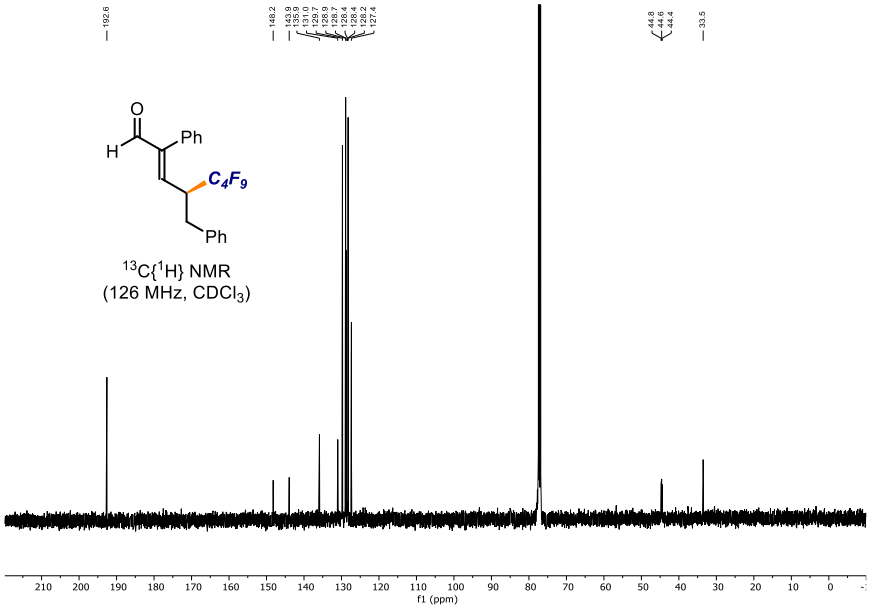
192.6
148.2
143.9
136.8
131.0
129.7
129.0
128.7
128.4
128.3
127.4
44.8
44.6
44.4
33.5
O
H
Ph
C4F9
Ph
13C{1H} NMR
(126 MHz, CDCl3)
f1 (ppm)

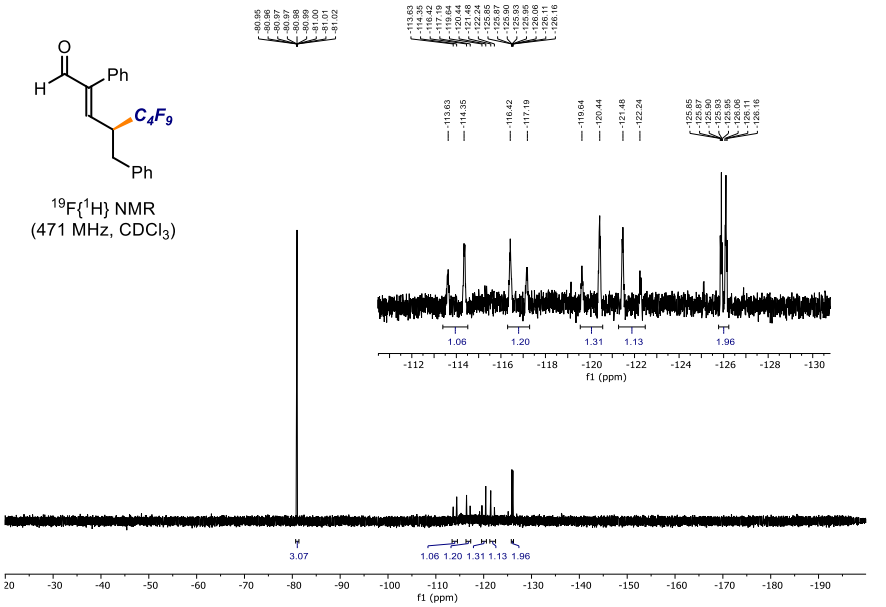
O
H
Ph
C4F9
Ph
19F{1H} NMR
(471 MHz, CDCl3)
-113.63
-114.35
-116.42
-117.19
-119.64
-120.44
-121.48
-122.24
-125.85
-125.87
-125.90
-125.93
-125.95
-126.06
-126.11
-126.16
1.06
1.20
1.31
1.13
1.96
3.07
f1 (ppm)

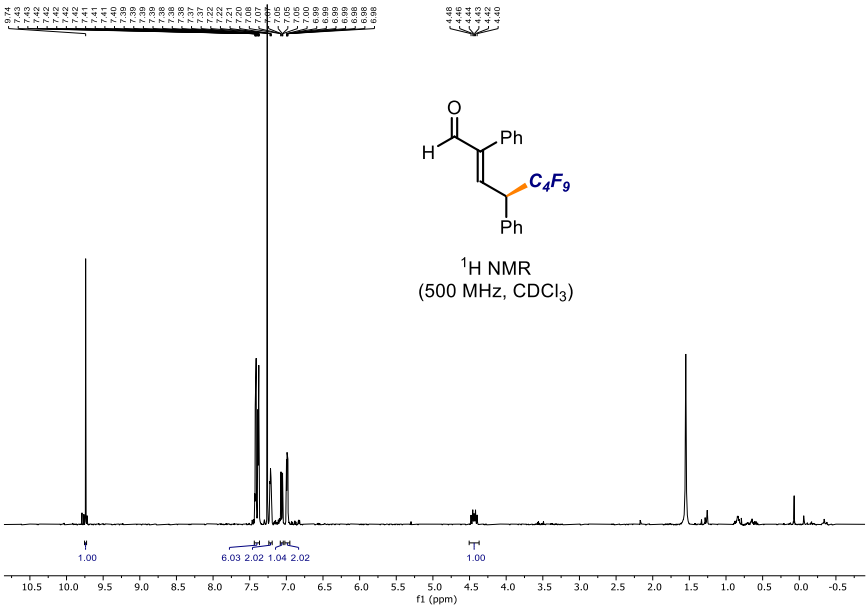
O
H
Ph
C_4F_9
Ph
^{1}H NMR
(500 MHz, $CDCl_3$)
1.00
6.03 2.02 1.04 2.02
1.00
f1 (ppm)

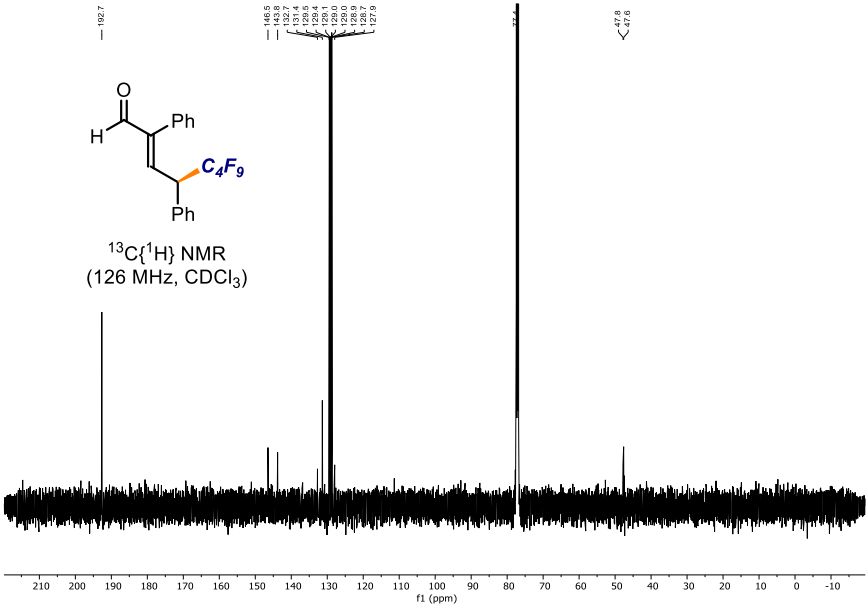
O
H
Ph
C_4F_9
Ph
^{13}C{^{1}H} NMR
(126 MHz, $CDCl_3$)
f1 (ppm)

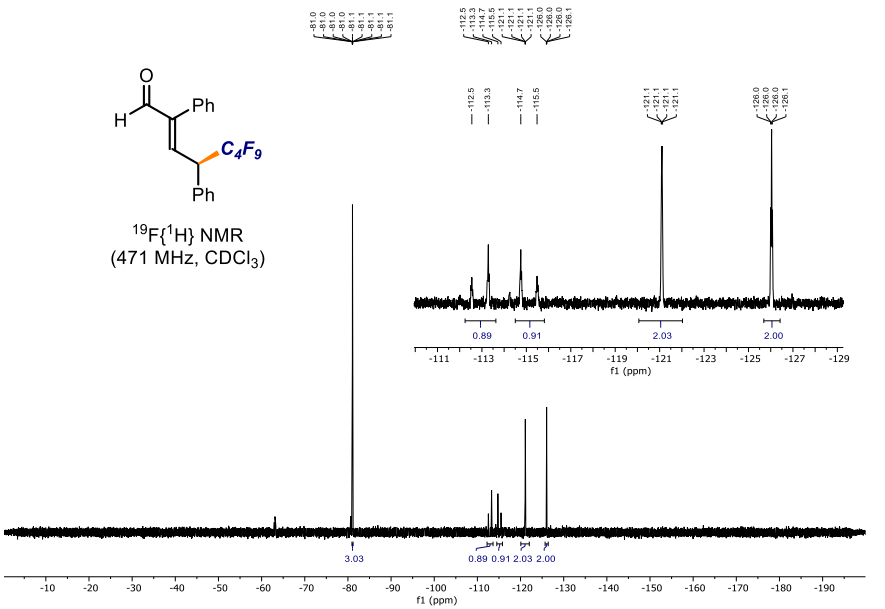
O
H
Ph
C_4F_9
Ph
$^{19}F\{^1H\}$ NMR
(471 MHz, $CDCl_3$)
f1 (ppm)

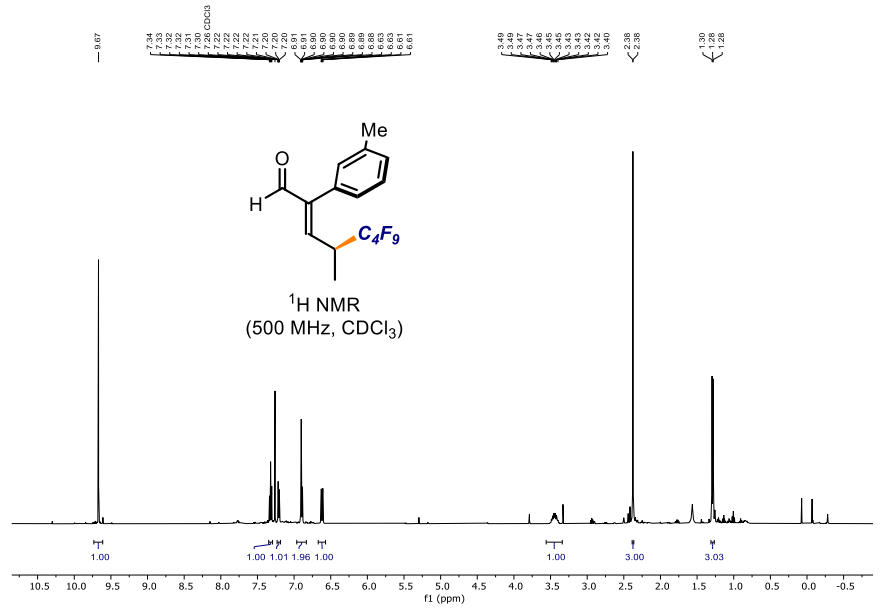
Me
O
H
C_4F_9
^1H NMR
(500 MHz, $CDCl_3$)
f1 (ppm)

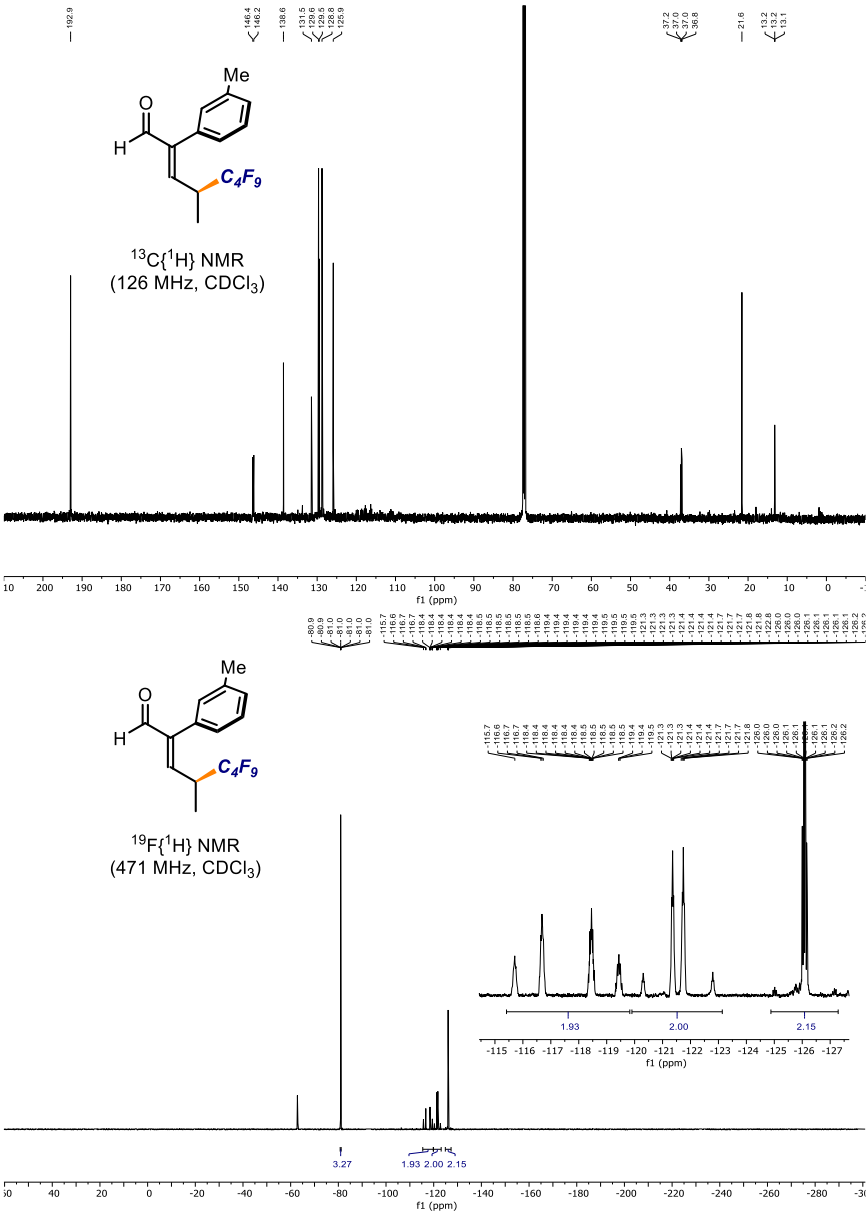
Me
O
H
C_4F_9
$^{13}C\{^1H\}$ NMR
(126 MHz, $CDCl_3$)
f1 (ppm)
Me
O
H
C_4F_9
$^{19}F\{^1H\}$ NMR
(471 MHz, $CDCl_3$)
3.27
1.93 2.00 2.15
1.93
2.00
2.15
f1 (ppm)

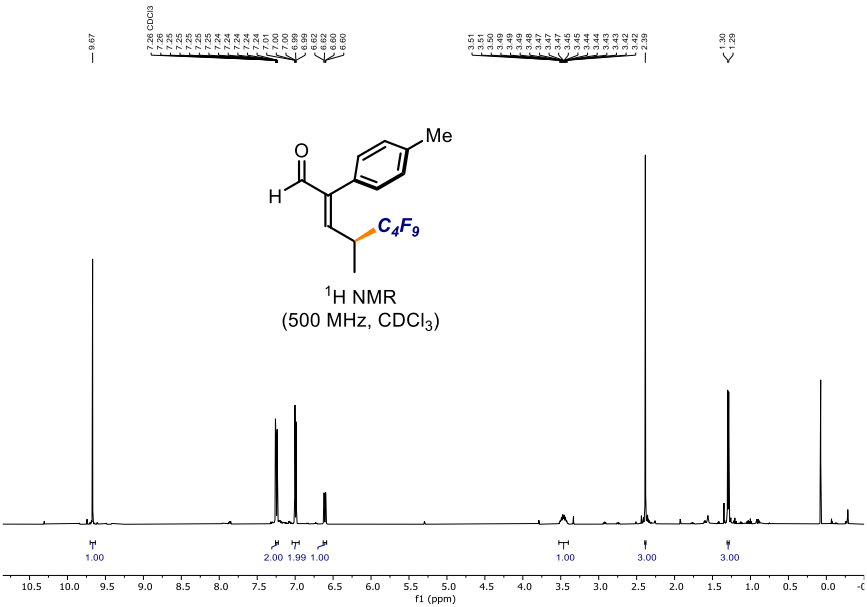
9.67
7.26 CDCl3
7.28
7.26
7.25
7.25
7.25
7.25
7.24
7.24
7.24
7.24
7.24
7.01
7.00
7.00
6.99
6.98
6.62
6.62
6.60
6.60
3.51
3.51
3.50
3.49
3.49
3.48
3.48
3.47
3.47
3.47
3.46
3.45
3.45
3.44
3.44
3.43
3.43
3.42
3.42
2.39
1.30
1.29
O
H
Me
C4F9
1H NMR
(500 MHz, CDCl3)
1.00
2.00
1.99
1.00
1.00
3.00
3.00
f1 (ppm)

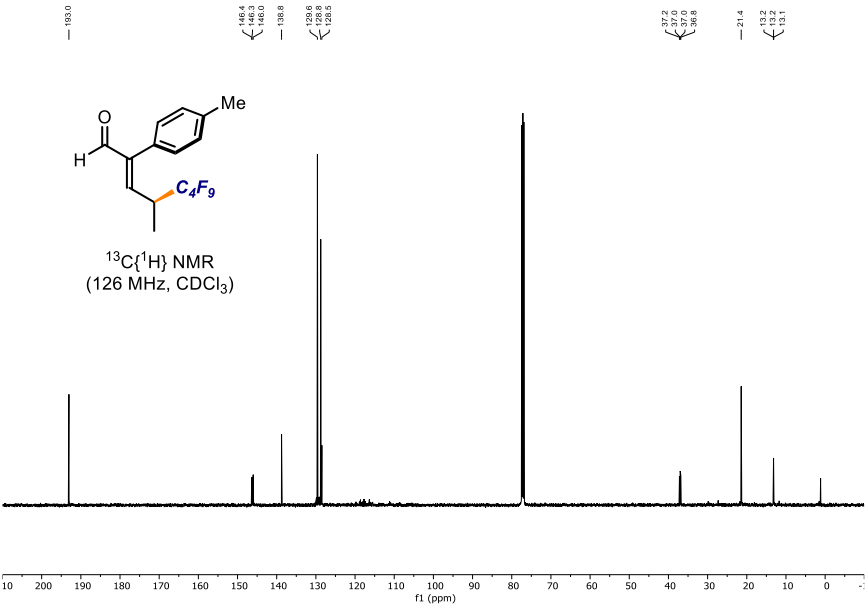
193.0
146.4
146.3
146.0
138.8
129.6
128.8
128.5
37.2
37.0
37.0
36.8
21.4
13.2
13.2
13.1
O
H
Me
C4F9
13C{1H} NMR
(126 MHz, CDCl3)
f1 (ppm)

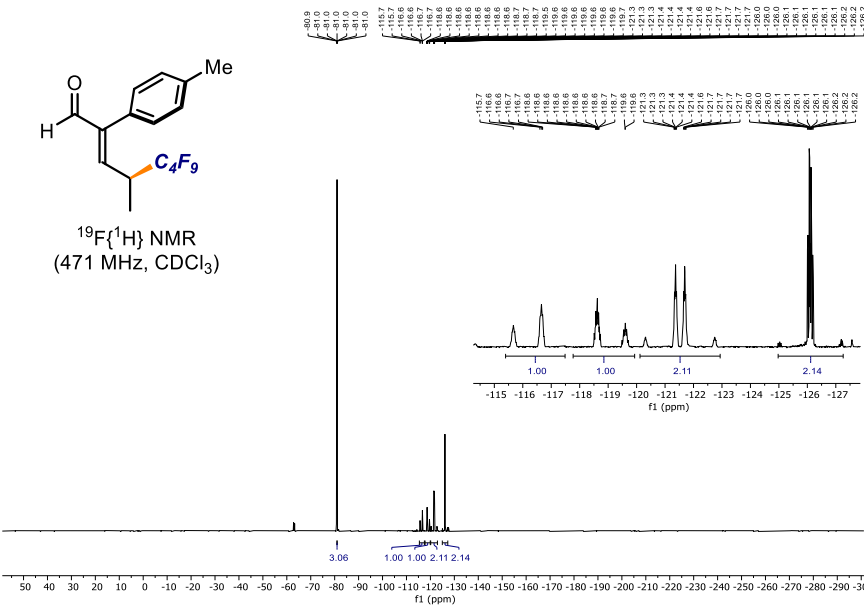
Me
O
H
C_4F_9
$^{19}F\{^1H\}$ NMR
(471 MHz, $CDCl_3$)
1.00
1.00
2.11
2.14
f1 (ppm)
3.06
1.00 1.00 2.11 2.14
f1 (ppm)

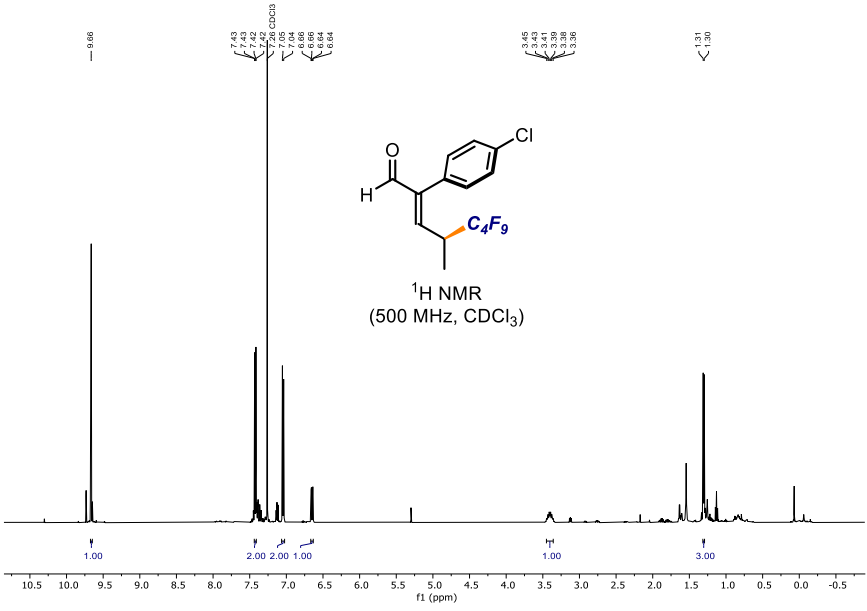
9.66
7.43
7.43
7.42
7.42
7.26 CDCl3
7.05
7.04
6.66
6.66
6.64
6.64
3.45
3.43
3.41
3.39
3.38
3.36
1.31
1.30
Cl
O
H
C_4F_9
^1H NMR
(500 MHz, $CDCl_3$)
1.00
2.00 2.00 1.00
1.00
3.00
f1 (ppm)

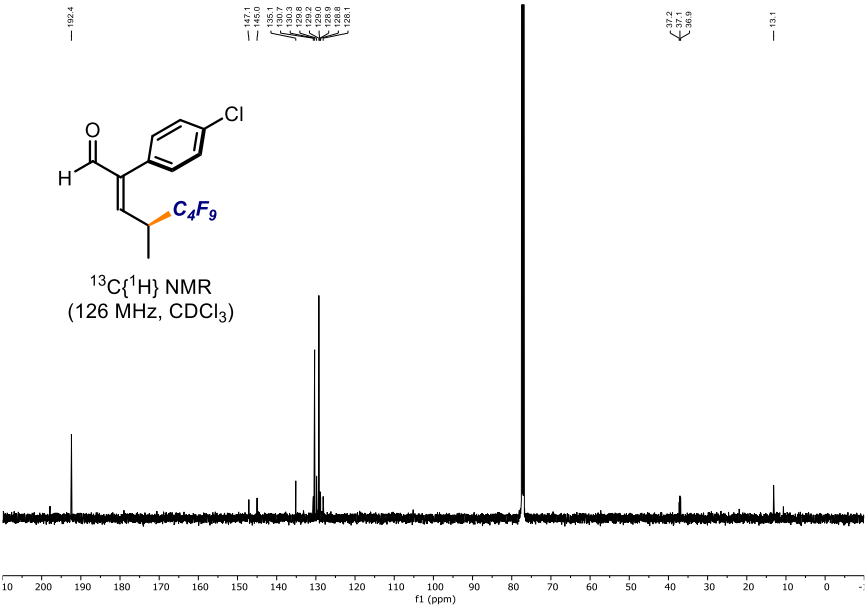
192.4
147.1
145.0
135.1
133.7
130.3
129.8
129.2
129.0
128.9
128.8
128.1
37.2
37.1
36.9
13.1
O
H
Cl
C4F9
13C{1H} NMR
(126 MHz, CDCl3)
f1 (ppm)

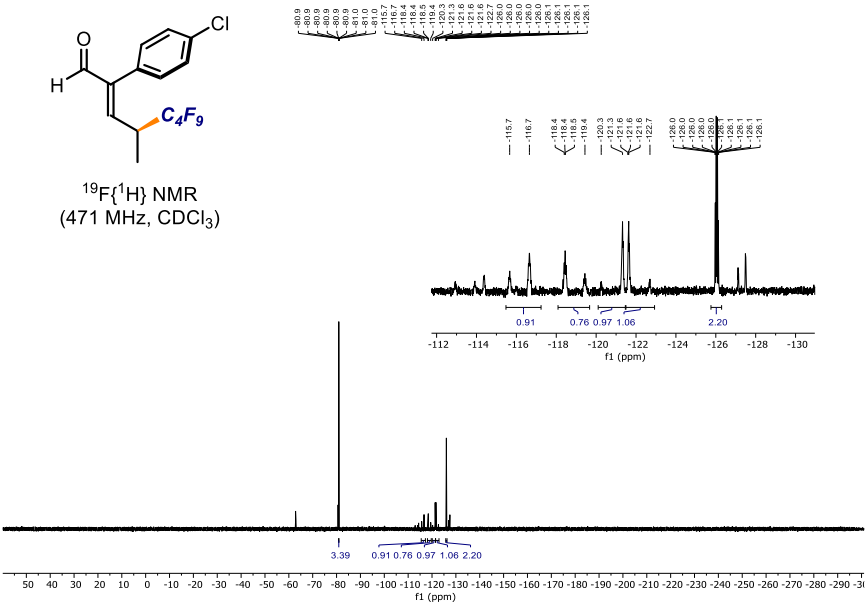
O
H
Cl
C4F9
19F{1H} NMR
(471 MHz, CDCl3)
0.91
0.76 0.97 1.06
2.20
3.39
0.91 0.76 0.97 1.06 2.20
f1 (ppm)

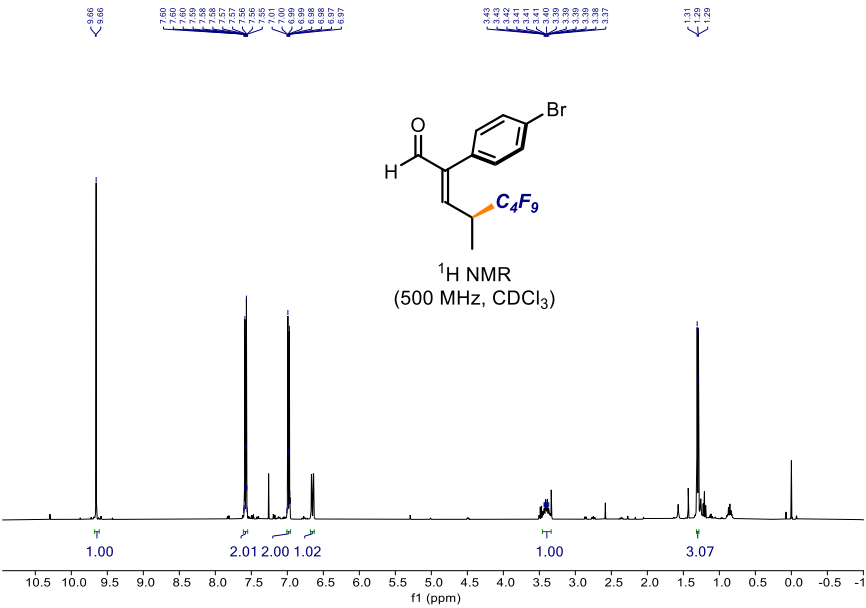
9.66
9.66
7.60
7.60
7.60
7.59
7.58
7.58
7.57
7.57
7.56
7.56
7.55
7.01
7.00
6.99
6.98
6.98
6.98
6.97
6.97
3.43
3.43
3.42
3.41
3.41
3.40
3.40
3.39
3.39
3.39
3.39
3.38
3.38
3.37
1.31
1.29
1.29
O
H
Br
C4F9
1H NMR
(500 MHz, CDCl3)
1.00
2.01
2.00
1.02
1.00
3.07
10.5 10.0 9.5 9.0 8.5 8.0 7.5 7.0 6.5 6.0 5.5 5.0 4.5 4.0 3.5 3.0 2.5 2.0 1.5 1.0 0.5 0.0 -0.5 -1
f1 (ppm)

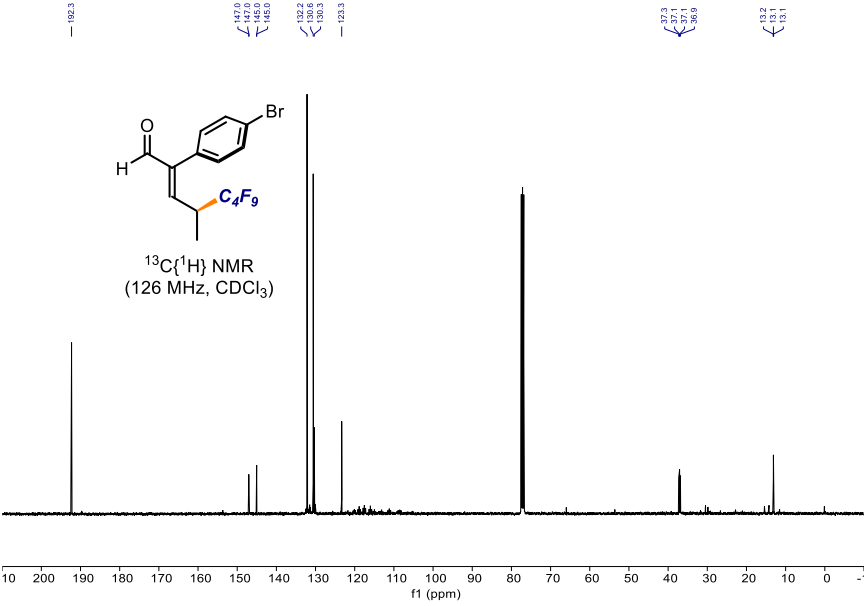
192.3
147.0
147.0
145.6
145.0
132.2
130.6
130.3
123.3
37.3
37.1
37.1
36.9
13.2
13.1
13.1
O
H
Br
C4F9
13C{1H} NMR
(126 MHz, CDCl3)
10 200 190 180 170 160 150 140 130 120 110 100 90 80 70 60 50 40 30 20 10 0
f1 (ppm)

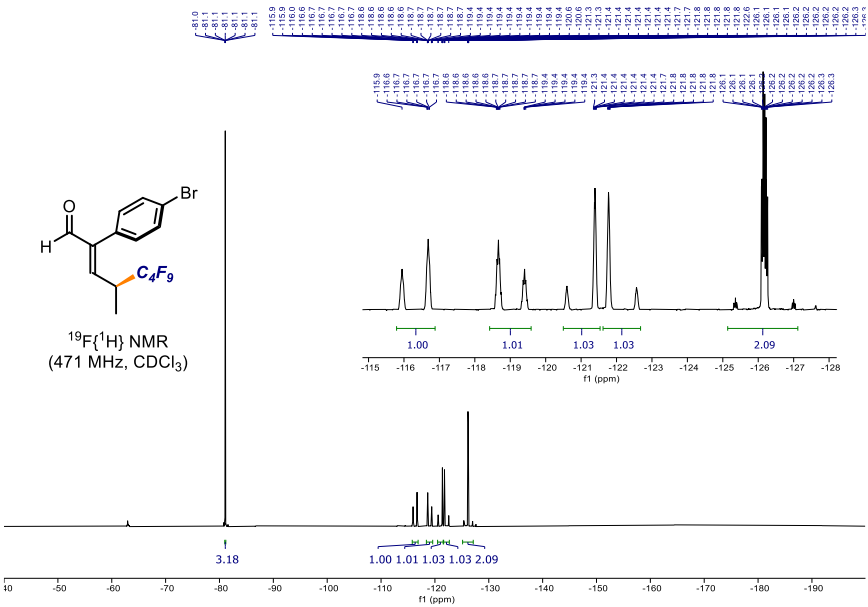
Br
O
H
C_4F_9
$^{19}F\{^1H\}$ NMR
(471 MHz, $CDCl_3$)
1.00
1.01
1.03
1.03
2.09
3.18
1.00 1.01 1.03 1.03 2.09
f1 (ppm)

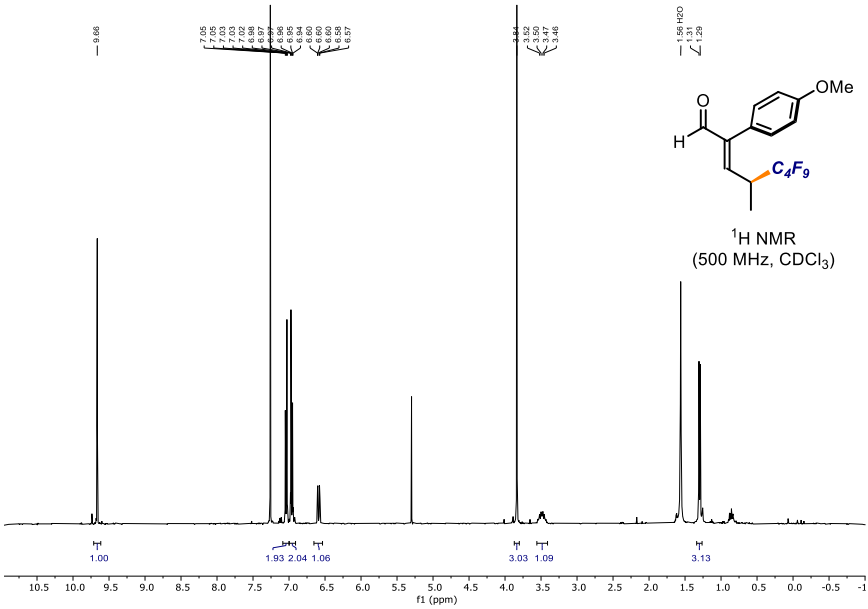
OMe
O
H
C_4F_9
^1H NMR
(500 MHz, $CDCl_3$)
1.00
1.93 2.04 1.06
3.03 1.09
3.13
f1 (ppm)

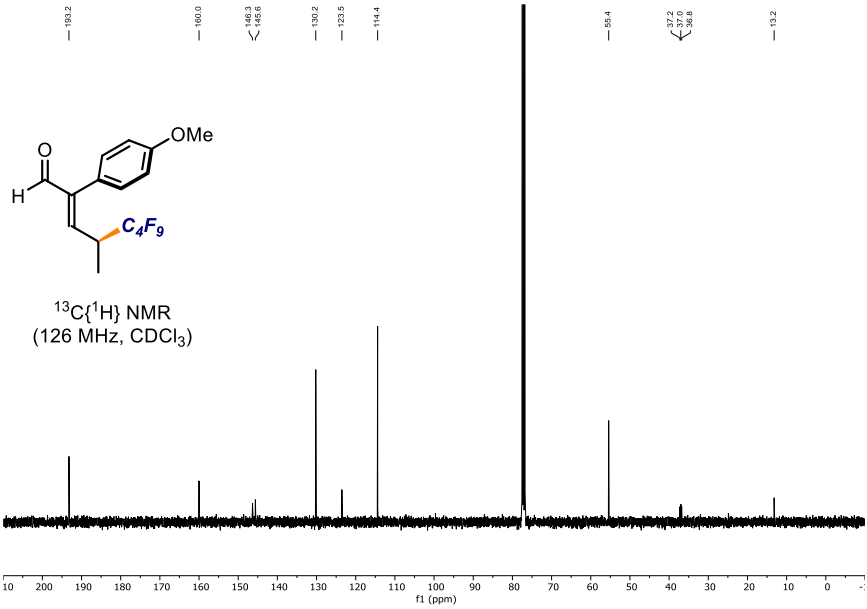
193.2
160.0
148.3
146.8
130.2
123.5
114.4
55.4
37.2
37.0
36.8
13.2
OMe
O
H
C4F9
13C{1H} NMR
(126 MHz, CDCl3)
f1 (ppm)

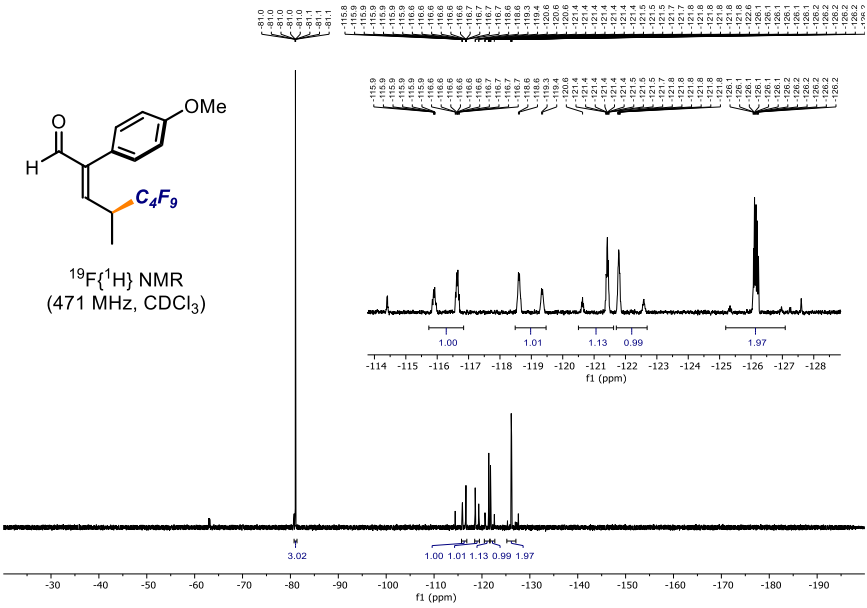
OMe
O
H
C4F9
19F{1H} NMR
(471 MHz, CDCl3)
1.00
1.01
1.13
0.99
1.97
f1 (ppm)
3.02
1.00 1.01 1.13 0.99 1.97
f1 (ppm)

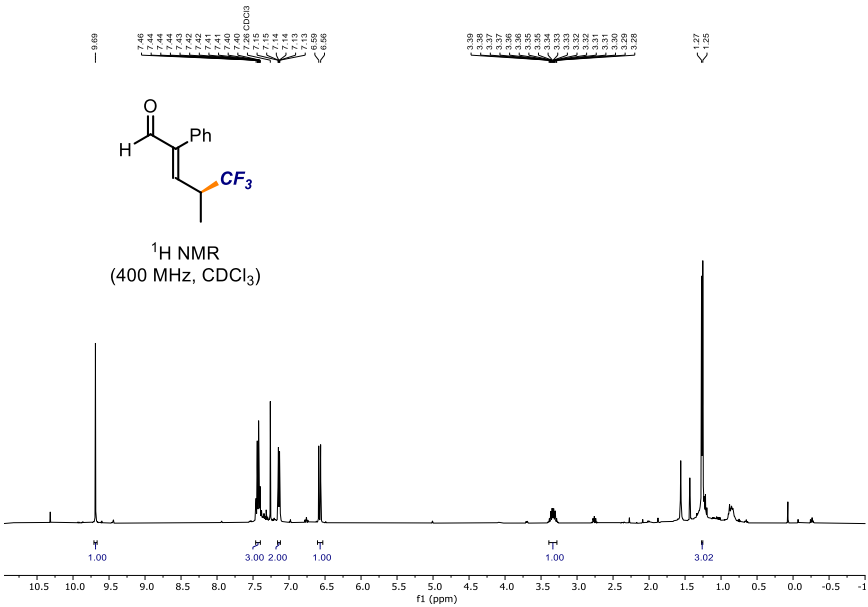
9.69
7.46
7.44
7.44
7.44
7.43
7.42
7.42
7.41
7.41
7.40
7.40
7.40
CDCl3
7.15
7.15
7.14
7.14
7.13
7.13
6.99
6.96
3.39
3.38
3.37
3.37
3.36
3.36
3.35
3.35
3.34
3.34
3.33
3.33
3.32
3.32
3.31
3.31
3.30
3.30
3.29
3.28
1.27
1.26
O
H
Ph
CF3
1H NMR
(400 MHz, CDCl3)
1.00
3.00
2.00
1.00
1.00
3.02
f1 (ppm)

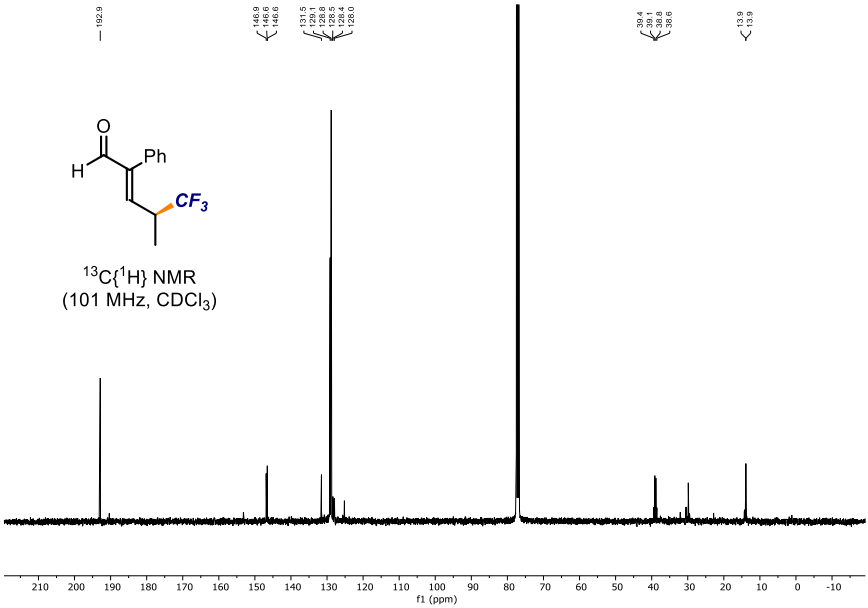
192.9
146.9
146.6
146.6
131.5
129.1
128.8
128.5
128.4
128.0
30.4
30.1
29.8
29.6
13.9
13.9
O
H
Ph
CF3
13C{1H} NMR
(101 MHz, CDCl3)
f1 (ppm)

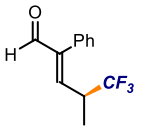

$^{19}F\{^{1}H\}$ NMR
(376 MHz, $CDCl_3$)

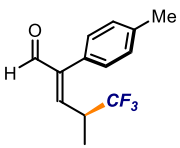

^{1}H NMR
(500 MHz, $CDCl_3$)

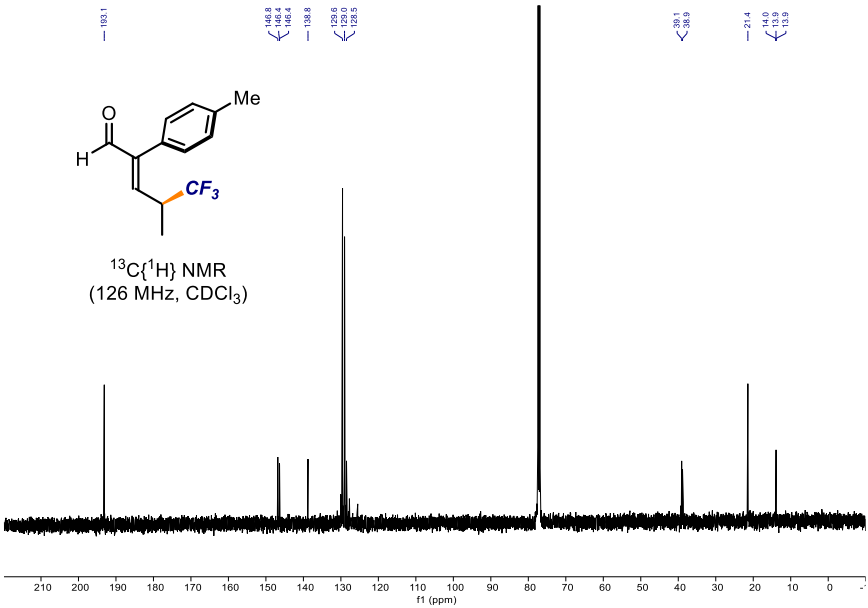

$^{13}C\{^{1}H\}$ NMR
(126 MHz, $CDCl_3$)

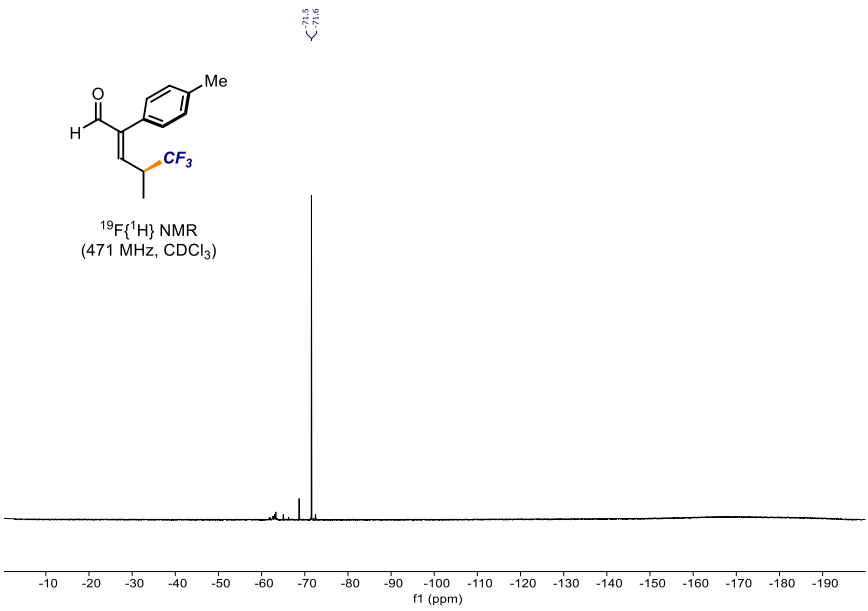

$^{19}F\{^{1}H\}$ NMR
(471 MHz, $CDCl_3$)

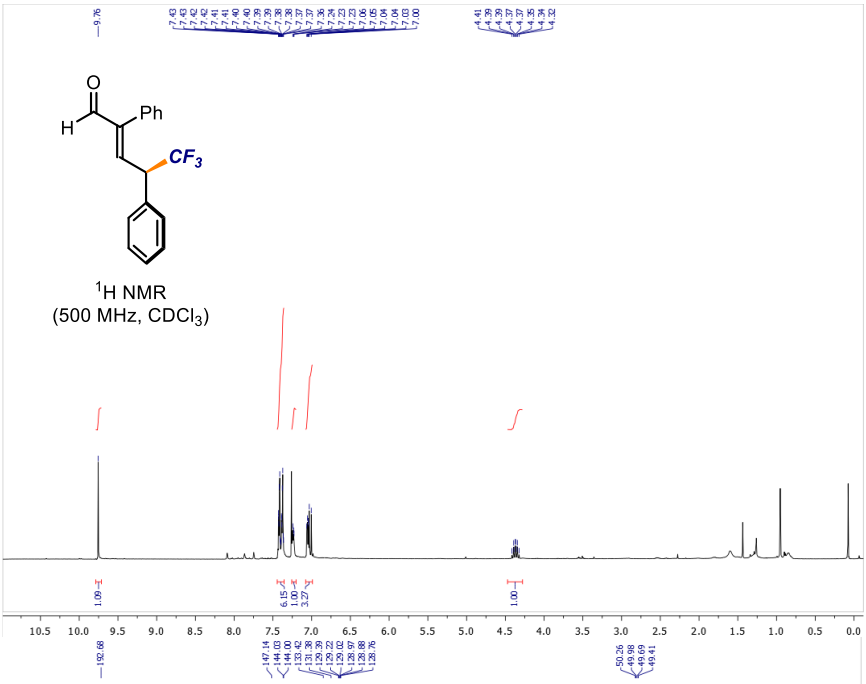

^{1}H NMR
(500 MHz, $CDCl_3$)

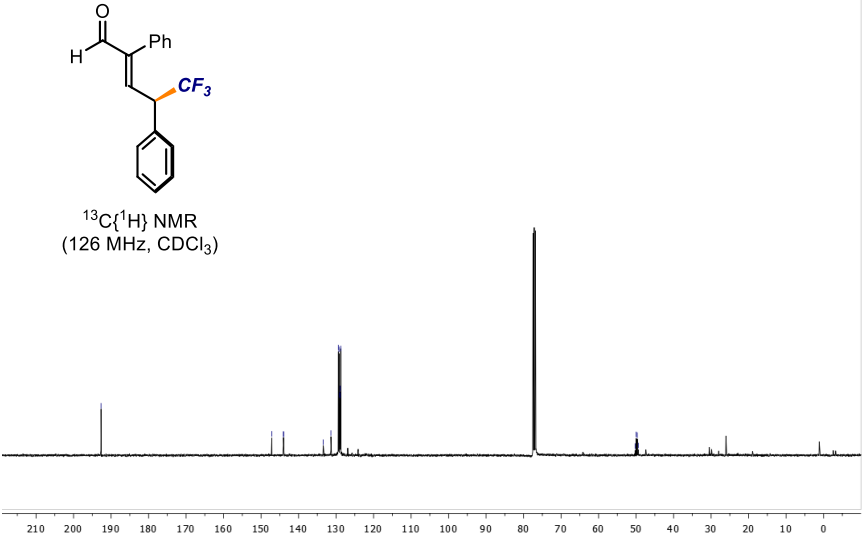

$^{13}C\{^{1}H\}$ NMR
(126 MHz, $CDCl_3$)

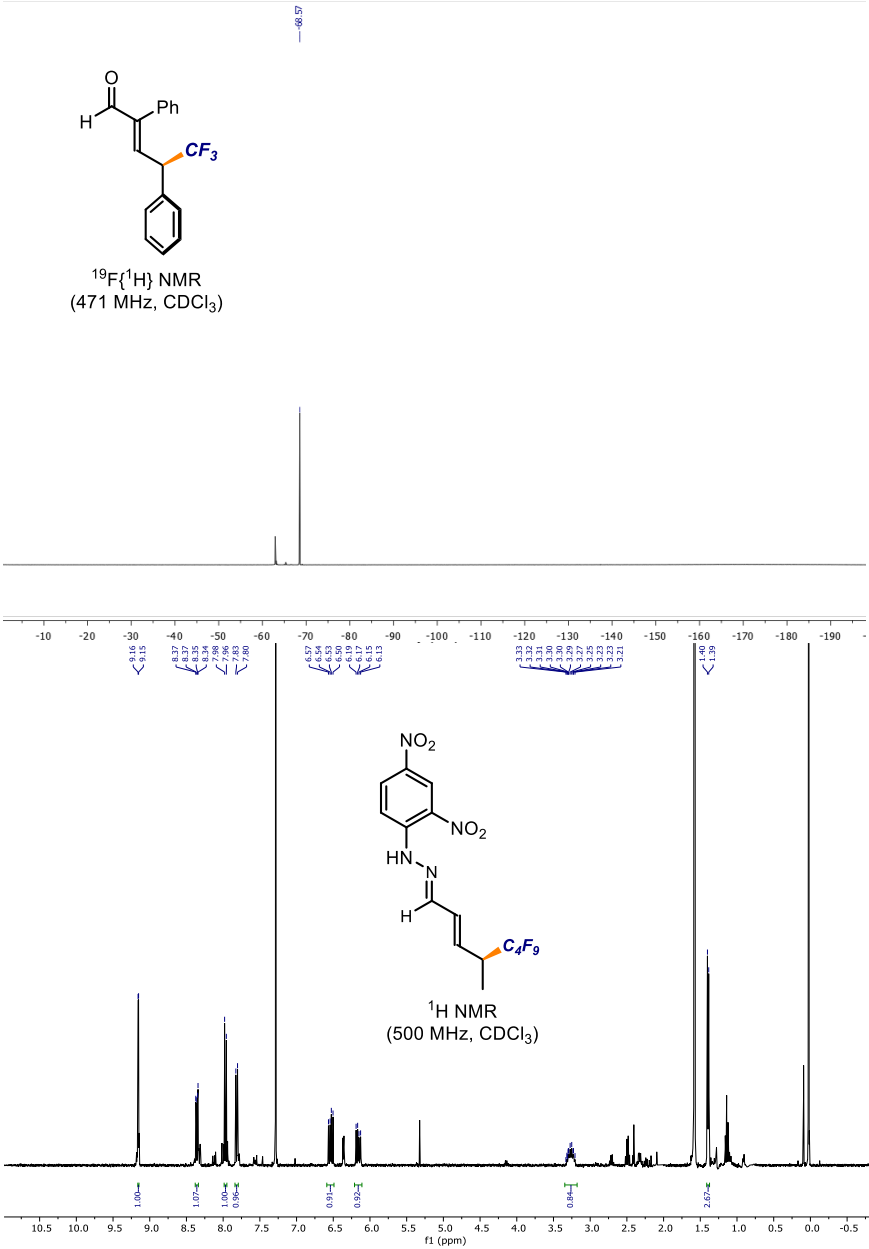
-68.57
O
H
Ph
CF3
19F{1H} NMR
(471 MHz, CDCl3)
NO2
NO2
HN
N
H
C4F9
1H NMR
(500 MHz, CDCl3)
f1 (ppm)

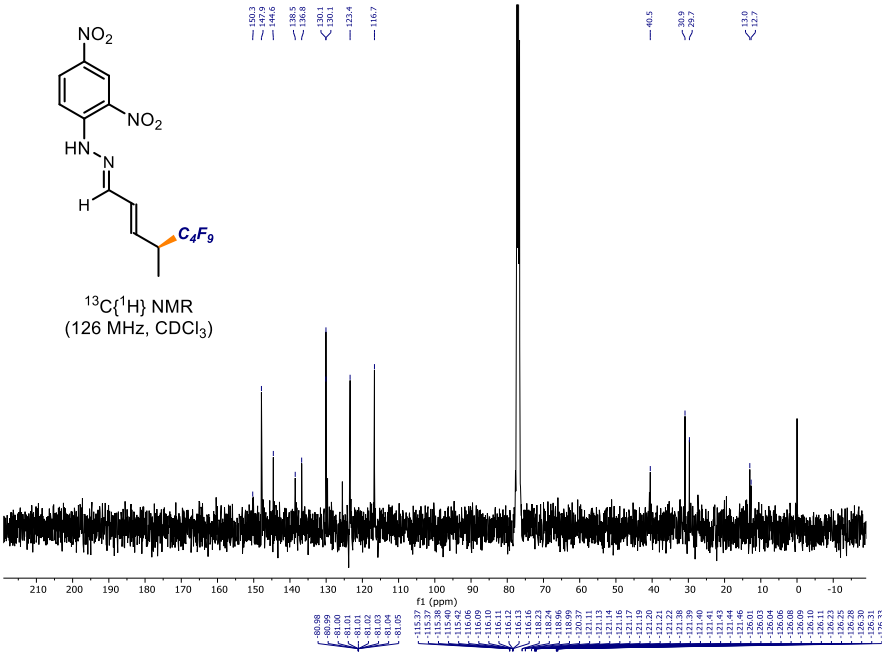

$^{13}C\{^{1}H\}$ NMR
(126 MHz, $CDCl_3$)

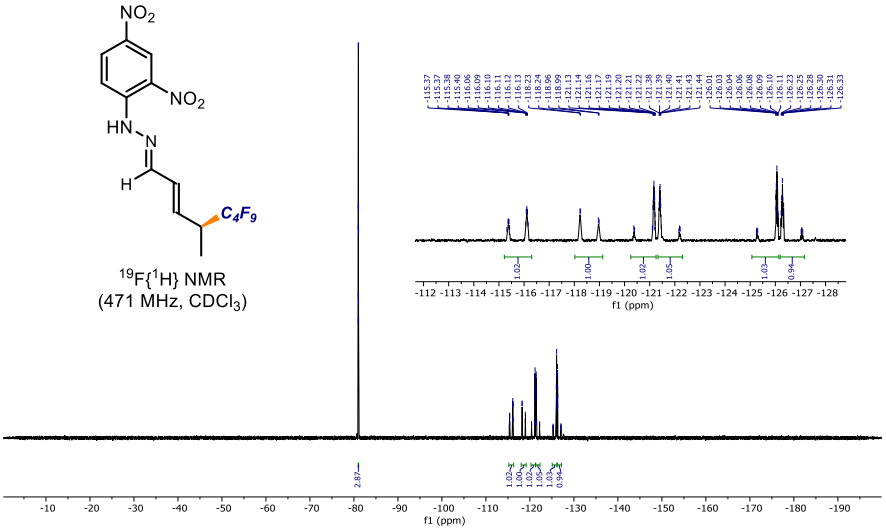

$^{19}F\{^{1}H\}$ NMR
(471 MHz, $CDCl_3$)

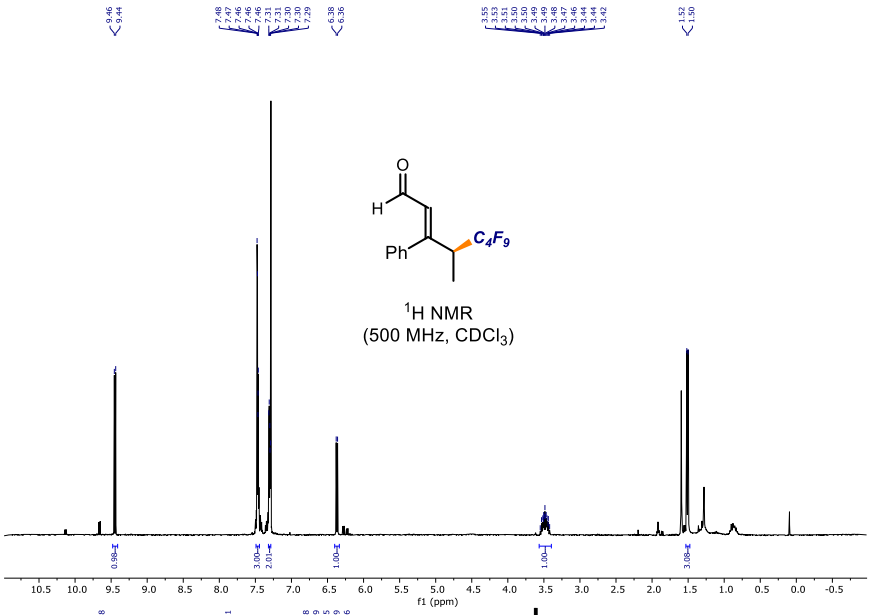
9.46
9.44
7.48
7.47
7.46
7.46
7.46
7.31
7.31
7.30
7.30
7.29
6.38
6.36
3.55
3.53
3.51
3.50
3.50
3.49
3.49
3.48
3.47
3.46
3.46
3.44
3.44
3.42
1.52
1.50
O
H
Ph
C4F9
1H NMR
(500 MHz, CDCl3)
0.98
3.00
2.01
1.00
1.00
3.08
f1 (ppm)

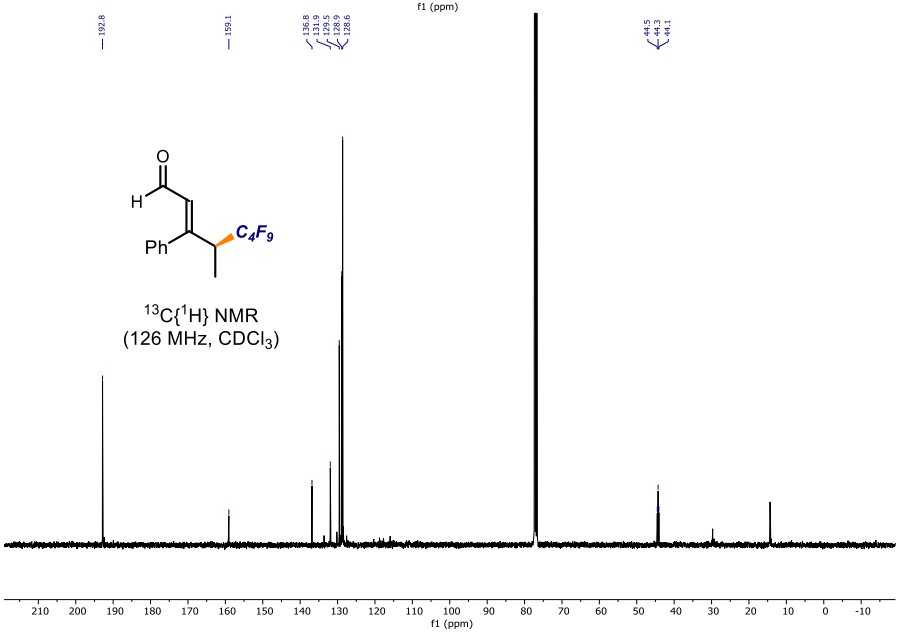
192.8
159.1
135.8
133.5
129.5
128.9
128.6
44.5
44.3
44.1
O
H
Ph
C4F9
13C{1H} NMR
(126 MHz, CDCl3)
f1 (ppm)

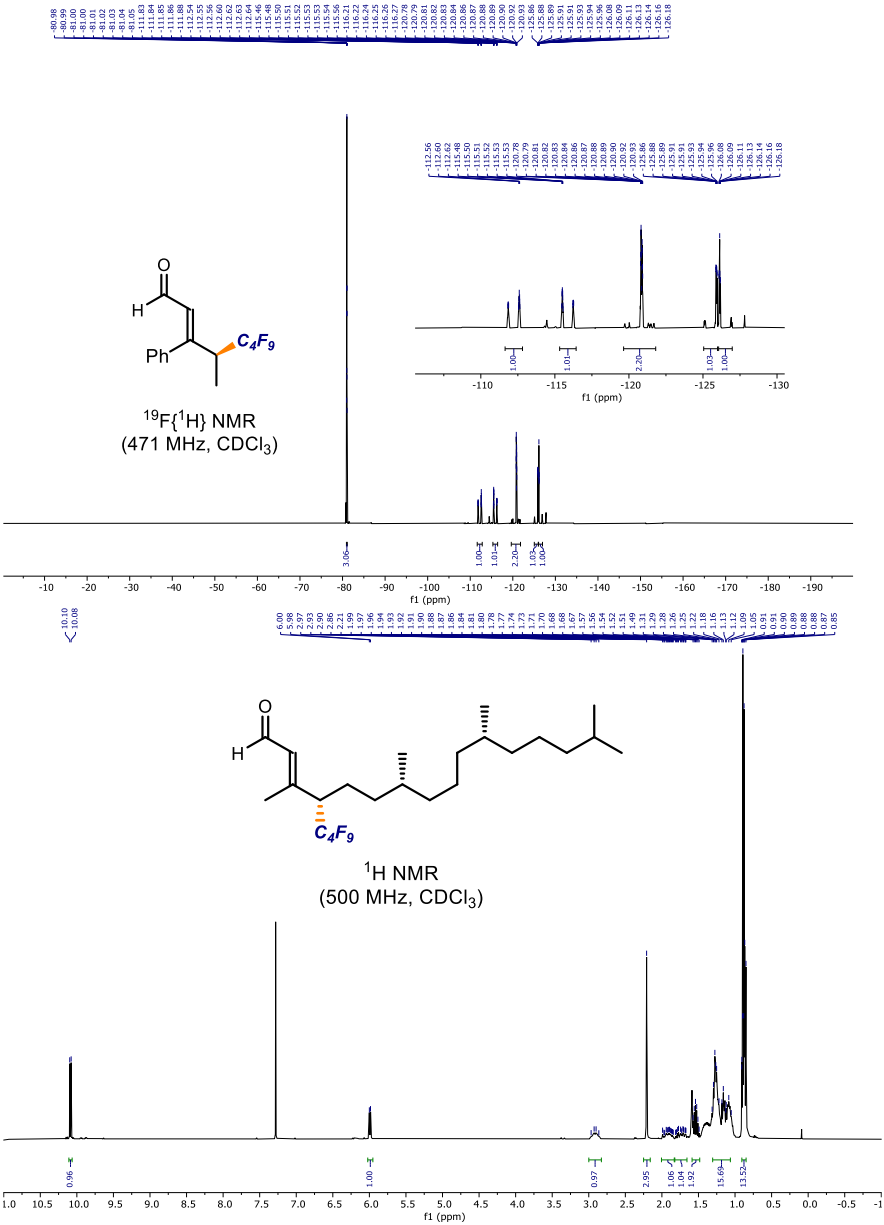
O
H
Ph
C_4F_9
$^{19}F\{^1H\}$ NMR
(471 MHz, CDCl$_3$)
f1 (ppm)
O
H
C_4F_9
^1H NMR
(500 MHz, CDCl$_3$)
f1 (ppm)

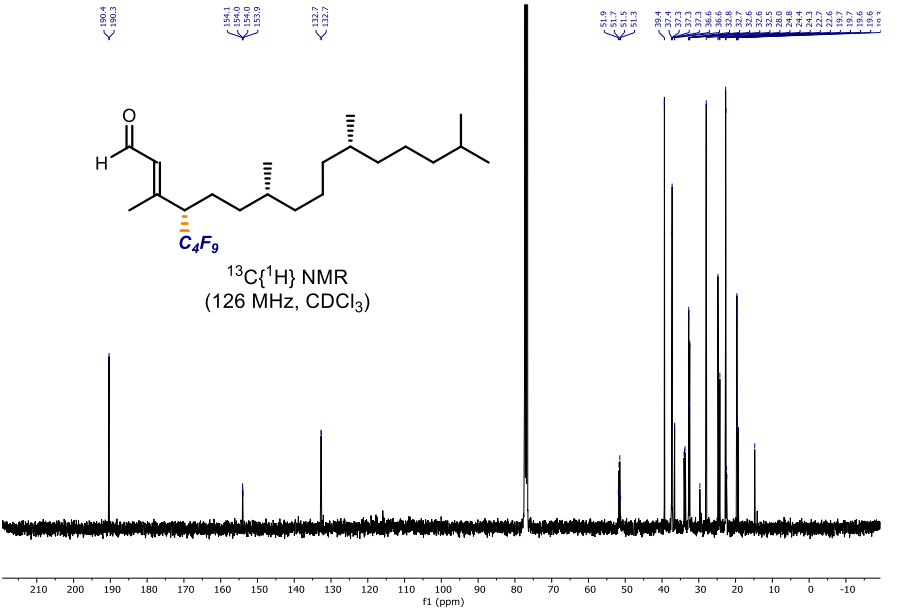
O
H
C_4F_9
$^{13}C\{^1H\}$ NMR
(126 MHz, $CDCl_3$)
f1 (ppm)

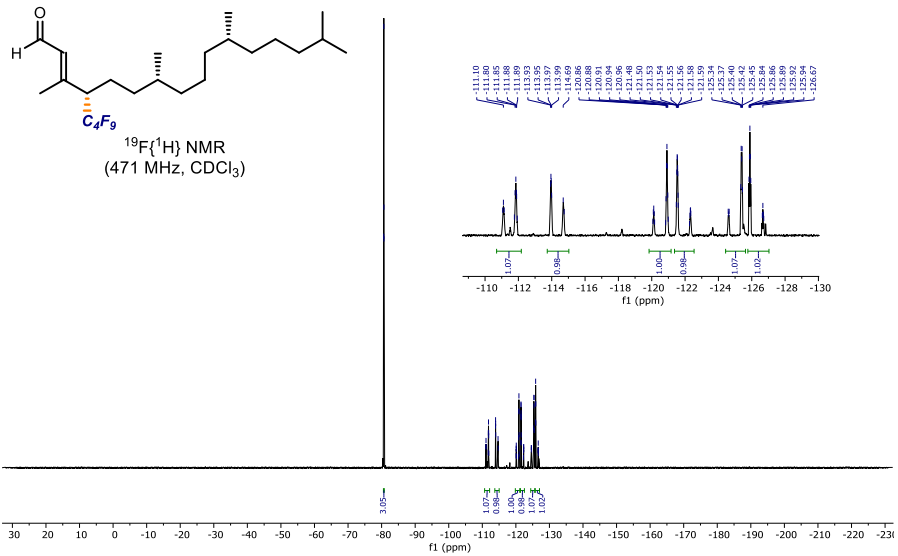
O
H
C_4F_9
$^{19}F\{^1H\}$ NMR
(471 MHz, $CDCl_3$)
f1 (ppm)

6. Bibliography

[1] T. P. Yoon, M. A. Ischay, J. Du, *Nat Chem* **2010**, *2*, 527–532.

[2] G. Ciamician, *The Photochemistry of the Future*, **1912**.

[3] P. Klán, J. Wirz, *Photochemistry of Organic Compounds : From Concepts to Practice*, Wiley, **2009**.

[4] J. A. Dantas, J. T. M. Correia, M. W. Paixão, A. G. Corrêa, *ChemPhotoChem* **2019**, *3*, 506–520.

[5] R. G. W. Norrish, C. H. Bamford, *Nature* **1937**, 195–196.

[6] P. J. Wagner, A. E. Kemppainen, P. J. Wagner, P. A. Kelso, R. G. Zepp, J. Amer Chem SOC, C. Walling, M. J. Gibian, W. D. K Clark, A. D. Litt, C. Steel, I. Kochevar, A. E. Kemppainen, J. Amer Chem, E. J. Baum, J. K. S Wan, J. N. Pitts, D. R. Burley, J. C. Mani, A. D. Broad, *Proc. Roy. Soc., Ser. A* **1968**, *90*, 462.

[7] A. G. Griesbeck, H. Heckroth, *J Am Chem Soc* **2002**, *124*, 396–403.

[8] J. N. Moorthy, P. Mal, *Tetrahedron Lett* **2003**, *44*, 2493–2496.

[9] N. Singhal, A. L. Koner, P. Mal, P. Venugopalan, W. M. Nau, J. N. Moorthy, *J Am Chem Soc* **2005**, *127*, 14375–14382.

[10] J. N. Moorthy, A. L. Koner, S. Samanta, N. Singhal, W. M. Nau, R. G. Weiss, *Chemistry - A European Journal* **2006**, *12*, 8744–8749.

[11] A. G. Griesbeck, H. Heckroth, J. Lex, *Chemical Communications* **1999**, 1109–1110.

[12] J. N. Moorthy, P. Mal, *Tetrahedron Lett* **2003**, *44*, 2493–2496.

[13] S. Yamada, Y. Oshima, Y. Fujita, S. Tsuzuki, *Tetrahedron Lett* **2019**, *60*, 1543–1546.

[14] S. Kamijo, T. Hoshikawa, M. Inoue, *Tetrahedron Lett* **2010**, *51*, 872–874.

[15] Y. Chen, J. Zhao, S. Li, J. Xu, *Nat Prod Rep* **2019**, *36*, 263–288.
[16] A. J. L. Ayitou, J. L. Jesuraj, N. Barooah, A. Ugrinov, J. Sivaguru, *J Am Chem Soc* **2009**, *131*, 11314–11315.
[17] F. Secci, S. Porcu, A. Luridiana, A. Frongia, P. C. Ricci, *Org Biomol Chem* **2020**, *18*, 3684–3689.
[18] P. Baas, H. Cerfontain, *A NOVEL TYPE II CYCLOBUTANOL FORMATION*, Pergamon Press, **1978**.
[19] P. Yates, J. Wong, S. Mclean, *Tetrahedron* **1981**, *37*, 3357–3363.
[20] A. J. L. Ayitou, J. L. Jesuraj, N. Barooah, A. Ugrinov, J. Sivaguru, *J Am Chem Soc* **2009**, *131*, 11314–11315.
[21] A. Natarajan, J. T. Mague, V. Ramamurthy, *J Am Chem Soc* **2005**, *127*, 3568–3576.
[22] J. L. Markley, T. L. Morse, N. P. Rath, T. A. Wencewicz, *Tetrahedron* **2018**, *74*, 2743–2753.
[23] J. S. Ham, B. Park, M. Son, J. B. Roque, J. Jurczyk, C. S. Yeung, M. H. Baik, R. Sarpong, *J Am Chem Soc* **2020**, *142*, 13041–13050.
[24] A. W. Harrison, S. H. Kable, *Journal of Chemical Physics* **2018**, *148*, DOI 10.1063/1.5019383.
[25] K. N. Rowell, S. H. Kable, M. J. T. Jordan, *Atmos Chem Phys* **2022**, *22*, 929–949.
[26] D. Shemesh, Z. Lan, R. B. Gerber, *Journal of Physical Chemistry A* **2013**, *117*, 11711–11724.
[27] C. D. Bray, G. Pattenden, *Tetrahedron Lett* **2006**, *47*, 3937–3939.
[28] B. Tang, R. S. Paton, *Org Lett* **2019**, *21*, 1243–1247.
[29] P. Gentili, S. Pedetti, *Chemical Communications* **2012**, *48*, 5358–5360.
[30] M. Baidya, H. Yamamoto, *J Am Chem Soc* **2011**, *133*, 13880–13882.
[31] P. Gentili, M. Nardi, I. Antignano, P. Cambise, M. D'Abramo, F. D'Acunzo, A. Pinna, E. Ussia, *Chemistry - A European Journal* **2018**, *24*, 7683–7694.

[32] V. Y. Kukushkin, A. J. L. Pombeiro, *Oxime and Oximate Metal Complexes: Unconventional Synthesis and Reactivity*, **1999**.
[33] P. Baas, H. Cerfontain, *Tetrahedron Lett* **1978**, *19*, 1501–1504.
[34] D. Eddings, C. Barnes, N. Gerasimchuk, P. Durham, K. Domasevich, *Inorg Chem* **2004**, *43*, 3894–3909.
[35] F. Mancin, P. Tecilla, U. Tonellato, *European J Org Chem* **2000**, 1045–1050.
[36] H. Saarinen, M. Orama, *Acta Chem Scand* **1998**, *52*, 1209–1213.
[37] M. Nardi, F. D'Acunzo, M. Clemente, G. Proietti, P. Gentili, *Polym Chem* **2017**, *8*, 4233–4245.
[38] I. Antignano, F. D'Acunzo, D. Arena, S. Casciardi, A. del Giudice, F. Gentile, M. Pelosi, G. Masci, P. Gentili, *Langmuir* **2022**, DOI 10.1021/acs.langmuir.2c02515.
[39] A. di Sabato, F. D'Acunzo, D. Filippini, F. Vetica, A. Brasiello, D. Corinti, E. Bodo, C. Michenzi, E. Panzetta, P. Gentili, *Journal of Organic Chemistry* **2022**, *2022*, 13803–13818.
[40] F. D'Acunzo, L. Carbonaro, A. D. Cort, A. di Sabato, D. Filippini, F. Leonelli, L. Mancini, P. Gentili, *European J Org Chem* **2021**, *2021*, 289–294.
[41] A. Padwa, *Chem Rev* **1977**, *77*, 37–68.
[42] A. Padwa, F. Albrecht, *J Am Chem Soc* **1974**, *96*, 4849–4857.
[43] A. G. Griesbeck, B. Porschen, C. Kropf, A. Landes, O. Hinze, U. Huchel, T. Gerke, *Synthesis (Germany)* **2017**, *49*, 539–553.
[44] Y. Huang, S. Thanneeru, Q. Zhang, J. He, *J Polym Sci A Polym Chem* **2018**, *56*, 1815–1824.
[45] A. G. Griesbeck, H. Heckroth, *J Am Chem Soc* **2002**, *124*, 396–403.
[46] J. N. Moorthy, P. Mal, *Tetrahedron Lett* **2003**, *44*, 2493–2496.

[47] J. N. Moorthy, S. Samanta, A. L. Koner, S. Saha, W. M. Nau, *J Am Chem Soc* **2008**, *130*, 13608–13617.
[48] N. Singhal, A. L. Koner, P. Mal, P. Venugopalan, W. M. Nau, J. N. Moorthy, *J Am Chem Soc* **2005**, *127*, 14375–14382.
[49] J. N. Moorthy, A. L. Koner, S. Samanta, N. Singhal, W. M. Nau, R. G. Weiss, *Chemistry - A European Journal* **2006**, *12*, 8744–8749.
[50] K. B. Wiberg, D. E. Barth, *J Am Chem Soc* **1969**, *91*, 5124–5130.
[51] J. Martens, R. E. van Outersterp, R. J. Vreeken, F. Cuyckens, K. L. M. Coene, U. F. Engelke, L. A. J. Kluijtmans, R. A. Wevers, L. M. C. Buydens, B. Redlich, G. Berden, J. Oomens, *Anal Chim Acta* **2020**, *1093*, 1–15.
[52] N. C. Polfer, *Chem Soc Rev* **2011**, *40*, 2211–2221.
[53] D. Corinti, M. E. Crestoni, S. Fornarini, M. Pieper, K. Niehaus, M. Giampà, *Anal Bioanal Chem* **2019**, *411*, 953–964.
[54] M. Mayer, K. R. Asmis, *Journal of Physical Chemistry A* **2021**, *125*, 2801–2815.
[55] J. Mehara, J. Roithová, *Chem Sci* **2020**, *11*, 11960–11972.
[56] J. Merx, K. J. Houthuijs, H. Elferink, E. Witlox, J. Mecinović, J. Oomens, J. Martens, T. J. Boltje, F. P. J. T. Rutjes, *Chemistry - A European Journal* **2022**, *28*, DOI 10.1002/CHEM.202104078.
[57] M. E. Crestoni, B. Chiavarino, D. Scuderi, A. di Marzio, S. Fornarini, *Journal of Physical Chemistry B* **2012**, *116*, 8771–8779.
[58] A. Bouchet, J. Klyne, G. Piani, O. Dopfer, A. Zehnacker, *Physical Chemistry Chemical Physics* **2015**, *17*, 25809–25821.
[59] S. S. Lee, S. Park, Y. Hong, J. U. Lee, J. H. Kim, D. Yoon, X. Kong, S. Lee, H. bin Oh, *Physical Chemistry Chemical Physics* **2017**, *19*, 14729–14737.

[60] A. Sinicropi, F. Barbosa, R. Basosi, B. Giese, M. Olivucci, *Angewandte Chemie - International Edition* **2005**, *44*, 2390–2393.
[61] C. M. Marian, *Wiley Interdiscip Rev Comput Mol Sci* **2012**, *2*, 187–203.
[62] R. Koch, H. J. Wollweber, C. Wentrup, *Aust J Chem* **2015**, *68*, 1329–1335.
[63] O. L. Chapman, R. W. King, W. J. Welstead, T. J. Murphy, *J Am Chem Soc* **1964**, *86*, 4968–4973.
[64] M. v. Sigalov, B. A. Shainyan, N. N. Chipanina, L. P. Oznobikhina, *European J Org Chem* **2017**, *2017*, 1353–1364.
[65] J. Gálvez, A. Guirado, *J Comput Chem* **2010**, *31*, 520–531.
[66] D. van der Spoel, E. Lindahl, B. Hess, G. Groenhof, A. E. Mark, H. J. C. Berendsen, *J Comput Chem* **2005**, *26*, 1701–1718.
[67] J. A. Levi, R. S. Aroney, D. N. Dalley, *Br Med J (Clin Res Ed)* **1981**, *282*, 2003–2004.
[68] N. Singh, A. Vik, D. B. Lybrand, C. Morisseau, B. D. Hammock, *Chem Res Toxicol* **2021**, *34*, DOI 10.1021/ACS.CHEMRESTOX.1C00347/SUPPL_FILE/TX1C00347_SI_001.PDF.
[69] N. Milosavljevic, C. Duranton, N. Djerbi, P. H. Puech, P. Gounon, D. Lagadic-Gossmann, M. T. Dimanche-Boitrel, C. Rauch, M. Tauc, L. Counillon, M. Poët, *Cancer Res* **2010**, *70*, 7514–7522.
[70] P. Maccarthy, *Simplified Experimental Route for Obtaining Job's Curves*, **1978**.
[71] Z. D. Hill, P. Maccarthy1, *Novel Approach to Job's Method An Undergraduate Experiment*, **n.d.**
[72] P. Job, **n.d.**
[73] G. E. M. Crisenza, D. Mazzarella, P. Melchiorre, *J Am Chem Soc* **2020**, *142*, 5461–5476.
[74] E. Arceo, I. D. Jurberg, A. Álvarez-Fernández, P. Melchiorre, *Nature Chemistry 2013 5:9* **2013**, *5*, 750–756.

[75] S. Purser, P. R. Moore, S. Swallow, V. Gouverneur, *Chem Soc Rev* **2008**, *37*, 320–330.
[76] N. A. Meanwell, *J Med Chem* **2018**, *61*, 5822–5880.
[77] W. K. Hagmann, *J Med Chem* **2008**, *51*, 4359–4369.
[78] K. Müller, C. Faeh, F. Diederich, *Science (1979)* **2007**, *317*, 1881–1886.
[79] F. Lovering, *Medchemcomm* **2013**, *4*, 515–519.
[80] F. Lovering, J. Bikker, C. Humblet, *J Med Chem* **2009**, *52*, 6752–6756.
[81] A. E. Allen, D. W. C. MacMillan, *J Am Chem Soc* **2010**, *132*, 4986–4987.
[82] H. Huo, X. Huang, X. Shen, K. Harms, E. Meggers, *Synlett* **2016**, *27*, 749–753.
[83] J. Liu, W. Ding, Q. Q. Zhou, D. Liu, L. Q. Lu, W. J. Xiao, *Org Lett* **2018**, *20*, 461–464.
[84] Q. H. Deng, H. Wadepohl, L. H. Gade, *J Am Chem Soc* **2012**, *134*, 10769–10772.
[85] P. Xu, W. Fan, P. Chen, G. Liu, *J Am Chem Soc* **2022**, *144*, 13468–13474.
[86] C. Jiang, L. Wang, H. Zhang, P. Chen, Y. L. Guo, G. Liu, *Chem* **2020**, *6*, 2407–2419.
[87] D. A. Nagib, M. E. Scott, D. W. C. MacMillan, *J Am Chem Soc* **2009**, *131*, 10875–10877.
[88] Ł. Woźniak, J. J. Murphy, P. Melchiorre, *J Am Chem Soc* **2015**, *137*, 5678–5681.
[89] I. D. Jurberg, I. Chatterjee, R. Tannert, P. Melchiorre, *Chemical Communications* **2013**, *49*, 4869–4883.
[90] S. Bertelsen, M. Marigo, S. Brandes, P. Dinér, K. A. Jørgensen, *J Am Chem Soc* **2006**, *128*, 12973–12980.
[91] V. Marcos, J. Alemán, *Chem Soc Rev* **2016**, *45*, 6812–6832.
[92] H. Jiang, Ł. Albrecht, K. A. Jørgensen, *Chem Sci* **2013**, *4*, 2287–2300.
[93] G. Bergonzini, S. Vera, P. Melchiorre, *Angewandte Chemie - International Edition* **2010**, *49*, 9685–9688.

[94] M. Silvi, C. Cassani, A. Moran, P. Melchiorre, *Helvetica Chimica Acta* **2012**, *95*, 1985–2005.
[95] J. Stiller, E. Marqués-López, R. P. Herrera, R. Fröhlich, C. Strohmann, M. Christmann, *Org Lett* **2011**, *13*, 70–73.
[96] B. S. Donslund, K. S. Halskov, L. A. Leth, B. M. Paz, K. A. Jørgensen, *Chemical Communications* **2014**, *50*, 13676–13679.
[97] M. Silvi, E. Arceo, I. D. Jurberg, C. Cassani, P. Melchiorre, *J Am Chem Soc* **2015**, *137*, 6120–6123.
[98] M. Balletti, M. Balletti, P. Melchiorre, *Chemical Communications* **2022**, DOI 10.1039/d2cc01638a.
[99] C. Ma, Z. J. Jia, J. X. Liu, Q. Q. Zhou, L. Dong, Y. C. Chen, *Angewandte Chemie International Edition* **2013**, *52*, 948–951.
[100] T. Ishino, T. Oriyama, *https://doi.org/10.1246/cl.2007.550* **2007**, *36*, 550–551.
[101] T. Inoshita, K. Goshi, Y. Morinaga, Y. Umeda, H. Ishikawa, *Org Lett* **2019**, *21*, 2903–2907.
[102] I. Arenas, A. Ferrali, C. Rodríguez-Escrich, F. Bravo, M. A. Pericàs, *Adv Synth Catal* **2017**, *359*, 2414–2424.
[103] D. D. M. Wayner, J. J. Dannenberg, D. Griller, *Chem Phys Lett* **1986**, *131*, 189–191.
[104] A. Bahamonde, P. Melchiorre, *J Am Chem Soc* **2016**, *138*, 8019–8030.
[105] F. Juliá, T. Constantin, D. Leonori, *Chem Rev* **2022**, *122*, 2292–2352.
[106] L. Buzzetti, G. E. M. Crisenza, P. Melchiorre, *Angewandte Chemie* **2019**, *131*, 3768–3786.
[107] M. A. Cismesia, T. P. Yoon, *Chem Sci* **2015**, *6*, 5426–5434.
[108] C. Cassani, P. Melchiorre, *Org Lett* **2012**, *14*, 5590–5593.
[109] R. H. Bradbury, J. S. Major, A. A. Oldham, J. E. Rivett, D. A. Roberts, A. M. Slater, D. Timms, D. Waterson, *J Med Chem* **1990**, *33*, 2335–2342.
[110] E. Larionov, L. Lin, L. Guénée, C. Mazet, *J Am Chem Soc* **2014**, *136*, 16882–16894.

[111] G. A. Molander, J. A. C. Romero, *Tetrahedron* **2005**, *10*, 2631–2643.
[112] H. Hopf, A. Krüger, *Chemistry A European Journal* **2001**, *7*, 4378–4385.
[113] G. Damilano, K. Binnemans, W. Dehaen, *Org Biomol Chem* **2019**, *17*, 9778–9791.
[114] P. Gentili, M. Nardi, I. Antignano, P. Cambise, M. D'Abramo, F. D'Acunzo, A. Pinna, E. Ussia, *Chemistry - A European Journal* **2018**, *24*, 7683–7694.
[115] T. Ikai, M. Okubo, Y. Wada, *J Am Chem Soc* **2020**, *142*, 3254–3261.
[116] P. J. Gilligan, B. K. Folmer, R. A. Hartz, S. Koch, K. K. Nanda, S. Andreuski, L. Fitzgerald, K. Miller, W. J. Marshall, *Bioorg Med Chem* **2003**, *11*, 4093–4102.
[117] Y. E. HU, J. KAUR, R. MCFADDEN, J. P. MURRY, B. E. SCHULTZ, H. H. TRUONG, H. YU, **2020**.
[118] W. L. Schreiber, A. O. Pittet, M. H. Vock, *J Agric Food Chem* **1974**, *22*, 269–273.
[119] K. J. Kolonko, H. J. Reich, *J Am Chem Soc* **2008**, *130*, 9668–9669.
[120] P. Teo, Z. K. Wickens, G. Dong, R. H. Grubbs, *Org Lett* **2012**, *14*, 3237–3239.
[121] I. Arenas, A. Ferrali, C. Rodríguez-Escrich, F. Bravo, M. A. Pericàs, *Adv Synth Catal* **2017**, *359*, 2414–2424.
[122] A. K. Rappé, C. J. Casewit, K. S. Colwell, W. A. Goddard, W. M. Skiff, *J Am Chem Soc* **1992**, *114*, 10024–10035.